

Copyright  
by  
Javier Allende Labastida  
2019

**The Dissertation Committee for Javier Allende Labastida Certifies that this is the  
approved version of the following dissertation:**

**Characterization and therapeutic evaluation of a traumatic brain injury  
model in compliance with common data elements**

**Committee:**

---

Ping Wu, M.D., Ph.D., Chair

---

Donald S. Prough, M.D.

---

Jose M. Barral, M.D., Ph.D.

---

John T. Povlishock, Ph.D.

---

Darren F. Boehning, Ph.D.

---

Dean, Graduate School

**Characterization and therapeutic evaluation of a traumatic brain injury  
model in compliance with common data elements**

**by**

**Javier Allende Labastida, M.D.**

**Dissertation**

Presented to the Faculty of the Graduate School of

The University of Texas Medical Branch

in Partial Fulfillment

of the Requirements

for the Degree of

**Doctor of Philosophy**

**The University of Texas Medical Branch**

**April 2019**

## Dedication

This dissertation is dedicated to all the broken hearts, disrupted minds and lives taken by this disease. This work was done in the hopes that it will contribute to solving the puzzle of this disease and helping these patients.

This work is especially dedicated to my family, who have always believed in me, even when I didn't.

**To my parents Javier and Ma. Del Pilar**, who instilled in me the spirit to always help others, and who showed me the value of a person's word, honesty and hard work. My parents have always encouraged me to follow my dreams, no matter how difficult.

**To my sister Pilar**, who has shown me always to push forward and maintain strength regardless of the hardships, and who is one of the strongest people I know.

**To my brother Andres**, who has shown me the true meaning of loyalty and selflessness, and who keeps surprising me of the great man he has and continues to become.

**To my nephew Jose Maria**, for making me want to be the best example I can.

This work is also dedicated to those who believed in me, supported my work and helped me to fulfill this goal:

**To José Marrón Cajiga and Inés Marrón Solorzano**, whose unwavering support through Fundación Marrón Cajiga was instrumental in my admission and success in graduate school.

**To Amalia Lopez De Nigris**, whose trust in me and support of my career has played a fundamental role in the completion of this project and the fulfillment of a dream.

Finally, I dedicate this work to every hurdle and obstacle, to every sleepless night and challenging time, because it has pushed me to work harder. It has increased the value of my work and has demonstrated to me my resilience and capacity for accomplishment. To all the good and the bad in my life, because all of it has led me in this direction.

## Acknowledgements

I want to thank Ping Wu for her mentorship through this program and all the members of the Wu Lab, including Tiffany Dun, Jungling Gao, James L. Sowers, Erica McGrath, Caitlin Schlagal, Hao Yan, Le Wang, Han Ding and Wenye Song, for their support and contributions.

I want to acknowledge friends who have become family, and without whom I could not have continued this long road: Joe Shearer, Sam Umbaugh, Shariq Ali, Ibdanelo Cortes, James L. Sowers, Iveth Garcia, Sanaalarab Al Enazy, Matt Mrazek, Brenda Wilson, Sergio Rodriguez, Mauro and Michela Montalbano, Lorenzo Ochoa, Claudia Marino, Emanuele Mocciano and Harris Weiz.

I would like to give special thanks to Tiffany J. Dunn, one of the most skilled people I have met in my time at UTMB, for teaching me everything she could, for being the ceaseless help I needed when work in the lab became exhausting or overwhelming, and for her numerous contributions to all parts of this project.

I want to thank The Moody Group for their great help and support throughout this lengthy project: Donald S. Prough, Csaba Szabo, Yuriy Petrov, Bridget Hawkins, Maria-Adelaide Micci, and Rinat Esenaliev. Additionally, I want to acknowledge Kelly T. Dineley for her teaching me about animal behavior testing and holding stimulating discussions with me. These helped me to develop a part of the work shown in this dissertation.

I want to thank the collaborators and contributors to these projects: Csaba Szabo for guiding in designing the olaparib dosing and testing paradigm; Yuriy Petrov, for design and implementation of the sensors and software for the model; Shariq Ali for guidance in the construction of the velocity sensor and the code that calculates it; Jungling Gao for contributions in cell culture, imaging and image quantification for the olaparib project;

Tiffany J. Dunn, for her assistance in the preparation and induction of injuries, scoring of behavior, tissue collection, sectioning, and staining, drug administration, and many other things; Han Zhang and Preston R. Klein for their contributions in confocal imaging; Gabor Toro and Akbar Ahmed for contributions with molecular analysis of the olaparib tissue; James L. Sowers for contributions in blinded behavioral quantification and assistance in TBI induction; Jutatip Guptarak for contributions on staining and imaging for the olaparib project; Yongjia Yu for his recommendation of the Kane paper for the model.

I also want to thank Jose Manuel Barral and Darren F. Boehning who believed in me and recommended my acceptance into the Cell Biology Program. They are great professors and have given me invaluable insight into science and life. Thanks to Andres Oberhauser, whose door was always open to discuss anything from an experiment to life or school problem. Thanks to Joan Nichols who helped me find the last support I needed to finish this dissertation and who has been an excellent champion for students in the Graduate School for Biomedical Sciences. Also, I would like to thank Pomila Singh for pushing and supporting me when it counted the most.

Thanks to the Cell Biology and Anatomy program for all their effort in training us and provide space that allowed us to improve our skills, particularly Pomila Singh, Aurora Galvan, and Debra Moncrief.

Thanks to my committee members for their insight, help, teachings, and patience: John T. Povlishock, Donald S. Prough, Jose Manuel Barral and Darren F. Boehning.

This work was funded by the Moody Project for translational TBI research. The Marron Cajiga Foundation, CONACYT-COPOCYT, and ConTex

# **Characterization and therapeutic evaluation of a traumatic brain injury model in compliance with common data elements**

Publication No. \_\_\_\_\_

Javier Allende Labastida, Ph.D.

The University of Texas Medical Branch, 2019

Supervisor: Ping Wu

Traumatic brain injury (TBI) is a major public health problem. It represents the leading cause of morbidity and mortality in children and young adults, resulting in long-term sequelae for a considerable number of survivors. Development of effective therapeutics for patients with TBI is an unmet need. A critical step to address this need is to establish reproducible and comparable animal models that will allow preclinical meta-analyses, and has led to an increasing interest in generating common data elements in TBI research.

This project addresses TBI and research-related issues in three ways. First, an existing closed-skull weight drop TBI model was optimized by the incorporation of three novel sensors, which allowed the detection of important factors that could induce variability. This finding led to the redesign of the model and the addition of an impactor. Additionally, the sensors allowed measurement and comparison of forces applied on the head of the animal to monitor mechanical reproducibility. The outcomes of these injuries were further evaluated with a comprehensive of battery of behavioral and pathological analyses. Second, an artificial model of a mouse, “the professional mouse” was developed

to aid the precise measurement for reproducibility of closed-head injury models or compare between models. Finally, this newly optimized TBI model was used to initiate the assessment of a potentially therapeutic drug to treat neurotrauma. Olaparib (Lynparza®) is a Poly(ADP-polymerase) 1 (PARP1) inhibitor approved by the FDA for the treatment of breast and ovarian cancer. Several studies reported the activation of PARP1 after injury in the central nervous system. This activation has been correlated with increased inflammation, mitochondrial dysfunction and necrosis. Furthermore, the inhibition of PARP1 is neuroprotective in different models of brain injury. This study shows that olaparib administered after TBI reduces astrogliosis and cognitive deficits. Although further studies are needed, we are enthusiastic that PARP inhibition may prove efficacious in the acute phase, as well as prevent the later-stage neurological deterioration secondary to single or repetitive TBI.

## TABLE OF CONTENTS

List of Tables .....	xviii
List of Figures.....	xix
List of Illustrations.....	xxiii
List of Abbreviations .....	xxiv
<b>TRAUMATIC BRAIN INJURY .....</b>	<b>28</b>
Chapter 1 Introduction.....	28
Traumatic brain injury (TBI).....	28
History of TBI .....	28
Definition of TBI.....	32
Classification of TBI .....	34
Classification of TBI by clinical severity .....	34
Classification of TBI by pathophysiology.....	37
Classification of TBI primary injury by distribution.....	38
Classification of TBI by mechanical force .....	39
Burden of disease and public health implications of TBI .....	40
Pathophysiology of TBI .....	46
Biomechanical injury.....	46
Mechanical loading and injury .....	47
Primary injury.....	50
Focal brain injury .....	51
Diffuse brain injury .....	59
Secondary Injury.....	62
Neurovascular changes.....	63
Neurometabolic cascade after TBI .....	65
Poly(ADP-Ribose) polymerase (PARP) in TBI.....	70
Neuroinflammation.....	73
Animal models of TBI.....	75
Open head injury models of TBI .....	76
Fluid percussion injury model .....	76

Controlled cortical impact injury model.....	77
Closed head injury models .....	78
Impact injury models.....	79
Impact-acceleration .....	79
Non-impact acceleration.....	82
Rationale, hypothesis, and aims .....	86
Aims	87
Chapter 2 Model development .....	89
Introduction .....	89
Materials and methods.....	91
Model evolution.....	91
Initial TBI apparatus.....	91
Evolution of the TBI apparatus (working model) .....	93
Current working TBI apparatus.....	95
Sensors.....	98
Professional mouse.....	102
Support systems to mimic other models.....	103
Software.....	106
Statistical Analysis .....	107
Results .....	108
Fishing line alters the velocity of the falling weight .....	108
Righting reflexes and behavioral deficits are object-weight dependent..	109
The novel apparatus with an impactor is highly reproducible.....	112
Velocities from the falling objects vary from theoretical calculations....	114
The impact sensor can detect double impacts .....	117
A tolerance curve for the weight drop model.....	118
Discussion and conclusions.....	121
Chapter 3 Model characterization.....	127
Introduction .....	127
Materials and methods.....	129
Animals.....	129

Selection and Randomization .....	130
Novel TBI apparatus.....	131
Signal processing and software .....	132
Injury system setup.....	133
Anesthesia and Physiological measurements setup.....	133
Injury and righting reflex.....	135
Behavioral tests.....	136
Neurological severity score (NSS) .....	136
Exploratory behavior and locomotor activity .....	138
Memory .....	140
Assessment for mood disorders.....	144
Assessment for Hippocampal damage.....	147
Gross pathology .....	149
Tissue Collection.....	150
Statistical analysis.....	150
Results of single TBI.....	153
Mortality .....	153
Force, acceleration and speed plateau in TBI from 1.5 m.....	153
Righting reflex and neurological deficits in single TBI .....	156
Fine motor function but not locomotion is affected after single TBI.....	158
Single TBI induces memory deficits in context discrimination .....	160
sTBI reduces acrophobia but not agoraphobia or depressive behavior ...	162
Marble burying and nestlet shredding tests show no differences after single TBI .....	166
Results of repetitive mild TBI .....	166
Peak force and acceleration are affected by object-weight at 1.0 m .....	166
Repetitive mild TBI increases RR and neurological deficits .....	170
Repetitive mild TBI affects fine motor function but not locomotion.....	172
Contextual memory is affected after RmTBI .....	174
RmTBI reduces acrophobia but not agoraphobia .....	176
Marble burying and nestlet shredding test show no differences after RmTBI.....	179
Gross morphology .....	179

Discussion and conclusions .....	181
Chapter 4 Repurposing of an FDA-approved Poly (ADP-ribose) polymerase 1 (PARP1) inhibitor (olaparib) to treat neurotrauma .....	189
Introduction .....	189
Materials and methods.....	191
Cell culture and injuries.....	191
Oxidative stress injury and kinetic lactate dehydrogenase (LDH) assay .....	191
Proliferation and differentiation of hNSCs.....	191
Rapid stretch injury and treatment .....	193
Molecular analysis.....	193
Necrosis and apoptosis assay.....	193
NAD, NADH, and NAD/NADH measurements .....	194
Immunofluorescence (immunocytochemistry).....	194
Animals and groups .....	196
Apparatus.....	196
Closed-skull weight drop injury .....	197
Dose and route of administration.....	198
Neurological and behavioral assessment.....	198
Righting reflex (RR).....	198
Locomotion activity.....	198
Novel object recognition (NOR) .....	199
Elevated plus maze (EPM) .....	200
Tissue processing.....	201
Immunohistochemistry .....	202
Molecular analysis.....	203
Malondialdehyde (MDA) Abundance.....	203
Myeloperoxidase (MPO) activity .....	203
Quantification of cytokine levels in plasma and tissue .....	204
Statistical analysis.....	205
Results .....	206
Olaparib protects neurons from oxidant-induced cell death.....	206

Olaparib reduces the formation of PARs and increases PARP1 expression .....	207
Olaparib reduces cell death and is neuroprotective after stretch injury ..	208
NAD levels are not restored with olaparib after stretch injury.....	211
Biomechanics of injury and RR.....	213
Both olaparib and TBI independently increase locomotor activity without a synergistic effect.....	215
Olaparib protects mice from TBI-induced cognitive deficits .....	217
TBI and olaparib individually decrease agoraphobia-related anxiety .....	219
Olaparib reduces astrogliosis and increases microglial activation after TBI .....	223
Olaparib shows neuroprotection after TBI in vivo .....	228
Olaparib increases activated caspase 3 positive cells in uninjured controls .....	229
TBI shows no changes in lipid peroxidation and hydrogen peroxide levels 4 days post injury.....	231
Differences in cytokine and chemokine profiles after TBI and olaparib treatment. ....	232
Discussion and conclusions .....	234
Chapter 5 Discussion and future directions .....	242
Conclusions .....	242
Overall impression of findings .....	242
Overview of impact, significance and innovation .....	246
Caveats and alternative explanations.....	247
Future directions.....	248
Appendix A Biomechanical comparison of the models .....	252
Appendix B Code .....	253
Appendix B1 Calibrator code.....	253
Appendix B2 Velocity sensor code for initial trials and biological characterization .....	253
Appendix B3 Velocity sensor code for biomechanical characterization.....	254
Appendix B4 Velocity sensor and force sensitive resistor (FSR) code.....	255

Bibliography/References .....	257
Vita ... ..	293

## List of Tables

Table 1.1. Clinical signs of traumatic brain injury .....	33
Table 1.2. Glasgow Coma Scale (GCS) .....	35
Table 1.3. Classification of traumatic brain injury according to severity .....	36
Table 3.1. Experimental groups of mice for model characterization .....	130
Table 3.2. Neurological severity score .....	138
Table 3.3. Multiple comparisons for analysis of repetitive mild TBI .....	153

## List of Figures

Figure 1.1. CDC data of TBI epidemiology in the US from 2001-2010.....	45
Figure 2.1. Initial TBI apparatus .....	92
Figure 2.2. Evolution of the TBI apparatus .....	94
Figure 2.3. Working model TBI apparatus.....	97
Figure 2.4. Sensors .....	101
Figure 2.5. Professional mouse model.....	103
Figure 2.6. Support systems for impact-acceleration models.....	105
Figure 2.7. Software screenshot. ....	107
Figure 2.8. Comparison of fishing lines for weight-drop.....	109
Figure 2.9. Mechanical and behavioral assessment of first working model of TBI..	111
Figure 2.10. Mechanical reproducibility with an aluminum foil support.....	113
Figure 2.11. Effect of friction on falling objects .....	116
Figure 2.12. Double impacts detected by impact sensor .....	118
Figure 2.13. A mouse tolerance curve.....	120
Figure 3.1. Experimental design.....	131
Figure 3.2. Injury system, anesthesia and physiological measurement systems .....	134

Figure 3.3. Neurological severity score (NSS).....	137
Figure 3.4. Novel object and location recognition paradigm .....	141
Figure 3.5. Fear conditioning experimental design and novel context setup .....	143
Figure 3.6. Thigmotaxis in open field (OF) and photobeam activity system (PAS).145	
Figure 3.7. Tail suspension test arena.....	147
Figure 3.8. Marble burying and nestlet shredding tests.....	149
Figure 3.9. Statistical analysis and group comparisons.....	152
Figure 3.10. Biomechanics of single injury.....	155
Figure 3.11. Righting reflex and neurological deficits in single TBI.....	157
Figure 3.12. Fine motor function but not locomotion is affected after single TBI ...	159
Figure 3.13. Single TBI induces memory deficits in context discrimination.....	161
Figure 3.14. sTBI reduces acrophobia but not agoraphobia.....	164
Figure 3.15. Biomechanics of repetitive mild TBI.....	168
Figure 3.16. Neurological deficits increase with the number of injuries .....	171
Figure 3.17. RmTBI affects fine but not gross locomotion.....	173
Figure 3.18. Contextual memory is affected after RmTBI.....	175
Figure 3.19. RmTBI reduces acrophobia but not agoraphobia.....	178

Figure 3.20. sTBI and RmTBI can produce concussion, contusion and hematomas	180
Figure 4.1. In vitro experimental design.....	195
Figure 4.2. In vivo experimental design for assessment of olaparib treated TBI.....	200
Figure 4.3. Olaparib protects neurons from oxidant-induced cell death .....	206
Figure 4.4. Olaparib reduces expression of PAR and cleaved PARP after stretch injury.....	208
Figure 4.5. Olaparib reduces cell death and is neuroprotective after stretch injury ..	210
Figure 4.6. NAD levels are not restored with olaparib after stretch injury in human neurons and astrocytes.....	212
Figure 4.7. Injury parameters and physiological outcomes.....	214
Figure 4.8. Olaparib and TBI increase locomotor activity without synergistic effect .....	216
Figure 4.9. Olaparib protects mice from TBI-induced cognitive deficits .....	218
Figure 4.10. No differences are found in acrophobia-related anxiety .....	220
Figure 4.11. TBI and olaparib individually decrease agoraphobia-related anxiety...	222
Figure 4.12. Olaparib reduces astrogliosis in the hippocampus after TBI .....	225
Figure 4.13. Olaparib increases TBI-induced microgliosis.....	227

Figure 4.14. Olaparib protects neurons from injury assessed by phosphorylated c-Jun .....	229
Figure 4.15. Olaparib increases the number of activated caspase 3 positive cells ....	230
Figure 4.16. No differences in lipid peroxidation and hydrogen peroxide levels assessed by MPO and MDA.....	231
Figure 4.17. Differences in cytokine and chemokine profiles after TBI.....	233

## **List of Illustrations**

Illustration 1.1 Types of intracranial hematomas .....	58
Illustration 1.2. Neurometabolic cascade of TBI.....	67
Illustration 1.3. Traumatic axonal injury .....	69
Illustration 1.4. Poly (ADP-ribose) polymerase 1 in TBI.....	72

## List of Abbreviations

aCas3	Activated caspase 3
ADP	Adenosine diphosphate
AMPA	$\alpha$ -Amino-3-hydroxy-5-methyl-4-isoxazolepropionic acid
AOC	Alteration of consciousness
APP	Amyloid precursor protein
AQ4	Aquaporin 4
ATRA	All-trans retinoic acid
ATP	Adenosine tri-phosphate
BBB	Blood brain barrier
bFGF	Basic fibroblast growth factor
BSA	Bovine serum albumin
BW	Body weight
CCI	Controlled cortical impact
CDC	Center for disease control and prevention
DAPI	4',6-diamidino-2-phenylindole
DMEM	Dulbecco's Modified Eagle Medium
DMSO	Dimethyl sulfoxide
DNA	Deoxyribonucleic acid
DoD	Department of defense
EAs	Excitatory amino acids
EDTA	Ethylenediaminetetraacetic acid
EGF	Epidermal growth factor
ELL	EGF, laminin and LIF
EPM	Elevated plus maze

FPI	Fluid perfusion injury
FDA	Food and drug administration
GCS	Glasgow coma scale
GCScore	Glasgow coma score
GFAP	Glial fibrillary acidic protein
H <sub>2</sub> O <sub>2</sub>	Peroxide
HEPES	4-(2-hydroxyethyl)-1-piperazineethanesulfonic acid
hNSCs	Human neural stem cells
HRP	Horseradish peroxidase
IACUC	Institutional animal care and use committee
Iba-1	Ionized calcium binding adaptor molecule 1
ID	Identification
IP	intraperitoneal
LDH	Lactic acid dehydrogenase
LIF	Leukemia inhibitory factor
LoC	Loss of consciousness
MBT	Marble burying test
MDA	Malondialdehyde
MPO	Myeloperoxidase
mTBI	Mild traumatic brain injury
NAD	Nicotinamide adenine dinucleotide
NADH	Nicotinamide adenine dinucleotide (reduced form)
NeuN	Neuronal nuclei
NLR	Novel location recognition test
NMDA	N-Methyl-D-aspartate
NOR	Novel object recognition test
NSS	Neurological severity score

NST	Nestlet shredding test
OF	Open field
P-C Jun	Phosphorylated C Jun
PAR	Poly (ADP-ribose)
PARP	Poly (ADP-ribose) polymerase
PARP1	Poly (ADP-ribose) polymerase 1
PAS	Photobeam activity system
PBS	Phosphate-buffered saline
PC	Polycarbonate
PEEK	Polyetheretherketone
PMMA	Poly (methyl methacrylate)
PMN	Polymorphonuclear leukocyte
PMSF	Phenylmethylsulfonyl fluoride
psi	Pound-force per square inch
PTA	Post-traumatic amnesia
PTSD	Post-traumatic stress disorder
PVDF	Polyvinylidene difluoride
RIPA	Radioimmunoprecipitation assay
RmTBI	Repetitive mild traumatic brain injury
RNS	Reactive nitrogen species
ROS	Reactive oxygen species
RR	Righting reflex
SDS-PAGE	Sodium dodecyl sulfate polyacrylamide gel electrophoresis
SI	Stretch injury
TBI	Traumatic brain injury
TBS	Tris-buffered saline
TBST	Tris-buffered saline + tween

TPPS	Transferrin, putrescine, progesterone and sodium selenite
TST	Tail suspension test
TuJ1	Neuron-specific class III $\beta$ tubulin
OCT	Optimal cutting temperature

# **TRAUMATIC BRAIN INJURY**

## **Chapter 1 Introduction**

### **TRAUMATIC BRAIN INJURY (TBI)**

Traumatic brain injury (TBI) is a complex and heterogeneous condition (Centers for Disease Control and Prevention 2015, World Health Organization 2006, Maas et al. 2010, Andelic 2013). It is referred to as “the most complex disease in the most complex organ” (Wheble and Menon 2016). Some of these complexities will be discussed in different portions of this chapter.

### **HISTORY OF TBI**

TBI has gained public attention in the last decade mainly due to Dr. Omalu’s findings of neurodegeneration in the brains of deceased football players (Omalu et al. 2005, Omalu et al. 2006) and the legal battle that ensued against the NFL years later. However, this is by no means a new disease; the study, attempted classification, and cure of TBI began in ancient times. The earliest record of a TBI and its consequences is a pediatric skull of a 12- or 13-years old child from the middle paleolithic period. The child had signs of blunt trauma to the skull and subsequent survival, as ascertained by a depressed compound skull fracture that underwent remodeling. The size of the endocranial cavity allowed the estimation of the child’s age to be 6 years old at the time of the trauma. On the other hand, the degree of tooth development helped to determine the age of death at 12- or 13-years old, suggesting skull growth retardation and reduced brain volume (Coqueugniot et al. 2014).

TBI has produced interest within humans, been a definite driver of understanding of the nervous system (CNS), and may have caused the generation of empirical care practices in antiquity. The latter can be illustrated with the over 1500 Neolithic trephined skulls found all over the world, particularly prevalent in Peru. Researchers believe that this practice may have arisen from the observation that people and animals sustaining trauma to the head would “die,” albeit momentarily, and finally come back to life. This observation may have led to the reasoning that if someone dies, a blow to the head could bring them back to life. Consistent with this theory is the finding of incomplete trepanations, which suggests that the “dead” might have woken up mid procedure. Due to the complicated nature of the procedure, the practice of trepanation was believed to be saved only for “important” people in the tribe (Faria 2015). Additionally, the description of TBIs and their effects are seen in myths and legends<sup>1</sup>

On the other hand, interesting examples throughout history exemplify the generation of knowledge from studying TBI. An Egyptian papyrus (named the Edwin Smith papyrus) found in 1862 near Luxor, Egypt (Stiefel, Shaner, and Schaefer 2006), is a surgical treatise and the oldest surviving surgical manuscript in existence today, dated from 1700 B.C.. It is believed to have been copied from an older document dating from 3000-2500 B.C. and may have been written by Imhotep, the first known physician (Breasted 1930, Stiefel, Shaner, and Schaefer 2006). The treatise contains 14 cases of head injuries, excluding external injuries only, spanning from a severe closed head injury (Stiefel, Shaner, and Schaefer 2006) to different types of skull fractures. This document contains the first reference to the word “brain,” mentions cerebrospinal fluid and meninges, and contains descriptions of paraplegia and aphasia in a case with a left temporal skull fracture, It also uses a rudimentary form of triage, dictating when to treat or not, based on known

---

<sup>1</sup> As shown in the description of TBI and its effect in mythological and literature stories all over the world, most famously, Hector in Homer’s Iliad (Homer and Rouse 1995, Courville 1953).

outcomes (Breasted 1930, Stiefel, Shaner, and Schaefer 2006, Sanchez and Burridge 2007, Rose 1997).

During the Greek and Roman eras, Hippocrates, Valerius Maximus and Galen of Pergamon (around 400 B.C., 30 and 130 A.D. respectively) described loss of consciousness, alexia, and aphasia in people suffering TBI, and observed that penetrating wounds to the temple will result in contralateral body spasm (Levin, Benton, and Grossman 1982). The trepanation was the treatment allowing the humors or pressure in the skull to be released, and was used in four out of five types of injury. It was not used if a depressed fracture was present, which represented the fifth kind in the Hippocratic treatise wounds of the head (McCrory and Berkovic 2001, Gross 2012). Of note, Aretaeus of Cappadocia (130 – 200 A.D) described how the level of injury (head or spine) will translate into contralateral or ipsilateral paralysis (respectively), being the first reference to the decussation of the fibers. This wasn't proven experimentally until 1710 by Pourfour de Petit, and half a century later by clinicopathological correlations of Morgagni (Levin, Benton, and Grossman 1982).

Around 900 A.D., Abu Bekr Muhammad el Razi (Rhazes), a Persian physician, was the first person to differentiate concussion from other kinds of brain injury, in which internal physiologic disruption could happen with no damage to skull or skin. It was not until 1306 that the term concussion was used again, when it was defined as a transitory injury of the brain with no external damage, and the pathophysiology conceptualized as commotion or “shaking of the brain” (McCrory and Berkovic 2001) Guido Lanfranchi also differentiated between *commotio* and *contusio cerebri*. This definition was further expanded by Berengario da Carpi (fifteenth century), classifying head injuries with fractures in lacerations, contusions or perforation, with *commotio* or concussion being a separate entity. However, Ambroise Paré, a French surgeon in the 1500s began exploring

the underlying mechanisms of these types of injury. The definition of *commotio* became a movement of the brain in the skull with edema and hemorrhage. It was also during this time that Paré explained the coup and contra coup lesions of both the brain and meninges, and the medical literature widely accepted the term “concussion” (Levin, Benton, and Grossman 1982, Rose 1997, McCrory and Berkovic 2001).

The eighteenth century brought forth essential advances in the understanding TBI, and this renewed interest in TBI because the Paris Academy of Medicine offered a prize to the best explanation of the contrecoup injury (Strauss and Savitsky 1934). Alexis Littré examined a young man that instead of facing the rack, committed suicide by running headfirst against a wall. There were no external or internal signs of injury, and the only finding was that the brain appeared firmer, confirming the concept of *commotio cerebri*. Confusion with the terminology persisted, until this century, when terms were better differentiated into *commotio*, *contusio*, and *compressio cerebri*. The brain and not the skull gradually became the focus of the treatment and, for the first-time, neurological state began to dictate treatment (Courville 1953, McCrory and Berkovic 2001, Levin, Benton, and Grossman 1982, Rose 1997). This paradigm shift was possible due to Joseph Lister Petit’s introduction of the concept that an impact to the skull produces vibrations that are transferred to the brain causing *commotio cerebri*, and this transmission is stronger and more severe if the skull remains unfractured (Strauss and Savitsky 1934). During the 19<sup>th</sup> century, physicians were intensely concerned about the severe neurological deficits with minimal or absent anatomical damage to the brain. Theories ahead of their time by Pierre Gamma (1775-1861) stated that fibers in the brain were breaking due to the trauma. In the 20<sup>th</sup> century, advances in experimental methods finally allowed Schmaus and Stritch to prove that there was in fact breakage of the axons and secondary degeneration due to the mechanical trauma. Concussion has now gained a clinical definition, and there is debate whether or not it causes an irreversible effect. Even today there is confusion in the

terminology, with some terms used interchangeably (Courville 1953, McCrory and Berkovic 2001, Levin, Benton, and Grossman 1982, Rose 1997), With advances in the understanding of the pathophysiology of TBI, new types of injuries such as blast injury have been included. There is still a debate in the definition of TBI, and different groups use different definitions. The concept of TBI being a disease process and not a single event is slowly permeating into the medical field (Corrigan and Hammond 2013, Masel and DeWitt 2010). Finally, the classification of TBI severity has recently been challenged, because the current system (Glasgow Coma Scale) does not always correlate with the outcome, and it cannot be translated from the clinic to the research setting.

#### **DEFINITION OF TBI**

The definition and delimitation of TBI have been a constant area of debate and controversy, as can be seen throughout history. After all, it took 500 years for the term concussion to be accepted and another 200 to define it, and even to this day, it is commonly misused.

TBI definitions are continually evolving and being refined. However, there are differences in wording and criteria between the definitions of different institutions. An example of this can be seen in the WHO definition of TBI. In the report, “Standards for surveillance of neurotrauma,” the definition is: “an occurrence of injury to the head (arising from blunt or penetrating trauma or from acceleration-deceleration forces,” with no mention of blast injury (Thurman 1995). By 2006 they renewed their definition in a report called “Neurological disorders: public health challenges” which included an explanation of the macro pathophysiology and mentioned that the injury is generated by “an external mechanical force,” without mention of blast waves (World Health Organization 2006). The 1995 outdated WHO definition has continued to be cited up to 2011 (Chen and Colantonio

2011), regardless of the changes made to the definition by the Center for Disease Control and Prevention (CDC) or the Department of Defense (DoD).

In 2010, the CDC finally incorporated blast injury into their definition of TBI stating “A TBI is an injury that disrupts the normal function of the brain. It can be caused by a bump, blow or jolt to the head or a penetrating head injury. Explosive blasts can also cause TBI” (Centers for Disease Control and Prevention 2015). Different definitions prevailed among different groups, like one by a task force on common data elements for research in TBI, “an alteration in brain function, or other evidence of brain pathology, caused by an external force” (Menon et al. 2010). The DoD in 2007 developed a more complete definition of TBI, reading: “a traumatically induced injury and/or physiological disruption of brain function a result of an **external force** that is indicated by new onset or worsening of at least one of the following **clinical signs**, immediately following the event” (signs are shown in Table 1). The **external force** can be defined as “head striking an object or an object striking the head, acceleration/deceleration movement of the brain without direct external trauma, foreign body penetrating the skull or forces generated from blasts or explosion” (Management of Concussion/mTBI Working Group 2009, Department of Defense 2010).

Clinical signs of traumatic brain injury
<ul style="list-style-type: none"><li>• Loss of consciousness (LOC).</li><li>• Alteration of consciousness/mental state (AOC).</li><li>• Memory loss/post traumatic amnesia (PTA).</li><li>• Neurological deficits, transient or permanent.</li><li>• Intracerebral lesion.</li></ul>

Table 1.1. Clinical signs of traumatic brain injury

**Table 1.1. Clinical signs of Traumatic brain injury.** To diagnose TBI at least one of these signs must be present (Management of Concussion/mTBI Working Group 2009,

Department of Defense 2010). Additionally, these play an important role in the classification of severity.

It is crucial to clarify commonly misused terminology, such as head injury, acquired brain injury (ABI) and, non-traumatic brain injury. Head injury has a broad definition, includes any injury to the head, such as injuries to the face, scalp or skull. Head injury can exist with or without a TBI (Rotatori and Burkhardt 2011, Bruns and Hauser 2003). Acquired brain injury, on the other hand, includes all traumatic and non-traumatic brain injuries that occur after birth. Non-traumatic brain injuries are any brain injury with the exception of TBI and congenital injuries. Stroke, anoxic and hypoxic brain injuries, infectious diseases and, toxic exposures are examples of these injuries (Giustini, Pistarini, and Pisoni 2013).

## **CLASSIFICATION OF TBI**

### **Classification of TBI by clinical severity**

The most common classification of TBI is by severity. The most common method to assess the severity has been the Glasgow Coma Scale (GCS). This scale, generated in 1974, was developed as a practical system to determine the level of consciousness and coma. The GCS determines the level of consciousness based on three components: the opening of the eyes, verbal response, and motor response. Each of these components has a specific score (Table 2), and their addition determines the levels of consciousness. During the development of the scale, a local hospital implemented it for the diagnosis of head injuries. This hospital lacked personnel with neurosurgical or neurological experience and needed a practical way to assess which patients required surgery (Teasdale and Jennett 1974). This practice led to the use of the Glasgow coma score (GCScore) to classify TBIs by severity. The GCScore stratifies the severity as mild (13 to 15), moderate (9 to 12) and

severe (3 to 9). The scale was modified for use with infants and nonverbal children. Responses to stimuli replaced the commands and the verbal response assessment was divided into younger than two, and 2-5 years of age. Verbal children and over five years of age undergo the standard version of GCS (Orliaguet, Meyer, and Baugnon 2008).

Glasgow coma scale components	
Response	Score
Eye opening	
Opens eyes spontaneously	4
Opens eyes in response to speech	3
Open eyes in response to painful stimulation (i.e. endotracheal suctioning)	2
Does not open eyes in response to any stimulation	1
Motor response	
Follows commands	6
Makes localized movement in response to painful stimulation	5
Makes non-purposeful movement in response to noxious stimulation	4
Flexes upper extremities in response to pain	3
Extends all extremities in response to pain	2
Makes no response to noxious stimuli	1
Verbal response	
Is oriented to person, place and time	5
Converses, may be confused	4
Replies with inappropriate words	3
Makes incomprehensible sounds	2
Makes no response	1

Table 1.2. Glasgow Coma Scale (GCS)

**Table 1.2. Glasgow Coma Scale (GCS).** The GCS has three components, each with a specific set of values. The addition of the three values is the Glasgow coma score (spanning from 3 to 15 points) and determines the classification of severity of TBI into mild (GCScore  $\geq 13$ ), moderate (GCScore 9 - 12) or severe (GCScore 3-9).

Although the GCScore has been instrumental in the determination of the severity of TBI for over 40 years, some conditions can act as confounders and affect the severity estimation. These confounders can be trauma (other than TBI), pre-existing diseases (neuropsychiatric or neuromuscular), medications (sedatives, opioids, paralytics, and hypnotics), intoxicants (alcohol and drugs), mechanical devices (tracheal tubes and splints)

(Teasdale et al. 2014, Zuercher et al. 2009, Barlow 2012), and even circadian rhythm (Yue et al. 2017). When the GCS is correctly employed, instead of the score, the examiner can annotate the reason for a section being untestable.

This metric for classification of severity of TBI later evolved into a multi-indicator of clinical criteria. The added metrics are duration of loss of consciousness (LOC), alteration of consciousness or mental state (AOC), and post-traumatic amnesia (PTA). GCS continues to be one of the stratifying factors, and structural neuroimaging was the last metric added (see table 3 for classification criteria) (Management of Concussion/mTBI Working Group 2009).

Classification of Traumatic brain injury according to severity (Management of Concussion/mTBI Working Group 2009)			
Criteria	Mild	Moderate	Severe
Loss of Consciousness (LOC)	0 – 30 min	> 30 min, < 24 h	> 24 h
Alteration of Consciousness/Mental State (AOC)	≤ 24 h	> 24 h	> 24 h
Post-traumatic Amnesia (PTA)	0 – 1 day	1 – 7 days	> 7 days
Glasgow Coma Scale (GCS) (best score in first 24 h)	13 – 15	9 – 12	< 9 (3 – 8)
Structural Imaging	Normal	Normal or Abnormal	Normal or Abnormal

Table 1.3. Classification of traumatic brain injury according to severity

There is one point of debate, however. There is a subset of patients who meet all the criteria for mild traumatic brain injury (mTBI), except that they present with a skull fracture or an abnormal structural image the day of the trauma, diagnosed as complicated mTBI. These two groups have shown differences in neurobehavioral outcomes, with worse results in the complicated mTBI group, which appear to correlate with the type of complication (Williams, Levin, and Eisenberg 1990, Lange, Iverson, and Franzen 2009). It seems that TBI has a spectrum of severity rather than a clear cut stratification (Whyte, Vasterling, and Manley 2010). Furthermore, mTBI was subcategorized into three degrees

of severity in the guidelines by the European Federation of Neurological Societies. These subcategories were based on the GCScore and the minor or major risk factors for indication of immediate head CT scan. The scale was composed of levels 1 to 3, in which mTBI category one was considered safe to discharge home, and categories two and three warranted a CT scan (Vos et al. 2012). Similarly, in the United States, CT is recommended in sports medicine when there is a suspicion of mTBI with a GCScore < 15, accompanied by LOC, PTA, persistent AOC, skull fracture, focal neurological deficits, or signs of deterioration (Giza et al. 2013).

### **Classification of TBI by pathophysiology**

TBI pathophysiology can be divided into two stages: primary and secondary injuries. Primary injury is the immediate damage induced by mechanical forces, deformation of tissue resulting in brain parenchyma and vasculature disruptions. This stage involves the concussion, contusion and laceration. Laceration of the brain, and intracranial hemorrhage along with shearing of blood vessels, neuronal axons, and glia, result in necrosis as the cell death mechanism. Thus, primary injury can only be prevented, but the consequences can be treated. Secondary injury (discussed further below) is comprised of a series of cellular, molecular, biochemical, metabolic and pathophysiological processes initiated by the primary injury and occurring at variable times. These processes are the usual targets for treatment interventions (Werner and Engelhard 2007, Cernak 2005, Hardman and Manoukian 2002, Ma et al. 2019, Faden 1993, DeKosky et al. 1998, Morales et al. 2005, Namjoshi et al. 2013, O'Connor, Smyth, and Gilchrist 2011, Wang et al. 2014, Xiong, Mahmood, and Chopp 2013).

## **Classification of TBI primary injury by distribution**

The nature of primary injury of TBI determines the extension or spatial distribution of TBI and is classified as focal, diffuse, or mixed injury. The different causes of TBI can predict these types of lesions. Focal brain injury is localized damage of the brain parenchyma, and it is generated by forces exerted on the skull and tissue underneath. This type of injury is commonly seen in direct impacts to the head, motor vehicle accidents with head collision, and violent assaults. The focal injury usually results in contusion (cortical or subcortical, based on severity), laceration, and hematomas (subdural, epidural, and intraparenchymal) with or without skull fracture (Ma et al. 2019, Gennarelli 1994, Finnie and Blumbergs 2002, Andriessen, Jacobs, and Vos 2010, Hardman and Manoukian 2002, O'Connor, Smyth, and Gilchrist 2011, Morales et al. 2005, Werner and Engelhard 2007).

On the other hand, a diffuse injury involves widespread damage to the brain and vasculature. Inertial forces on the brain cause shearing and distortion of the tissue. This lesion is seen in rapid acceleration-deceleration conditions such as a high-speed vehicle accident with unrestricted head movement, child abuse (such as shaken baby syndrome) or by the propagation of blast waves. The result is a concussion, diffuse injury of axons and blood vessels, diffuse brain swelling, ischemic or hypoxic damage, increased intracranial pressure, or in some cases traumatic subarachnoid hemorrhage. A mixed injury is a combination of both types in which there is a focal and diffuse injury. This lesion is seen predominantly in sports injuries and falls, in which there is an impact as well as acceleration and deceleration (Ma et al. 2019, Gennarelli 1994, Finnie and Blumbergs 2002, Andriessen, Jacobs, and Vos 2010, Hardman and Manoukian 2002, O'Connor, Smyth, and Gilchrist 2011, Morales et al. 2005, Werner and Engelhard 2007).

## **Classification of TBI by mechanical force**

The initial cause of TBI is the effect of an external mechanical force exerted on the head. The force can be static or dynamic. Static loading is dependent upon amplitude and duration, which is usually slow (above 200 ms), and thus it does not generate acceleration. The static or semi-static mechanical force is rarely seen in TBI, it is usually correlated with building or structures collapsing or earthquakes and it requires substantial force over a long period of time. It follows a crushing mechanism, only generating brain damage through skull fracture. This type of injury is focal and can result in brain compression, herniation and death (Ommaya and Gennarelli 1974, Meaney and Cullen 2017, Cernak 2005). A dynamic mechanical force possesses amplitude, acceleration, and duration, which is usually less than 50ms. Dynamic loading is a common cause of TBI, with severity depending on the magnitude and rate of strain on the brain. Dynamic loading is usually divided in impact and inertial loadings (Ommaya and Gennarelli 1974). The understanding of the mechanical forces that generate the trauma allows us to predict the primary injury, and thus the pathophysiology of the individual TBI. Specifically, static loading tends to produce focal damage due to depressed fractures, while dynamic loading will generate focal damage in penetrating, direct brain deformation, and impact acceleration injuries (when the head is constrained). On the other hand, a diffuse injury will be present in impulse and blast loading TBI. Finally, an impact acceleration injury with a free moving head will produce a mixture of focal and diffuse injury (Ommaya and Gennarelli 1974, Meaney and Cullen 2017, Cernak 2005).

## **BURDEN OF DISEASE AND PUBLIC HEALTH IMPLICATIONS OF TBI**

In 2006, estimates of the number of yearly worldwide cases of TBI were 150-300 people per 100,000 inhabitants. There were a calculated 9.9 to 19.8 million cases around the world (World Health Organization 2006). Dewan et al. (2018) estimated the global incidence of TBI using data from national registries, the global burden of disease initiative and the world bank. They calculated that there are 939 per 100,000 TBIs worldwide (from all causes and all severities), resulting in approximately 69 million (64-74 million) people suffering a TBI each year (in a population of 7.348 billion). These figures correspond to 2 TBIs happening every second worldwide. Furthermore, they estimated the incidences per severity as 740 per 100,000 (55.9 million or 81%) for mild, and 73 (5.48 million or 8%) for severe (Dewan et al. 2018). These figures may still be an underestimation due to underreporting and because people who suffer mild TBI may not attend the emergency department and outpatient consults are seldomly included in these studies.

The World Health Organization (WHO) states that TBI is the leading cause of morbidity and mortality in children and young adults, and a significant cause of morbidity and mortality in other age groups (World Health Organization 2006).

In the United States, there is a surveillance system for TBI quantification established by the CDC. This system uses databases from the Healthcare Cost and Utilization Project's Nationwide Emergency Department Sample, the National Inpatient Sample, and CDC multiple-cause-of-death public-use data files (Faul et al. 2010, Taylor et al. 2017). This methodology may underestimate the total number of TBIs. It does not account for patients seen in physicians' offices, outpatient hospital settings, the military, people not seeking medical attention and people that died outside of a hospital. The ratio of reports of TBI to true incidence of TBI may be as high as 1:2 and as low as 1:6. It may

be even higher in sport and recreation activity-related TBIs, when the loss of consciousness is a requisite for diagnosis, reporting is as low as only 1:9 cases (Langlois, Rutland-Brown, and Wald 2006, Gardner and Yaffe 2015, Laker 2011).

There has been a steady increase in the yearly incidence of TBIs in the USA. The CDC reported an estimated 1.7 million TBIs on average from 2002-2006. It accounted for 4.8% of all injuries seen in the ER but was a factor in 30.5% of all injury-related deaths. An average of 51,538 TBI related deaths occurred during that period, equating to 142 people dying every day due to TBI (Faul et al. 2010, Taylor et al. 2017). Further reports included an overall incidence of TBI in the US of 1.7 million in 2007, 2.1 million in 2008 (Pearson et al. 2012), 2.5 million in 2010 (Korley et al. 2016) and 2.8 million reported in 2013. It represented 10% of all injuries seen in the ER and 29% of all injury-related deaths, with 55,927 TBI related deaths (Taylor et al. 2017). TBI definitions are essential for epidemiological studies. Hale et al. reported an incidence of 1.6 million TBI cases for 2013, significantly differing from other studies. Researchers calculated the incidence based on the response to the question if in the past 12-months anybody in the household had “a serious or traumatic brain injury?” (Hale et al. 2019).

The changes in the epidemiology and demographics of TBI in the last CDC report (2007-2017) were an increase of 47% in ER visits, with small decreases in hospitalizations and deaths (2.5 and 5% respectively). Children 19 years of age or younger with sport-related TBIs seen in the ER more than doubled in the 2000s, with approximately 329,290 in 2012. An aging population in the US reflects in the epidemiology of TBI. The highest overall rate of TBI was in people aged over 75 years (2,232.2 per 100,000), followed by 0-4 years, (1,591.5 per 100,000) and 15-24 years (1,080.7 per 100,000). ER visits followed the same trimodal distribution (Taylor et al. 2017), and this trend was previously reported in different countries around the world (Bruns and Hauser 2003). Even when overall TBI

hospitalization and deaths decreased in this period, there was an increase among the oldest age groups. The main causes of TBI leading to ER visits were falls, except for the age group of 15-24 years old, in which being struck by or against an object was the primary cause. Falls was also the most common mechanism causing TBI-related hospitalizations in children under 14 and adults over 45, while motor vehicle crashes were the main cause in the 15-44 age group. TBI deaths had different mechanisms depending on the age group. The primary mechanism for these deaths in people 65 years of age and older was falling. The most common cause in 25 to 64-year-old age group was intentional self-harm. The age group of 5-24 years died more often due to motor vehicle accidents. Assaults were the leading cause of death in children under the age of four (Taylor et al. 2017, Albrecht et al. 2016).

Between 2008-2010 the prevalence of people living with some disability due to TBI was roughly five million in the U.S. (Centers for Disease Control and Prevention 2015, World Health Organization 2006). Approximately 43.1% of patients with TBI acutely hospitalized and released (124,000 patients) will develop a long-term disability, resulting in a significant economic burden to the health care system (Corrigan, Selassie, and Orman 2010). In Scotland, a population-based cohort study reported that disability was present in 78%, 54% and 51% of severe, moderate and mild TBI survivors respectively. Moreover, late disability was not correlated with initial injury severity and was present in 47% of mild, 45% of moderate and 48% of severe TBI patients one-year post-injury (Thornhill et al. 2000). In the year 2000 (Centers for Disease Control and Prevention 2010), the lifetime expense of treating TBIs was estimated to be \$60.4 billion. However, this figure does not account for costs associated with extended rehabilitation; support services; loss of productivity for patients, parents, and caregivers; lost quality of life of the patients; and TBI victims that did not seek medical care (Corrigan, Selassie, and Orman 2010). More recent studies have measured direct and indirect costs, accounting for the loss of

productivity (31%) and intangible (quality of life, 62%) costs. Their estimates were \$221 billion in 2009 and, ranged from \$85.6 to \$252.2 billion in 2017 depending on the measurements of the intangible costs (Maas et al. 2017).

TBI was named the silent epidemic. It is a condition affecting people that may seem physically fine, while the cognitive, motor and neuropsychiatric disabilities persist (Vaishnavi, Rao, and Fann 2009). It is paramount to emphasize that TBI is a disease and not a single event, it has acute and chronic consequences (Masel and DeWitt 2010, Corrigan and Hammond 2013). If we accept that TBI is a chronic disease, why is the epidemiology of this disease treated as a single event? When will we start speaking of the prevalence of TBI? Why do we continue to reference the prevalence of people with TBI-related disabilities in the US as 5 million, today, if this was the amount calculated between 2008-2010? The 5 million cases do not correlate with the current understanding that about 50% of patients that suffer a TBI will develop late disabilities, and there has been a steady increase of TBI cases since 2001. How can we believe that the prevalence of people with TBI related disabilities remains the same?

mTBI and Repetitive mild TBI (RmTBI) can be named in their own right a silent epidemic. The definition of mTBI is “an acute brain injury resulting from mechanical energy to the head from external physical forces” (Carroll et al. 2004). The most widely used operational definition is a head injury with a Glasgow Coma Scale (GCS) of  $\geq 13$  (Carroll et al. 2004, Ozdogan, Zeynep, and Basar 2013, Gardner and Yaffe 2015). mTBI has gained increased attention recently due to long-term deficits found in professional athletes (Barkhoudarian, Hovda, and Giza 2011, Kane et al. 2012). However, mTBI is a worldwide public health problem, with an estimated 42-60 million cases worldwide every year (Gardner and Yaffe 2015, Langlois, Rutland-Brown, and Wald 2006, Dewan et al.

2018), representing 75-87% of all TBI cases (Barlow et al. 2010, Kane et al. 2011, Laker 2011, Centers for Disease Control and Prevention 2015, Dewan et al. 2018).

It is important to note that the CDC estimates mTBIs based on number of TBIs treated and discharged from the emergency departments (without hospitalization, see green line in Figure 1.1); With this method it is calculated that 1.4-3.8 million mTBIs occur each year in the US (Laker 2011, Centers for Disease Control and Prevention 2015). mTBI is a significant risk factor for RmTBI, (Gardner and Yaffe 2015) and both are underestimated and underreported (Gardner and Yaffe 2015, Centers for Disease Control and Prevention 2010, 2015, Weber 2007, Langlois, Rutland-Brown, and Wald 2006). While the number of moderate and severe TBIs has remained stable from 2001-2010, the number of cases of mTBI has increased since 2007 (Figure 1.1) (Centers for Disease Control and Prevention 2015). However, with more than 200,000 patients out of the reported 1.4 million showing long-term deficits, the categorization of these injuries as “mild” comes into question (Kane et al. 2011).

Figure 1.1. CDC data of TBI epidemiology in the US from 2001-2010

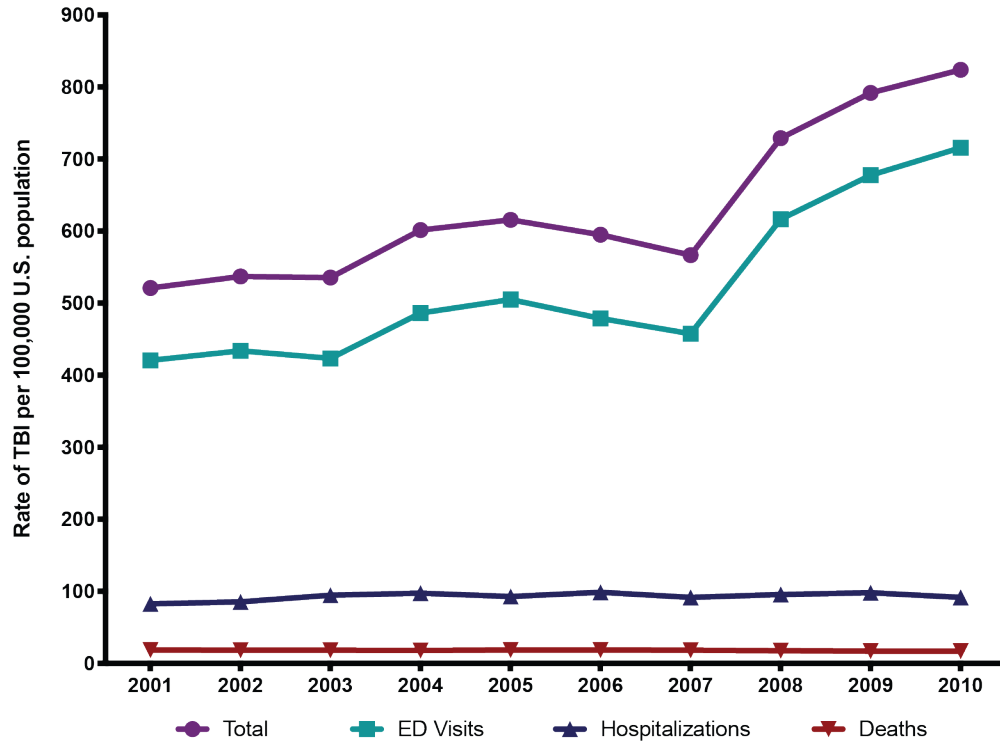


**Figure 1.1. CDC data of TBI epidemiology in the US from 2001-2010.** Used from CDC report to Congress (Centers for Disease Control and Prevention 2015). The prevalence of emergency department (ED) visits, hospitalization, and deaths due to TBI. It is noteworthy that only the number of visits has increased while hospitalizations and deaths remain constant. TBIs treated and discharged from the emergency department drive this increase, categorized as mTBI.

In 2007 sports-related injuries represented 10% of the total mTBIs (Weber 2007). Subpopulations at high risk for mTBI (and thus RmTBI) are contact sports players, military personnel, victims of abuse, truck drivers, and construction and farm workers (Laker 2011, Weber 2007, Gardner and Yaffe 2015, Gubata et al. 2014). Five to twenty percent of mTBI patients will experience persistent post-concussive symptoms (Table 1.3), and 3% will undergo neurological deterioration (Ozdogan, Zeynep, and Basar 2013, Thornhill et al. 2000). Recent findings show that repeated episodes of mild TBI lead to deterioration of

brain function; this phenomenon was first seen in boxers with *dementia pugilistica* and is now seen in individuals that participate in contact sports (Kane et al. 2011). Furthermore, patients with RmTBI demonstrated more severe symptoms, extended recovery periods, and earlier onset of memory disturbances and dementia. Also, when a patient suffers a second TBI within a vulnerable period there is a possibility, although rare, of catastrophic severe brain injury (second concussive syndrome) that can lead to death (Barkhoudarian, Hovda, and Giza 2011).

## **PATHOPHYSIOLOGY OF TBI**

TBI pathophysiology will be divided into three parts for this section: (1) biomechanical injury, which includes the mechanical forces acting on the skull and brain; (2) primary injury, consisting of the morphological damage of the brain and vascular tissues; and (3) secondary injury, encompassing all the biochemical and neurometabolic cascade that can continue for days, months and years after the traumatic event.

### **Biomechanical injury**

Biomechanics is the study of the effect of forces on biological systems and their responses to those forces. As previously mentioned, these forces can be static or dynamic. In TBI, biomechanics attempts to understand the physical or mechanical loads (forces or stress) and the responses (deformation or strain) generated in the head, neck, and ultimately brain. The point at which loading surpasses the adaptability (tolerance or threshold) of the tissue and causes damage will depend on the type of load, its magnitude, and duration (LaPlaca et al. 2007, Namjoshi et al. 2013). Understanding the threshold at which TBI induces injury is essential for preventive campaigns and safety mechanisms, such as public health policy, motor vehicle safety features and helmet design for sports and military

(Namjoshi et al. 2013, Institute of Medicine National Research Council 2014, Post et al. 2019).

Important concepts to define are force, deformation, and stress. Force is measured in Newtons (N), which is the required load to provide an acceleration of 1 m/s<sup>2</sup> to an object of 1 kg of mass. When forces are applied on a body, it may generate deformation, which is the change in shape of an object due to a force. The degree of deformation of a body will depend on its physical characteristics, such as density and rigidity. Another factor that will dictate the effects of force on a body is stress. Stress is the distribution of the force over an area, shear stress ( $\tau$ ) in particular is applied tangentially to a surface. Thus, the strain (or deformation of the tissue) is dependent upon the amount of force applied to an area, meaning strain is greater if a force is applied over a smaller area (LaPlaca et al. 2007). Even though the particular strain involved in the severity of an injury is still being debated, the brain strain theory accounts for the findings seen in cerebral contusion (Ivancevic 2009).

#### ***MECHANICAL LOADING AND INJURY***

As previously mentioned, insults are generated by two mechanical loading conditions, static or quasi-static and dynamic conditions (Meaney and Cullen 2017, LaPlaca et al. 2007). A simple classification developed by Cernak (Cernak 2005), based on the work of Denny-Brown and Russell (Denny-Brown and Russell 1940) and Ommaya et al. (Ommaya and Gennarelli 1974), divided dynamic loading into indirect and direct injuries, where direct was both impact and non-impact head acceleration injuries. Moreover, indirect, defined as a force applied to the whole body that produces kinetic energy (KE) and pressure waves that affect the brain, referred to blast-wave injuries (Cernak 2005).

Others, however, classify the loading conditions as direct (or impact injury), and indirect (or impulse loading) (LaPlaca et al. 2007). A third loading has been proposed as blast overpressure, although the mechanism is still not clearly understood and remains under debate (Meaney and Cullen 2017). Recent studies regard blast wave and blast wind loading as an impulse injury, comprised of peak pressure, duration and pulse shape. Blast wind induces an acceleration-deceleration mechanism of injury through the “bobblehead effect” (Bandak et al. 2015, Goldstein et al. 2012, McKee and Robinson 2014). As stated above, a direct injury is a mechanical force directly applied to the head and brain. The impact injury can be a penetrating, or direct brain deformation injury; and non-penetrating, or impact acceleration injury (Ommaya and Gennarelli 1974, Meaney and Cullen 2017, Cernak 2005). Indirect injury, on the other hand, is the result of head motion generated by forces applied elsewhere in the body (Cernak 2005).

The different types of strain that generate a deformation in the tissue originate from different types of mechanical loads. A translational or linear load induces an extensional strain that can be positive (tensional) or negative (compressive). When a rotational load generates the strain, it is classified as a shear strain. The third type of acceleration, angular acceleration, is a combination of the two and the most commonly seen in TBI. This type of acceleration better explains the focal and diffuse injuries seen in the same patient after a TBI and this combination of accelerations can produce most types of brain injury (LaPlaca et al. 2007, Meaney and Cullen 2017).

Original studies showed that linear loads could cause compressional strains and minor shear strains. However, these strains were considered negligible in comparison to the ones generated by rotational loads and their contribution in the generation of concussion and contusion (Holbourn 1943, Namjoshi et al. 2013, Ommaya and Gennarelli 1974, LaPlaca et al. 2007). Gurdjian, Lissner, and others made counterarguments in favor of

linear acceleration. They believed that linear acceleration through direct impacts to the head and pressure gradients, generated by skull deformation, were the culprit for brain injury. These authors dismissed rotational acceleration and negative pressures as negligible (Deck and Baumgartner 2007, Meaney and Smith 2011). More recently, a set of experiments showed that helmets protect from brain injury by reducing linear loads but not rotational loads. However, they contribute to the reduction of TBI severity, indicating the importance of linear acceleration (King et al. 2003).

Due to technical limitations in the 1950s, TBI was evaluated through the effects of intracranial pressure and time of impact duration (Lissner, Lebow, and Evans 1960). Later, with the ability to measure acceleration it was correlated with linear acceleration (tensional) and duration of impact. These measurements were used to generate the Wayne State Tolerance Curve, which assesses the tolerance of the skull and brain to suffer a fracture or concussion, respectively (Gurdjian et al. 1961, Meaney and Smith 2011). Newer curves have been generated with the use of linear, rotational or angular acceleration.

Further experiments extended the insult parameters studied in TBI. Ommaya measured the angular accelerations required to induce a concussion in rhesus monkeys (40,000 rad/s<sup>2</sup>, to induce concussion in 99% of the monkeys). Furthermore, Houlbourn understood that in order to induce injury to a smaller brain the forces required had to be much larger. This concept was later tested by Ommaya and Hirsch using three species of monkeys with different brain sizes (Ommaya and Hirsch 1971). Following Holbourn's law, Ommaya calculated that humans would require 7500 rad/s<sup>2</sup> to suffer a concussion based on the monkey experiments (Ommaya et al. 1967). These and other experiments led the author to describe that both linear and rotational accelerations can generate a TBI. Ommaya concluded that both points of view were partly correct, and described the type of injury

generated by each direction of acceleration. Linear loading was the main cause for focal injuries and rotational originated diffuse injuries (Ommaya and Gennarelli 1974).

There is a plethora of variables in play to determine the tissue's response to a mechanical insult. The insult parameters, force magnitude (mass, hardness, area, and velocity of the impacting object), location, plane (coronal, horizontal or sagittal), and direction, will determine the types of loads and accelerations on the tissue. Conversely, mechanical properties of the tissue, viscoelasticity (change in stiffness in response to a loading rate), cellular orientation, tissue composition, and surrounding structures determine the tissue response to the insult. The tissue properties are different between individuals, brain region and modified by age or previous injuries or diseases. The viscoelasticity of the brain is also responsible for the non-linear correlation of mechanical force applied and tissue strain and stress, such that there is an increase in the latter if the former increases (LaPlaca et al. 2007, Namjoshi et al. 2013, Meaney and Smith 2011, Meaney and Cullen 2017).

### **Primary injury**

As mentioned previously, primary brain injury is the resulting injury of the brain and vasculature inflicted by a mechanical force, and it can be focal or diffuse. The primary injury is usually classified as either penetrating (or open head) or non-penetrating (or closed head) TBI (Morales et al. 2005, Finnie 2016, Sanchez and Burr ridge 2007, Breasted 1930). Penetrating TBI is usually caused by a projectile breaching the skull (such as bullets, shrapnel, or others), or skull fractures in which the bone and dura are compromised. Open head brain trauma is usually a focal or multifocal injury affecting the path of the penetrating object and the site of entry (LaPlaca et al. 2007, Morales et al. 2005). Closed head injury is further classified as focal or diffuse injury (Nyanzu et al. 2017, Povlishock and Katz

2005, Pervez, Kitagawa, and Chang 2018, Hardman and Manoukian 2002). Although these injuries are categorized separately, they usually coexist, especially in more severe cases of TBI (Meaney and Cullen 2017).

### ***FOCAL BRAIN INJURY***

Focal brain injury is localized damage to the brain, secondary to direct loading (or impact). It is an important cause of moderate and severe traumatic brain injury, and it accounts for two-thirds of the severe TBIs that result in death. The primary mechanisms for death are herniation and brain stem compression. Intracranial hematomas or skull fractures may accompany a focal injury, and result in contusion or lacerations, which differ from each other by the integrity of the pia (LaPlaca et al. 2007, Hardman and Manoukian 2002, O'Connor, Smyth, and Gilchrist 2011, Morales et al. 2005).

### **Fracture**

Focal TBI may be associated with skull fractures in about 25% of moderate (Gennarelli 1994) and 25% of fatal TBIs (Hardman and Manoukian 2002). Closed head TBI is mainly associated with linear, depressed and basilar skull fractures. Linear fractures are most commonly seen in children due to falls. It can cause an underlying contusion or extra-axial hematomas by damaging blood vessels in the meningeal groove, dural venous sinuses or the temporal bone. Additionally, the impact is often accompanied by head acceleration generating other types of TBI (Meaney and Cullen 2017, Hardman and Manoukian 2002, Pervez, Kitagawa, and Chang 2018).

Depressed fractures are common in the frontal and parietal regions. These fractures are generated by low-velocity impacts with a hard, small (less than 2 in) objects on some regions of the skull. The fracture occurs immediately under the impact site, and one or

more bone fragments are displaced towards the meninges and the brain. These fragments displaced inward can cause damage of the meninges with cerebrospinal fluid (CSF) leakage, hemorrhage and brain injury that can result in seizures (Meaney and Cullen 2017, Hardman and Manoukian 2002, Pervez, Kitagawa, and Chang 2018).

Basilar fractures are fractures affecting the ethmoid bone (cribriform plate), frontal bone (orbital plate), the petrous and squamous portions of the temporal bone, the sphenoid or occipital bones. Remote impacts in the skull, direct impacts in the base of the skull, facial or mandibular bones, as well as falls and crushing injuries generate basilar fractures. An extra-axial hematoma is one of the complications that can arise from these fractures (Meaney and Cullen 2017, Hardman and Manoukian 2002, Pervez, Kitagawa, and Chang 2018).

### Contusion

Contusions represent a focal bruise in the surface of the brain. Based on the force of impact they can be cortical or subcortical contusions (King 2017, Povlishock and Katz 2005, Hardman and Manoukian 2002). Contusions most commonly occur in the inferior frontal and temporal regions of the brain (Pervez, Kitagawa, and Chang 2018). Cortical contusions are generally wedge-shaped, involve the gyri and are characterized by cortical and leptomeningeal hemorrhage and necrosis of the contusion area of the tissue. Subcortical contusions are usually multifocal and caused by temporal or occipital impacts (O'Connor, Smyth, and Gilchrist 2011). Different types of contusions have been identified based on the biomechanics causing them. These are coup, contrecoup and intermediate coup.

Coup contusions are primarily due to mechanical loading causing the skull to bend or fracture. The contusion appears under the site of impact and is an injury of the pia, vasculature and cortical brain tissue. The mechanism of injury is an impact on a motionless free head, such as an object striking the head (Hardman and Manoukian 2002, O'Connor, Smyth, and Gilchrist 2011, Meaney and Cullen 2017, LaPlaca et al. 2007, Morales et al. 2005, King 2017).

Conversely, contrecoup contusions appear in an area not immediately under the impact site. The injury is produced when the accelerating head impacts against a hard or unmovable surface (i.e. falls or car crashes). The most commonly injured regions are related to the anatomic irregularities in the bone surfaces of the anterior and middle cranial fossae, causing contusions as the brain impacts these areas. However, if the impact in the skull is lateral, the contusions will be produced in the contralateral frontotemporal regions. There are two predominant theories on how contrecoup contusions are generated. The first, known as the cavitation theory, suggests that the deceleration of the skull induces the brain to move towards the impact site. The void left behind creates a negative pressure area; this causes strains in the brain parenchyma forming air or gas bubbles (named cavitations) within the tissue. Due to the elastic nature of the brain tissue, when it returns to its normal position it generates positive pressure that eliminates the bubbles. This theory fails to explain why contrecoup lesions can appear in areas that are not directly opposite to the impact site. Another possibility of contrecoup origin is the inertial theory. The impact generates translational, rotational or angular acceleration, causing strains in the brain parenchyma and blood vessels, generating the contrecoup lesions. This theory explains the generation of these lesions based on mechanical loading. If the force is transmitted by an object that is rigid and has a small area, the injury will most likely be at the site of impact (coup). On the other hand, a contrecoup injury is more common when the area of the impacting object is compressible or has a large area. This type of collision generates a

deceleration injury since the forces are stopping the head in motion and thus generating inertial loading (King 2017, Hardman and Manoukian 2002, Meaney and Cullen 2017).

A less studied type of contusion is the intermediate coup, which includes vascular disruptions or brain parenchyma injury separate from the skull. It is believed to originate from inertial or compressive loading by a tensile strength on the tissue or herniation contusions by the falx or tentorium. This herniation contusion is observed in the cingulate gyrus (Meaney and Cullen 2017, Hardman and Manoukian 2002). Finally, the gliding contusion is a diffuse injury in the parasagittal plane. It is comprised of deep hematomas in the gray and white matter junction, associated with diffuse axonal injury (DAI) (Hardman and Manoukian 2002).

### Laceration

Laceration has similar localization as contusions, although it requires a greater mechanical loading. Lacerations, unlike contusions, involve mechanical tearing of the tissue. They can be associated with fractures and penetrating injuries or can appear on their own. Unlike in contusions, the pia and arachnoid are usually compromised in lacerations. It is an important cause of intracranial hemorrhage. Common locations include the ventral face of the frontal lobes and the temporal poles. In combination with DAI, they are usually present in the corpus callosum (CC), and the most severe injury involves the cerebral peduncles and pontomedullary junction, frequently resulting in death. The few exceptions that survive suffer “locked-in syndrome” (King 2017, Hardman and Manoukian 2002).

### Hematomas and Hemorrhages

Intracranial hemorrhages are secondary to the rupture of blood vessels and accumulation of blood in the brain and meninges. The severity of hemorrhages is dependent on location and volume. They often have significant neurological sequelae and

are an important cause of death when surgical treatment is lacking. They are classified anatomically as epidural, subdural, subarachnoid and intracerebral hematomas (Meaney and Cullen 2017, Hardman and Manoukian 2002, King 2017, O'Connor, Smyth, and Gilchrist 2011, Morales et al. 2005, Pervez, Kitagawa, and Chang 2018).

### Epidural hematoma (EDH)

Epidural hematomas are more common in young people. These hematomas are an accumulation of blood between the skull and the dura mater due to rupture of the meningeal blood vessels. It is associated with skull fractures in up to 80% of the cases, very commonly with linear fractures. This lesion is present in about 3 to 5% of TBI patients (Gennarelli 1994, Pervez, Kitagawa, and Chang 2018). The accumulation of blood causes the periosteum to be separated from the dura, giving the hematoma its characteristic biconvex shape. The limitation between these two structures limits the hematomas expansion along the cranium, unable to cross sutures and thus most commonly unilateral (Pervez, Kitagawa, and Chang 2018, Finnie 2016). This type of hematoma is life-threatening, and since it is arterial, in nature it can produce rapid expansion and have a clinical evolution of hours or days with a high mortality rate if untreated. This rapid evolution is most commonly caused by the damage of the medial meningeal artery and has a temporoparietal distribution. As it accumulates it creates a mass effect displacing and compressing the brain leading to herniation and death. Clinically, the patient suffers loss of consciousness with the impact, and a period of recovery. As the blood continues to accumulate the patient will present focal neurological deficits and coma, before dying. When diagnosed early and treated surgically it has good prognosis (Pervez, Kitagawa, and Chang 2018, Finnie 2016, Hardman and Manoukian 2002, Meaney and Cullen 2017, O'Connor, Smyth, and Gilchrist 2011). In the occasions in which the ruptured vessel is a vein, the evolution of this hematoma is chronic lasting from 6 days to years. In children slow progression can be

present due to extracranial communication through a fracture line, generating a subgaleal hematoma (Iwakuma and Brunngraber 1973).

### Subdural hematoma (SDH)

A subdural hematoma is the accumulation of blood in a potential space generated by the hemorrhage penetration between the dura and the arachnoid. The main cause is the ruptures of the parasagittal bridging veins, which connect the cerebral hemispheres with the sagittal sinus by bridging the subdural space. These veins are particularly susceptible to acceleration-deceleration strains (Yokobori et al. 2018, Finnie 2016, Meaney and Cullen 2017, Hardman and Manoukian 2002, Pervez, Kitagawa, and Chang 2018).

Differently from epidural hematomas, subdural hematomas are more common in older adults due to a larger subdural space secondary to brain atrophy. It is associated with worse prognosis in severe TBI with 60% of severely disabled or dead patients. SDH has a mortality rate that ranges from 30% in patients operated within 4 hours post injury and 90% on patients who received delayed or no surgery. SDH are not limited by sutures, they have a classic crescent moon shape when seen in a CT scan. Hematomas can spread across the cerebral hemispheres, and they exert a mass effect on the brain, this generates increase intracranial pressure that result in herniation of the brain, while simultaneously decreasing cerebral blood flow. When the skull is decompressed through a craniotomy it leads to reperfusion injury due to the ischemic event (Yokobori et al. 2018).

Based on its clinical evolution, SDH can be divided in acute, subacute, and chronic hematomas. The acute hematoma presents symptoms within 3 days of the injury or it is composed of dark red and black clotted blood (Finnie 2016, Hardman and Manoukian 2002). This fast-occurring hematoma is most likely generated by a combination of the

cortical arteries and the parasagittal bridging veins (Pervez, Kitagawa, and Chang 2018, O'Connor, Smyth, and Gilchrist 2011). A subacute hematoma presents symptoms between 3 and 21 days and contains both clotted and liquid blood. The chronic hematoma presents symptoms over 21 days from the time of the injury and is filled with liquid dark chocolate blood (Finnie 2016, Hardman and Manoukian 2002).

#### Traumatic subarachnoid hemorrhage (tSAH)

Traumatic subarachnoid hemorrhage is associated with the rupture of the pial vessels. It quickly disseminated across the subarachnoid space. The most common locations are the sulci, basal cisterns, and Sylvian fissure. It is often cited as a common effect of TBI with reports that range from 35% (Pervez, Kitagawa, and Chang 2018) to 80% (Ditty et al. 2015) of TBI cases. Generally, tSAH is mild and may present with mild gliosis and has a good recovery. tSAH is usually localized when associated with a contusion. In more severe cases, usually along contusions or lacerations, they can be extensive, have a mass effect and cause death (Finnie 2016). Moderate and severe TBIs with tSAH are at increased risk of poorer prognosis or death (Eisenberg et al. 1990). One of the main complications of tSAH is the cerebral vasospasm leading to ischemia as a secondary insult (Finnie 2016).

#### Intracerebral or intraparenchymal hematoma (ICH)

The rupture of blood vessels in the brain parenchyma generate an intracerebral or intraparenchymal hematoma. They are present in about 40% of TBI cases (Hardman and Manoukian 2002). ICHs have a 20% co-occurrence with acute subdural hematomas and appear in up to 9% of patients that undergo decompressive surgeries to treat intracranial hematomas (Ninchoji et al. 1984, Hardman and Manoukian 2002). Also, these hematomas

are known to undergo expansion in the first 24 hours in up to 51% of the patients (Perel et al. 2009).

ICHs are named “burst” lobe when formed in the margins of contusions and lacerations. When they appear in the temporal and frontal lobes, they can extend into the lateral ventricles. These hematomas can be formed in the caudate nucleus, thalamus, and basal ganglia. The gliding contusion mentioned earlier is the cause of parasagittal white matter hematomas in the frontal lobes (Hardman and Manoukian 2002). If symptoms appear after a week or more, they are named delayed onset intracerebral hematomas (Ninchoji et al. 1984).

Illustration 1.1 Types of intracranial hematomas

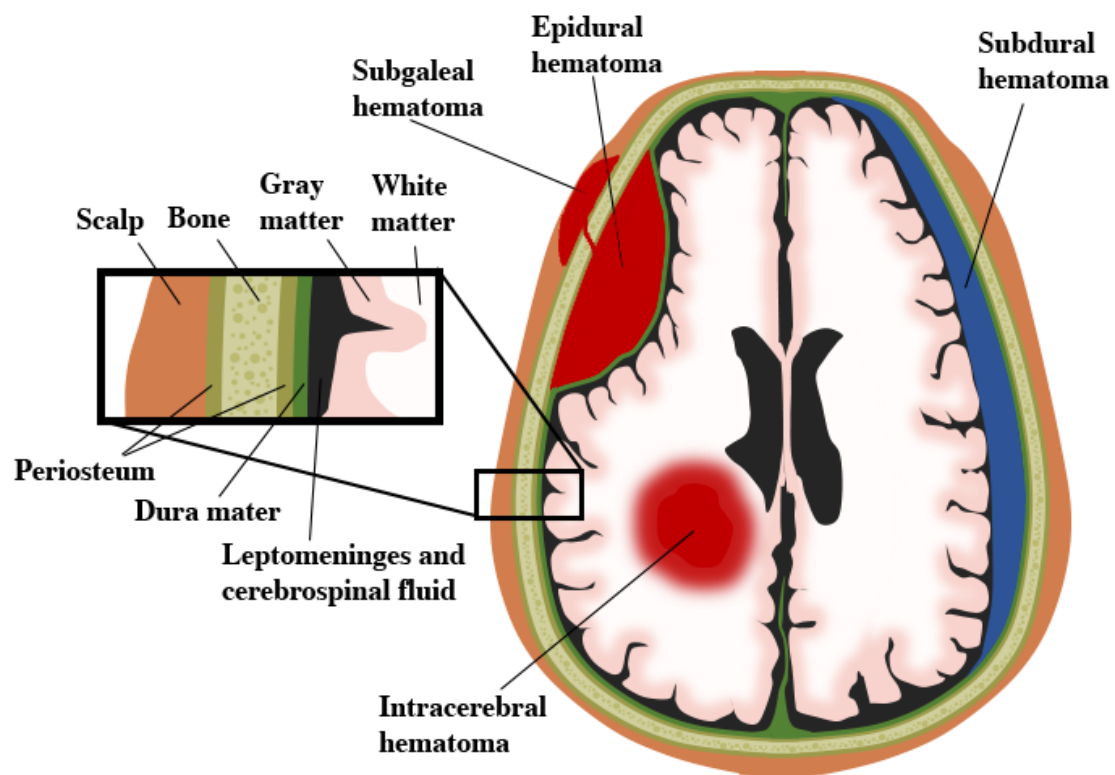


**Illustration 1.1. Types of intracranial hematomas.** *Illustration by Shariq Ali.* Three of the major types of intracranial hematomas are shown. Epidural hematoma with a biconvex

shape limited by sutures due to the dura attachment to the skull. Subdural hematoma with the characteristic crescent shape, this type of hematoma can traverse sutures. Intracerebral hematomas form in the cerebral parenchyma. All these hematomas have a mass effect inside the skull, this translates into brain compression and can lead to death if the hematoma is large enough to induce herniation of the brain.

### ***DIFFUSE BRAIN INJURY***

Diffuse brain injury as its name implies is the widespread damage of the brain and is considered the primary mechanism of brain damage in closed head injury (Levin, Benton, and Grossman 1982). This injury is believed to result from inertial loading that distorts the tissue and produces shear strains during the trauma. Furthermore, the acceleration and deceleration are the culprits of this type of injury due to uneven distributions of a fast-moving force. The leading cause of injury is motor vehicle accidents or high-speed collisions (LaPlaca et al. 2007). This distortion causes diffuse neural, vascular, and brain swelling injuries. The different types of diffuse brain injuries are concussion (Hardman and Manoukian 2002, Meaney and Cullen 2017), DAI (Strich 1956, Levin, Benton, and Grossman 1982, Hardman and Manoukian 2002, LaPlaca et al. 2007, Finnie 2016, Povlishock and Katz 2005), and diffuse vascular injury (Finnie and Blumbergs 2002, O'Connor, Smyth, and Gilchrist 2011, Morales et al. 2005, Andriessen, Jacobs, and Vos 2010, LaPlaca et al. 2007).

### **Concussion**

Concussion has been a highly debated term; part of this has been the misuse as the equivalent of mTBI (Romeu-Mejia, Giza, and Goldman 2019, McCrory and Berkovic 2001). However, for a concussion to occur there has to be a widespread functional disruption of the brain (Meaney and Cullen 2017). The current definition of concussion is

a TBI induced by biomechanical forces with the rapid appearance of functional neurological impairments. They lack macroscopic disturbances as observed by structural neuroimaging studies. It is a disruption of the physiological function, experienced as ionic, metabolic, and neurotransmission changes, or microstructural disruptions that cannot be detected by computed tomography, magnetic resonance or diffusion tensor imaging (Giza and Hovda 2014, McCrory et al. 2017). The primary mechanism is believed to be angular acceleration since the combination of translational and rotational acceleration causes deformation of deeper structures of the brain. The affection of deep brain structures generates a widespread effect. The disruption tends to be reversible. However, microstructural damage or physiological dysfunction may persist (McCrory et al. 2017, Meaney and Cullen 2017).

#### Diffuse axonal injury (DAI)

Diffuse or traumatic axonal injury is the most common type of diffuse TBI. It is associated with all severities of injury and is caused by rotational and angular acceleration/deceleration (Siedler et al. 2014, Andriessen, Jacobs, and Vos 2010, Meythaler et al. 2001, Hardman and Manoukian 2002). It has high morbidity and mortality in moderate or severe injury. DAI is present in 50% of severely disabled and 80% of brain death patients (Lajtha and Banik 2007).

DAI was first described in 1946 named “diffuse degeneration of the cerebral white matter” in patients who survived TBI but were severely demented or decerebrate (Strich 1956). Adams and collaborators introduced the term “diffuse axonal injury” along with a severity classification based on the depth of the lesions in the brain. There are three severities, grade 1 lesions confined to the lobar white matter, grade 2 includes lesions in the corpus callosum, and grade 3 has lesions in the dorsolateral region of the rostral brainstem (Adams et al. 1982, Adams et al. 1984). Historically, DAI was a complete axonal

disruption by a mechanical force (primary axotomy). After the mechanical insult, the axon would swell and form a “retraction ball” resulting in degeneration. Additionally, it included macroscopic damage to the corpus callosum, and the dorsolateral quadrant of the midbrain (Buki and Povlishock 2006, Povlishock 1993, Povlishock and Katz 2005, Lajtha and Banik 2007). Gennarelli et al. showed in experiments with monkeys, that rotational acceleration was the cause of DAI and unconsciousness (Gennarelli et al. 1982). Two decades later, in experiments using an inertial loading swine TBI model the extent of DAI in the rostral brainstem, dorsolateral region, was directly correlated with the duration and severity of post-traumatic coma. Moreover, coma was only present in the rotational loading of the axial plane (Smith et al. 2000).

While there were advances in the understanding of the biomechanics that induced DAI and unconsciousness, there were also advances in the understanding the pathophysiology. An elegant experiment, using different animal species and two TBI models, as well as human tissue, analyzed anterograde transport in axons and cytoskeletal changes. Different timepoints were analyzed including hours to months post-TBI. There were no signs of axonal shearing directly caused by mechanical loading. Also, anterograde axonal transport impairments appeared in discrete regions that evolved into axonal swelling and lobulations hours post injury. Additionally, the process takes longer in humans, starting around 12 hours after injury (Povlishock 1993). These results were confirmed in further experiments with a different set of human tissues (Christman et al. 1994).

Primary axotomy is rare and only happens in severe brain injury when there is white matter tissue tearing (Smith, Meaney, and Shull 2003). The rapid mechanical load surpasses the viscoelasticity of the brain tissue, and the axons appear “stiff and brittle.” The stiffness is particularly true in highly anisotropic areas (like the white matter tracts). Thus, the rapid tensile and compressive stretch induces cytoskeletal damage, membrane

mechanoporation or aberrant channel activation (Wolf et al. 2001). The following steps pertain to secondary injury beginning a slow process that can finish in axotomy (Buki and Povlishock 2006).

### Diffuse vascular injury (DVI)

Diffuse vascular injury is associated with severe TBI. It commonly co-occurs with DAI. It is caused by lateral and rotational acceleration and requires high energy inertial loading. It is characterized by multiple macroscopic and microscopic hemorrhages distributed in the cerebral hemispheres and brainstem. Microscopic hemorrhages are surrounding arteries, veins, and capillaries with extravasation of erythrocytes. The common areas affected by DVI are the white matter of the frontal, temporal and parietal lobes, corpus callosum, internal capsule, basal ganglia, periventricular tissues, and brainstem. Microscopically, there is disruption of the blood-brain barrier and changes to the endothelium. Patients that suffer this kind of injury have poor prognosis dying minutes or up to 24 hours post-TBI or suffers immediate and prolonged coma (Meaney and Cullen 2017, Onaya 2002, Tomlinson 1970, Blumbergs 2005).

### **Secondary Injury**

After the initial mechanical insult to the brain and vasculature, there is a complex physiological, cellular and biochemical response known as “secondary injury.” This cascade of events will affect long-term consequences induced by the trauma. Secondary injury includes neurovascular changes, a neurometabolic cascade (involving neurotransmission impairments, bioenergetic deficits, neuronal cytoskeletal disruptions, and cell death) and inflammation.

## *NEUROVASCULAR CHANGES*

Neurovascular control of the cerebral blood flow (CBF) is tightly coupled with the tissue requirements for glucose and oxygen (MacFarlane and Glenn 2015). However, after severe TBI the CBF is dysregulated and undergoes a triphasic neurovascular response (Romeu-Mejia, Giza, and Goldman 2019, Barkhoudarian, Hovda, and Giza 2016, MacFarlane and Glenn 2015). A period of hypoperfusion or decreased cerebral blood flow (CBF) in relation to metabolic rate (MR), was found in patients the day of the TBI. A period of hyperemia or increased CBF in relation to normal or decreased MR, followed on days 1 to 3 post-injury (Barkhoudarian, Hovda, and Giza 2016). Followed by another episode of hypoperfusion, or vasospasm with hypoperfusion in <30% of patients with TBI, that may present at day 2 to 15 post-injury (Romeu-Mejia, Giza, and Goldman 2019). Vasospasm is significant in about 50% of the patients that suffer it and indicates severe brain damage. If the CBF is below 15 ml per 100 g<sup>-1</sup> per min<sup>-1</sup>, the brain will be ischemic and irreversible damage will occur. Any length of ischemia after TBI correlates with poor neurological outcome, vegetative state or death (Werner and Engelhard 2007).

These critical changes in CBF correlate with the severity of symptoms and take longer than cognitive tests and symptom reports to return to normal (Romeu-Mejia, Giza, and Goldman 2019, Barkhoudarian, Hovda, and Giza 2016, MacFarlane and Glenn 2015). The leading causes are theorized to be due to compromise of autoregulatory mechanisms such as CO<sub>2</sub> reactivity. Vasospasm is correlated with the depletion of potassium, nitric oxide and cyclic GMP (the latter in endothelial smooth muscle). It can also be correlated with increases in the presence of endothelin, prostaglandins or reactive oxygen species (Werner and Engelhard 2007, Romeu-Mejia, Giza, and Goldman 2019).

## Blood brain barrier disruption

The blood-brain barrier (BBB) is a highly complex and dynamic barrier between the vascular lumen and the brain parenchyma (Romeu-Mejia, Giza, and Goldman 2019). It is composed of endothelial cells, pericytes, astrocytes, and neurons at the capillaries; this group of cells is called the “neurovascular unit.” Every cell in the unit plays a critical role in controlling the transit from the blood to the brain and back. Endothelial cells possess tight junctions to avoid paracellular transit, and the cells are selectively permeable to metabolites, ions, and nutrients required by the brain. Pericytes regulate the permeability of the BBB, control the hemodynamic responses (including CBF), regulate neuroinflammatory response and are responsible for the removal of toxic metabolites. Astrocytes control the hydric balance through Aquaporin 4 (AQ4) channels (Hagos et al. 2019, Pop and Badaut 2011, Rodriguez-Grande et al. 2017).

TBI disrupts the BBB through mechanical disruption in blood vessels, as evidenced by hemorrhage or microbleeds (MacFarlane and Glenn 2015, Rodriguez-Grande et al. 2017, Pop and Badaut 2011). The inflammatory response (secondary to oxidative stress generated by infiltrating cells, proteins or other substances) in concert with the CBF dysregulation increase the flow of water into the brain generating vasogenic edema. This type of edema may induce ischemia via the increase of intracranial pressure and decreased CBF. Other mechanisms that cause barrier compromise are the alteration of the endothelial cell channels and transcytosis which may cause indiscriminate transit. The permissive ionic flow into the brain induces hyperosmolarity in the neurons and astrocytes generating cytotoxic edema. This hyperosmolarity in astrocytes activates the AQ4 channels leading to further brain edema (Pop and Badaut 2011, Rodriguez-Grande et al. 2017). Another mechanism is the increase in reactive oxygen species (ROS) and reactive nitrogen species (RNS) which activate metalloproteinases which will degrade tight junctions and decrease the physical stability of the barrier. The final mechanism is through activation of

neuroinflammatory cells which will damage the barrier further by the release of cytokines and chemokines, and the attraction of peripheral inflammatory cells perpetuating a negative cycle of ROS and inflammation (Abdul-Muneer, Chandra, and Haorah 2015, Pop and Badaut 2011, Rodriguez-Grande et al. 2017).

### ***NEUROMETABOLIC CASCADE AFTER TBI***

As previously mentioned, the mechanical injury induced by acceleration/deceleration forces may cause mechanoporation (Figure 1.2) of the membrane [transient (initial or delayed) or permanent] and the stretching of axons (Farkas, Lifshitz, and Povlishock 2006, Barkhoudarian, Hovda, and Giza 2011, Blennow, Hardy, and Zetterberg 2012). The injury causes an indiscriminate flux of ions through transient membrane defects and dysregulated ion channels, resulting in  $K^+$  efflux and excessive  $Ca^{2+}$  influx (Barkhoudarian, Hovda, and Giza 2011, Weber 2012, Povlishock et al. 1997). An additional mechanism of  $Ca^{2+}$  entry is through the dysregulation of  $Na^+$  channels, the reversal of  $Na^+/Ca^{2+}$  exchanger and the activation of voltage-gated  $Ca^{2+}$  channels. The deformation of the membrane activates mechanical sensitive  $Na^+$  channels that initiate this cascade of events (Wolf et al. 2001). Changes in the membrane potential cause non-specific depolarization, initiating action potentials that release primarily excitatory amino acids (EAAs, most commonly glutamate and aspartate) (Faden et al. 1989, Katayama et al. 1990). Glutamate in the synaptic clefts activates  $\alpha$ -amino-3-hydroxy-5-methyl-4-isoxazolepropionic acid (AMPA) and N-methyl-D-aspartate (NMDA) receptors, the latter through the reduction of  $Mg^{2+}$  block (Furukawa et al. 2000). This activation allows further ionic dysregulation, causing depolarization of the membrane, adding to  $K^+$  efflux and  $Ca^{2+}$  influx through further activation of receptors (Barkhoudarian, Hovda, and Giza 2011, Faden et al. 1989, Katayama et al. 1990, Furukawa et al. 2000). The unspecific depolarizations and ionic dysregulation lead to a diffuse state that resembles a spreading

depression and may be the reason for immediate postconcussive symptoms (Giza and Hovda 2014, Barkhoudarian, Hovda, and Giza 2016).

Neurons attempt to restore ionic homeostasis by activating Na<sup>+</sup>/K<sup>+</sup> ATPases, causing depletion of intracellular ATP stores. Oxidative phosphorylation is activated, and the neurons enter hyperglycolysis to generate more ATP (30 minutes after injury, metabolic rates increase 30-40% and may last up to 4 hours) (Barkhoudarian, Hovda, and Giza 2011, Yoshino et al. 1991, Barkhoudarian, Hovda, and Giza 2016). The hypermetabolic state most likely coexists with a decreased blood flow to the brain, leading to a greater metabolic disturbance (Giza and Hovda 2014).

The hyperconsumption of glucose for ATP production through an anaerobic route generates lactate, which accumulates extracellularly (Kawamata et al. 1995). Lactate accumulation contributes to the acidosis of the microenvironment and may play a part in increasing membrane permeability and edema (Barkhoudarian, Hovda, and Giza 2011), along with other factors, perpetuating Ca<sup>2+</sup> influx. The excess influx of Ca<sup>2+</sup> to the cytosol is sequestered by mitochondria, causing mitochondrial swelling and dysfunction and leading to impaired oxidative metabolism and decreased ATP production (Blennow, Hardy, and Zetterberg 2012, Brown, Sullivan, and Geddes 2006, Yokobori et al. 2014). The mitochondrial accumulation of calcium results in decreased NAD/NADH and ATP/ADP ratios, explained further below (Barkhoudarian, Hovda, and Giza 2016, Vagnozzi et al. 2007). The metabolic cascade in mTBI is usually transient and does not end in apoptosis. However, the cell stays in a vulnerable state and exhibits glucose hypometabolism that may last for days or months depending on the severity of TBI (Bergsneider et al. 1997, Barkhoudarian, Hovda, and Giza 2016). It has been reported that total Ca<sup>2+</sup> uptake by the tissues in TBI is increased and cerebrospinal fluid Ca<sup>2+</sup> concentration reduced from 1 to 0.01 mM; this phenomenon is explained by the massive influx of Ca<sup>2+</sup> into the injured

neurons, exhibiting intracellular  $\text{Ca}^{2+}$  elevation following trauma (Weber 2012, Nilsson et al. 1993, Weber, Rzigalinski, and Ellis 2001). This process is also known as excitotoxicity.

Illustration 1.2. Neurometabolic cascade of TBI

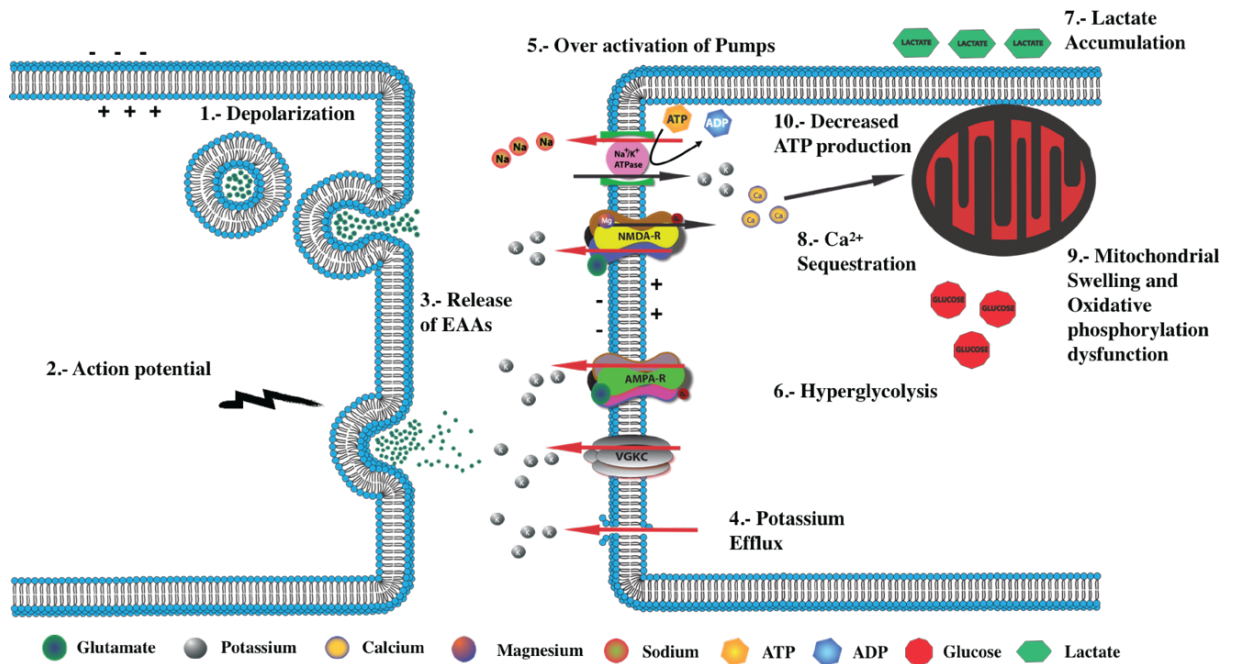


**Illustration 1.2. Neurometabolic cascade of TBI.** Conceptualized from (Giza and Hovda 2001, 2014, Barkhoudarian, Hovda, and Giza 2011, 2016). Neurometabolic cascade after TBI. Injury induces membrane permeability allowing ionic flux, which causes (1) non-specific depolarization and (2) action potentials that (3) release excitatory amino acids (EAAs). (4) There is massive  $\text{K}^+$  efflux through the membrane and channels.  $\text{Na}^+/\text{K}^+$  pump over activation, to return to ionic homeostasis, depleting ATP stores which leads to (6) hyperglycolysis to produce ATP. Energy requirements and production leads to (7) extracellular lactate accumulation causing acidosis and increasing membrane permeability. Activation of N-methyl-D-aspartate (NMDA) receptor by glutamate causes  $\text{Ca}^{2+}$  influx (8)  $\text{Ca}^{2+}$  is sequestered by mitochondria leading to (9) mitochondrial swelling and dysfunction, causing impaired ATP production. After injury the cell maintains a vulnerable state, exhibiting glucose hypometabolism that can last for days.

Traumatic axonal injury (TAI) is one of the hallmarks of TBI and the most common injury across severities (Maxwell, Povlishock, and Graham 1997, Werner and Engelhard 2007). TAI is mainly a non-disruptive injury to the axons (that may result in secondary axotomy due to biochemical processes) (Maxwell, Povlishock, and Graham 1997). Mechanical damage through acceleration/deceleration forces causes axonal membrane disruption, cytoskeletal damage and the activation of ionic channels (Farkas, Lifshitz, and Povlishock 2006, Staal et al. 2010, Johnson, Stewart, and Smith 2013, Meythaler et al. 2001). During the ionic dysregulation mentioned above, resulting in the accumulation of  $Ca^{2+}$  in the axons.  $Ca^{2+}$  influx will cause neurofilament compaction through the phosphorylation or calpain-mediated cleavage of the sidearms of neurofilaments (Farkas, Lifshitz, and Povlishock 2006, Maxwell, Povlishock, and Graham 1997, Barkhoudarian, Hovda, and Giza 2011, Johnson, Stewart, and Smith 2013). Trauma also causes misalignment of neurofilaments and microtubules (Maxwell, Povlishock, and Graham 1997, Johnson, Stewart, and Smith 2013). Depolymerization of microtubules is activated in the presence of  $Ca^{2+}$ , to correct the alignment, contributing to organelle accumulation and axonal swelling (Maxwell, Povlishock, and Graham 1997, Johnson, Stewart, and Smith 2013). This process leads to organelle accumulation, axonal swelling, and may ultimately cause axotomy, axonal retraction, and Wallerian degeneration depending on the extent of cytoskeletal disruption. Studies in RmTBI have shown an increase in microtubule and neurofilament markers and translocation of staining near the perikarya (Kanayama et al. 1996). The translocation correlates with the disruption in protein transport, translating into the accumulation of these proteins in the soma of the neuron instead of being transported along the axons. Although this process was believed to occur in the hours following injury, recent findings show that axonal degeneration may still be present years after injury in human brains (Johnson, Stewart, and Smith 2013).

### Illustration 1.3. Traumatic axonal injury

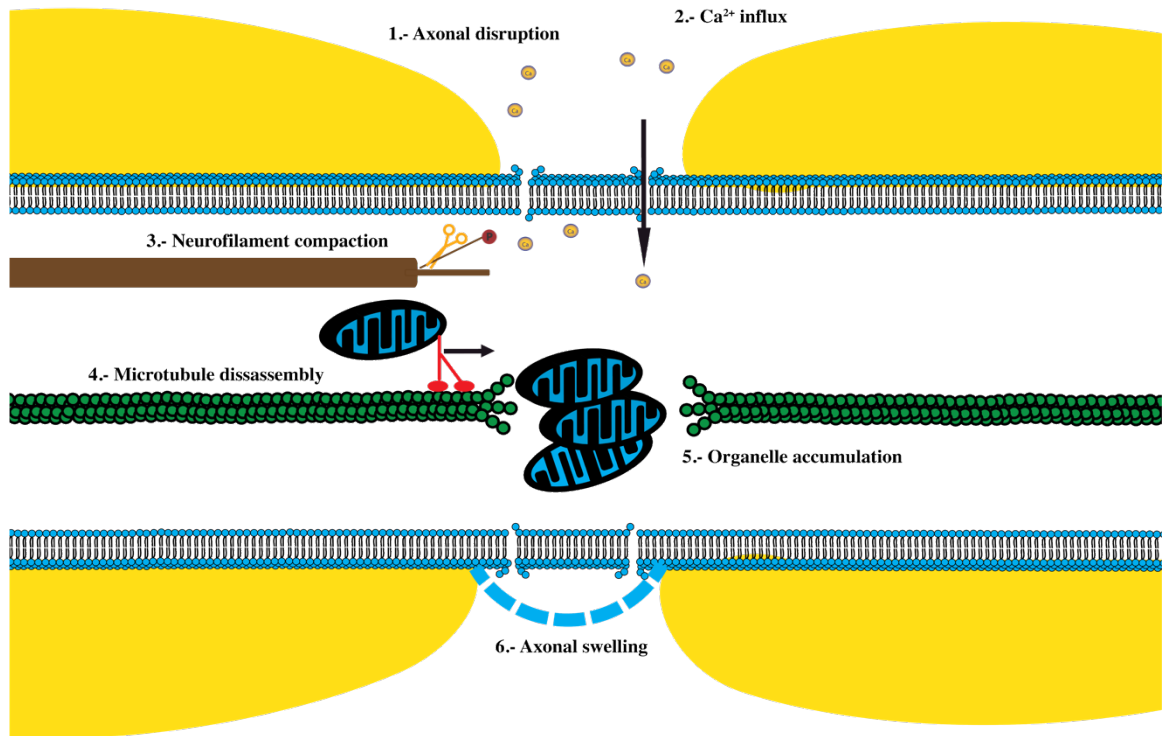


**Illustration 1.3. Traumatic axonal injury.** Conceptualized from (Giza and Hovda 2001, 2014, Barkhoudarian, Hovda, and Giza 2011, 2016). Neurometabolic cascade at the axonal level. 1) Mechanical injury induces activation of mechanosensitive channels and membrane permeability. 2) The disruption of the axonal membrane allows ionic flux, and Ca<sup>2+</sup> entry into the axon. 3) Ca<sup>2+</sup> entry leads to neurofilament instability and collapse, initiating in compaction through phosphorylation or calpain-mediated sidearm cleavage. 4) Ca<sup>2+</sup> also contributes to the microtubule disassembly and breakdown. 5) the disruption of microtubules generates accumulation or organelles in the site of disruption. 6) This accumulation leads to axonal swelling and may even lead to axotomy, producing the characteristic axonal bulbs seen in histological studies. This whole process takes from minutes to weeks.

### ***POLY(ADP-RIBOSE) POLYMERASE (PARP) IN TBI***

Poly(ADP-ribose) polymerase 1 (PARP1) is the best-known isoform of the PARP family. PARP1 can be found in the nucleus and mitochondria (Du et al. 2003, Jagtap and Szabo 2005). This enzyme was first linked to the repair of single or double DNA break repair. This repair achieved by binding to the DNA and attracting DNA repair enzymes by tagging the site with Poly ADP-ribose polymers (PARs). This process is NAD<sup>+</sup> dependent, and if it is overactivated, it can produce a metabolic crisis and ultimately cell death. PARP is also involved in regulation of transcription, cell cycle, activation of pro-inflammatory transcription factors, apoptosis and necrosis (Berger et al. 2018, Jagtap and Szabo 2005, Charriaut-Marlangue et al. 2018). Additionally, PARP1 has been implicated in TBI. Activation of PARP1 has been reported in neurons of the pericontusional tissue of patients with severe TBI (Berger et al. 2018). Also, poly(ADP-ribos)ylated (PARylated) proteins have been found in CSF of pediatric TBI patients (Fink et al. 2008), and single nucleotide polymorphisms in the PARP1 gene have been correlated with favorable outcome after TBI (Sarnaik et al. 2010). PARP1 is also known to play an essential role in excitotoxicity (Abramov and Duchon 2008, Alano et al. 2010, LaPlaca et al. 2001, Hortobagyi et al. 2003).

As previously mentioned, during excitotoxicity the membrane disruption allows a Ca<sup>2+</sup> overload of the cells. This overload initiates Ca<sup>2+</sup> sequestration by the mitochondria and cascades that produce ROS and RNS in the cytosol, generating DNA damage and activating nuclear PARP1. Concomitantly, the sequestration activates mitochondrial Ca<sup>2+</sup> dependent nitric-oxide synthase, producing peroxynitrites. The mitochondrial membrane potential is affected, and PARP1 becomes activated (Duan, Gross, and Sheu 2007, Du et al. 2003, Alano et al. 2010). PARP1 initiates PARylation of mitochondrial proteins depleting the mitochondrial stores of NAD<sup>+</sup> and inducing membrane depolarization (Alano

et al. 2010, Du et al. 2003). The PARylated proteins include the electron transport chain complexes III, IV, and V, which compromise the cellular respiration further (Lai et al. 2008). Additionally, PARP depletes NAD in the cytosol (Alano et al. 2010) and inhibits glyceraldehyde-3-phosphate dehydrogenase (GAPDH) and hexokinase leading to NADH depletion and inhibition of glycolysis (Abramov and Duchon 2008, Andrabi et al. 2014, Lai et al. 2008, Alano et al. 2010, Virag et al. 2013). These metabolic disruptions cause the inability to produce ATP by the respiration chain and the depletion of the ATP stores to resynthesize NAD<sup>+</sup> (Owens et al. 2013).

The cell at this point has an energetic compromise in the mitochondria and cytosol. Both mitochondrial and cytosolic PARP1 produce PAR polymers (Cipriani et al. 2005). By mechanisms yet to be identified, PARs induce the caspase-independent calpain cleavage of the apoptosis inducible factor (AIF) (Wang et al. 2004, Andrabi et al. 2014, Alano et al. 2010, Vosler et al. 2009, Du et al. 2003, Andrabi et al. 2006). After cleavage, the truncated AIF is released by the mitochondrial permeability pore and translocated to the nucleus where it initiates cell death (Vosler et al. 2009, Ying 2006, Dawson and Dawson 2004).

Illustration 1.4. Poly (ADP-ribose) polymerase 1 in TBI

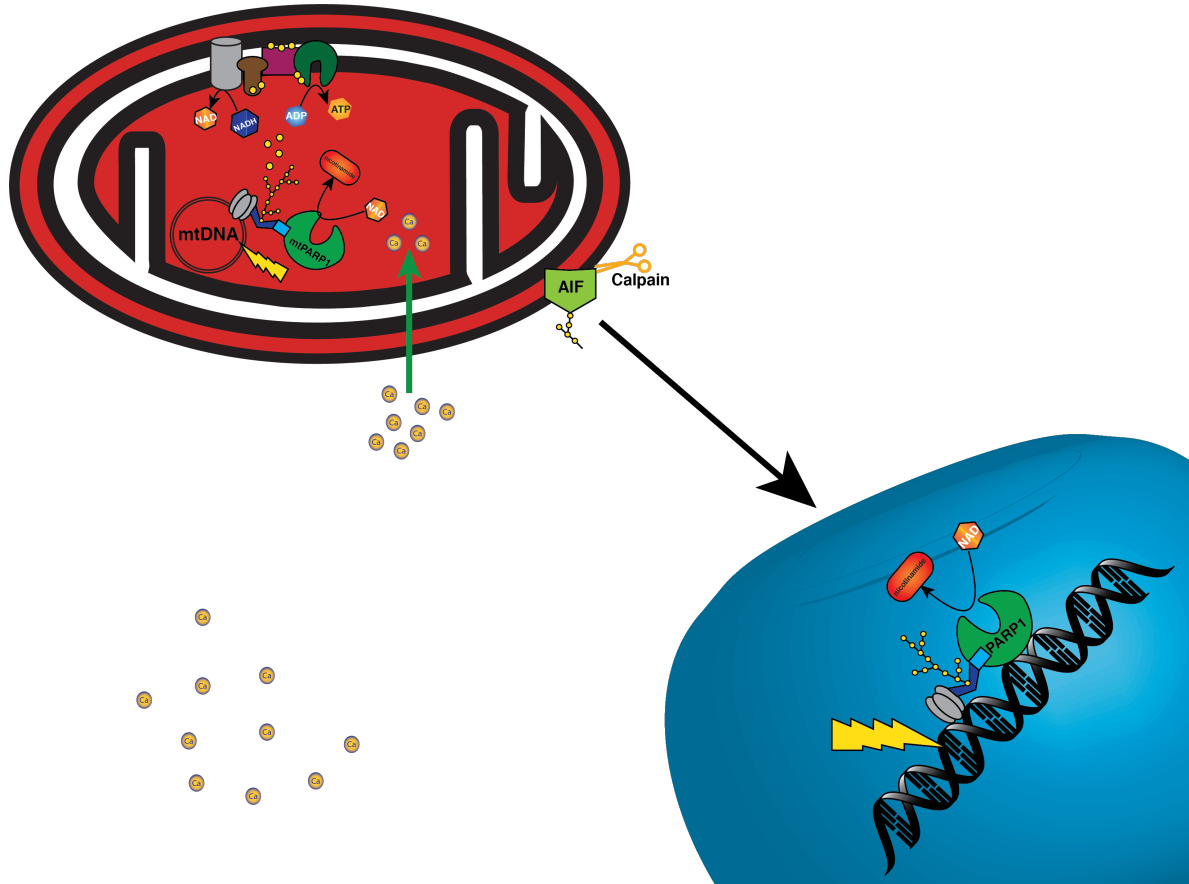


**Illustration 1.4. Poly (ADP-ribose) polymerase 1 in TBI.** While the neurometabolic cascade of TBI is underway, the overload of  $\text{Ca}^{2+}$  in the cell (yellow circles) bypasses the buffering capacity of cytosolic proteins, which leads to the sequestration of  $\text{Ca}^{2+}$  by the mitochondria. The free  $\text{Ca}^{2+}$  generates reactive oxygen and nitrogen species (yellow lightning) which induce DNA damage in the nucleus and mitochondria. The DNA damage activates PARP1 in the nucleus and mitochondria (mtPARP1) which stimulates the production of poly (ADP-ribose) polymers (PARs) which are used to PARylate three of the four complexes of the oxidative phosphorylation chain, inhibiting the production of NAD and ATP, leading to the complete depolarization of the mitochondrial membrane. The free PARs will induce the release of the apoptosis inhibitory factor (AIF) by the mitochondria on their own or by a calpain mediated process. AIF will be translocated to

the nucleus where it will initiate the big fragment DNA defragmentation and ultimately lead to parthanatos cell death.

### *NEUROINFLAMMATION*

Neuroinflammation is an incredibly complex process following traumatic brain injury that involves central and peripheral reactions (Simon et al. 2017). It is an important driver of the secondary injury in TBI; however, it is also an important component of injury recovery (Xiong, Mahmood, and Chopp 2018). This process begins immediately after the primary injury with the activation of glial cells (also termed reactive gliosis), which include microglia, astrocytes and oligodendrocytes. These activation mediates the release of cytokines and chemokines to attract peripheral leukocytes which contribute to the permeability of the BBB and release more inflammatory mediators generating an inflammatory cycle (Kumar and Loane 2012, Chiu et al. 2016).

The reactive gliosis was believed to start with microglial activation followed by astrocytes. However, recent reports suggest that astrocytes may be activated first. Astrocytic markers, with glial fibrillary acidic protein (GFAP) and complement component 3 (C3), were upregulated 8 hours after injury while microglia marker, allograft inflammatory factor 1, also named ionized calcium adapter molecule 1 (Aif1/Iba-1), were upregulated 24 hours post injury. Regardless of gene expression, both astrocytic and microglial markers peaked at 72h post-TBI (Clark et al. 2019).

The two main glial cells involved in the initiation of the inflammatory response are microglia and astrocytes. There have been reports of both having multiple phenotypes. In an oversimplified description, there are pro-inflammatory or neurotoxic astrocytes and microglia (dubbed A1 and M1, respectively) and anti-inflammatory or neuroprotective

astrocytes and microglia (A2 and M2, respectively) (Gao et al. 2016, Clark et al. 2019, Skaper et al. 2018). Thus, the shift in balance of this duality of the primary immune defense cells of the CNS will determine repair versus prolonged inflammation and persistent damage (Xiong, Mahmood, and Chopp 2018).

Microglia represent about 10 to 20% of the brain's cells and have been known as the “first responders” of the brain. One of the functions of these cells is to actively sense the microenvironment of the brain and maintain homeostasis. At this stage microglial cells present multiple fine processes that are used for monitoring the microenvironment (Witcher, Eiferman, and Godbout 2015, Jassam et al. 2017, Chiu et al. 2016). After trauma, injured cells release signaling molecules [Damage-associated molecular patterns (DAMPs) and Pathogen-associated molecular patterns (PAMPs)] that induce the microglia to proliferate (Bianchi 2007). Once activated, they release inflammatory mediators, these include cytokines (interleukin (IL)-1 $\beta$ , IL-6 and tumor necrosis factor  $\alpha$  (TNF  $\alpha$ )) and oxidative metabolites (ROS, RNS, and nitric oxide among others) (Kumar and Loane 2012). This activation is accompanied by a change in morphology that ranges from cells with shortened and hypertrophic processes to an amoeboid morphology. A measured inflammatory reaction is required after TBI and can be neuroprotective. If this process is over stimulated or becomes chronic, it will be detrimental to the brain. Simultaneously, microglia are also producing an anti-inflammatory response with the release of IL-4, IL-10, and transforming growth factor  $\beta$  (TGF  $\beta$ ) among others. The delicate balance between a spectrum of these microglia will lead to neuro-recovery or induce a detrimental and long-lasting or chronic neuroinflammation (Simon et al. 2017).

Astrocytes also play an important role in the inflammatory response. After activation, there is an upregulation of glial fibrillary acidic protein (GFAP), vimentin, and release of cytokines and chemokines. Astrocytes are involved in the clearance of

neurotransmitters, which can limit excitotoxic damage (Maragakis, Dykes-Hoberg, and Rothstein 2004, Zou et al. 2010). Additionally, astrocytes limit the injured area by forming a scar, avoiding the spread of injury to healthy parts of the brain. The upregulation of AQP4 following injury contributes to the formation of edema which can be detrimental. The upregulation of AQP4 is also involved in the clearance of noxious molecules by the glymphatic system (Chiu et al. 2016, Simon et al. 2017, Jassam et al. 2017).

### **ANIMAL MODELS OF TBI**

As previously mentioned, TBI is a highly heterogeneous condition, from the types of trauma, forces involved, the location of impact, secondary injury, and presence of secondary insults among other variables. This heterogeneity makes TBI challenging to study and replicate. For purposes of understanding the pathophysiology of TBI and test potential treatment options, a “simplification” of the injury has to be made (LaPlaca et al. 2007). The first classification of animal models is the use of large (or gyrencephalic) or small (lissencephalic) animal models. Gyrencephalic brains have a closer resemblance to the organization of the human brain. However, the use of these animals is costly which limit their use in TBI research. The small animal models, although with some morphological differences of the brain can recreate a large part of the molecular and behavioral deficits seen in human TBI. Rodents are the most common animals used in TBI research due to their modest cost, the repertoire of behavioral tests similar to the human condition, as well as the possibility of using transgenic techniques to allow for a more precise view of pathophysiological processes (Xiong, Mahmood, and Chopp 2013). There is a multitude of classifications of TBI. The models can be classified based on the type of mechanical insult, type of primary injury, and integrity of the skull among others.

The integrity of the skull can classify TBI as an open or closed head injury. Each of these broad groups has sub-classifications. This work will discuss the most common animal models of each group, for more information on multiple animal models, please refer to the following excellent review articles (Xiong, Mahmood, and Chopp 2013, Angoa-Perez et al. 2014, Bodnar et al. 2019, Cernak 2005, Finnie 2001, O'Connor, Smyth, and Gilchrist 2011, Morales et al. 2005).

### **Open head injury models of TBI**

Open head injury models rely on the use of a craniotomy to provide access to the meninges or brain, and usually, the head has to be fixed. The two most commonly used models of open head injury are fluid percussion (FP) and controlled cortical impact (CCI), which apply the mechanical load directly onto the dura. Another subset of models penetrates the dura inflicting penetrating injuries, such as penetrating ballistic-like injury models (Williams et al. 2005, Xiong, Mahmood, and Chopp 2013) or needle stab models (Amat et al. 1996, Eugenin et al. 2001).

#### ***FLUID PERCUSSION INJURY MODEL***

Fluid percussion injury is one of the most commonly used models in TBI research (Stalhammar et al. 1987, Hayes et al. 1987, Sullivan et al. 1976). This model is composed of a cylindrical container filled with saline solution. One end of the cylinder has a piston, transducer or membrane, and is directly positioned in the path of a pendulum. The other end of the container connects to a craniotomy in the skull of an animal through a cemented cap. The injury severity depends on the height at which the piston is released. The piston impacts the side of the container, generating a pressure pulse that travels through the

cylinder pushing a small amount of saline into the animal's skull (Xiong, Mahmood, and Chopp 2013).

There are two varieties of fluid percussions injuries based on the site of the craniotomy, it can be central or lateral. Both models have been extensively characterized, and share a brief period of coma, cerebrovascular and metabolic deficits and BBB permeability. Central percussion has a craniotomy in the midline between the bregma and lambda. It produces small contusions near the site of the impact accompanied by scattered axonal injury, with brainstem compromise. In lateral fluid percussion, the craniotomy is over the parietal cortex. The injury with this model shows greater damage ipsilateral to the impact site. It is considered a mixed model due to the generation of a focal and diffuse injury. It produces a contusion lateral to the site of impact and affects the hippocampus. It produces cell death with necrosis, vascular damage and DAI (McIntosh et al. 1987, Gennarelli 1994). In severe injuries it can induce death due to pulmonary edema or long apnea. This procedure can accommodate intubated animals with a fixed head. The use of this model is labor intensive and requires extensive training to reach high reproducibility. The site of craniotomy is an essential cause of variability (Xiong, Mahmood, and Chopp 2013). Biomechanical monitoring can be challenging due to the diffusion of water inside the skull.

#### ***CONTROLLED CORTICAL IMPACT INJURY MODEL***

The controlled cortical impact (CCI) model introduces a rigid impactor into the skull through a craniotomy to hit the dura. This impactor is controlled by a weight drop (does not share all the controlled parameters as the rest), a pneumatic, or electromagnetic device. This model is highly reproducible, it has adjustable biomechanical settings, time, depth of impact and velocity can be controlled and does not produce rebound injury (Xiong,

Mahmood, and Chopp 2013, Mao et al. 2006, Manley et al. 2006, O'Connor, Smyth, and Gilchrist 2011, Feeney et al. 1981). These parameters control the severities that can be achieved based on the duration and depth of cortical deformation. This model mimics a focal injury, and the damage includes loss of the cortical tissue and damage to the underlying hippocampus and thalamus, axonal injury, subdural hematoma, BBB permeability, and increased ICP (Saatman et al. 2006, Fujimoto et al. 2004). Behaviorally this model shows long-term cognitive decline as well as mood disorders (Xiong, Mahmood, and Chopp 2013). While highly reproducible variability between laboratories can make comparisons difficult. This variability is due to differences in the device (pneumatic, electromagnetic, weight drop), the shape, size, material and rigidity of the tip, and size and location of the craniotomy (Smith et al. 2015).

### **Closed head injury models**

Closed head injury can be divided into impact, impact-acceleration, and non-impact which include the blast and inertial loading models. The intact skull during impact is the primary characteristic of the closed head injury models. Although, in some models, the scalp is surgically opened, either to direct the impact on the naked skull (Bennett and Brody 2014) or to cement a metal helmet to protect against skull fractures (Marmarou et al. 1994). The full breadth of closed head injury models lays outside of the scope of this work. We will focus on the impact-acceleration models, in particular, the weight-drop injury model as it relates to the model generated in this project. Other types of closed head injury models will be briefly mentioned.

### ***IMPACT INJURY MODELS***

The main characteristic of the impact injury models is that the head is fixed or unable to move during impact which results in no acceleration. Historically, there have been several of this type model, such as modified mouse traps (Shaw 1985, 1986), weight drop models (Flierl et al. 2009) and models that use devices similar to the CCI (Bennett and Brody 2014, Jamnia et al. 2017). There is a wide range of devices to induce impact TBI, ranging from simple to incredibly elaborate, which have been used for single and repetitive injuries. These models have reported a range of injuries, characterized by the increased permeability of the BBB, microgliosis, astrogliosis, axonal injury, and in some cases focal injuries. The use of metal discs is commonly used to avoid skull fractures and induce more diffuse injuries (Ziebell, Corrigan, and Vink 2012).

### ***IMPACT-ACCELERATION***

Impact-acceleration models characteristically have a free moving head. The best-known models of this type are a range of weight-drop models and piston driven models. The piston driven models have proven to be reproducible and allow for a range of severities of injury. The “Closed-Head Impact Model of Engineered Rotational Acceleration” (CHIMERA) was developed by Dr. Cheryl Wellington’s group, and is one of the piston-driven models. It has been extensively characterized in term of biomechanics and outcomes. The device has a square shape; on its top, it has an inclined bed that ends in a horizontal plate with a hole. Under this plate is the piston. The mouse is placed in the supine position on the inclined plane with the head resting over the horizontal plate with the hole and is strapped in place by the body. Once the piston is activated it impacts the skull and induces an upward acceleration of the head (Namjoshi et al. 2014). Additional optimizations have been made recently to induce a moderate injury, for which they changed the inclined plane for a moving platform and added a helmet for the mouse. The platform

is attached on one edge; upon impact, the mouse moves upward which creates a semicircular motion. Both of these models induce neurobehavioral changes, such as cognitive deficits and morphological alterations including microgliosis and diffuse axonal injury, with the addition of cell death in the moderate version (Namjoshi et al. 2014, Sauerbeck et al. 2018).

The weight-drop model has a multitude of versions. It is commonly used due to its low cost and simplicity. It is based on dropping an object of known weight from a known height onto the animal head through a guiding tube. The best-known weight-drop model was developed by Marmarou and colleagues (Marmarou et al. 1994). This model was intended as a severe model of TBI and used a 450 g object dropped from a height of 2 meters. This magnitude of impact required the placement of a metallic helmet on top of the rat and had a mortality rate of 44% and 12.5% of skull fractures. This model uses foam as a support for the rat, which allows acceleration of the head after impact. Biomechanical analysis of the acceleration and compression of the head was performed mathematically and concluded accelerations of 630 to 900 G and compression of the skull of 0.2 to 0.3 mm. One of the main problems with this model was the possibility of double impacts in the head of the rats (Marmarou et al. 1994).

The Marmarou model has been the basis for a multitude of variations of the weight drop models. The weight and material of the objects used, the shape, material, and rigidity of the impacting surface, the height of the drop, the use of helmet, and type of support for the animal are some of the frequent changes seen in these models. Concomitantly all of these are also part of common data elements for this model. The support systems range from foam, spring-loaded platforms (Engelborghs et al. 1998), and more recently Kimwipes (Khuman et al. 2011, Meehan et al. 2012), aluminum foil (Kane et al. 2012, Mychasiuk et al. 2014) and trap doors (Briggs, Angoa-Perez, and Kuhn 2016). All of the

variables discussed above have significant consequences on the type of injury and severity. The foam allows limited head movement and induces a moderate to severe TBI with the DAI as the primary component of the injury (Marmarou et al. 1994). The Kimwipes break after impact, allowing unrestricted movement of the head, generating rotational acceleration in the sagittal plane. This movement of the head eliminated the need for surgery or helmet in the mouse. The original Kimwipe model used a 53g object dropped from a height of approximately 1.6m and reported a range of 10 to 20% mortality. This model also induced axonal injury, astrogliosis and microgliosis, and showed locomotion and cognitive deficits (Khuman et al. 2011). The model developed by Kane et al. uses a box with foam, and places a scored aluminum foil as support for the mice or rats. The foil is secured at the top of the open box 10cm above the foam and breaks with minimal effort. The movement after impact is similar to the Kimwipe model. This model uses a 75 g, or a 95 g object dropped from a height of one meter. Kane reported a very mild injury and with a mortality of 5% and 10% in single and repetitive injury, respectively. A 10% chance of intracranial hemorrhage in single injury was also reported. He also reported increased locomotion and protein expressions of GFAP, Iba-1 and phosphorylated tau (Kane et al. 2012). This group modified their apparatus by adding a trap door system. However, a comparison is difficult since the new support system was used for a repetitive injury paradigm of 30 TBIs over 40 days. They report no locomotion deficits in the open field, although they found a late impairment in the rotarod test, an early decrease in strength, spatial cognitive deficits and overall depressive behavior. Immunohistological studies showed myelin thinning, diffuse axonal injury, and accumulation of degenerative markers associated with chronic traumatic encephalopathy (Briggs, Angoa-Perez, and Kuhn 2016).

A recently generated model has an interest approach. This model induces acceleration followed by blunt impact, contrary to the models described in this section, resembling what is usually seen in falls. They have shown sexual dysmorphic effects in

rats, with milder symptoms seen in male rats when compared to females. Rats presented locomotion and memory deficits, however no anxiety effects were seen when assessed by open field (Wirth et al. 2017).

### *NON-IMPACT ACCELERATION*

Non-impact acceleration is represented by two models, inertial loading and blast loading injuries. Inertial loading models were some of the original models of TBI. These models are based on acceleration and deceleration forces. Initially, this was used in nonhuman primates and large animals. These models were paramount in the discovery of the importance of rotational acceleration in the genesis of concussion (Ommaya et al. 1967). More recently, animal models have been generated for smaller animals, in particular rodents. These models can be divided into a sagittal and coronal rotation. Models with rotation in the sagittal plane can follow a rear or forward rotation. These models produce diffuse axonal injury, degenerating neurons, bradypnea and bradycardia during the period of unconsciousness, astrogliosis, microgliosis and degenerating neurons (Wang et al. 2018). A coronal plane rotation model used for mild TBI reported increased locomotor activity and decreased anxiety (or increased disinhibition), similar to what is seen in concussed athletes (Stemper et al. 2016). A different model showed spatial cognitive deficits 72 hours after rotational injury (Fang et al. 2014) .

The increase in blast injuries in military personnel has led to the study of this unique type of TBI. There are several models of blast-induced neurotrauma (BINT) that mimic different conditions of exposure to explosions (Wang, Wei, et al. 2011, Cheng et al. 2010, Risling and Davidsson 2012, Long et al. 2009). An explosion generates a shock front-blast wave pulse which is composed of a sharp increase in blast overpressure and by underpressure (this is considered primary injury). It can be accompanied by shrapnel,

acceleration-deceleration, as well as fire and toxic gases. The accompanying components depend on the distance to the explosive device, with fire and toxic gases present when distance is small. There are currently five theories on the mechanism that generates the brain damage after blast injury: 1) A direct inertial loading due to the over and under pressure; 2) the compression of the brain due to skull flexure; 3) the acceleration-deceleration caused by the explosive blast pushing the person; 4) the cavitations that are formed in the inertial trauma; and 5) an increase in pressure in the thoracic cavity that elevates intracranial blood pressure and transmits the inertial load to the brain tissue (Chandra, Sundaramurthy, and Gupta 2017).

These models are classified based on the generation of the shockwave by detonating an explosive or by rupturing a diaphragm, they are further divided based on the environment for the propagation of the wave and positioning of the animal, into inside or outside of a tube, bunker or open field area. The models that contain the shockwave inside the tube can end in an open tube or have an incorporated wave eliminator. The models in which the animal is outside of a tube are further classified based on the position of the animal in reference to the tube axis. Animals may be directly on the blast path or outside of it (Bailey, Hubbard, and VandeVord 2016). Severity can be adjusted based on the peak overpressure and has been extensively characterized (Kuriakose et al. 2016, Petraglia, Dashnaw, et al. 2014, Mishra et al. 2016, Skotak, Alay, and Chandra 2018). Mild blast injuries produce deficits in spatial memory, decreased locomotion activity and food intake behaviorally. Histopathological effects it produces are a diffuse axonal injury with demyelination, neuroinflammation, and blood-brain barrier disruption (Mishra et al. 2016, Petraglia, Dashnaw, et al. 2014). In injuries of higher severity, animals showed more robust diffuse axonal injury, swelling of the brain, hemorrhage, and other vascular conditions such as vasospasm. Blast-wave pulse has shown to increase axonal damage when the thoracic

area of the animals is exposed to injury (Petraglia, Dashnaw, et al. 2014, Mishra et al. 2016, Begonia et al. 2014, Cheng et al. 2010, Long et al. 2009).

As stated earlier, TBI has been considered the most complex disease in the most complex organ in the human body. An essential part of this complexity stems from the heterogeneity of this condition— “No two TBIs are alike.” The diversity of TBI begins with the type, location, intensity, and duration of loads that are applied to the head, and the transfer of those loads to the brain. It continues with the response of the different tissues to the insults suffered, and the type of primary injury generated. Next is the secondary injury being produced, which can have particular characteristics and extensions based on the primary injury. This heterogeneity has complicated the study of TBI, and the assessment of benefits of treatments in clinical trials, due to a one size fits all approach. The lack of treatment options for patients of TBI is of great concern, due to the high incidence and the high proportion of long-term consequences suffered by survivors.

Significant advances in the understanding of the pathophysiology of TBI have been achieved through the generation and use of animal models. However, models are designed to recreate certain conditions of the pathology, and fail to reproduce the full scope of the disease. In order to understand what induces certain aspects of TBI, models must be experimentally controlled, homogenous (as much as possible) and reproducible. To achieve this, a considerable proportion of animal models have focused on the open skull and focal injuries, an approach in which a direct impact and deformation of the brain can be accomplished. Additionally, several parameters of this impact can be controlled, as explained in the CCI model where location, speed, depth, duration, and displacement of the impact can be programmed. These models show high reproducibility and consistency when the same parameters of injury are followed. Even in these highly reproducible models

there is a tendency to modify the injury parameters yielding different outcomes; added to the vast array of animal models currently in use, there has been an increased interest to find common factors to standardize the reporting of injuries and outcomes. This standardization of injury parameters is believed to increase the comparability of the results from a particular device, model, laboratory or group. With improved comparability, better extrapolations of the results can be achieved, increasing the probability that successful treatments of pre-clinical models may translate to the clinic.

In contrast, closed head injury models have proven to induce less reproducible injuries, though they exhibit higher similarities to the biomechanical characteristics of the injuries seen in the clinical setting. Among these models, the weight-drop models have proven attractive due to their low cost and simplicity. Some of the main concerns in these models have been the high mortality, high incidence of skull fractures, probability of double impacts and variability, though recent modifications to the original models have decreased these concerns. The addition of a breakable support system allows the animals to fall into a foam cushion after impact. This acceleration of the head after impact has increased the clinical relevance of the model, as it may better mimic injuries more commonly seen in assaults and sports. Also, decreases in skull fractures have eliminated the need for surgery (to adhere helmets to the skull), consequently making these models higher throughput. Yet the concern of variability remains.

This work aims to address three of the major challenges in TBI research stated above: 1) The assessment of reproducibility of the weight-drop TBI model, 2) the generation of comparable metrics for inter-experiment and inter-laboratory comparison of injury, 3) a pilot study of an FDA-approved therapeutic compound that could be potentially repurposed from cancer to neurotrauma.

## **Rationale, hypothesis, and aims**

As previously discussed, TBI results in unspecific neuronal depolarization, leading to the release of excitatory amino acids, mainly glutamate. The abundance of glutamate in the microenvironment of the brain initiates a process called excitotoxicity. Thus, TBI results in the overload of  $\text{Ca}^{2+}$  in the cell. When the buffering capacities of the cytosol of the cell have been overwhelmed, the mitochondria sequester  $\text{Ca}^{2+}$  in an attempt to return ionic homeostasis. This process leads to the generations of ROS in the mitochondria and is known to activate mitochondrial PARP1, which in turn poly(ADP-ribose)ylates complexes of the respiratory chain, compromising the production of energy and further generating ROS. Simultaneously, ROS produced in the cytosol induce DNA damage in the cell and activate nuclear PARP1. The activation of PARP1 consumes  $\text{NAD}^+$  and increases the energetic crisis in the cell. If PARP1 depletes  $\text{NAD}^+$ , the cell will undergo necrosis. If the mitochondria's membrane depolarizes first, PAR molecules formed by PARP1 activate calpain and release AIF from the mitochondria. AIF travels to the nucleus and initiates DNA fragmentation and a specific type of cell death called parthanatos. Regardless of the path, the process ultimately leads to cell death and inflammatory signaling that will eventually produce tissue injury.

We and others have shown that PARP1 activation exists after TBI. Patients that suffered severe TBI showed PARP1 activation in the pericontusional tissue (Berger et al. 2018). Children presented poly(ADP-ribose)ylated proteins in the cerebrospinal fluid after TBI (Fink et al. 2008). Furthermore, PARP1 single nucleotide polymorphisms have been correlated with better outcomes after TBI (Sarnaik et al. 2010). The deficiency or inhibition of PARP1 is neuroprotective *in vitro* and *in vivo* in animal models of TBI and stroke (Whalen et al. 1999, Rom et al. 2015, LaPlaca et al. 2001, Besson et al. 2005, Clark et al. 2007). However, most of these studies were done with previous generations of PARP1

inhibitors. Recently, three PARP1 inhibitors were approved by the FDA for use in cancer. Olaparib (Lynparza™) was the first ultrapotent PARP inhibitor approved for the treatment of ovarian cancer in 2014 and has shown cytoprotective characteristics in non-oncological diseases.

Interestingly, olaparib is neuroprotective in models of neuronal death by oxygen-glucose deprivation and NMDA receptor activation (Xu et al. 2016). Likewise, the therapeutic dose of olaparib to confer neuroprotection (1-5mg/kg/day) (Berger et al. 2018) is significantly lower than the doses required to show efficacy in the treatment of cancer (50-200 mg/kg/day) (To et al. 2014, Henneman et al. 2015), reducing the probability of side effects. Due to the lack of an effective treatment for TBI, as well as the characteristics of olaparib stated above, we believe that olaparib holds the potential for being repurposed for the treatment of neurotrauma.

These led to the hypothesis that **olaparib will protect against neurological and cognitive deficits in a clinically relevant murine model of TBI by improving the metabolic state of the cells and reducing neuroinflammation.**

### *AIMS*

The overall aim of this project was to assess if olaparib is a good candidate for further characterization with the ultimate goal of repurposing to treat TBI.

The implementation of an animal model of TBI was necessary to achieve this goal. The model developed by Kane et al. from Wayne State University was chosen because, unlike other weight-drop models, this model allows induction of injury on an intact skull and scalp with an unconstrained head, yields low mortality and skull fractures, and

recreates the clinical components of blunt impact and acceleration. However, after building and testing the weight drop model, we found areas that could induce variability between injuries. Thus, the specific aims were:

**Aim 1:** To generate a system in which the identified areas of variability are quantified and addressed to reduce the mechanical variability of the model (Chapter 2, model used in Chapter 4).

**Aim 2:** To generate a system that allows the quantification of the forces involved in the induction of TBI, thus permitting objective comparison of injuries among laboratories, support systems and even different models (Chapter 2).

**Aim 3:** To characterize the range of injuries and outcomes generated by the new TBI model (Chapter 3).

**Aim 4:** To assess the protective effects of olaparib on acute neurological and behavioral deficits following a closed-skull weight drop TBI (Chapter 4).

## Chapter 2 Model development

### INTRODUCTION

Traumatic brain injury (TBI) is a significant public health issue. In the United States, there were approximately 2.8 million cases diagnosed in emergency departments in 2010 (Taylor et al. 2017), or 3.5 million taking into account non-hospital based medical attention in 2009 (Coronado et al. 2012). Cohort based studies have shown that there is a high prevalence of sequelae after TBI, regardless of the severity. Reportedly around 40% of patients will show long term sequelae after suffering a TBI (Thornhill et al. 2000). Approximately, 75-87% of all TBIs are considered mild TBI (Barlow et al. 2010, Kane et al. 2011, Laker 2011, Centers for Disease Control and Prevention 2015, Dewan et al. 2018). Additionally, the leading cause for mild and moderate TBIs are falls, in both young and elderly; In the 15 to 44-year old range, being struck against an object constitutes the primary cause of mild TBI, and motor vehicle crashes for moderate (Taylor et al. 2017, Albrecht et al. 2016). These mechanisms mainly produce closed head injuries, making it the most common type of TBI seen in the clinical setting (Zhang et al. 2014).

Animal models have been used to obtain a deeper understanding of TBI and the pathophysiological processes that follow. No single animal model can recreate the full complexity and heterogeneity of TBI. These models attempt to reproduce portions of the pathophysiology that can be replicated in an experimental environment with controlled parameters (LaPlaca et al. 2007, Xiong, Mahmood, and Chopp 2013). There have been a plethora of different animal models that mimic different conditions of TBI; even within closed head injuries, a multitude of models can be found (Bodnar et al. 2019). Due to the lack of translation to humans of successful treatments in pre-clinical studies and the vast array of animal models available, a reproducibility and comparability problem has been

identified. To address this, researchers shifted towards elements that can be used to compare outcomes across models and laboratories, named “Common Data Elements” (CDEs). Since even small modifications to the settings of a device can affect the outcome and make comparisons impossible, a list of reportable settings and properties of the models has been created (Smith et al. 2015).

Historically, some of the first assessments to understand the pathophysiology of TBI were focused on the biomechanics generating the injury (Holbourn 1943, Ommaya and Gennarelli 1974). These studies led to the assessment of tissue tolerance to inertial forces. The objective was to determine the points at which these translational or rotational forces resulted in a concussion, contusion or skull fracture, concluding in the Wayne State Tolerance Curve (Lissner, Lebow, and Evans 1960). Recently, there has been an increasing interest in the biomechanics behind the injuries produced in animal models (LaPlaca et al. 2007, Namjoshi et al. 2013, Namjoshi et al. 2014, Mishra et al. 2016, Kuriakose et al. 2016, Hsieh et al. 2017, Li et al. 2011) and humans (Romeu-Mejia, Giza, and Goldman 2019, Post et al. 2019).

A variety of weight-drop models have gained acceptance in the field due to their simplicity, clinical relevance, and low cost. However, one of the main concerns in the use of these models is variability (Xiong, Mahmood, and Chopp 2013). Typically, in the weight drop model, the head of a rat or mouse was placed on a hard surface or foam. This model can induce severe injuries and skull fractures are common. To reduce the probability of skull fractures the scalp is surgically open, and a metal “helmet” is adhered to the skull (Marmarou et al. 1994). A more recent version of this model has changed the support of the animal from foam to an aluminum foil or Kimwipe that can be suspended, allowing the animal to traverse the support and accelerate downward to a foam cushion. This modification significantly reduced the skull fractures and has shown different severities of

outcomes based on the support system (Khuman et al. 2011, Meehan et al. 2012, Kane et al. 2012, Mychasiuk et al. 2014).

This new impact-acceleration model developed by Kane et al. was implemented in our laboratory due to its clinical relevance, reduction of skull fractures and double impacts, and its low cost of fabrication. To address the concerns of variability, an assessment of the biomechanical characteristics of the model was done and warranted modifications to the apparatus. This study focuses on further understanding the mechanical properties of this newly generated weight-drop model through the development of two systems of sensors. The first system is a set of sensors to monitor the forces applied to the animals during the induction of TBI. After obtaining some unexpected results regarding the forces applied to the head of the animals, a second system was generated. The artificial mouse was composed of three sensors in or on the head to measure the magnitude of forces in different portions of the head.

## **MATERIALS AND METHODS**

### **Model evolution**

#### ***INITIAL TBI APPARATUS***

A closed-skull weight drop injury model was built based on the model developed by Dr. Kuhn's group in 2012 (Kane et al. 2012). Briefly, the model consisted of a brass cylinder 19 mm in diameter milled to 95 g, suspended by a fishing line (Orvis® Super Strong knotless tapered leader [5X] fishing line) inside a vertical guide polyvinyl chloride (PVC) tube (22 mm internal diameter x 1.5 m length). The tube was suspended by a lab stand above a two-sided polycarbonate box (15 cm x 15 cm x 23 cm) inside of which lies a foam cushion (14 cm x 14 cm x 9.5 cm) (Figure 2.1). The vertical distance between the

top edge of the box sidewall and the bottom opening of the tube was 3.5 cm, and the vertical distance between the top edge of the box and the top of the cushion was 10 cm. A sheet of 18  $\mu\text{m}$  thick aluminum foil (01-213-101, Fisher Scientific, Hampton, NH) was placed across the top of the sidewalls of the box (Figure 2.1, B6). The aluminum foil was scored linearly with a razor blade from one edge to another and oriented such that the slit was parallel to the sidewalls and directly below the tube.

Figure 2.1. Initial TBI apparatus



**Figure 2.1. Initial TBI apparatus.** A) A 3D render of the first apparatus before its construction. B) The apparatus after assembly and in place in the lab. A1-B1) polyvinyl

chloride (PVC) tube; A2) falling object; B2) clamps holding the tube from the shelving and lab stand; A3-B3) the lab stand; A4-B4), the acrylic box; A5-B5), foam cushion; B6) scored aluminum foil.

### ***EVOLUTION OF THE TBI APPARATUS (WORKING MODEL)***

The initial TBI apparatus was modified. In place of the PVC tube, a polycarbonate (PC) guiding tube (22 mm I.D. x 1.7 m length) was used (Figure 2.2, A1), first suspended by clamps fastened to laboratory shelves, and later suspended with clamps secured to an iron rod fixed to the wall (Figure 2.2, A3 and H1, respectively). A larger box was built in order to accommodate both mice and rats (38 x 28 x 22 cm), similar to the one reported previously (Mychasiuk et al. 2014). Two additional brass weights (120 g and 150 g) were milled with holes through the center along the longitudinal axis, through which fishing line was threaded, knotted and glued with silicon.

Additionally, four systems were added to enhance reproducibility. (1) A sensor to measure the velocity of the falling objects (composed of two photodiodes and two phototransistors) was placed in the last 10 cm of the guiding tube to calculate the kinetic energy (KE) of the falling weight immediately before impact (see complete specifications in sensor section of the final apparatus below) (Figure 2.2, C-D). (2) A head positioning guide built with a triangular clamp with padding ensured a reproducible position of the mouse head underneath the guiding tube (Figure 2.2, H3), (3) A pulley system to reduce drag of the fishing line against the border of the tube and breaking of the fishing line (Figure 2.2, E), and (4) the first attempted iteration of a force sensor were added (Figure 2.2, F and G). Data generated with the velocity sensor showed that the Orvis Super Strong knotless tapered leader (5X) fishing line increased drag and reduced the velocity of the falling object, thus reducing the KE and injury severity. Therefore, the line was replaced with

Super Strong Trilene® Big Game™ (20 LB, BGQS20C-81, Berkley®) fishing line. This version of the model (Figure 2.2, H) was used for initial experiments in this Chapter (Figure 2.8 and 2.9) and all experiments in Chapter 4.

Figure 2.2. Evolution of the TBI apparatus

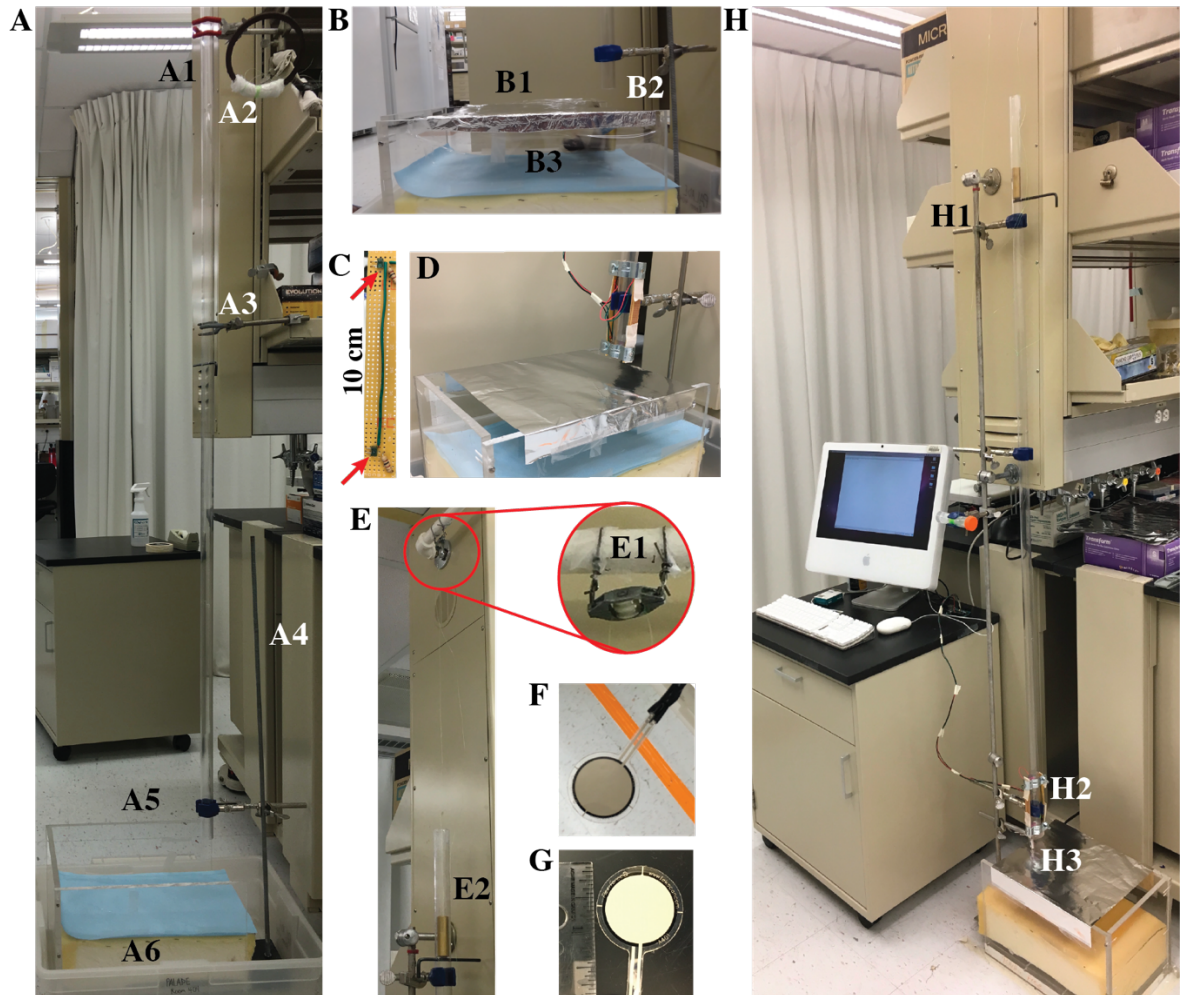


**Figure 2.2. Evolution of the TBI apparatus.** Two different iterations of the model are shown. A) The modified model, A1) the polycarbonate (PC) tube, A2) a fishing line holder, A3) clamps securing the PC tube fixed to the lab shelving, A4) a lab stand, that secures the lowest portion of the tube, A5) the larger box with thicker walls for stability, and A6) the foam cushion. B) The new box, B1) the aluminum foil support for mouse, B2) separation

of 3.5 cm between the bottom of the tube and the foil, and B3) a mouse falling into the foam cushion after impact. C) The velocity sensor, photodiodes (red arrows) in place 10 cm apart. D) The velocity sensor attached to the end of the tube, to measure the final velocity before impact. E) The pulley system suspended above the tube, E1) a pulley with the fishing line passing through, and E2) the fishing line and brass weight parallel to the tube. F) Force sensitive resistor (FSR). G) Dimensions of the FSR. H) Working model for experiments in chapter 4, H1) an iron rod to stabilize the tube, H2) the velocity sensor, and H3) the triangular head positioning system beneath the tube.

### ***CURRENT WORKING TBI APPARATUS***

Use of our previously generated closed-skull weight-drop injury model (Figure 2.2, H and Chapter 4) and observation of potential areas of variability led to further modifications and optimizations of the model. Briefly, the new apparatus (Figure 2.3) consists of a solid aluminum breadboard (12 x18 x 1/2 in, MB1218, ThorLabs, Newton, NJ) that serves as the base (Figure 2.3, A1, B and F) of the system, and is raised by four aluminum rods (30 cm height x 1.2 cm diameter). Attached to the base is a construction rail (Figure 2.3, A3 and B) (two 0.98 x 0.98 x 36 in long rails connected to reach a height of 72 in, XE25L900/M, ThorLabs, Newton, NJ). The construction rail secures the PC guiding tube (Figure 2.3, A4 and B) (22.22 mm I.D., 25.4 mm O.D. x 1.7 m length, 175-54, AAA Plastics, Inc., Cypress, TX) that has three 5 mm holes drilled at 0.5, 1.0 and 1.5 meters corresponding to dropping heights (Figure 2.3, B). Under the base is a steel plaque (17.6 x 11.3 x 1.3 cm) with a 10 mm cylindrical perforation on one edge. The hole is surrounded by three 5 mm neodymium magnets. Additionally, there is one plastic polyetheretherketone (PEEK) (28 mm height x 3 mm in diameter) tube (Figure 2.3, C) on each side of the hole that serve as a head position indicator. The PEEK tubes were filled with a cotton-tipped applicator wood rod (2.2 mm diameter, 8884540500, Covidien Curity,

Dublin, Ireland) for rigidity. The circular perforation holds an impactor. The impactor (Figure 2.3, D) (24.5 g total) consists of a cylindrical poly (methyl methacrylate) (PMMA) rod (9mm in height, 10mm in diameter) that concentrates the impact on the animal's head, along the midline of the skull and equidistant from ears and eyes. Between this rod and the body of the impactor (PMMA rod 11 cm in length, 10mm outer diameter) lies an impact force sensor (PVDF film [Precision Acoustics, UK], Figure 2.3, E) within a PMMA disc (8mm in height, 19mm outer diameter) that has a metal ring on its superior surface. At the top of the body of the impactor, two hard rubber rings (5mm thick, 20mm O.D.) are screwed into place with a steel washer in between.

Similar to the models mentioned above, an open acrylic chamber (38 cm length x 28 cm width x 21 cm depth, with walls 15 mm thick) that contains a foam cushion (36.5 cm x 20 cm x 13.5cm [Premium poly foam 4"x22"x22", American Excelsior Company, Arlington, TX]). The vertical distance from the top of the box to the top of the cushion is 10 cm.

Three cylindrical brass objects (19 mm in diameter, 95, 120 and 150 g) were milled (Figure 2.3, B). Each brass weight was attached to a 1.0 m fishing line (Super Strong Trilene® Big Game™ 20 LB, Berkley®), allowing it to be raised or lowered into a polycarbonate guide tube to the desired drop height (Figure 2.3, B). The guide tube was used to ensure the brass objects drop directly onto the impactor.

Aluminum foil (01-213-101, Fisher Scientific, Hampton, NH) was cut into sheets measuring 30 x 25 cm. Fifteen sheets were stacked and perforated perpendicularly in the midline from the edge to the center (12 cm with one perforation per cm) with a #15 stainless-steel surgical blade (0086, Bard-Parker, Aspen Surgical, Caledonia, MI). Aluminum foil is then attached to the sidewalls of the open acrylic chamber with

approximately 10 cm of invisible tape (520928, Office Depot, Boca Raton, FL) so that the foil covered the top aperture (Figure 2.3, B); the space between third and fourth perforation was under the impactor.

Figure 2.3. Working model TBI apparatus

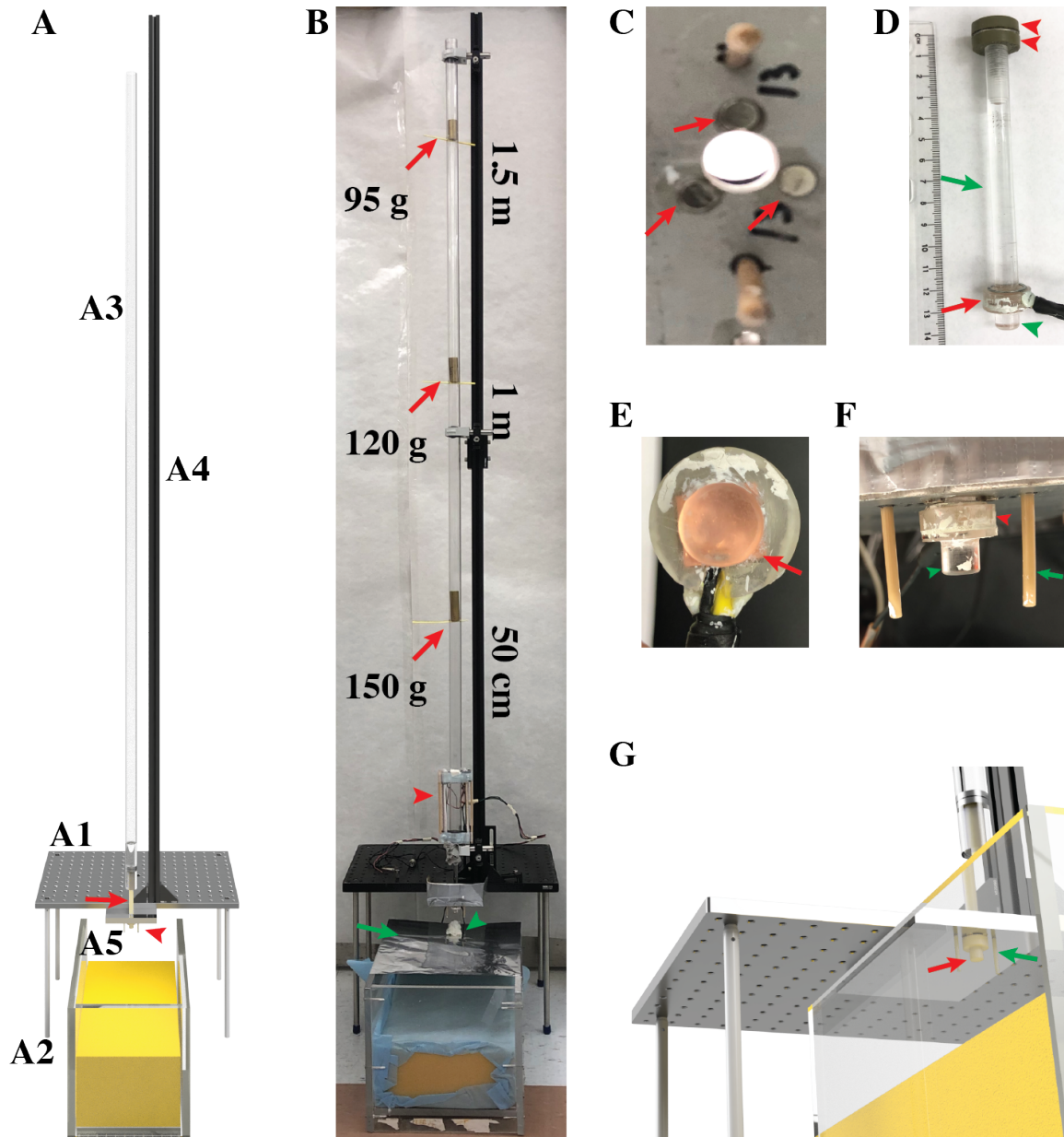


**Figure 2.3. Working model TBI apparatus.** The current TBI apparatus. A) A 3D render of the model. A1) the base breadboard, A2) aluminum rods, A3) the Polycarbonate (PC)

guiding tube, A4) and the supporting construction rail. The PC tube ends on the impactor (red arrow). A5) The steel plaque holding the impactor (red arrow) and the plastic polyetheretherketone (PEEK) tubes (red arrowhead). B) Constructed model is shown with the same components, three objects (red arrows) at the three drop heights and the velocity sensor in place (red arrowhead). The box with the aluminum foil (green arrow), supports a cast mouse (green arrowhead) in between the head positioning PEEK tubes. C) A bottom view of the steel plate with a 10 mm perforation for the impactor to go through and the 5 mm neodymium magnets (red arrows) to hold the impactor in place. D) The impactor consisting of a poly (methyl methacrylate) (PMMA) rod (green arrowhead), a PMMA disc (red arrow), the body (green arrow) and the hard rubber rings (red arrowheads). E) A close up of the impactor with the force sensor (PVDF film). F) A close-up view of the impactor composed of a rod for focusing impact (green arrowhead) and PMMA ring with an impact force sensor (red arrowhead) and, G) a close-up view of the PEEK tubes (green arrow) and the impactor (red arrow),

## ***SENSORS***

The system was built containing three sensors: A phototransistor velocity sensor, an accelerometer, and an impact force sensor (Figure 2.4).

### **Phototransistor velocity sensor**

Two light-emitting diodes (LEDs) coupled with two phototransistor detectors (PT) (Figure 2.4, A and B) were used to calculate the average velocity of the falling object in the last ten cm of the PC guiding tube. Two infrared (IR) LEDs (880 nm, SEP8736-003, Honeywell, Morristown, NJ) were used as the light emitters. Two IR PTs (880 nm, SDP8436-003, Honeywell, Morristown, NJ) were used as the detectors. These wavelengths were chosen to limit interference from visible light. The two IR LEDs were placed in series

with a 100  $\Omega$  resistor going to ground (Figure 2.4) and positioned 10 cm apart pointed in a parallel direction across the PC tube. The two PTs were also spaced 10 cm apart, parallel facing. Each directed towards one of the IR LEDs on the other side of the PC tube, such that an object passing through the tube would obstruct the light emitted towards the PT. The components were driven by 5 volts supplied by a microcontroller board (Arduino Uno Rev3, Arduino.cc, Somerville, NJ), and the signal from the PT was interpreted by the analog input pins of the microcontroller board.

The analog pins monitor the signal coming from the PT. The falling object passed between LED and PT, altering the signal emitted by the PT. As soon as the signal from the PT was below a threshold value, the timer was started. The obstruction of the signal from the second PT stopped the timer. The measure of elapsed time between the break of both signals was used to calculate the velocity of the falling object. Velocity was calculated as  $[V = d/t]$  where  $d$  is the distance between detector 1 and 2 (10 cm) and  $t$  is the elapsed time. The result was converted to meters per second. Velocity was used to calculate the kinetic energy  $[KE = \frac{1}{2}m * v^2]$  where  $m$  is the mass in Kg and  $v$  is the velocity of the falling object.

### Impact force sensor

The force sensor was assembled in our laboratory and was incorporated into the impactor directly above the impacting rod (Figure 2.4, C), allowing the measurement of the force applied to the top of the animal head during impact. It was made from uniaxially poled PVDF film (Precision Acoustics, UK). For the calibration of the force sensor, the force transducer under calibration was placed on the top of a plastic block. A Plexiglas tube (1 in O.D.) was fixed above the transducer and a factory calibrated Accelerometer 352A73 (PCB Piezotronics, Inc., Depew, NY) was attached to a cylindrical aluminum object (67g). During calibration, the object was dropped on the transducer along the Plexiglas tube. The

entire impact area was covered by the transducer to avoid error in calibration. The tube served only to keep the object aligned with the transducer vertically.

The force of the impact on the transducer was calculated as  $[F = m * a]$  (1), where  $F$  is the applied force in Newtons,  $m$  is the applied mass in kilograms (0.067 kg in this calibration), and  $a$  is the acceleration in  $g$  shown by an accelerometer. The signal from the piezoelectric force sensor was recorded with an oscilloscope (TDS 3012, Tektronix, Beaverton, OR). The amplitude of the signal is  $[V = \frac{F}{k}]$  (2), where  $V$  is a signal measured with the oscilloscope in volts, and  $k$  is the transducer's sensitivity. The transducer's sensitivity could then be determined by (1) and (2),  $k = \frac{F}{V} = m * \frac{a}{V}$ . Using five points for the calibration line, the  $R^2=0.999$ , the sensitivity of the force transducer was  $43 \frac{N}{V}$  at the beginning of the experiments and remained unchanged after all measurements were finished.

### Accelerometer

A factory calibrated accelerometer (352A73, PCB Piezotronics, Inc., Depew, NY) measuring 8.6 x 4.1 x 2.8 mm in size, and weighting 0.3 g (sensitivity  $5.25 \frac{mV}{g}$  [where mV is millivolt and  $g$  is acceleration due to gravity], and frequency range: 0.7 – 40000 Hz) was used. The accelerometer was attached to a plastic equilateral triangle sheet (1.7 cm height x 2.0 cm base, and 0.2 mm thick) (Figure 2.4, D). The total weight of the accelerometer and triangle sheet was 0.65 g. The triangle had two white plastic twist ties (Figure, 2.4 D), one in the vertex and the second on the base of the triangle to attach the accelerometer to the head of the mouse (nose and neck respectively). This accelerometer was used for animal experiments in Chapter 3.

The signals from all transducers were digitized with three 2-channel digital oscilloscopes (USB-5132, National Instruments, Austin, TX) at 200 kHz sampling rate and recorded on a computer.

Figure 2.4. Sensors

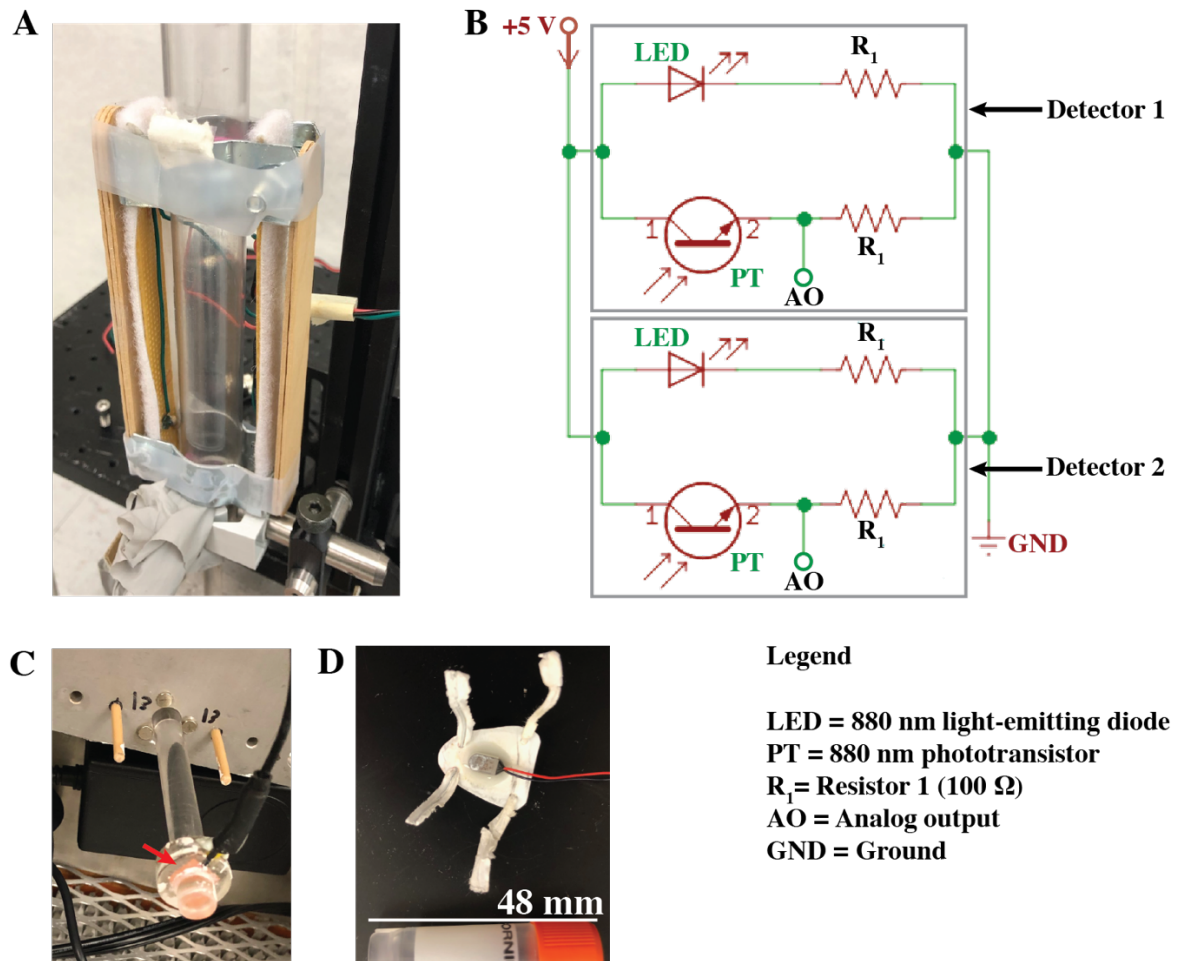


**Figure 2.4. Sensors.** The use of sensors to measure the biomechanics of traumatic brain injury in the closed-skull weight-drop injury model. A) A phototransistor velocity sensor placed at the bottom portion of the PC guiding tube. B) The circuit schematic for the phototransistor velocity sensor. C) A PVDF film (red arrow) used as an impact force sensor was placed in the poly (methyl methacrylate) PMMA ring of the impactor. D) An

accelerometer was attached to a plastic triangle with two twisty ties to secure it to the mouse head.

### ***PROFESSIONAL MOUSE***

A cast mold of a mouse was prepared with Mold Star® 16 FAST Platinum Silicone Rubber (Smooth-on, Macungie, PA), and a silicone model was generated with Dragon Skin® 10 Medium Platinum Silicone - Medium Cure (Smooth-on, Macungie, PA). The head of the silicone mouse was cut at the neck. A new head was carved out of a silicone block (23mm length x 18mm base x 13mm height, Sylgard 184, Dow Corning, Midland, MI) (Figure 2.5). The silicone head was equipped with two PVDF films (middle and bottom impact sensors discussed below) and an accelerometer. The factory calibrated accelerometer (8.6 x 4.1 x 2.8 mm in size, 0.3 g in weight, a sensitivity of  $5.25 \frac{mV}{g}$  and a frequency range of 0.7 – 40000 Hz; 352A73, PCB Piezotronics, Inc., Depew, NY) was placed in a recess in the bottom of the silicon head (Figure 2.5, B green arrowheads).

The two 28  $\mu\text{m}$  thick gold plated PVDF films (Precision Acoustics Corporation, UK) placed inside the silicone head make up two impact sensors. One sensor was placed in the middle of the head (perpendicular to the axis of impact) (Figure 2.5, B green arrows). The sensitivity of the middle force transducer was  $6.5 \frac{N}{V}$  throughout the experiments. The additional sensor was placed in the bottom surface of the silicon head, (Figure 2.5, B red arrow) and calibrated to the accelerometer. The sensitivity of the bottom force transducer was  $100 \frac{N}{V}$  and confirmed at the end of the experiment. The silicon head was attached to the silicone mouse with a size 5-0 perma-hand silk (640G, Ethicon, Somerville, NJ), which allows the “head” to have movement independently from the body.

Figure 2.5. Professional mouse model

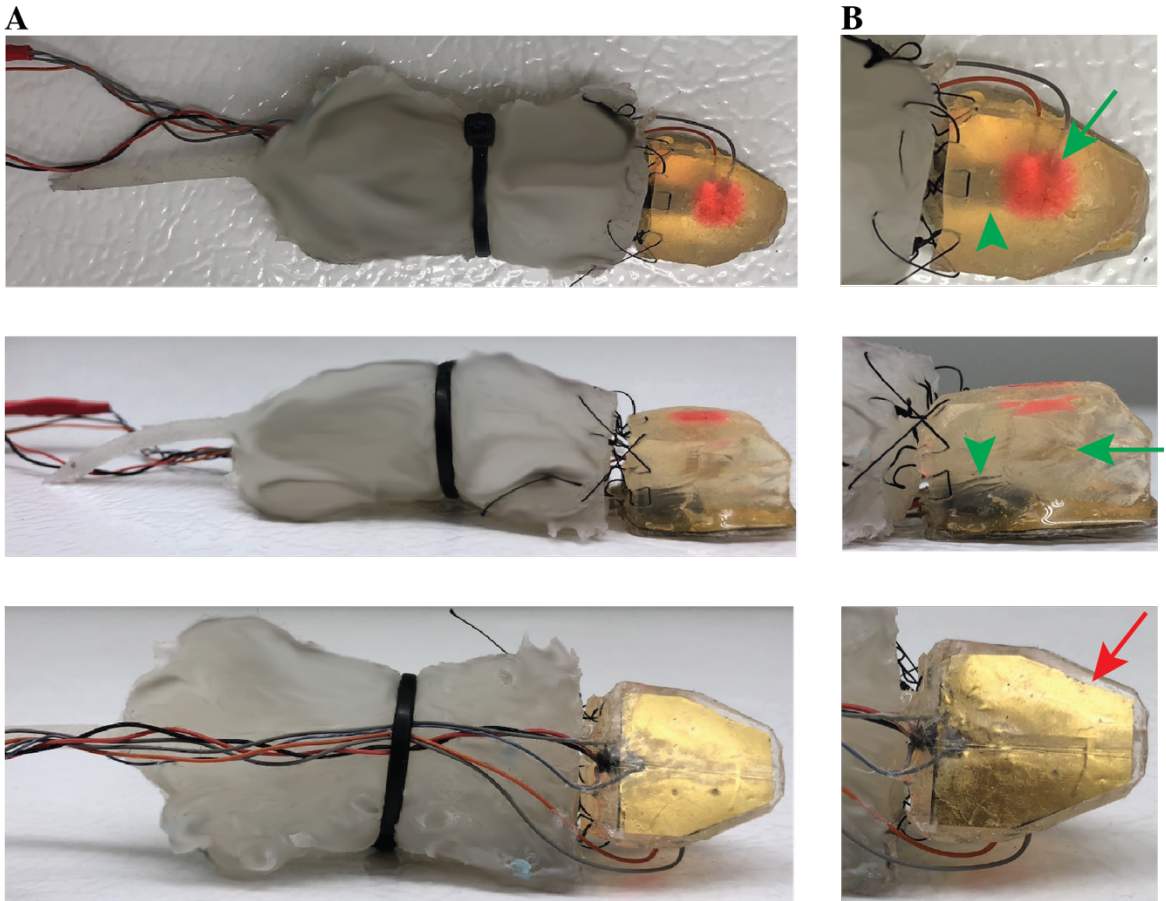


**Figure 2.5. Professional mouse model.** A) A silicone cast with the shape of a mouse was produced, and a mouse head generated out of silicon attached to the body by perma-silk simulating the free motion of the head, seen from the top, side and bottom. B) The silicone head was equipped with two impact force sensors, one in the middle of the head (green arrows) and one on the bottom (red arrow), and an accelerometer (green arrowheads) embedded in a recess at the bottom of the head.

#### *SUPPORT SYSTEMS TO MIMIC OTHER MODELS*

To be able to compare the biomechanics of our recently generated model and prove the utility of our sensor system beyond our model, we generated two sets of support

systems to mimic other models and quantify the forces involved in the injury of two published methods.

The first support system was made to mimic the weight-drop TBI models that use Kimwipes® (Kimberley-Clark Inc., Irving, TX) to hold the animal below the impactor (Khuman et al. 2011), such as the Laboratory weight-drop system (LWDS) (2700-300, Northeast Biomedical Inc., Tyngsborough, MA) (Yates et al. 2017). In these models, objects ranging between 53-83 g for mice and 250 g for rats are used and usually dropped from a distance that ranges between 71 cm and 1.67 m (Mannix et al. 2014, Mannix et al. 2013, Meehan et al. 2012, Kobeissy et al. 2016, Dapul et al. 2013, Khuman et al. 2011, Yates et al. 2017). The support system to mimic these injury models consisted of two 25 x 25 mm construction rails (Figure 2.6, A-B) 375 mm in length (XE25L375/M, ThorLabs, Newton, NJ) with clamps to hold the open acrylic box of our system. Kimwipes® were placed across the scaffold and held in place with invisible tape. The smaller objects (95 g and 120 g dropped from one meter and 95 g dropped from 1.5 m) were used to mimic experimental conditions that are used in the field. Height and range of weights do not match exactly because we wanted to compare between the two models.

The second support system consists of a set of trapdoors kept closed by magnets, and to our knowledge this has only been used in one model (Briggs, Angoa-Perez, and Kuhn 2016). The doors were intended to overcome some of the potential variability in the tension of aluminum foil or Kimwipes® between experiments. This support system was constructed with a solid aluminum breadboard (Figure 2.6, C) (12 in x18 in x 1/2 in, MB1218, ThorLabs, Newton, NJ) that serves as a base for the frame that holds the doors. Attached to the breadboard are four slotted bases (BA1/M, ThorLabs, Newton, NJ) for four post holders (PH1, 2 in, ThorLabs, Newton, NJ). The slotted bases allow movement to change the separation between both sides of the frame. Each post holder secures an 8 in

long SR assembly rod (for 16mm cage systems, SR8, ThorLabs, Newton, NJ). These rods end in right-angle brackets (Figure 2.6, D, green arrowhead) for 25 mm rails (XE25A90, ThorLabs, Newton, NJ) connecting to 2 in long SR assembly rods (Figure 2.6, D, red arrowhead) (for 16 mm cage systems, SR20, ThorLabs, Newton, NJ). These parts form the frame for two custom-built aluminum doors (Figure 2.6, D, Red arrows) (13.3 cm long x 5.3 cm wide and 27g each), with one 5 x 1 mm neodymium magnet (HHOOMY, US) near each edge of each door to keep them closed together. All objects and heights were used to compare with the aluminum foil support.

Figure 2.6. Support systems for impact-acceleration models

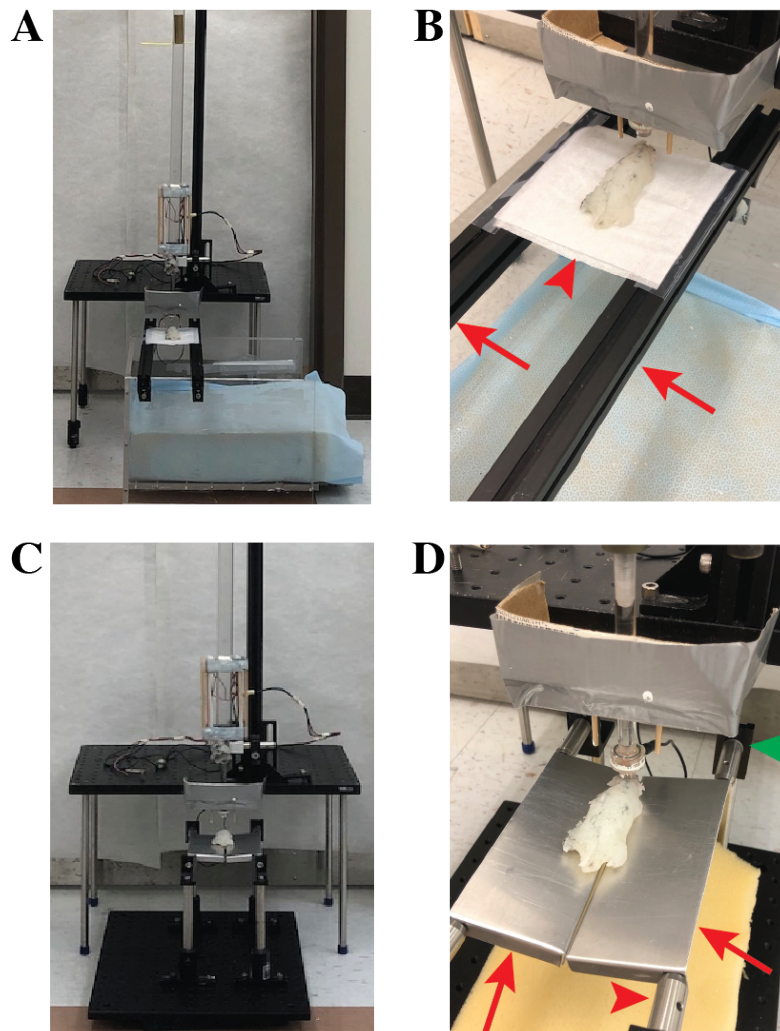


**Figure 2.6. Support systems for impact-acceleration models.** Different support systems were generated to mimic various weight drop TBI models. A) One model uses Kimwipes® as a support system. B) In a close-up image the rails (red arrows) used to hold Kimwipes® (red arrowhead) are displayed, Kimwipe is placed along its longitudinal axis, single ply. C) The second model uses a trapdoor system elevated by a frame constructed of rods. D) A close-up of the doors (red arrows) where the rods (red arrowhead) and right-angle brackets (green arrowhead) are shown.

### *SOFTWARE*

A custom-made program written in LabVIEW (Version 2018, National Instruments, Austin, TX) was used to collect, process and store the temporal profiles of the signals from the force sensor in the impactor, the force sensor in the center of the head, the force sensor in the bottom of the head and the accelerometer (Figure 2.7).

A custom-written code was used to measure collect and process the phototransistor velocity sensor data, using the Arduino software (Version 1.8.1, Arduino.cc, Somerville, NJ) (see appendix for code).

Figure 2.7. Software screenshot.

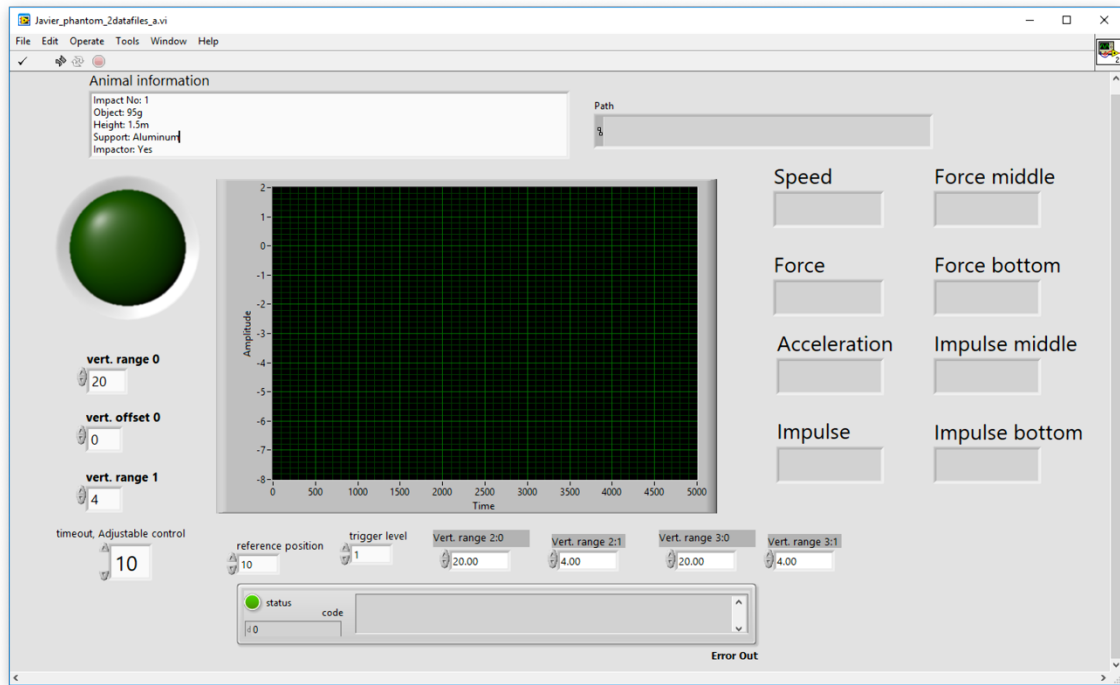


**Figure 2.7. Software screenshot.** A screenshot of the custom-made software utilized to quantify various parameters of the weight drop injury is shown. The information collected includes the force of the hit on the mouse head by the impact force sensor located inside the impactor, the compression of the head with the middle force sensor, the pressure exerted by the support material on the head with the bottom force sensor, and the acceleration and speed of the head of the mouse after impact with the accelerometer.

## Statistical Analysis

The statistical analysis for the fishing line comparison was two-way ANOVA and multiple comparisons was done with Tukey's post hoc test. The behavioral outcomes of TBI and the effect of friction on the falling objects was analyzed by one-way ANOVA and Tukey's post hoc test. To compare the velocity of the two falling objects the Student T' test was used. Data was analyzed using Graphpad Prims version 8.0 (Graphpad software,

San Diego, CA). Significance was considered when  $p < 0.05$ . Mechanical data is shown as mean  $\pm$  standard deviation (SD) and biological data including behavior is shown as mean  $\pm$  standard error of the mean (SEM).

## **RESULTS**

### **Fishing line alters the velocity of the falling weight**

In the first set of experiments, the use of the fishing line (Orvis® Super Strong knotless tapered leader (5X) fishing line) described by Kane (Kane et al. 2012) resulted in the line breaking on several occasions, induced by friction against the top edge of the tube. Fishing line breaks were directly correlated to the weight of the object used. The use of a stronger, less elastic, fishing line (Super Strong Trilene® Big Game™ (20 LB, BGQS20C-81, Berkley®)) resulted in fewer line breaks.

For the next set of experiments, a velocity sensor and a pulley system were installed. With these new additions, the use of the Orvis® fishing line was revisited. Drops with the Orvis® fishing line exhibited lower velocities than previous experiments using the Big Game™ line. Further, line breaks persisted, even with no friction against the top edge of the tube due to the pulley system. A direct comparison was made between the drops using the Orvis® line with a new set of drops using the Big Game™ line. Drops with the Orvis® line developed significantly lower velocities ( $p < 0.05$ ) regardless of object-weight (Figure 2.8). Another interesting finding was an object weight-dependent difference ( $p < 0.05$ ) in velocity between drops with the 95 g and 120 g objects using the Orvis® line. This difference was absent in the drops made with the Big Game™ line.

Figure 2.8. Comparison of fishing lines for weight-drop

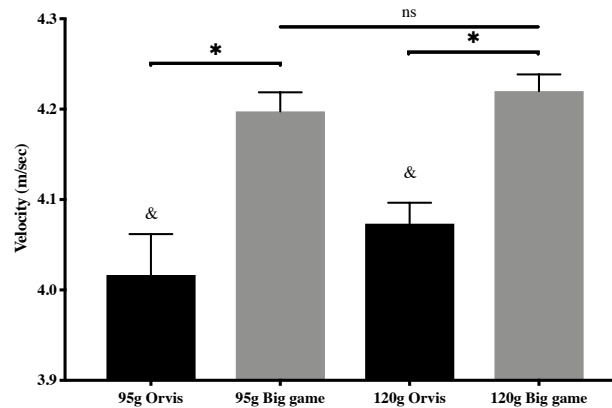


**Figure 2.8. Comparison of fishing lines for weight-drop.** Velocity measurements were used to compare the drag generated by two fishing lines, the Orvis® Super Strong knotless tapered leader (5X) and the Super Strong Trilene® Big Game™. The Orvis® line generated more drag and reduced the velocity of the falling weight when compared to the Trilene® Big Game™ line. The increase drag was object weight dependent making the velocities different between weights. (Orvis n=3 per object and Big Game n=8) Data is presented as mean  $\pm$  SD, analyzed by two-way ANOVA with Tukey’s post-hoc test. “\*” indicates significance between brands and “&” between objects of the same brand  $p < 0.05$ .

### Righting reflexes and behavioral deficits are object-weight dependent

The TBI apparatus with the Big Game™ fishing line, pulley system, and velocity sensor, was used to test if there were differences between the mechanical and biological outcomes of after TBI. For this purpose, male 2-month-old C57Bl/6 mice (n=5) were injured by the 95 g and 150 g objects dropped from 1.0 m and compared to sham. The mechanical measurement was velocity (m/s), from which KE (J) was calculated. The biological outcomes measured were righting reflex and locomotor activity. Locomotor activity was measured using the photobeam activity system, starting 30 minutes after the anesthesia wore off and recording for 12 hours. This was repeated four days post-injury.

Even though there was no difference in the velocity of the falling objects (95 g and 150 g) (Figure 2.9, A), as expected, due to the mass difference, the KE was different between the two groups ( $p < 0.05$ ) (Figure 2.9, B). There was a significant difference between the RR of the mice injured with the 150 g object when compared to sham (Figure 2.9, C). An inverse correlation was seen between the object weight used in impact and a decrease in exploratory behavior, assessed as rearing events, distance traveled and total locomotion activity (Figure 2.9, D, E and F, respectively) the day of the injury. The patterns in distance and total locomotor activity changed at four days post injury, to an equivalent distance and beam breaks between sham and the mice injured with the 95 g object except in rearing. Also, the differences remained with the animals injured with the 150 g object in all measurements (Figure 2.9, G, H and I).

Figure 2.9. Mechanical and behavioral assessment of first working model of TBI

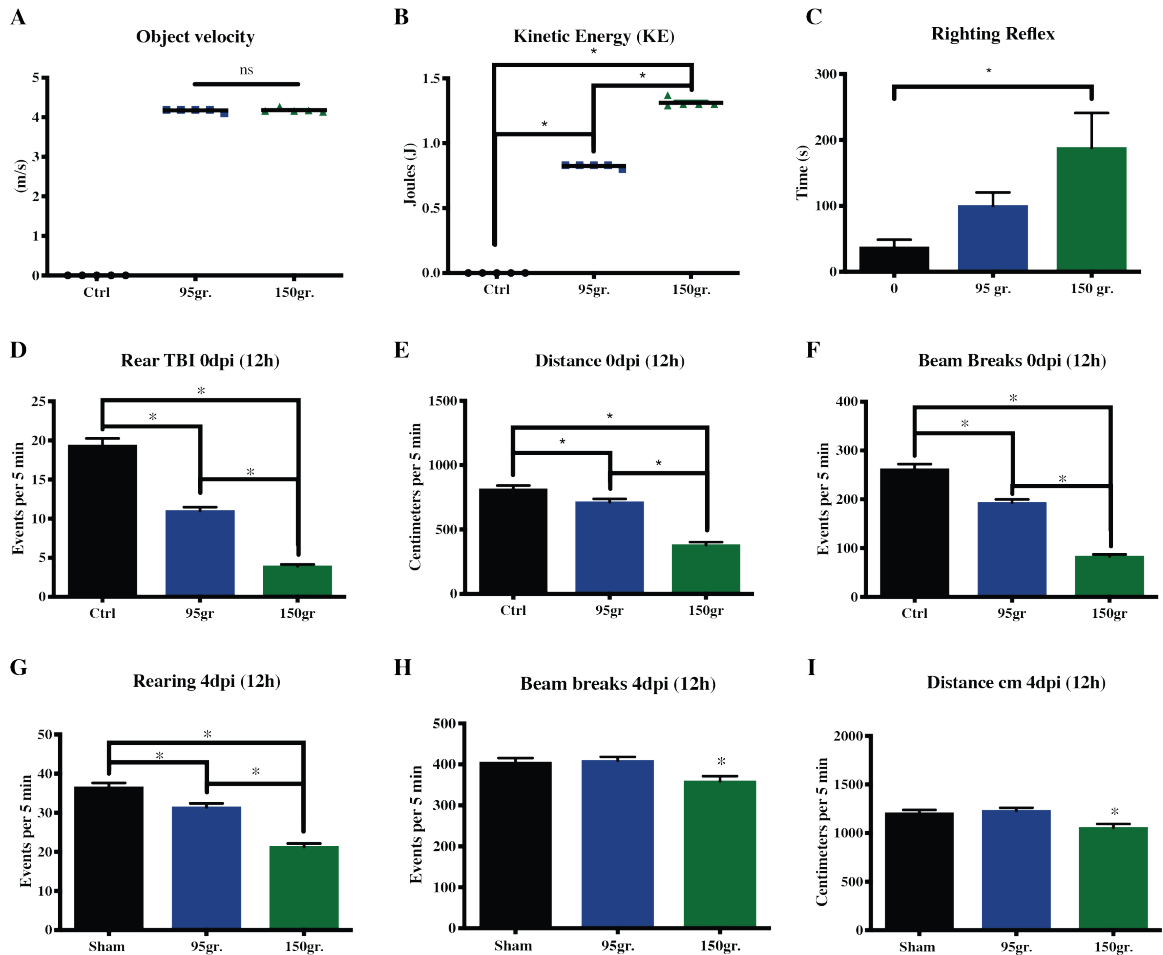


**Figure 2.9. Mechanical and behavioral assessment of first working model of TBI.**

Mechanical analysis of the weight-drop model of TBI along with acute and subacute neurobehavioral outcomes. A) Measured velocity in m/sec of two falling objects of different weights (95 g and 150 g), with no differences. B) Calculated kinetic energy [ $KE = \frac{1}{2} m * v^2$ ], in joules (J), generated by the two objects, where m is the mass of the object in Kg and v is the measured velocity. C) Duration of unconsciousness after injury (recovery from anesthesia), was significantly increased in the group injured with the 150 g object when compared to uninjured control animals. D-F) Changes in locomotor activity in 12 hours measured 30 minutes after the effect of anesthesia wore of. There is a inverse correlation between the increase in object mass and the decreases in exploratory behavior

measured as D) rearing events, E) distance measured in mm and total exploration assessed as beam breaks. G-H) Same behavior measured 4 days post-injury. Data represented as mean  $\pm$  SEM (n=5) \*p<0.05. Student's T test to compare the velocity of the two weights and one-way ANOVA with Tukey's multiple comparisons test as post-hoc.

These results, in addition to preliminary imaging of neuroinflammatory and cell death markers in TBIs with objects dropped from 1 and 1.5 meters (data not shown), verified that the model was able to induce varying severities of injury, allowing the use of this model for the project reported in Chapter 4.

### **The novel apparatus with an impactor is highly reproducible**

The experiments mentioned above and below in Chapter 4 revealed a high degree of intracranial bleeding and 15- 20% mortality in the animals injured with the 150 g object dropped from 1.5 m. In a given experimental day the object's travel distance seemed to increase with the number of drops likely due to the elasticity of the line. This led to the addition of an impactor that included a force sensor to measure the impact force on the head of the mouse. Additionally, the impactor would stop the falling weight, eliminating the need for a fishing line (model used for experiments in Chapter 3). Once the experiments for the characterization of the model were finished, we noticed that there was a plateau of the force applied to the top of the mouse head (see Chapter 3, Figure 3.10), the acceleration and speed of the head following impact with the 95, 120 and 150 g objects dropped at 1.5 m. Even though this plateau existed, the neuroscore showed weight dependent increases in neurological deficits, that albeit not significant between them, the 150 g weight showed differences from sham (Chapter 3, Figures 3.10 and 3.11). These data led us to hypothesize that this plateau was the product of skull compression, absorbing the shock of the impact and reducing the peak impact force. To test this hypothesis, the "Professional mouse"

model was developed to measure the different forces acting throughout the head of the mouse.

The impact forces increased with the object-weight and height of drop. This increase was measured by the multiple sensors on the top, middle and bottom of the Professional mouse's head (Figure 2.10, A, B, and C). The different forces applied to the head remain consistent across multiple drops within each object weight and drop height.

Figure 2.10. Mechanical reproducibility with an aluminum foil support

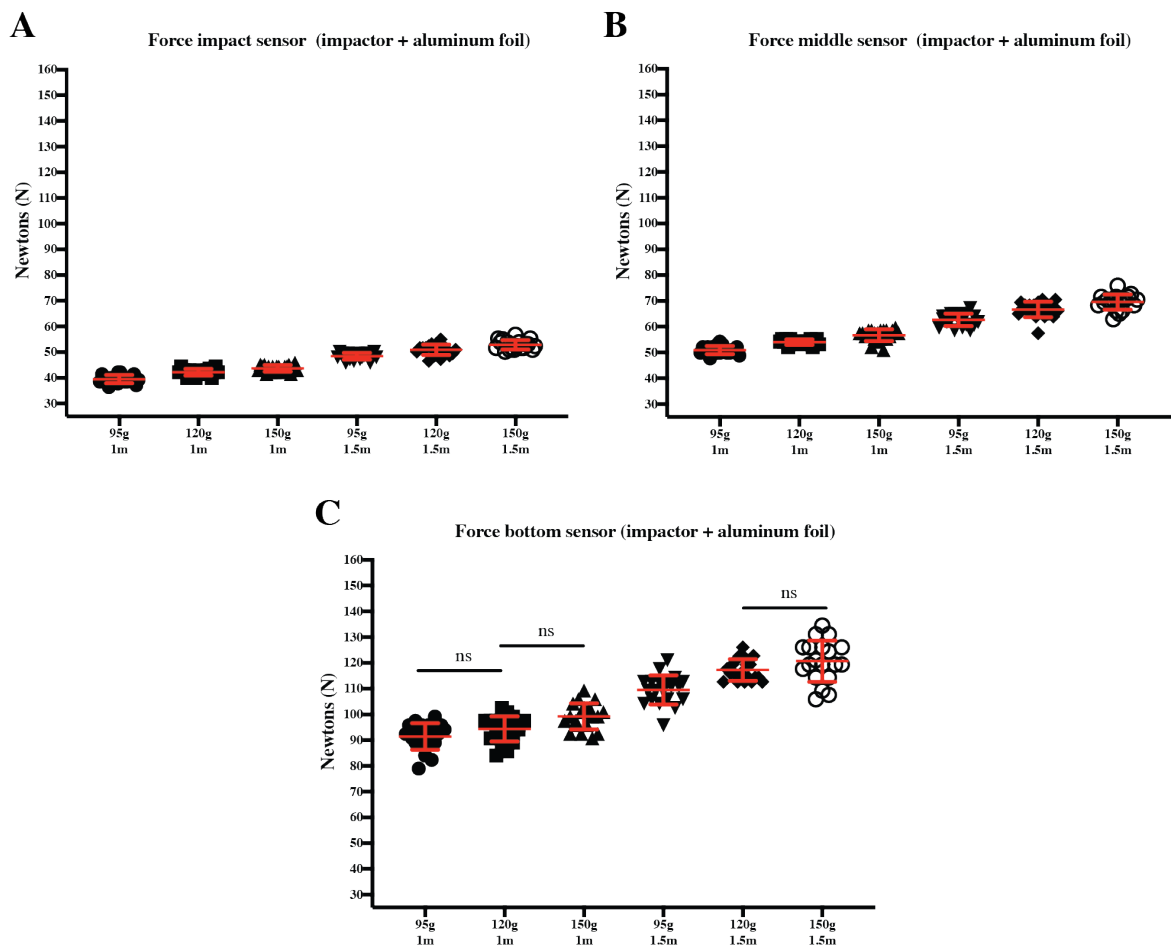


**Figure 2.10. Mechanical reproducibility with an aluminum foil support.**

Biomechanical analysis of the forces applied to the professional mouse head with

aluminum foil as support. A) The forces of impacts in Newtons applied to the head of the Professional mouse model (95, 120 and 150 g objects dropped from 1 and 1.5 m) were recorded by the sensor in the impactor. B) Force from the same impacts recorded in the “middle” sensor (placed in the middle of the head of the Professional mouse), and C) bottom sensor, registering the resistance from the aluminum foil. Note that the increase in force is object and height dependent, as well as the reproducibility of impacts. Data shown as mean  $\pm$  SD n=20 per condition.  $p < 0.05$ , ns =  $p \geq 0.05$ , one-way ANOVA with Tukey’s multiple comparisons post hoc test.

### **Velocities from the falling objects vary from theoretical calculations**

To assess the degree of drag due to different components of the weight-drop system, the velocity of the falling objects was measured using the two working iterations of the apparatus. The apparatus that uses the fishing line without the impactor (first apparatus) and the apparatus with the impactor but no fishing line (last apparatus) were used. The velocities of the three falling objects (95 g, 120 g, and 150 g) at two heights (1.0 m and 1.5 m) were compared between the two iterations of the apparatus (Figure 2.11). The velocity of the falling object in the last apparatus was done with the three different mouse support systems (scored aluminum foil, Kimwipes, and aluminum doors).

- First apparatus (weight-drop with fishing line):
  - Fishing line, no impactor + aluminum foil (Alu): 95 g and 120 g objects dropped from 1.0 m and 150 g object from 1.5 m.
- New apparatus (Impactor):
  - Impactor + aluminum foil (Imp Alu): 95 g, 120 g and 150 g objects dropped from 1 and 1.5 m.
  - Impactor + Kimwipes (Imp KW): 95 g dropped from 1.0 and 1.5 m and 120 g object dropped from 1.0 m.

- Impactor + doors (Imp Do): 95 g, 120 g and 150 g objects dropped from 1 and 1.5 m.

All velocities measured were compared against the theoretical velocity reached due to gravity by an object falling from the height of 1.0 m and 1.5 m. Theoretical velocity was calculated  $v = gt$ , where  $v$  is velocity,  $g$  is the acceleration due to gravity (9.81 m/s<sup>2</sup>) and  $t$  is time. Time of fall was calculated  $t = \sqrt{\frac{2d}{g}}$  where  $t$  is time,  $d$  is distance and  $g$  is acceleration due to gravity (9.81 m/s<sup>2</sup>). The theoretical velocity was higher than the measured velocity in all conditions dropped from 1.0 m. In objects dropped from 1.5 there was no difference in velocity between the theoretical velocity and the 95 g object dropped from 1.5 m in the Imp KW group, the 150 g object from 1.5 m (except the Alu group), and the 120 g object dropped at 1.5 m. The objects suspended by the fishing line (Alu) from were slower than all other groups in the three conditions tested (chosen due to previous experiments done in the laboratory). Surprisingly, there was a significant difference between aluminum foil and door impacts with the 150g object dropped from 1.5 m, which may indicate a minimal variability due to the pulling of the drop pin by the operator.

Figure 2.11. Effect of friction on falling objects

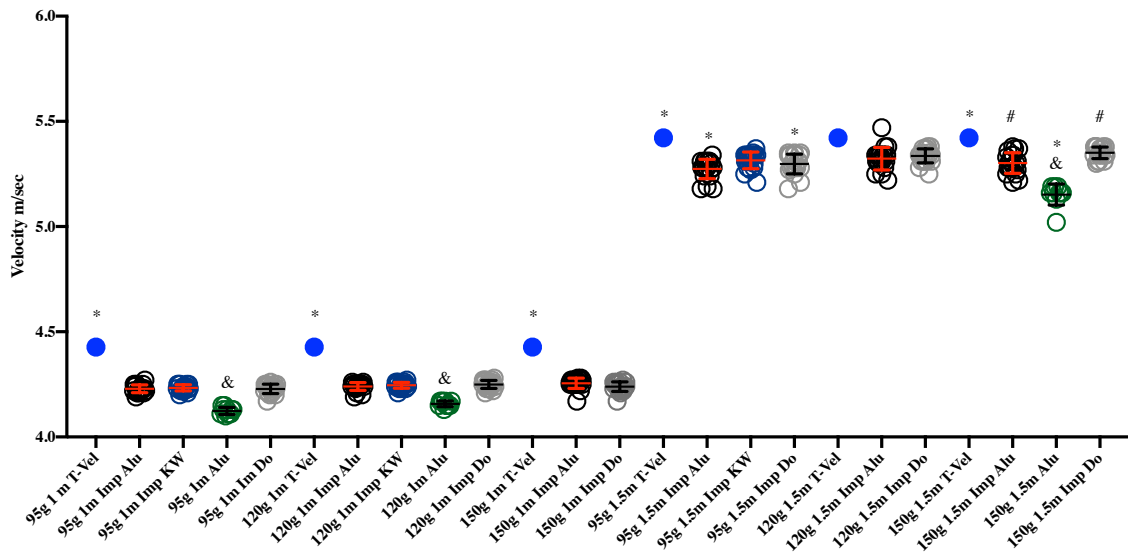


**Figure 2.11. Effect of friction on falling objects.** The effect of friction was assessed by comparing the velocity of the falling objects in different conditions used for this mechanical characterization of the model. Each condition is named by the weight of the object being dropped, followed by the height of the drop and finally the specific condition in which it is used. T-Vel = theoretical velocity; Imp = Impactor; and is followed by the type of support for the mouse: Alu = Aluminum; KW = Kimwipe; and Do = trap-doors. The group only labeled Alu, seen in green is the version of the apparatus that uses the fishing line. The dropped object velocities were significantly lower than the theoretical velocity attributed to gravity in a frictionless environment in all conditions at the height of 1.0 m. The differences decreased when the height increased at 1.5 m. However, some differences remained. Interestingly, in the 150 g object dropped from 1.5 m there was a difference between seemingly equal drops (black and grey). The use of a fishing line showed slower velocities in all the conditions dropped. Data shown in mean  $\pm$  SD, one-way ANOVA and multiple comparisons with Tukey's post-hoc test (Conditions with impactor n=20, conditions with fishing line n=10),  $p < 0.05$ .

## **The impact sensor can detect double impacts**

The impact sensor signal curve tells a broader story of the injury. A first impact (green arrow) can be seen for each of the support conditions. The impact on the Professional mouse supported by the aluminum foil (black line) and Kimwipes (blue line) follow a similar pattern. However, the impact with the trap-door support (gray line) shows an increase in amplitude and duration, that translates to a more severe injury. Additionally, different peaks were noted in the trap-door and Kimwipe supports which is suggestive of double impacts to the head of the mouse. In the trap-door support the second peak is immediate after the first impact and of considerable force (approximately 50 N) (Figure 2.12, red arrow). In contrast, the second peak with the Kimwipe support (Figure 2.13, black arrow) has longer elapsed time between peaks. This time between peaks suggests that it is likely an artifact, since the mouse is already on the foam cushion at that point. This demonstrates that the implementation of this model and sensors can differentiate between single and multiple impacts during injury.

Figure 2.12. Double impacts detected by impact sensor

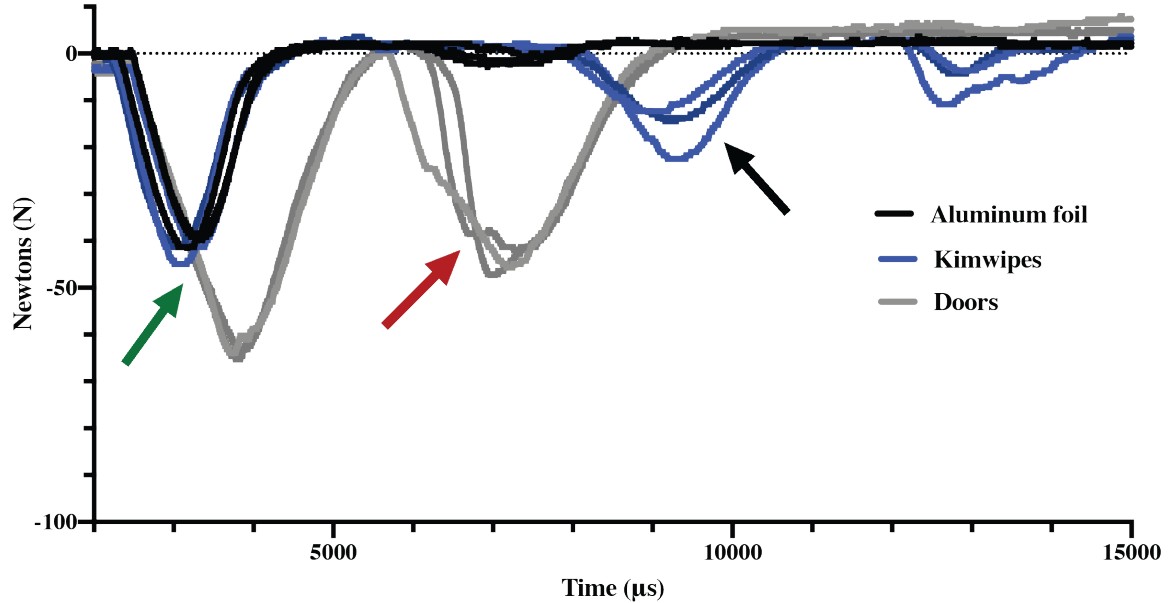


**Figure 2.12. Double impacts detected by impact sensor.** Different peaks were noted. All support conditions show a first impact (green arrow). The impact with the aluminum foil (black line) and Kimwipes (blue line) support follow a similar pattern. The impact is longer and yields more force with the trap-doors support (gray line). This support appears to induce a second impact (red arrow) immediately after the first. Kimwipes support also shows a second peak (black arrow) which is most likely an artifact, due to the time elapsed between peaks.

### A tolerance curve for the weight drop model

A mouse tolerance curve (like the one created for humans by researchers at Wayne State University) can be generated out of the measurements from our system. To accomplish this the duration of acceleration of every drop was measured (excluding the first iteration of the model, in which an accelerometer was not implemented). The acceleration of the head of the professional mouse was plotted against the time of acceleration for each object, height and support system. The impactor + aluminum foil

group clustered tightly with an increasing acceleration as the weight of the objects increased. The exception is the 95 g object dropped from 1.0 m, which exhibits a slightly larger variability in the time of acceleration than the other objects in this group. Kimwipes group shows higher accelerations with lower object mass and a longer acceleration periods, this is shown as a larger spread in both acceleration and duration, and are shifted to the right of the graph, which could account for empirical reports that the weight-drop model that uses Kimwipes as support produces a more severe injury with smaller object-weights and lower drop heights, when compared to the model by Kane. Finally, the trap-door group showed a greater range of accelerations and almost double the duration of acceleration of the other groups (Figure 2.13).

Figure 2.13. A mouse tolerance curve

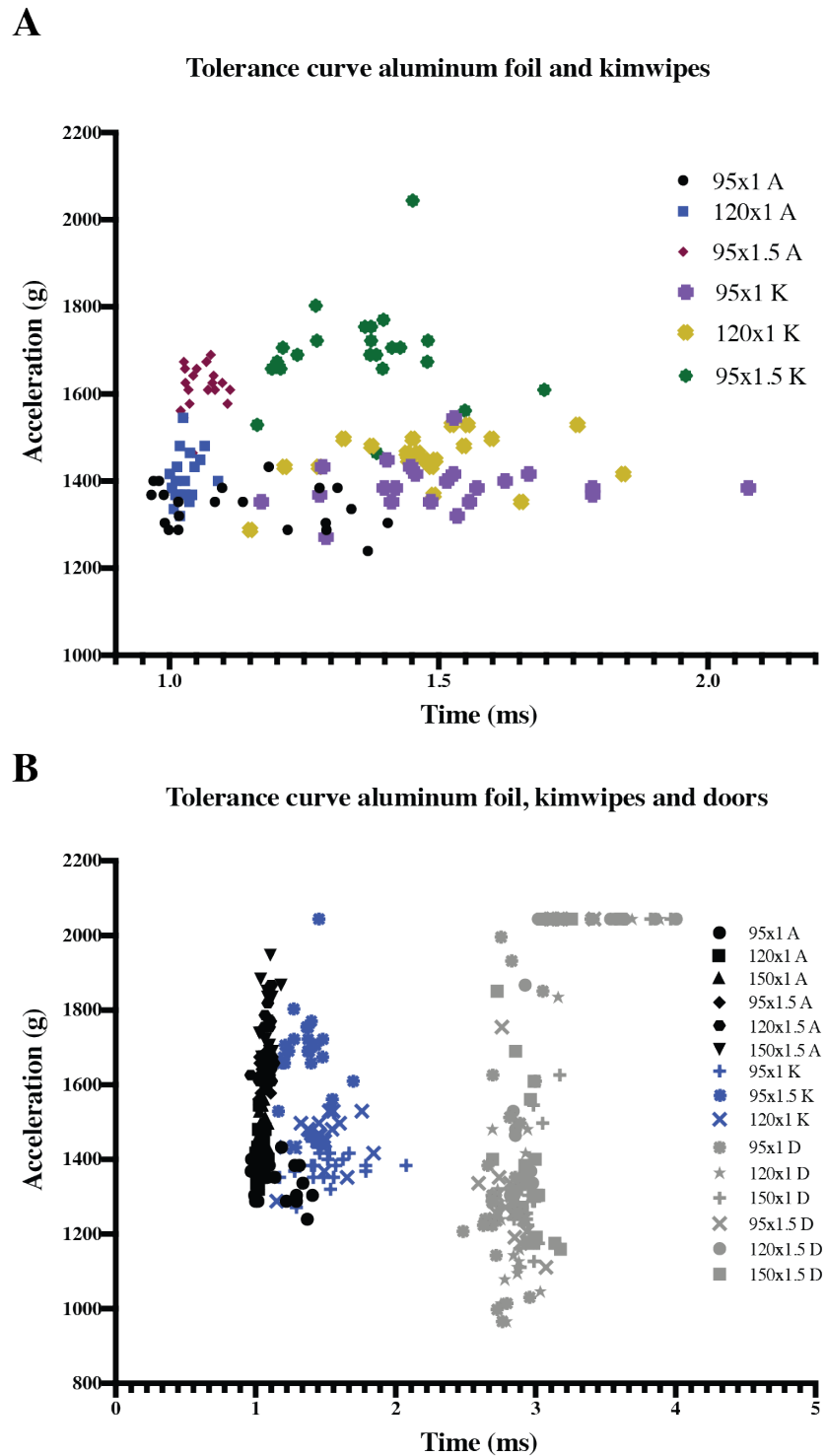


**Figure 2.13. A mouse tolerance curve.** A plot of acceleration in g (acceleration due to gravity) and duration in milliseconds (ms) was generated. A) The measurement from the

aluminum foil support system (labels ending in “A”) and Kimwipes (“K”). The aluminum foil group shows a more compact cluster on all three conditions when compared to the Kimwipes, which are spread wider and to the right. B) Clear groupings can be observed based on support systems. Aluminum foil groups show a tightly packed cluster (black). The Kimwipes group (blue) shows a wider spread and is shifted to the right. Trap-door group (gray) is the most variable and reaches higher accelerations. The variability of the trap-door groups is found in the acceleration of the head after injury. The duration of acceleration in the trap-door group almost doubled that of the other groups.

## **DISCUSSION AND CONCLUSIONS**

Weight-drop TBI models are one of the four most commonly used animal models in preclinical TBI research (Morales et al. 2005). Additionally, the weight drop group counts with the largest number of models within a group (Bodnar et al. 2019). Their popularity stems from the low cost, easy construction, and simplicity. However, the lack of controlled biomechanics of the weight-drop models and outcome variability has been a concern (Cernak 2005, Xiong, Mahmood, and Chopp 2013). Because of these concerns, there is a need for the generation of new systems that allow for the quantification of the mechanical inputs of the model and the biomechanical responses by the animals. In this study, we modified the weight-drop TBI model developed by Kane et al. (Kane et al. 2012). The primary objective was to optimize the model by detecting and fixing the areas of potential variability. The final result was a new apparatus with an integrated system that would allow for the continuous monitoring of the forces involved in the induction of TBI on the animals. To achieve this, we generated a new apparatus and integrated a system of sensors into the model to measure the kinematic parameters of the components that generate an injury.

The first modifications to the model developed by Kane et al. was a sensor generated to measure the velocity of the falling object immediately before impact. This sensor showed that the type of fishing line used had a significant effect on the velocity of the falling object, due to differences in the drag generated by the line. After choosing a fishing line that generated less drag and adding a pulley system, a set of experiments was conducted. These experiments showed low variability in the velocity of the falling weight. However, it was noticeable that as multiple drops were conducted, the fishing line became more elastic and the falling object would travel further, which might increase the variability of the outcomes after injury. These observations led to the modification of the system with the inclusion of an impactor between the falling object and the head of the animal. This impactor also housed the sensor designed to measure the force applied on the head of the animal. It eliminated the need for fastening the weight to a fishing line, since the falling object could not pass the impactor and the impactor traveled a fixed distance. Also, it provided a more consistent direction of the impact and eliminated lateral movement of the impactor's surface ensuring it was perpendicular to the horizontal plane. In the model where the animal gets impacted by the falling object alone, the surface of impact may change. This variability is generated by the falling object impacting the sides of the tube which may induce a change in angle of the objects axis once it leaves the tube and before it impacts on the animal head. These events may lateralize the impact and increase variability due to differences in the impacting surface (Cernak 2005, Namjoshi et al. 2014).

An unexpected finding in the force measurements with the use of the impactor was that all objects (95 g, 120 g, and 150 g) dropped from 1.5 m generated approximately the same force on the head of the mice, yet different behavioral outcomes. These results are contrary to reports in rats, in which variations in the skull size, shape and thickness can generate significant variations within drops of the same height and weight (Li et al. 2011). We theorized that higher weights of the falling objects resulted in increased skull

compression, even though force on the top of the head remained relatively unchanged. To test this, we generated a “Professional mouse,” an artificial silicone model of a mouse that had the head embedded with sensors to measure the effect of the forces induced by the impactor. This model allowed the recording of the forces applied to top of the head by an impact sensor in the impactor, the forces in the middle of the head by a force sensor and the resistance of the support system underneath by another force sensor. Additionally, it also allowed the measurement of the acceleration and speed of the head after impact. Increases in the forces recorded in the middle and on the bottom of the head demonstrate both an object-weight and drop-height dependent compression of the animal’s head.

Next, we compared the velocities of the falling objects between the different iterations of the apparatus (fishing line vs. impactor) and with the different support systems. Slower velocities were observed when the fishing line suspended the object. This difference in velocity could correspond to the increase in drag produced by the fishing line on top of the tube or higher movement of the falling object inside the tube, increasing friction and reducing speed (Cernak 2005, Piper, Thomson, and Miller 1996). Additionally, the velocities of the falling objects were slower than the theoretical velocities calculated solely based on gravity, confirming that a combination of tube and air resistance imparts friction on the falling object (Namjoshi et al. 2014).

Similar to the variability reported by Carre et al. (Carre et al. 2004), our measured speed variabilities in the apparatus with the impactor were 1% or lower, across all objects and all heights and generally less than 0.5% (SD ranged from 0.01395 to 0.05362 across all heights and objects). Our model shows less variability than other weight-drop models (Li et al. 2011). This variability could be reduced even further with the use of a metallic tube (Carre et al. 2004) and an automatic release mechanism (Li et al. 2011). The latter could reduce the variability seen in figure 2.11 in the 150 g object dropped from 1.5 m. In

general, the velocities of the objects in our model are lower than those in a modified Marmarou model for rats, using a 450 g weight. For objects without the fishing line dropped from 1.0 m, the velocities recorded in our model were  $4.22 \pm 0.01$ ,  $4.24 \pm 0.02$  and  $4.25 \pm 0.02$  m/s for the 95 g, 120 g and 150 g, respectively. In contrast, the rat model recorded faster speeds,  $4.54 \pm 0.06$  m/s for the 450 g object dropped from 1.25 m (Li et al. 2011).

Even though falling object velocities are similar across these models, our system induced significantly higher accelerations of the head and less variability. Accelerations ranging from  $1,339.82 \pm 49.58$  (g) to  $1,747.54 \pm 89.10$  (g) were generated by different object-weights and drop-heights on the artificial mouse model (variability represented as standard deviation). These acceleration measurements are higher when compared to Marmarou based models that generate  $907 \pm 501$  (g) and  $666 \pm 165$  (g) hit with a 450 g object dropped from 2.25 and 1.25 m, respectively (Li et al. 2011). This difference is maintained when compared to actual animal experimental data where 95 g object dropped from 1.0 m generated a mean head acceleration of  $804.00 \pm 82.12$  (g) and 150 g object dropped from 1.5 generated a mean acceleration of  $1,110.00 \pm 145.10$  (g). These values are significantly higher than those reported by Hsieh et al. of  $211.19 \pm 11.12$  (g) for a 450 g object dropped from 1.0 m and  $249.24 \pm 5.82$  (g) when dropped from 1.5 m (Hsieh et al. 2017). The higher accelerations in our model are most likely due to the breaking of the support system that does not decrease the acceleration as much as the foam support directly beneath the animal's head used in the Marmarou based models.

There are reports of variability due to the foam support in the Marmarou model (Piper, Thomson, and Miller 1996). Additionally, different laboratories use various breakable support systems (aluminum foil, Kimwipes, and trap-doors), and reports of higher severity of injuries with smaller object-weights and lower drop-heights in the Kimwipes model (Khuman et al. 2011, Meehan et al. 2012) when compared to the trap-

door and Kane's models (Kane et al. 2012, Briggs, Angoa-Perez, and Kuhn 2016). We therefore analyzed the kinematic and biomechanical differences of the head of the Professional mouse generated by these support systems. The impact sensor detected multiple hits on the head of the Professional mouse when using a door system held together by magnets. This finding is contrary to the report by Briggs et al. in which no double impacts were detected when using acrylic doors suspended by magnets (Briggs, Angoa-Perez, and Kuhn 2016).

Additionally, support systems affected the force and duration of impact, and thus may affect the severity of injury. Kimwipes showed higher variability, along with higher accelerations of the head after impact and longer impact durations when compared to aluminum foil. Similarly, doors showed higher forces (see Appendix A), acceleration and almost twice the impact duration when compared to aluminum foil and Kimwipes. The door system was also the one with the highest variability in these metrics.

Even though the biomechanical analysis of the weight-drop model has been done in the past (Li et al. 2011, Piper, Thomson, and Miller 1996, Hsieh et al. 2017, Carre et al. 2004), to our knowledge, our study is the first biomechanical and kinematic characterization of the new generation of weight drop models that incorporated the acceleration through falling after impact. Additionally, this is the first time that different models with similar characteristics have been compared biomechanically, including the forces induced on the object being impacted and the resulting kinematics after impact. It is essential that these systems are implemented in more laboratories to allow for comparison across laboratories and models. We showed that knowing the velocity of the falling object is not enough, since the variability in outcomes may be due to the response of the head to the impact. We hope that, by designing and characterizing a low-cost system like the one we used, that precludes any need for surgery or modifications to the animal, more

laboratories using weight drop models start implementing it and reporting the results. The limitations of this study included the use of a uni-axial accelerometer and the lack of angular acceleration measurements of the head of the animal. Also, the use of trap-doors made of aluminum instead of acrylic like the ones reported in the paper by Briggs et al. (Briggs, Angoa-Perez, and Kuhn 2016). The support system used for Kimwipes only represented one of the methods reported for that model. A different version of this model in which the Kimwipes are stretched by the hands of an investigator while supporting the mouse, instead of a fixed system (e.g. Kimwipes attached to a box), was not tested. Another limitation is that the materials used in the mouse do not mimic the scalp and skull. For this reason, the comparison with the other models included data from the experiments performed with animals, which were not included in this chapter. The use of this system opens up the possibility to determine the thresholds (in forces and accelerations) to induce different degrees of injuries in mice and rats. The accurate determination of these thresholds will help the field to objectively determine the severity of injury based on biomechanical measurements and reach a higher consistency in the injury severity.

## **Chapter 3 Model characterization**

### **INTRODUCTION**

Traumatic brain injury (TBI) is defined as an injury or physiological disruption of the brain induced traumatically by an external force that presents with at least one clinical sign: alteration of consciousness, memory loss, neurological deficits, or structural brain damage (Management of Concussion/mTBI Working Group 2009, Department of Defense 2010). This broad definition fits with the current view of TBI as a complex and highly heterogeneous disease (Centers for Disease Control and Prevention 2015, World Health Organization 2006, Maas et al. 2010, Andelic 2013). This complexity is also present in TBI classification. Clinically, TBI is classified as mild, moderate or severe based on the Glasgow Coma Scale, specific neurological parameters and structural imaging (Management of Concussion/mTBI Working Group 2009, Department of Defense 2010). However, TBI is not without nuance in its presentation, and all ranges of severity have the same probability of presenting long term consequences, ranging from approximately 40 to 50% (Thornhill et al. 2000). Thus, it appears that severity of TBI should be considered a spectrum, rather discretely stratified (Whyte, Vasterling, and Manley 2010).

TBI represents the primary cause of morbimortality in children and young adults (World Health Organization 2006). In the United States, 2.8 – 3.8 million cases of TBI are estimated to occur every year (Centers for Disease Control and Prevention 2015, Langlois, Rutland-Brown, and Wald 2006, Coronado et al. 2012). These cases can be divided into 75-80% mild, 12% moderate and 8% severe TBIs (Centers for Disease Control and Prevention 2015). In order to study TBI, many models have been generated. These models represent a simplification of the disease to study specific mechanisms and test potential treatments (LaPlaca et al. 2007). However, each degree of severity poses challenges when

generating animal models, since they should ideally reproduce the critical characteristics of the human pathology (Dewitt et al. 2013). This multitude of models generated to study TBI lacks the metrics that would allow the comparison of their results between laboratories. The inability to compare results between laboratories is considered one of the main reasons for the failure in therapeutic translation in TBI. With no means of comparison, the effect sizes of treatments cannot be assessed. For this reason, there has been an increased interest in the generation and report of common data elements (CDEs), which aim to standardize the data for comparison among laboratories (Smith et al. 2015).

Biomechanics of TBI have been instrumental in the understanding of the processes that generate primary injury and the subsequent secondary pathology (Holbourn 1943, Ommaya and Gennarelli 1974, Lissner, Lebow, and Evans 1960, Gurdjian et al. 1961). It is regrettable that the measurement of these metrics has not been broadly incorporated, since these could bridge the gap and improve the comparability of injuries among laboratories. Several groups have integrated these measurements to their models of TBI, including fluid percussion (Wahab et al. 2015), blast injury (Chandra, Sundaramurthy, and Gupta 2017, Kuriakose et al. 2016, Skotak, Alay, and Chandra 2018, Mishra et al. 2016), and impact-acceleration models based on the Marmarou weight drop model (Li et al. 2011, Piper, Thomson, and Miller 1996, Hsieh et al. 2017, Carre et al. 2004).

The impact-acceleration weight-drop models have been increasingly utilized due to their low-cost and simplicity. This animal model generates diffuse injury, and provides the possibility of graduating the severity of injury based on the weight of the object and the height of the drop (Marmarou et al. 1994, Foda and Marmarou 1994). The extensive characterization of the Marmarou model has highlighted a few areas of concern, including high mortality, skull fractures, double impacts, and low reproducibility in terms of the injury severity (Marmarou et al. 1994, Foda and Marmarou 1994, Xiong, Mahmood, and

Chopp 2013, Cernak 2005). Newer models have been generated that addressed some of these concerns. The high mortality, skull fractures, and double impacts were eliminated by creating a suspended support system (aluminum foil or Kimwipes) that break upon impact. This break of the support allows the animal to accelerate downward until landing on a foam cushion or being suspended by the tail (Mannix et al. 2014, Mannix et al. 2013, Meehan et al. 2012, Kobeissy et al. 2016, Dapul et al. 2013, Khuman et al. 2011, Yates et al. 2017, Kane et al. 2012, Mychasiuk et al. 2014).

To address the reproducibility concerns in the impact-acceleration model of weight drop, we generated a new apparatus (Chapter 2) based on the model developed by Kane et al. (Kane et al. 2012). This new apparatus has a system for quantifying the forces involved in the induction of TBI and the biomechanical response of the animal's head. Additionally, its mechanical reproducibility has been extensively characterized (Chapter 2). This new model was designed to generate a spectrum of injuries and be used in single TBI (sTBI) and repetitive mild TBI (RmTBI). Since substantial modifications were done to generate the new apparatus, this study focusses on the biomechanical and behavioral characterization of the model. To our knowledge, this is the first time that biomechanics of the head of the animal are assessed on these new versions of the impact-acceleration weight-drop models with a breakable support systems.

## **MATERIALS AND METHODS**

### **Animals**

All animal procedures were approved by the University of Texas Medical Branch Institutional Animal Care and Use Committee (IACUC). One hundred two-month-old C57BL/6j male mice (000664, Jackson Lab, Sacramento, CA) underwent habituation to the housing area for seven days. Mice were group-housed in a light-controlled room with

12-hour light/dark cycle and *ad libitum* access to food and water. All tests were performed in the light cycle, between 6:00 am and 6:00 pm. After habituation, ear tags with ID numbers were applied and a general health assessment was done, including physical characteristics (body weight [BW], fur and whisker appearance), basic neurological reflexes (righting reflex [RR], whisker reflex, ear twitch and eye blink), and behavior in the home cage (regular activity and rest, exploratory behavior, grooming and nesting). Baseline BW was measured every day, and handling of the mice for one minute every day for six days was done to reduce handler generated anxiety.

### ***SELECTION AND RANDOMIZATION***

Mice were randomly assigned into one of ten groups based on the bodyweight of the day before the injury (Day -1):

Table 3.1. Experimental groups of mice for model characterization

Group #	Object mass (g)	Drop height (m)	# Injuries	Day of Injury
1	Sham	0	0	D0-D4
2	95	1	1	D0
3	120	1	1	D0
4	95	1.5	1	D0
5	120	1.5	1	D0
6	150	1.5	1	D0
7	95	1	5	D0-D4
8	120	1	5	D0-D4
9	95	1	1	D4
10	120	1	1	D4

Figure 3.1. Experimental design

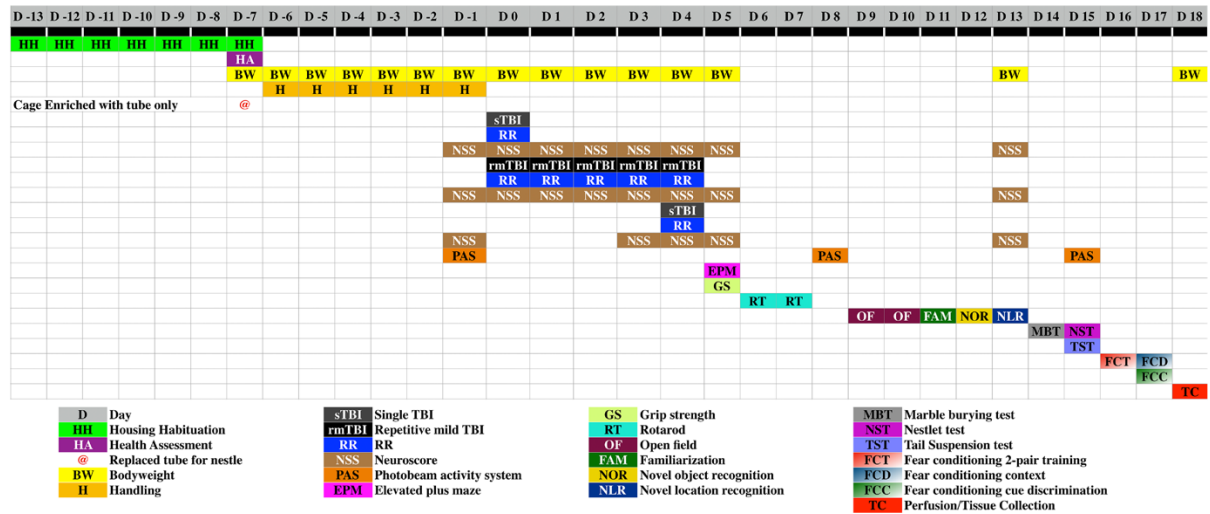


**Figure 3.1. Experimental design.** The schedule for all tests performed. Every procedure is color coded and placed on a different row. Columns represent the number of days before or after the first injury (set as D0). Legends can be seen underneath the table.

### Novel TBI apparatus

A new closed-skull weight-drop injury system was established (see Chapter 2) optimized from the model developed by Kane et al. in 2012 (Mychasiuk et al. 2014, Kane et al. 2012). Briefly, the model (Figure 3.2) was constructed with a solid aluminum base (MB1218, ThorLabs, Newton, NJ), 30 cm above the ground, with a steel plate that holds an impactor. A 72 in high construction rail (XE25L900/M, ThorLabs, Newton, NJ) was attached to the base, holding a 22.22 mm I.D. and 1.7 m length PC guiding tube (175-54, AAA Plastics, Inc., Cypress, TX) oriented vertically such that the bottom opening is above the steel plate. The impactor was placed inside the bottom of the guiding tube, and outside of the tube and above the impactor, the velocity sensor was attached (Chapter 2). Three holes (5 mm in diameter) at 0.5, 1.0 and 1.5 m above the impactor were drilled to serve as sites from which the brass objects were held and dropped. The 24.5 g impactor containing

a force sensor (uniaxially poled PVDF film, Precision Acoustics, UK) (Chapter 2) was held in place by three 5 x 1 mm neodymium magnets (HHOOMY, US) placed in the bottom of the steel plate. Two plastic PEEK tubes were also attached here to serve as indicators for head positioning.

Below the solid aluminum base of the system, an open acrylic chamber with a foam cushion (Figure 3.2) (premium poly foam 4"x22"x22", American Excelsior Company, Arlington, TX) was placed to hold an aluminum foil sheet that support a mouse under the impactor.

Three cylindrical brass objects (95, 120 and 150 g), custom milled from a 19 mm diameter brass rod, a fishing line (1.0 m, Super Strong Trilene® Big Game™ 20 LB, BGQS20C-81, Berkley®) traversed the objects through a central hole and was glued inside. The fishing line permitted the lowering of the objects through the guiding tube to the designated drop heights.

### **Signal processing and software**

Signals from both transducers were digitized with a 2-channel digital oscilloscope (USB-5132, National Instruments, Austin, TX) at 200 kHz sampling rate and transferred to a computer. A custom-designed program written in LabVIEW (Version 2018, National Instruments, Austin, TX) was used to collect, process and store the temporal profiles of the signals from the force sensor and accelerometer (see Chapter 2). A custom-written code was used to measure, collect and process the phototransistor velocity sensor data, using the Arduino software (Version 1.8.1, Arduino.cc, Somerville, NJ) (see appendix for code).

### ***INJURY SYSTEM SETUP***

Before the injury day, 30 x 25 cm sheets of aluminum foil (01-213-101, Fisher Scientific, Hampton, NH) were cut. Fifteen sheets were stacked together, and twelve perforations (one every cm starting at the edge) were made along the midline (about 15cm from each side) with a stainless-steel surgical blade #15 (0086, Bard-Parker, Aspen Surgical, Caledonia, MI). The aluminum foil sheet was used as support for the mice by covering the top aperture of the acrylic chamber. The sheet was placed with the edge where the perforations began toward the impactor. The impactor was directly over the space between the second and third perforation in the aluminum foil sheet. The edges of the aluminum foil sheet were held in place to the sidewall of the chamber with approximately 10 cm of invisible tape (520928, Office Depot, Boca Raton, FL).

White Washable Art-Time Tempera paint (17-3496, Sargent Art®, Hazelton, PA) was added to the tip of the impactor to mark the area of impact on the head of the mouse.

### ***ANESTHESIA AND PHYSIOLOGICAL MEASUREMENTS SETUP***

SomnoSuite® anesthesia system (Figure 3.2) (Kent Scientific, Torrington, CT) with a 0.5 L chamber (SOMNO-0705, Kent Scientific, Torrington, CT) and a small low-profile anesthesia mask (SOMNO-0801, Kent Scientific, Torrington, CT) used to administer general anesthesia. Before the injury, mouse ID number and BW were collected. The ID and BW were input into the Somnosuite® anesthesia system, and isoflurane was set to 2.5% mixed with room air. The anesthesia flow volume is based on the inputted BW. The ID was input into the Physiosuite® system with MouseSTAT® pulse oximeter & heart rate monitor module (Figure 3.2) (Kent scientific, Kent Scientific, Torrington, CT). The recording was captured by Serial software (Version 1.3.5, Decisive Tactics, Inc.) for both systems. The ID, BW, object mass, drop height and number of injuries were input into our

custom-made Labview (Version 2018, National Instruments, Austin, TX) injury system software.

Figure 3.2. Injury system, anesthesia and physiological measurement systems

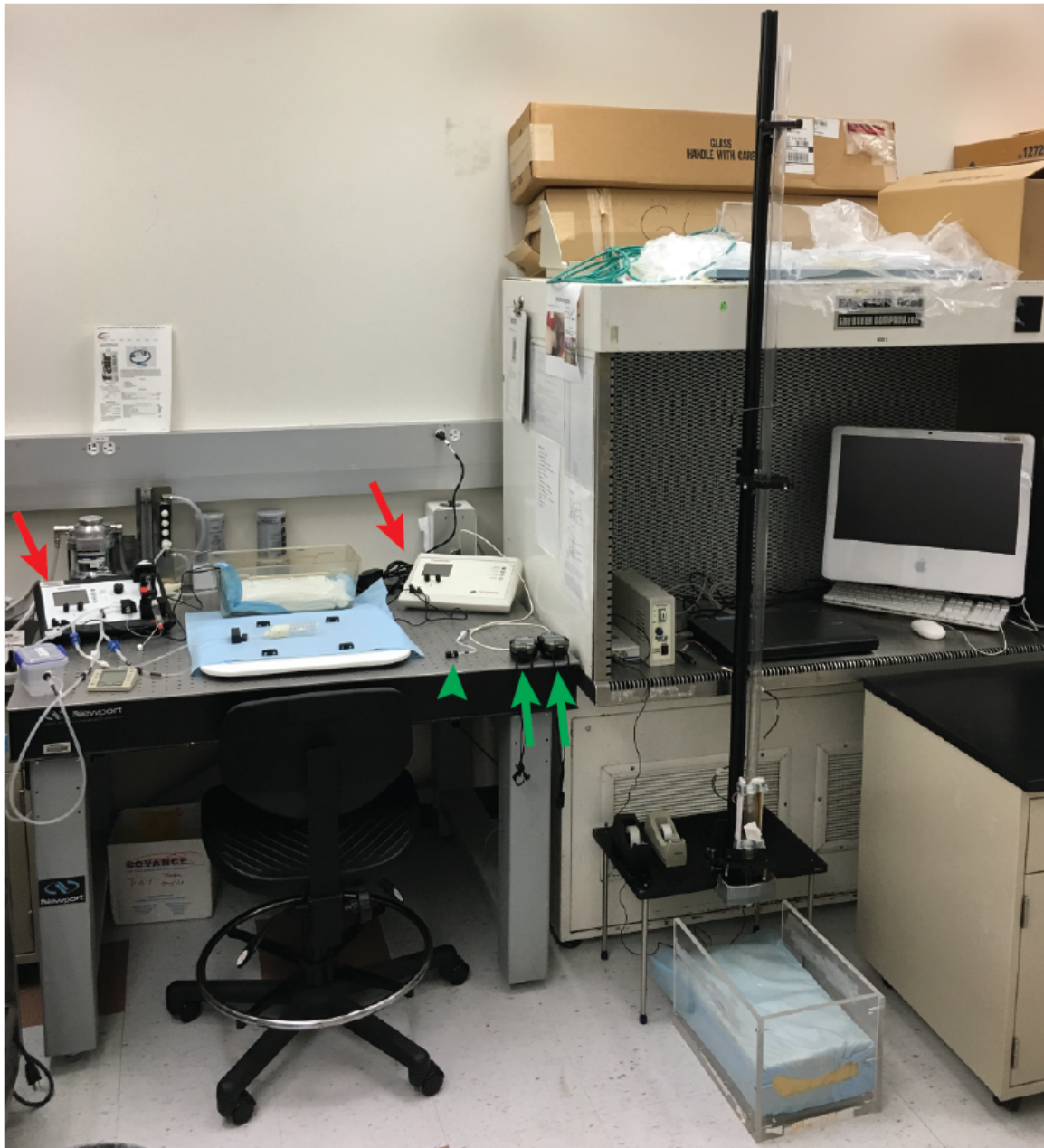


**Figure 3.2. Injury system, anesthesia and physiological measurement systems.** The complete injury setup includes the weight-drop injury apparatus and two computers used

for all data collection (sensors, physiological measurements, and anesthesia) on the right. On the left, the arrangement of the Somnosuite®, and Physiosuite® modules (red arrows), a heated pad to maintain the body temperature of the mouse during the anesthesia and righting reflex (RR) (between the two modules). In the middle, a pulse oximeter (green arrowhead) and two chronographs are kept in the area to measure the time elapsed to the recovery of the RR.

### **Injury and righting reflex**

Mice were individually transported from their home cage to the anesthesia system chamber, and isoflurane 2.5% was initialized until the mouse lost its righting reflex. The system was flushed (anesthesia was removed from the chamber; this takes 10 seconds) and the animal was transferred from the chamber to the anesthesia cone. At this point the accelerometer (352A73, PCB Piezotronics, Inc., Depew, NY) was secured to the head of the mouse via two plastic twist ties that were pushed together above the neck and nose of the mouse; simultaneously, a pulse-oximeter clip was placed in the mouse's right hind paw. Pinch paw and tail reflexes were evaluated, and the anesthesia was turned off as soon as both disappeared. At this point, a chronograph was initiated to measure the elapsed time to the recovery of the righting reflex (RR). The animal was placed above the aluminum foil directly underneath the impactor aimed to hit in the midline between the ears and eyes. Injury system software was armed, and the Allen key holding the brass object was pulled, allowing it to drop. The falling object pushed the impactor which in turn hit the top of the animal's head mounting pressure on the aluminum foil underneath, causing it to break and allowing the animal to accelerate downward and forward in free fall until it landed on the cushion 10 cm below the aluminum foil. After removing the accelerometer, the mouse was recovered from the system and transported to a warming pad (37°C) and placed in the supine position. The pulse-oximeter was placed again in its right hind paw, and any further

stimulation was avoided until the mouse recovered the prone position at which time the chronograph was stopped, and a photo was taken of the mouse head to show the position of impact.

## **Behavioral tests**

### ***NEUROLOGICAL SEVERITY SCORE (NSS)***

NSS (Chen et al. 1996) was established as a rodent equivalent of the functional neurological and cognitive outcome assessment, the Glasgow outcome scale (GOS) in humans (King, Carlier, and Marion 2005). The NSS evaluates deficits in neurological motor function. After several iterations, the NSS was finally condensed into a 10-item test (Flierl et al. 2009, Khalin et al. 2016, Tsenter et al. 2008). One point is awarded for each failed task; therefore, a healthy or uninjured mouse should score 0. The ten tasks of NSS are shown in Table 3.2. Briefly, in task 1, a mouse was placed in the center of a round arena (30 cm diameter) with an opening. The mouse was allowed to explore (Figure 3.3, B) and expected to leave the arena within 3 minutes; failure to do so resulted in one point. In task 2, signs of seeking behavior were evaluated by examining the mouse via a mirror that was placed on top of the round arena to visualize behavior during task one. In task 3, mice were placed back on the arena and gait was observed; a point was given if animals did not walk straight or other gait impairments were seen. In task 4, the experimenter performed a loud clap and the mouse reaction was observed. Lack of a reaction was graded as one point. In task 5, mice were observed for paralysis, lateralization in locomotion and ability to grip anatomic forceps. Animals were suspended by the tail and allowed to grab the forceps; the strength of the hold was tested. Failure to grip or low grip strength was counted as one point. In task 6, mice were placed in a 7 mm wide square beam (Figure 3.3, A and C), and mice were expected to maintain balance for 10 seconds. Failure to do so resulted in one point. In tasks 7, 8 and 9, mice were placed in one side of a beam (Figure 3.3, A and C)

and were expected to cross to the other side. Mice were given 3 minutes to cross three beams of decreasing width (3, 2 and 1 cm). Mice were given 3, 2 or 1 points if they failed to cross the wide, middle or narrow beams, respectively. In task 10, mice were helped to perch on a round beam (Figure 3.3, A and C) (5 mm in diameter) and were given one point if unable to maintain balance for 10 seconds.

Figure 3.3. Neurological severity score (NSS)

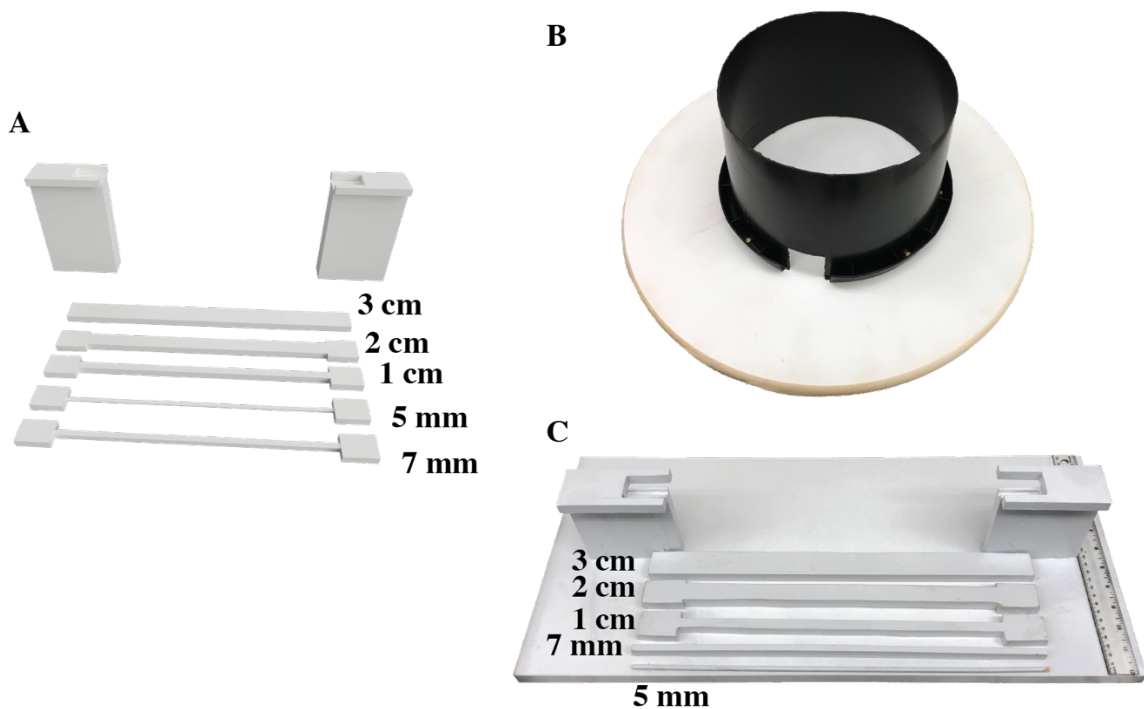


**Figure 3.3. Neurological severity score (NSS).** The different components for the NSS test were built. A) A 3D render of the bases and beams with the different widths, which can be 3D printed in the future. B) The arena was made with a bucket (30 cm in diameter) and screwed to a wooden baseboard. C) The beams were made out of wood, and cut to the desired width. All components were painted white with a waterproof paint.

Table 3.2. Neurological severity score

<b>TASK</b>		<b>POINTS FAILURE</b>
1	Circle exit	1
2	Seeking behavior	1
3	Straight walk	1
4	Startle reflex	1
5	Monoparesis/hemiparesis	1
6	Beam balance 7mm square beam	1
	Beam walk	
7	Beam 3cm wide	1
8	Beam 2cm wide	1
9	Beam 1cm wide	1
10	Round stick balance 5mm in diameter	1
Maximum score		10

#### ***EXPLORATORY BEHAVIOR AND LOCOMOTOR ACTIVITY***

To measure exploratory behavior and locomotor activity two systems were used: open field (OF) and photobeam activity system (PAS).

#### **Open field (OF)**

This test was used as part of the habituation for the novel object (NOR) and location recognition (NLR) tests (Figure 3.5, see below). Following a protocol described elsewhere (Cortez et al. 2017) with minor modifications, mice were introduced in the center of a white Plexiglas™ open field box (38 x 38 x 38 cm) and allowed to explore freely for 10 minutes. The light was adjusted to be approximately 100 lux in the center of the box. Behavior was captured and analyzed in digital video with the TopScan software (Ver 3.0, CleverSys Inc., Reston, VA). Center and periphery arenas were created for thigmotaxic analysis (see below and Figure 3.6). Distance traveled, average velocity, time spent, and percent of exploration were measured in the center, periphery, and entire arena.

### Photobeam activity system (PAS)

PAS was used to measure exploratory behavior and locomotion activity, including rearing events, distance traveled, time spent in the center, periphery and entire box (see thigmotaxis below). Briefly, mice were randomly assigned to a box at baseline (day D-1) and repeated all time points (days D8, D15) in the same box. Mice were placed in the center of a clear acrylic (40x40x40 cm) OF box and allowed to explore for 10 minutes. Behavior information was collected by photo-cell beam breaks placed in two frames at different heights: the first with a photo-cell height of 2.5cm from the ground (for horizontal exploration) and a second frame at 4.5cm from the ground (for rearing or vertical exploration). Information was recorded automatically by the PAS software and analyzed in PAS Reporter (San Diego Instruments, San Diego, CA). Equipment was cleaned with 50% ethanol and allowed to air dry in between each animal.

### Rotarod test

Balance, motor coordination and learning were assessed with the accelerating rotarod test following a Hernandez et al. protocol (Hernandez et al. 2010) with modifications. Mice were placed on a cylindrical bar in the Dual Species Economex Rotarod (0207-003M, Columbus Instruments, Columbus, OH) and assessed balance was assessed on a static and constant speed rotating bar at 4 RPM for 30 seconds each. Following the habituation to the bar, motor coordination was assessed on a rotating bar that accelerated 0.1 RPM/sec by measuring latency to fall. Mice underwent three trials per day with an inter-trial rest of no less than 30 minutes on days D6 and D7.

### Grip strength

Grip strength test was used to assess forelimb strength (Cortez et al. 2017). Briefly, a mouse was grabbed by the base of the tail and lowered to a metal frame connected to a gauge meter DFIS-2 Digital Force Gauge (Chantillon®, Largo, FL). The mouse was then gently pulled away horizontally until it could no longer grasp the metal frame. The

procedure was performed in triplicate, and average grip strength was measured in Newtons (N).

## ***MEMORY***

### Novel object (NOR) and novel location (NLR) recognition

Novel object recognition was used to assess spontaneous memory following the one-trial protocol described elsewhere (Ennaceur and Delacour 1988, Dere, Huston, and De Souza Silva 2007, Leger et al. 2013) with minor modifications. Briefly, animals were randomly assigned to one of four arenas and completed the whole protocol in the same arena. Animals underwent a five-day paradigm (D9-D13) (Figure 3.4). On days D9 and D10 mice underwent a habituation stage to the OF (see above for behaviors analyzed) to reduce neophobia-induced anxiety.

On day D11 mice were subjected to the familiarization stage for 10 minutes. During this stage two familiar (equal) objects (T75 culture flasks with non-vented caps [156472, Thermo Scientific, Waltham, MA] filled with corn cob bedding [Bed-o’cobs®, The Anderson Lab Bedding, Maumee, OH] for added weight [Figure 3.4, E]) were placed in the corners of the OF, 10cm apart from each wall. The mice were permitted to habituate and explore the objects (Figure 3.4, B). The objects were positioned radially, allowing the camera (placed above, in the center of the four boxes) to record each animal with the same angle. When animals were introduced in the maze, they had the same perspective regardless of the arena. The light was adjusted to measure 95-105 lux in the center of each box and was maintained for the five-day paradigm. Time exploring each object (nose to object, sniffing and the combination of both) was analyzed to ensure no object or place preference was found in any of the four arenas. Additionally, all open field metrics were measured.

Twenty-four hours after the familiarization stage, on day D12, mice were re-exposed to the OF for the NOR test (Figure 3.4, C). A novel object (a 150ml analytical filter [130-4045, Nalgene™, Thermo Scientific, Waltham, MA] filled with corn cob bedding [Bed-o’cobs®, The Anderson Lab Bedding, Maumee, OH], for added weight [Figure 3.4, E], every opening filled with cold silicon, meticulously cleaned with 50% ethanol and allowed to dry to avoid odors) replaced one of the familiar objects in the OF. Mice explored freely for ten minutes, novel and familiar object exploration and open field metrics were recorded and analyzed.

Mice were re-introduced into the OF on D13 for the NLR test, after a 24-hour inter-trial period. The familiar object left in the OF was changed to a different corner location (Figure 3.4, D). Mice were allowed to explore the arena and object for 10 minutes, and the same parameters as in NOR were recorded. To eliminate residual odor cues a 50% ethanol-water solution was used to thoroughly clean the arena and objects before and after each animal. This was done for all stages of the test. Digital video recording and analysis was done with the TopScan software (Ver 3.0, CleverSys Inc., Reston, VA).

Figure 3.4. Novel object and location recognition paradigm

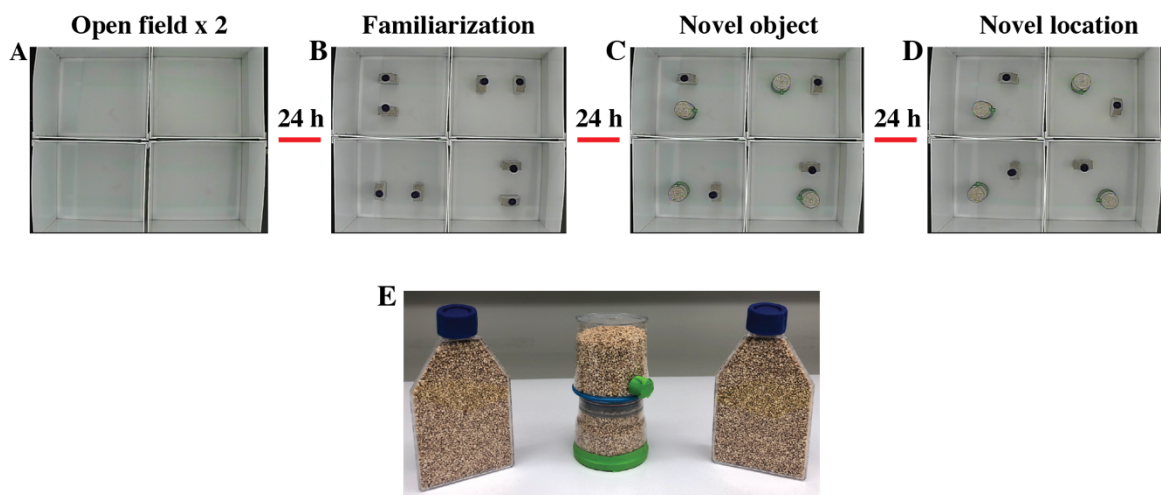


**Figure 3.4. Novel object and location recognition paradigm.** This experimental design followed the one-trial paradigm for novel object (NOR) and location recognition (NLR) tests. A) Animals were exposed to the open field arena for habituation twice for 10 min, 24h apart. B) The third day was the familiarization of the animals to the objects. Note the radial distribution of the objects allowing the camera to record every arena from the same angle, and so that the animals to experience identical perspectives when released in the inside corner of the boxes. C) After an inter-trial period of 24h animals were tested for NOR where one of the objects was exchanged for a novel object. D) After another inter-trial period of 24h, the animals were tested for spatial memory in the NLR where the familiar object was moved to a new location. E) The objects used were non-vented T75 flasks and 150 ml Nalgene filter.

### Fear Conditioning (FC)

FC and conditioned fear-tested associative learning were assessed using a protocol published elsewhere (Dineley et al. 2002, Rodriguez-Rivera, Denner, and Dineley 2011, Hernandez et al. 2014), with modifications. On day D16 mice underwent a 7-min two-pairing paradigm of an acoustic-cue and a mild foot-shock. Briefly, mice were introduced in the FC system (80004AT, Lafayette Instruments, Lafayette, IN) and allowed to explore for 3 minutes, followed by the first of two pairings of a 30-s acoustic conditioned stimulus (aCS; white noise, 70-74 dB) with a 2-s shock unconditioned stimulus (sUS; 0.5 mA) during the last 2 seconds of the aCS. This pairing was repeated at 5 minutes of exploration. On day D17 after a 24-hour inter-trial period, mice were assessed for contextual fear learning. They were reintroduced into the FC system, without any modifications to the environment. The freezing behavior was recorded for 5 minutes. Finally, cued fear learning was evaluated. The transport to the test room was modified, using 1-200  $\mu$ l pipette tip boxes (1111-0810, TipOne, USA Scientific, Inc., Ocala, FL). The fear conditioning boxes context was also changed. A white corrugated twinwall plastic sheet (COR-2436-15, Home Depot,

Atlanta, GA) custom cut was used to cover the grid floor. A black corrugated twinwall plastic sheet (COR-4896-BK, Home Depot, Atlanta, GA), custom cut to form a three-part insert was used to change the shape of the box into a triangle, and a new odor was introduced (5  $\mu$ l of peppermint extract [041313011130, Adams, Gonzales, TX] pipetted to a paper towel pasted behind the newly introduced wall). Mice were introduced into the new environment and allowed to explore for three minutes to record baseline behavior. Immediately after, the aCS was played for three minutes, and freezing behavior was recorded. Video capture and analysis of freezing behavior were done with FreezeFrame 4 software (Actimetrics, Wilmette, IL). Freezing behavior was observed for each animal, a threshold was set (distinguishing between freezing and grooming or sniffing) and percent of freezing was calculated.

Figure 3.5. Fear conditioning experimental design and novel context setup

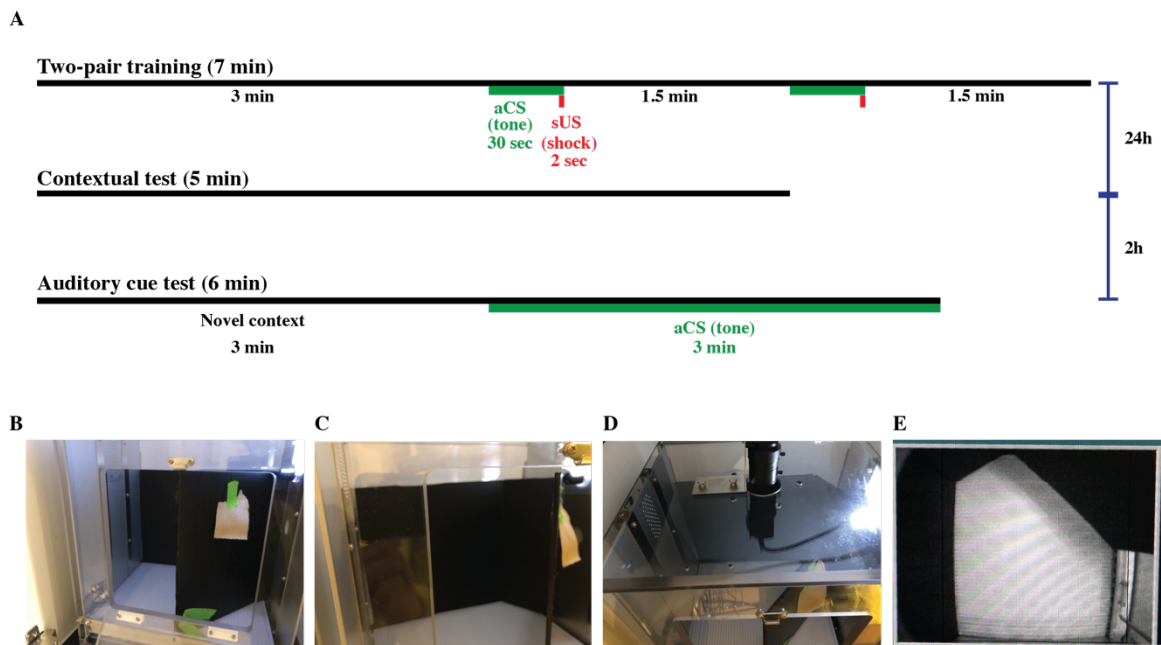


**Figure 3.5. Fear conditioning experimental design and novel context setup.** A) Fear conditioning experimental design begins with a two-pair training paradigm in which a shock unconditioned stimulus (sUS) comprised of a mild foot shock (0.5 mA) is paired

with an acoustic conditioned stimulus (aCS), white noise (70-74 dB). This pair of stimuli are done twice, at 3 min and 5 min of the 7 min training. Twenty-four hours after training, the mice are reintroduced in the same boxes and recoded for five minutes to measure contextual memory. Two hours later, they are introduced in the boxes with a modified environment, recoded for 3 minutes as freezing baseline, followed by the aCS for three minutes at which point cued memory is assessed. B) Side view of the FC box with the context modification depicted. A black plastic wall is visible with a paper towel attached to the wall with a green tape. This paper towel is used to absorb 5 $\mu$ l of peppermint extract to generate a new smell. A white plastic floor is covering the metal grid. C) A different side view where the inside of the area enclosed by the black plastic wall can be seen. D) A view of the top of the box showing the lighting and position of the recording camera. E) The camera view shows the new shape of the arena with the black plastic insert, used as walls and the grid floor is covered by a white plastic insert.

### ***ASSESSMENT FOR MOOD DISORDERS***

#### **Thigmotaxis (open field)**

Thigmotaxis is the response of an organism to a stimulus. In behavioral experiments in mice (Barnett 1976) and humans (Walz, Muhlberger, and Pauli 2016), it has been defined as the choice to stay close to walls or away from open spaces, (i.e. the center of the open field). Thigmotaxis has been related to agoraphobia-mediated anxiety in humans (Walz, Muhlberger, and Pauli 2016) and rodents (Kurhe et al. 2014) in the OF test. The open field and PAS tests were used to evaluate anxiety-like behavior, following previous protocols. For open field (Cortez et al. 2017), the arena was split into a central area (12.6 cm<sup>2</sup>) and a peripheral area (25.4 cm<sup>2</sup>) used to measure distance traveled, velocity, time and percent of time spent in each area (Figure 3.6, A). For the PAS, two different protocols were used to analyze anxiety-like behavior. For the first protocol, the field was split into

periphery (from the wall to 10 cm) and center [10 cm to the center (20 cm)] (Figure 3.6, B). Thigmotaxis was calculated from time spent or distance covered in each area as  $\frac{Periphery}{Periphery + Center}$ , in which the higher the result, the higher predilection of the mouse to stay close to the walls. The second protocol, which might show higher sensitivity splits the arena into eight concentric squares (A-H) each measuring 2.5 cm wide (Figure 3.6, C).

Figure 3.6. Thigmotaxis in open field (OF) and photobeam activity system (PAS)

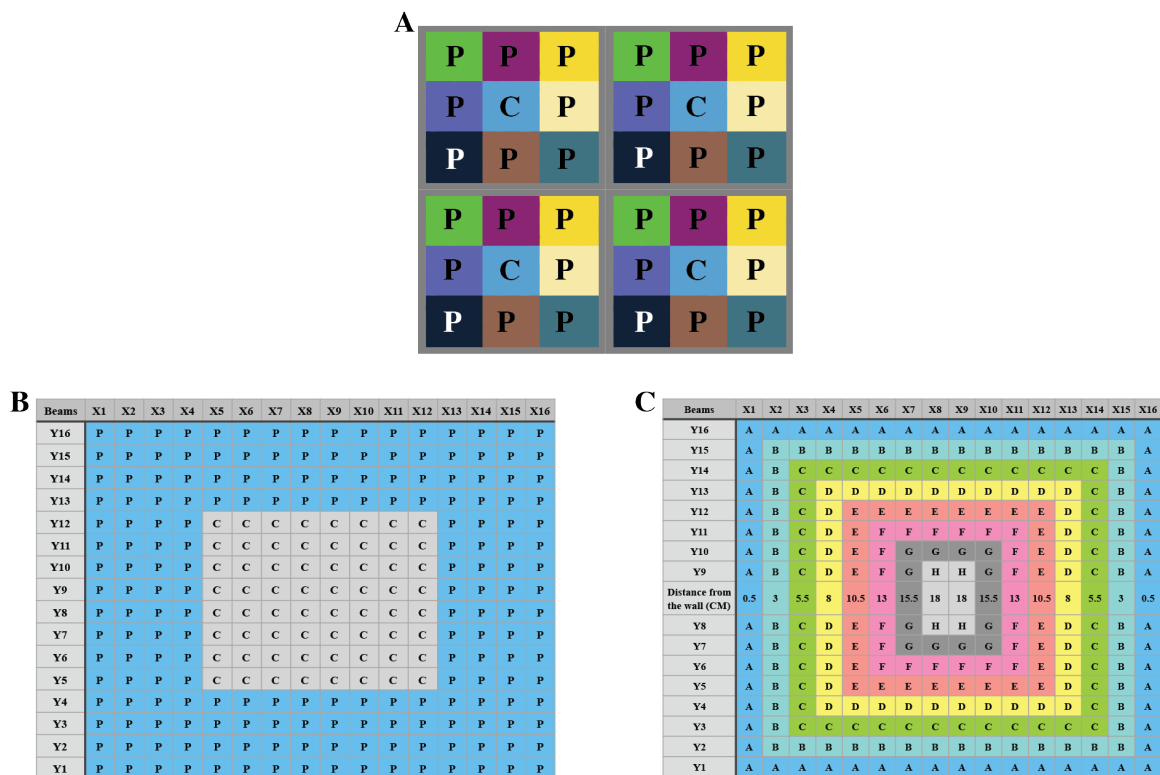


Figure 3.6. Thigmotaxis in open field (OF) and photobeam activity system (PAS).

Thigmotaxis was used to study anxiety-like behavior. This behavior was measured in two different OF test. A) The Topscan open field arena was split into nine squares of equal size divided in center “C” and periphery “P.” B) Similarly in the PAS OF, two zones, center “C” and periphery “P,” were generated. C) Additionally, to gain higher resolution of mapping anxiety-like behavior, the PAS OF was divided into concentric squares, with a known distance from the wall.

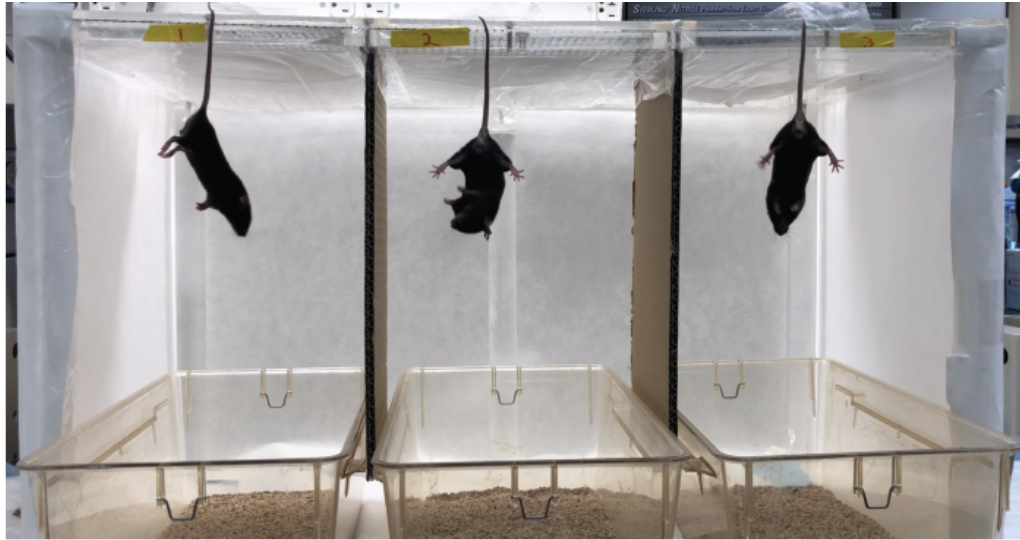
### Elevated plus maze (EPM)

A single exposure paradigm of EPM (platforms 50 cm off the ground, 30 cm long x 6 cm wide with walls in the closed arms 13 cm tall) was used to measure anxiety-like behavior (Walf and Frye 2007, Cortez et al. 2017). The EPM is known to induce acrophobia-related anxiety in rodents and humans (Biedermann et al. 2017, Walf and Frye 2007, Ari et al. 2019). The light was adjusted to 100-106 lux in the closed arms, 120-126 in the center and open arms. Briefly, on day D5 mice were placed in the center of the EPM facing an open arm and allowed to explore for 5 minutes. Entries, time, distance, velocity and percent time in center, open and closed arms were recorded and calculated with the TopScan software (Ver 3.0, CleverSys Inc., Reston, VA). EPM was cleaned with 50% ethanol and allowed to air dry between animals.

### Tail suspension test (TST)

This test was used to assess depression-like behavior as stress-induced immobilization (Cryan, Mombereau, and Vassout 2005). Using methods described elsewhere (Steru et al. 1985, Castagne et al. 2010) with modifications, total immobility and percent of immobility in 5 minutes were measured. Briefly, mice were randomized to one of three arenas, in a Vonn Frey frame split into three sections (Figure 3.7) and hung by their tail (with tape 1 cm from the tip of the tail) from the acrylic border of the frame. Behavior was recorded for 5.5 minutes. Videos were analyzed blinded, and immobility time was measured in 5 minutes of test and calculated as a percentage of the total time.

Figure 3.7. Tail suspension test arena



#### ***ASSESSMENT FOR HIPPOCAMPAL DAMAGE***

##### **Marble burying test (MBT)**

MBT has been used as a measure of anxiety or compulsive-like behavior (Angoa-Perez et al. 2013, Londei, Valentini, and Leone 1998, Taylor, Lerch, and Chourbaji 2017, Thomas et al. 2009). However, disputes in interpretation exist (Wolmarans, Stein, and Harvey 2016, Deacon 2006) because marble burying is considered species-typical behavior, correlated with digging and burying (Deacon 2006). MBT is considered a test to assess the effect of anti-anxiolytics and antidepressants (Deacon 2006, Nicolas, Kolb, and Prinssen 2006, Broekkamp et al. 1986). Interestingly, MBT alterations have been associated with hippocampal lesions (Deacon and Rawlins 2005). In this study, MBT was used to assess changes in species-typical behavior and as a proxy for hippocampal damage. Briefly, 28 black glass marbles 1.25 cm in diameter were placed in a grid, separated equidistantly in four columns and seven rows in a standard rat polycarbonate cage (26 x 48 x 20 cm) with 5 cm of bedding (Figure 3.8, A and B). A mouse was placed in a cage and allowed to explore for 30 minutes. The number of buried marbles (2/3 of total volume

covered by bedding), which was measured as a percent of the total number of marbles, was counted by two observers blinded to the injury status of the mice (Figure 3.8, C), and the average of both observers was calculated.

#### Nestlet shredding test (NST)

NST has also been used in the past as a measure of repetitive or compulsive-like behavior in rodents (Angoa-Perez et al. 2013). However, recent studies have considered NST as an indicator of well-being (Nichols et al. 2016, Jirkof 2014) or species-typical behavior (Deacon 2012, Deacon and Rawlins 2005). Furthermore, there have been several studies showing a correlation between this behavior and hippocampal damage (Deacon, Croucher, and Rawlins 2002, Deacon and Rawlins 2005, Jedynak et al. 2012, Kondratiuk et al. 2013). NST also correlates with apathy or depressive behavior (Filali, Lalonde, and Rivest 2009) rather than locomotion ability. Briefly, a mouse was placed in a standard mouse home cage (27 x 21 x 14 mm, 1264C001, Tecniplast, Italy) that contains a cotton nestlet (Figure 3.8, D). Each nestlet is 51 mm<sup>2</sup> x 5 mm in size and is weighed before the test (Figure 3.8, E), usually measuring approximately 3 g (NC9365966, Ancare, Bellmore, NY). Mice was allowed to explore for 30 minutes. The nestlet is taken out of the home cages, allowed to air-dry overnight and weighed the following day to quantify how much was shredded (Figure 3.8, F).

Figure 3.8. Marble burying and nestlet shredding tests

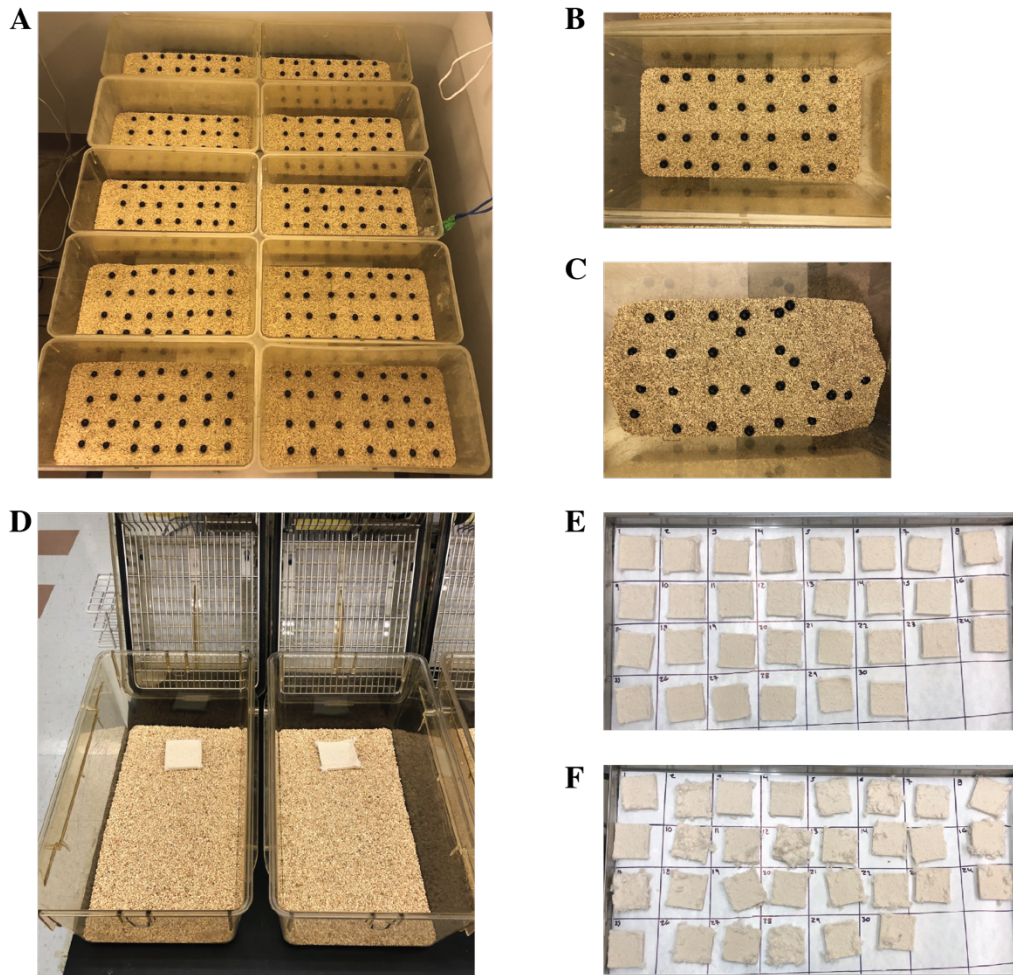


**Figure 3.8. Marble burying and nestlet shredding tests.** This experimental setup was to assess hippocampal damage through two tests: A) First, the marble burying test setup in standard rat cages with 5 cm of bedding. B) Marbles were organized in a grid pattern prior to the test. C) Marbles displaced and buried by the mice after the test. D) Second, the nestlet shredding test setup, in a standard mouse cage. E) pre-weighed nestlet was placed near one end of the cage. F) The shredded nestlets were air-dried overnight and weighed to calculate the percentage of shredding

### Gross pathology

### ***TISSUE COLLECTION***

Tissue was collected as previously reported (Gao et al. 2006), with modifications. Briefly, six mice per group were euthanized on day D18 (day 14 or 18 after the last injury) by intraperitoneal (IP) injection of ketamine (90 mg/kg) and xylazine (10 mg/kg). Once pain reflex was abolished, the thoracic cavity of the mouse was opened, and approximately 0.3-0.5 mL of blood was retrieved from the heart and collected in a 1.5 mL microcentrifuge tube. Blood was allowed to clot for 60 minutes and then centrifuged at 5,000 x g for 10 minutes. The serum was collected and stored at -80°C. Following blood collection, 5 mL of ice-cold 0.1 M phosphate-buffered saline (PBS) was perfused intracardially, followed by 30 ml of 4% paraformaldehyde (PFA) in phosphate buffer (PB). Mouse brains were collected, post-fixed overnight in 4% PFA and immersed in 30% (w/v) aqueous sucrose solution for 3 to 4 days or until tissue sank (indicating it became isotonic). Tissue was embedded in OCT (Fisher Scientific, Hampton, NH) and fast frozen in a cold bath of 2-methyl butane in dry-ice with isopropyl alcohol. Tissues were cut in serial coronal sections with a thickness of 20 $\mu$ m (Leica CM3050 S, Meyer Instruments Inc., Houston, TX). Four sections were mounted per slide (separated 200 $\mu$ m apart) on Superfrost™ Plus microscope slides (Fisherbrand, Hampton, NH) and stored at -20°C.

### **Statistical analysis**

Statistical analysis was carried out as follows (Figure 3.9): Results of sTBI groups injured on day D0 were analyzed by two-way ANOVA repeated measures (RM) with Tukey's post hoc test when the test span across multiple days. If data was missing as in PAS, due to machine malfunction, a mixed model with RM and Tukey's post hoc test were performed. When the test was a single event, one-way ANOVA was used with Tukey's post hoc test.

For the repetitive injury analysis, five controls were utilized: uninjured sham, sTBI 95 g x 1.0 m injured and 120 g x 1.0 m injured on D0, and 95 g x 1.0 m and 120 g x 1.0 m injured on D4. The following analysis was done. For all biomechanical measurements and RR, the D0 and D4 were analyzed by one-way ANOVA, and multiple comparisons were selected (Table 3.3, A and B, respectively) thus Bonferroni's post hoc test followed. The rest of the days D1-D3 two-way ANOVA RM was done between Sham, 95 g x 5 and 120 g x 5 injuries.

For NSS results two analyses were performed: 1) Two-way ANOVA RM was performed for all groups injured on day D0, days included in this analysis are D-1, D0, D1, D2, D3, D4, D5 and D13. 2) Another two-way ANOVA RM was done for the controls injured on D4, in comparison to sham and both RmTBI injury groups, days included in the analysis were D-1, D4, D5, and D13. For the rest of the tests that included more than one day, a standard two-way ANOVA RM was performed. Where data was missing, a mixed analysis RM was done. For all single day experiments, a one-way ANOVA with Bonferroni's post hoc test was done to select specific multiple comparisons (Table 3.3, C). No time interactions were further analyzed.

Data was analyzed with GraphPad Prism version 8.0 (GraphPad software, San Diego, CA). Significance was considered when  $p < 0.05$ . Mechanical data is shown as mean  $\pm$  standard deviation (SD) and behavioral data as mean  $\pm$  standard error of the mean (SEM).

Figure 3.9. Statistical analysis and group comparisons

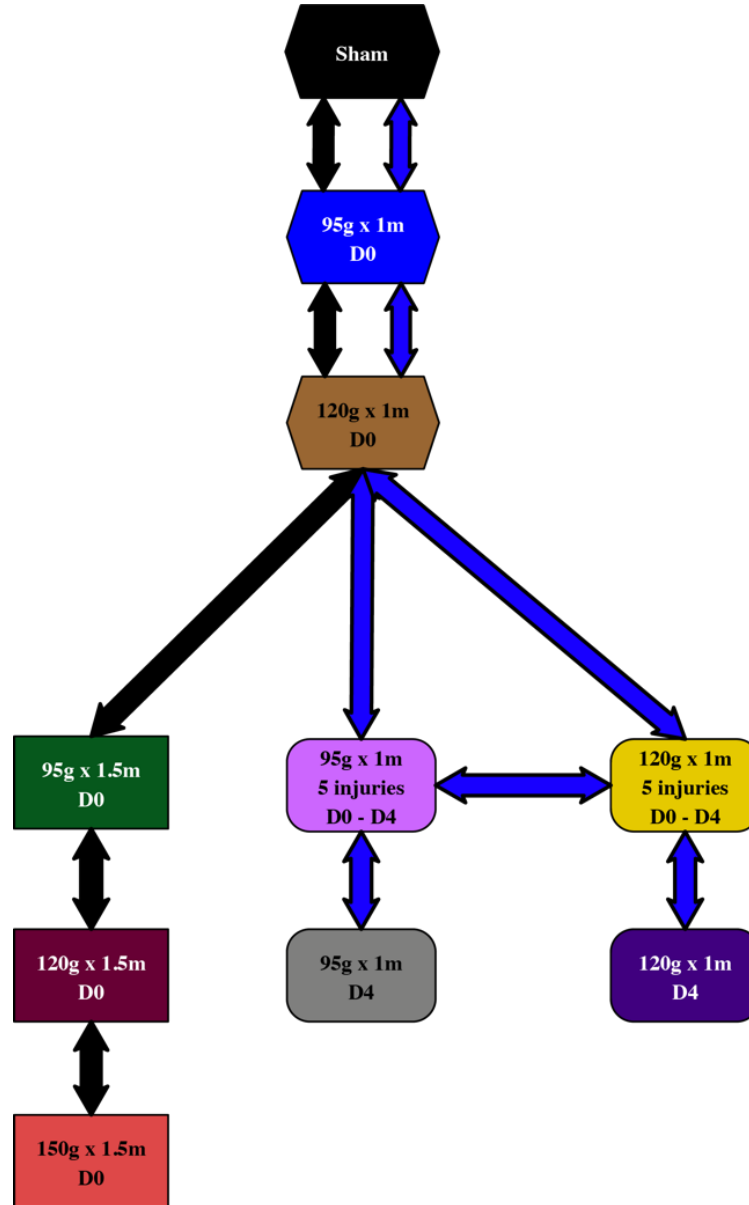


**Figure 3.9. Statistical analysis and group comparisons.** Analysis was divided in two broad comparisons. The groups connected with the black arrow were analyzed as differences between single TBIs. On the other hand, the groups connected in blue were analyzed as differences between RmTBIs. Since the groups in the RmTBI analysis that received only one impact are used as controls for the repetitive group, they were only compared to their respective RmTBI injury group (i.e. 95 g at 1.0 m for 1 vs. 5 injuries, and 120 g at 1.0 m for 1 vs. 5 injuries) (see Table 3.3 for specific comparisons).

Table 3.3. Multiple comparisons for analysis of repetitive mild TBI

<b>A) Comparisons D0</b>	Group	Day of injury	Group	Day of injury
1	Sham	0	95 g x 5 injuries	0
2	Sham	0	120 g x 5 injuries	0
3	95 g x 1.0 m	0	95 g x 5 injuries	0
4	120 g x 1.0 m	0	120 g x 5 injuries	0
5	95 g x 5 injuries	0	120 g x 5 injuries	0
<b>B) Comparisons D4</b>	Group	Day	Group	Day
1	Sham	4	95 g x 5 injuries	4
2	Sham	4	120 g x 5 injuries	4
3	95 g x L (1.0 m)	4	95 g x 5 injuries	4
4	120 g x L (1.0 m)	4	120 g x 5 injuries	4
5	95 g x 5 injuries	4	120 g x 5 injuries	4
<b>C) Comparisons one-way ANOVA all RmTBI groups</b>	Group	Day	Group	Day
1	Sham	0	95 g x 5 injuries	0
2	Sham	0	120 g x 5 injuries	0
3	95 g x 1.0 m	0	95 g x 5 injuries	0
4	120 g x 1.0 m	0	120 g x 5 injuries	0
5	95 g x L (1.0 m)	4	95 g x 5 injuries	0
6	120 g x L (1.0 m)	4	120 g x 5 injuries	0
7	95 g x 5 injuries	0	120 g x 5 injuries	0
L = Last day of injuries (D4)				

## RESULTS OF SINGLE TBI

### Mortality

No mortality due to TBI was observed in these experiments.

### Force, acceleration and speed plateau in TBI from 1.5 m

The velocity of the falling objects and the forces applied to the head of the animals were recorded and analyzed (Figure 3.10). Three objects (95 g, 120 g, and 150 g) were

dropped from two different heights (1.0 m and 1.5 m) to graduate the injury severity on the animals. The peak force (N) of impact was measured and showed  $17.59 \pm 2.54$ ,  $20.43 \pm 1.71$ ,  $23.09 \pm 2.06$ ,  $22.92 \pm 2.22$  and  $22.28 \pm 1.81$ , for 95 g x 1.0 m, 120 g x 1.0 m, 95 g x 1.5 m, 120 g x 1.5 m, and 150 g x 1.5 m, respectively. The peak force measured by the impact sensor on the top of the mice heads were significantly lower in the animals injured with the 95 g x 1.0 m when compared with all other groups, except 120 g x 1.0 m. Also, 120 g x 1.0 m peak force was significantly smaller than 95 g x 1.5 m (Figure 3.10, A). Similarly, the peak acceleration (g) of the mice heads was significantly lower in the animals injured with the 95 g x 1.0 m,  $804.00 \pm 82.12$  (g), when compared to all other groups, except 120 g x 1.0 m,  $957.40 \pm 171.00$  (g). The other groups generated accelerations of  $1,100.00 \pm 172.00$  (g),  $1,109.00 \pm 158.10$  (g), and  $1,110.00 \pm 145.10$  (g), for 95 g x 1.5 m, 120 g x 1.5 m, and 150 g x 1.5 m, respectively (Figure 3.10, B). The peak speed of the mice heads after impact followed a similar trend. Speed was significantly higher in the 95 g x 1.5 m, 120 g x 1.5 m, and 150 g x 1.5 m, when compared to the speed of the mice heads generated by the objects dropped from 1.0 m (Figure 3.10, D). Contrary to the expected object-weight and drop-height dependent increase in peak force, acceleration and speed of the mice heads after injury, these results show a plateau of these parameters in injuries induced by objects dropped from 1.5 m.

The velocity (m/s) of the falling objects was measured to assess the effect of friction produced by the tube on the variability of the model. The velocity increased based on the height of drop but not the weight of the object (Figure 3.10, E). The kinetic energy was calculated as  $KE = \frac{1}{2}mv^2$ , where  $m$  is mass in kg and  $v$  is velocity in m/s. An object-weight and drop-height dependent increase in KE was observed, as expected.

Figure 3.10. Biomechanics of single injury

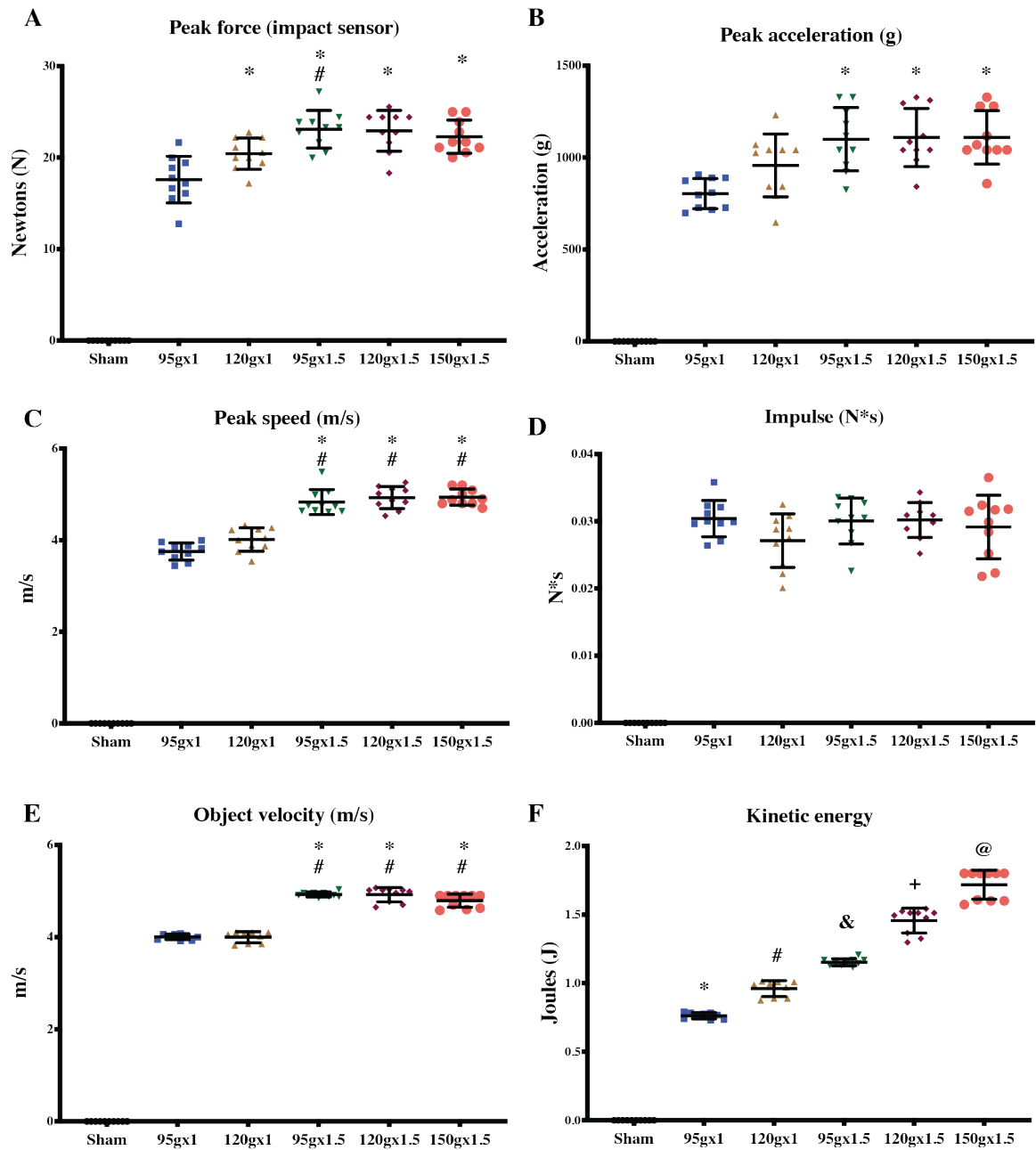


**Figure 3.10. Biomechanics of single injury.** Biomechanical assessment of the animal heads' response to TBI. A plateau was found in injuries by objects dropped from 1.5 m in A) peak force of impact, B) peak acceleration (g, acceleration due to gravity), and C) peak speed, (in meters per second, m/s). D) No differences in impulse (Newtons seconds) was found among any group. E) Velocity of the falling objects as expected showed drop-height

differences. F) Conversely, kinetic energy (KE) generated by the falling object was object-weight and drop-height dependent increase. Data is shown as mean  $\pm$  SD (n=10 per group). One-way ANOVA analysis was performed with Tukey's test for multiple comparisons. Differences were considered significant if  $p < 0.05$ . \* compares against 95 g x 1.0 m group and # compares against 120 g x 1.0 m group. F) all groups are significantly different.

### **Righting reflex and neurological deficits in single TBI**

TBI is known to induce loss of consciousness in humans, and this can be assessed in rodents as the RR, which is the time it takes the animal to regain consciousness and acquire the prone position after anesthesia or trauma. The RR times of animals injured with objects dropped from 1.5 m,  $302 \pm 25.66$ ,  $348.1 \pm 65.48$ , and  $358.4 \pm 54.96$  seconds (95 g, 120 g and 150 g x 1.5 m groups, respectively) were longer than the times for the sham group,  $43.80 \pm 4.027$  seconds, and the groups injured with objects dropped from 1.0 m,  $116.3 \pm 9.836$  and  $122.4 \pm 36.95$  seconds  $\pm$  SEM (95 g and 120 g x 1.0 m, respectively) (Figure 3.11, A). The neurological dysfunction of the mice after trauma was assessed with the NSS. The animals that score higher in this test show worse neurological deficits. After TBI, the group injured with the 150 g x 1.5 m had significantly higher neurological compromise 2 hours after injury (D0) when compared with all groups, except 120 g x 1.5 m. This difference persisted on D2, except animals injured with 120 g at both heights, and on D3 animals injured with both 120 g and 150 g objects dropped from 1.5 m showed higher neurological deficits than all other groups. Furthermore, the 150 g x 1.5 m group exhibited a much slower NSS recovery throughout the testing period.

Figure 3.11. Righting reflex and neurological deficits in single TBI

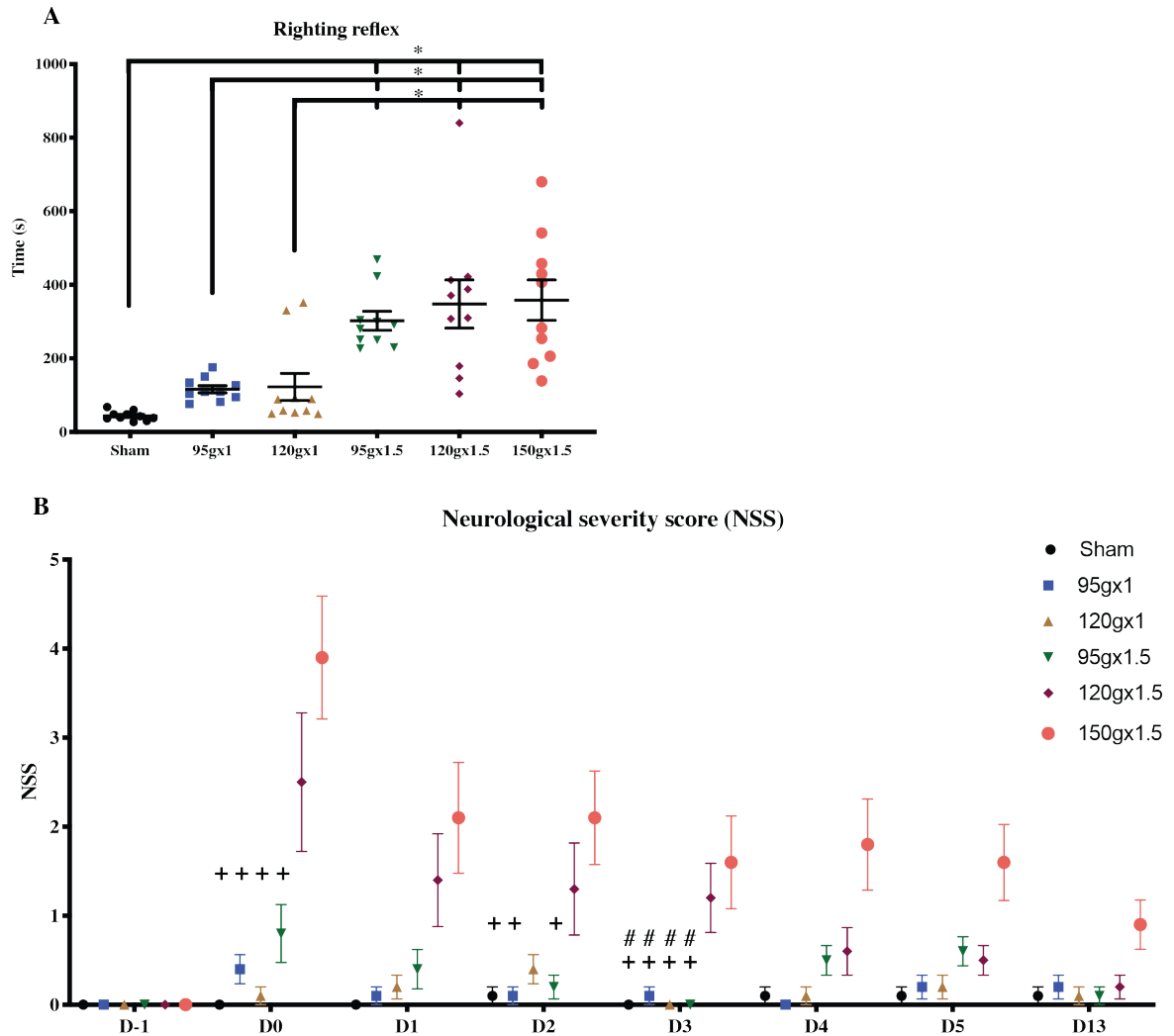


**Figure 3.11. Righting reflex and neurological deficits in single TBI.** Two neurobehavioral outcomes were assessed acutely after injury and one continued until D13. A) Righting reflex (RR) was drop-height dependent but not object. B) Neurological deficits were seen in the group injured with the 120 g and 150 g objects x 1.5 m, on D3, and 2 hours post-injury (D0), D2 and D3, respectively. Data is shown as mean  $\pm$  SEM, with  $n=10$  per group. Analysis for RR and NSS were one-way ANOVA and two-way ANOVA RM, respectively, with Tukey's post hoc test for multiple comparisons.  $*p<0.05$ .  $+$  different from 150 g x 1.5 m,  $\#$  different from 120 g x 1.5 m.

### **Fine motor function but not locomotion is affected after single TBI**

We had previously shown locomotion deficits immediately after the injury that persisted up to 4 days (Chapter 2). In order to assess the dysfunction of the motor system, fine motor function (grip strength) and gross locomotion (PAS, OF and Rotarod) were assessed after TBI. Animals injured with 120 g and 150 g objects dropped from 1.5 m showed a reduction in grip strength five days post-injury (Figure 3.12, A) when compared to sham and the group injured with 95 g x 1.0 m. The rotarod test has been used as a mean to evaluate motor coordination and cerebellar dysfunction. We tested the performance of the mice in the rotarod, and no differences were found between groups on D6 and D7 or performance between days on each group (Figure 3.12, B). To assess potential locomotor deficits that could influence other tests, mice were subjected to the PAS and OF tests. There were no differences in exploration measured by the PAS on D8 and D15 (Figure 3.12, C). However, on D9 in the open field, mice injured with 95 g object dropped from 1.5 m showed longer distance traveled when compared to sham (Figure 3.12, D).

Figure 3.12. Fine motor function but not locomotion is affected after single TBI

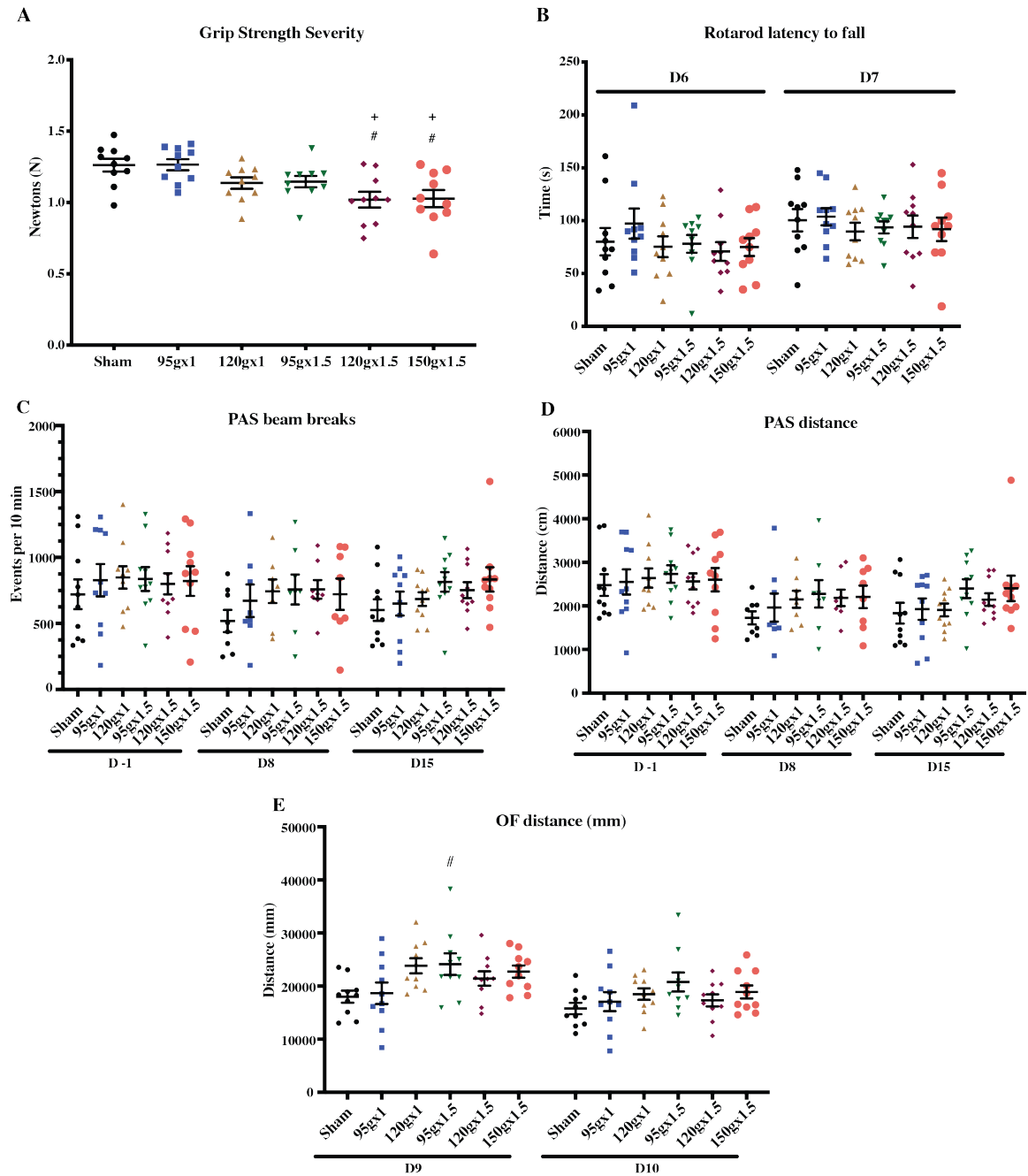


**Figure 3.12. Fine motor function but not locomotion is affected after single TBI.** A) Fine motor function was assessed by grip strength (GS) in Newtons. GS significantly decreased in the animals injured with 120 g and 150 g objects x 1.5 m when compared to sham and 95 g x 1.0 m. B) Animals showed no difference in latency to fall from the Rotarod regardless of injury. C) Total exploratory behavior and D) horizontal exploration were not

different among the groups measured by photobeam activity system. E) On D9 in the open field (OF) the group injured with the 95 g object x 1.5 m traveled a longer distance than sham. GS was analyzed with one-way ANOVA, Rotarod, and OF were analyzed with two-way ANOVA repeated measures, and PAS was analyzed with mixed model repeated measures due to missing data. Multiple comparisons were made with Tukey's post hoc test. Data is shown as mean  $\pm$  SEM, with n=10 per group  $p < 0.05$ . # different from sham, + different from 95 g x 1.0 m.

### **Single TBI induces memory deficits in context discrimination**

Different areas of the brain are known to be important for different types of memory. Four different tests—the NOR, NLR, FC context discrimination and FC cue discrimination —were used to assess memory post-injury on days D12, D13, D17 and D17, respectively. These tests assess spontaneous memory involving the perirhinal cortex, and hippocampus, and associative learning involving the hippocampus or amygdala. Contextual memory was enhanced in the animals injured with 95 g object x 1.0 m when compared to the sham group and decreased in animals injured with 95 g x 1.5 m, measured as the percentage of time frozen within the aversive context. All groups showed significantly lower percentage of freezing time when compared with 95 g x 1.0 m (Figure 3.13, A). Cued conditioning was preserved in all groups, which was assessed by an increased freezing behavior in a novel context when animals were exposed to the cue stimulus (Figure 3.13, B). In NOR, the time of exploration of the novel object was not significantly different from the familiar in the groups injured with the objects 95 g and 120 g x 1.5 m (Figure 3.13, C). However, when the discrimination and investigation indexes were calculated (accounting for exploration differences), all groups recognized the novel object above the 50% chance of choosing one object randomly (Figure 3.13, D). On the

other hand, only the group injured with 120 g x 1.5 m explored the object in the novel location more than the familiar one (Figure 3.13, E).

Figure 3.13. Single TBI induces memory deficits in context discrimination

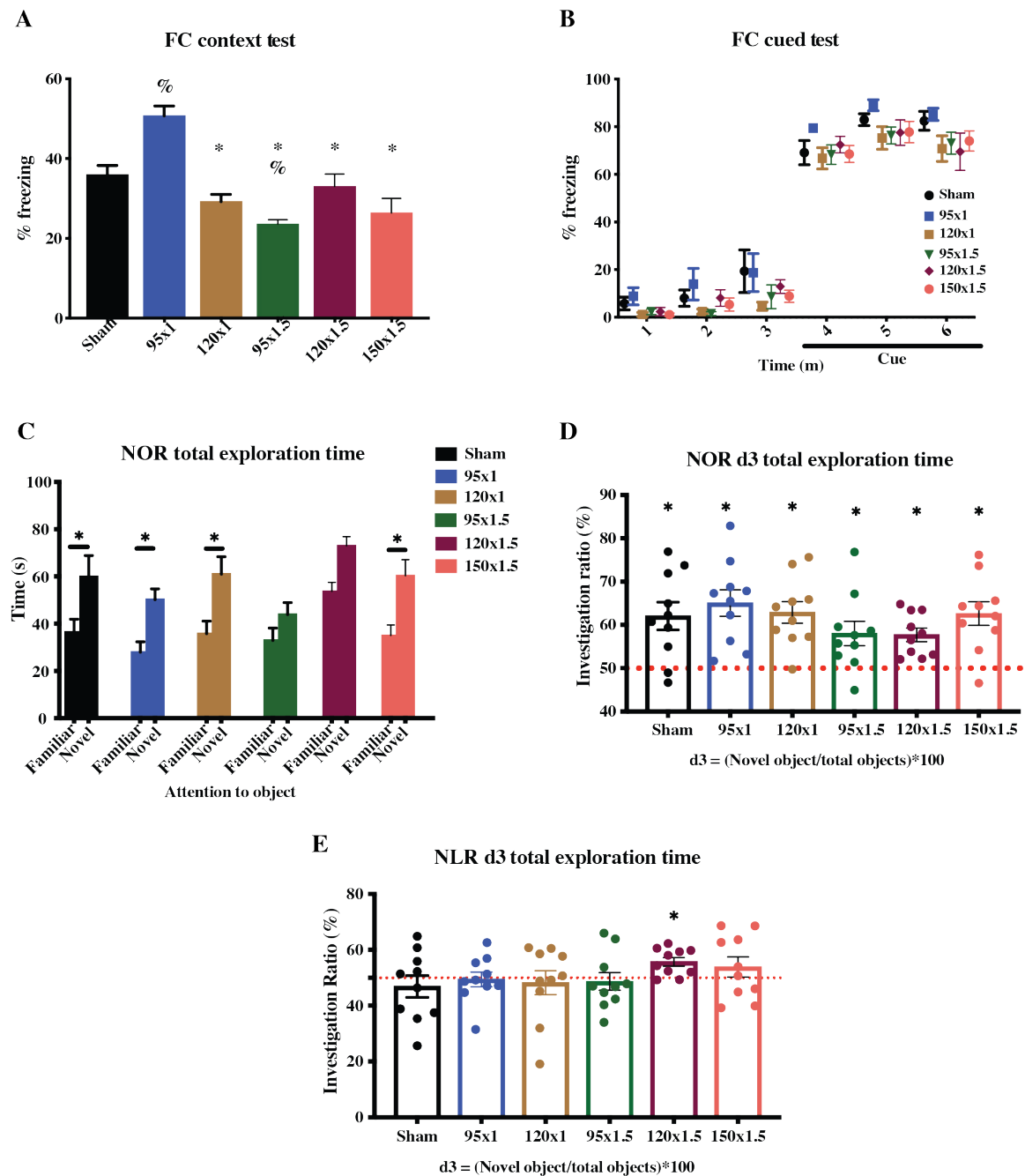


**Figure 3.13. Single TBI induces memory deficits in context discrimination.** A) sTBI induced memory deficits in contextual memory in the group 95 g x 1.5 m when compared to sham, and enhanced memory in 95 g x 1.0 m. B) Cued conditioning was preserved in all groups shown as increased freezing. C) In the novel object recognition test, the groups injured with 95 g x 1.5 m and 120 g x 1.5 m did not explore the novel object significantly longer than the familiar. D) The investigation ratio d3 (calculated to account for animal exploration differences) showed that all groups recognized the novel object beyond chance. E) Only the group injured with 120 g x 1.5 m recognized the novel location. FC context was analyzed by two-way ANOVA and Tukey's post hoc test. Total exploration time of familiar and novel objects was analyzed with two-way ANOVA and Bonferroni's multiple comparisons post hoc test. D3 of NOR and NLR were calculated with one sample T and Wilcoxon tests against a 50% theoretical mean. All data is shown as mean  $\pm$  SEM, with n=10 per group.  $p < 0.05$ , % compared to sham, \* compared to 95 g x 1.0 m. D and E) \* Different from 50% theoretical mean.

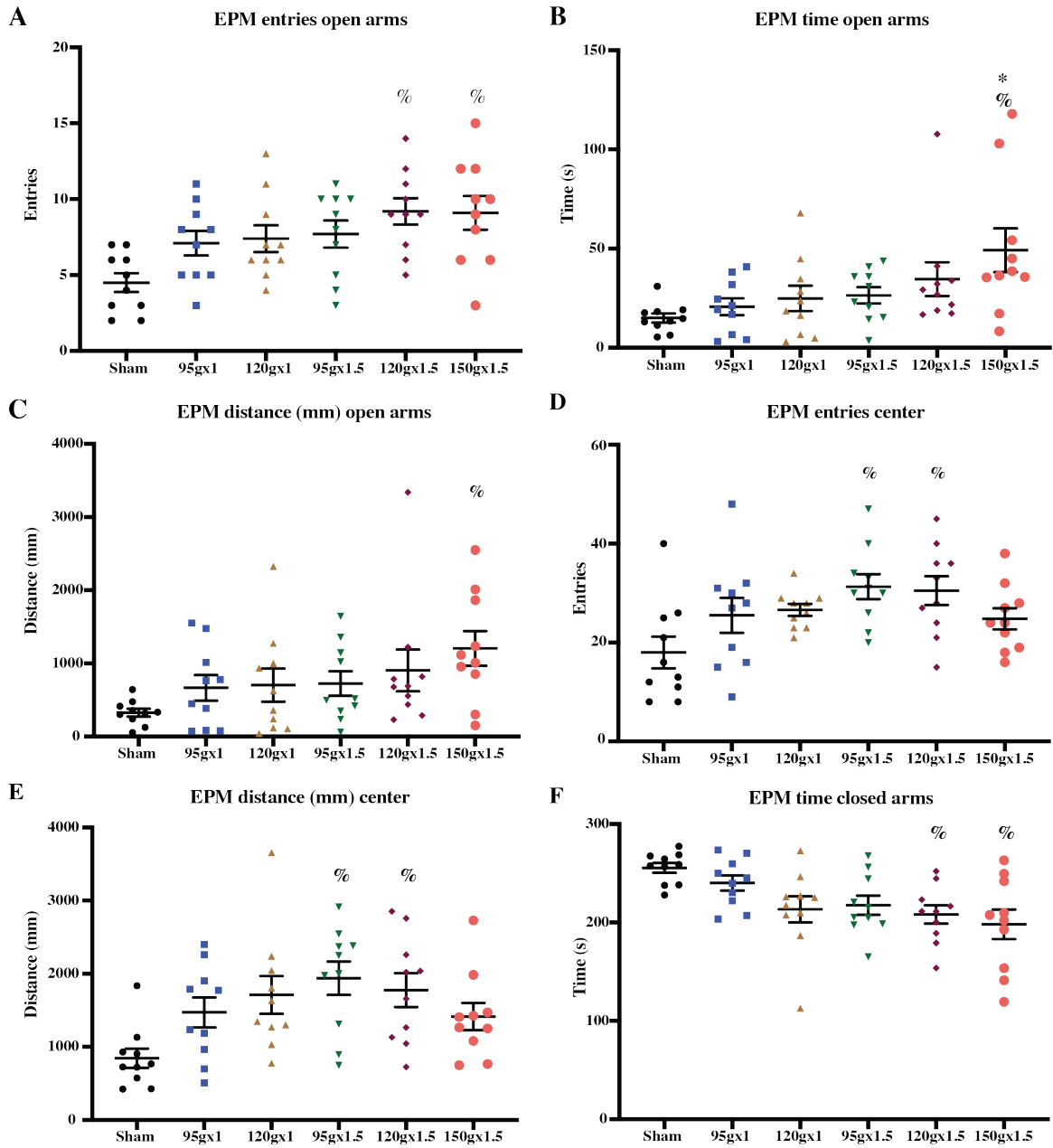
### **sTBI reduces acrophobia but not agoraphobia or depressive behavior**

TBI has been reported to induce mood disorders, such as depressive and anxiety behaviors, while paradoxically increasing risk-seeking behavior. Anxiety-like behavior was analyzed by EPM, for acrophobia-mediated anxiety (Biedermann et al. 2017, Walf and Frye 2007, Ari et al. 2019), and thigmotaxis in PAS and OF, for agoraphobia-mediated anxiety (Walz, Muhlberger, and Pauli 2016, Kurhe et al. 2014). After sTBI with 120 g or 150 g objects from 1.5 m, mice increased entry into open arms (Figure 3.14, A). Mice injured by 150 g x 1.5 m also had increased time spent and distance traveled on the open arms, and significantly decreased time on closed arms of the EPM, when compared to sham (Figure 3.14, B, C, and F). Interestingly, groups injured with 95 g and 120 g objects x 1.5 m increased entries into the center and the distance traveled when compared with sham

(Figure 3.14, D and E). Conversely, there were no differences in thigmotaxis behavior in the PAS or the OF (Figure 3.14, G and H).

Depressive behavior assessed by tail suspension test showed no differences when comparing any of TBI groups with the sham group. However, the group injured with the 150 g object x 1.5 m spent significantly more time immobile than the group injured with 120 g object x 1.5 m ( $38.70 \pm 1.096$  vs.  $27.97 \pm 3.763$  seconds, mean  $\pm$  SEM).

Figure 3.14. sTBI reduces acrophobia but not agoraphobia



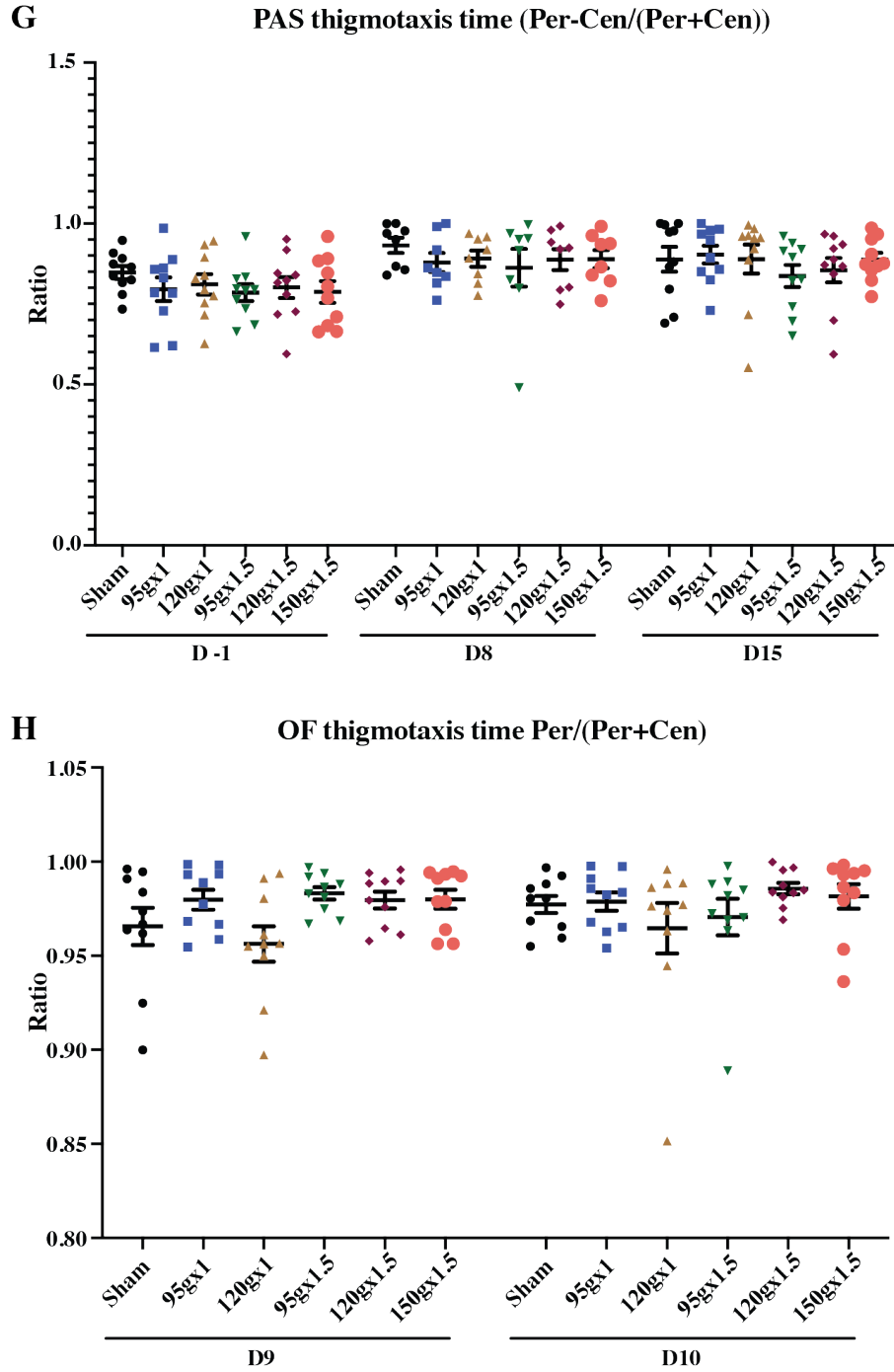


**Figure 3.14. sTBI reduces acrophobia but not agoraphobia.** sTBI reduced acrophobia in the group injured with 150 g object x 1.5 m, as assessed by A) increased number of entries into the open arms (120 g and 150 g x 1.5 m), B) increased the time of open arm exploration, and C) increased the distance traveled on open arms. D) The groups injured with 95 g and 120 g objects x 1.5 m increased entries and E) distance on the center of the

maze. F) Animals in the 120 g and 150 g x 1.5 m injury groups decreased time spent on the closed arms, in comparison to sham. G) No differences in thigmotaxis was found in the photobeam activity system, and H) open field. Per = Periphery, Cen = Center. Data is shown as mean  $\pm$  SEM, with n=10 per group. EPM was analyzed with one-way ANOVA, and PAS and OF were analyzed with two-way ANOVA RM multiple comparisons test with Tukey's post hoc test.  $p < 0.05$ . % different from sham, \* different from 95 g x 1.0 m.

### **Marble burying and nestlet shredding tests show no differences after single TBI**

The behavioral tests used to assess compulsivity or hippocampal damage showed no difference among groups. However, in the MBT, the group injured with the 150 g object dropped from 1.5 m showed a trend to decrease the number of buried marbles when compared to sham ( $p = 0.0744$ , one-way ANOVA, Tukey's post hoc test, data not shown)

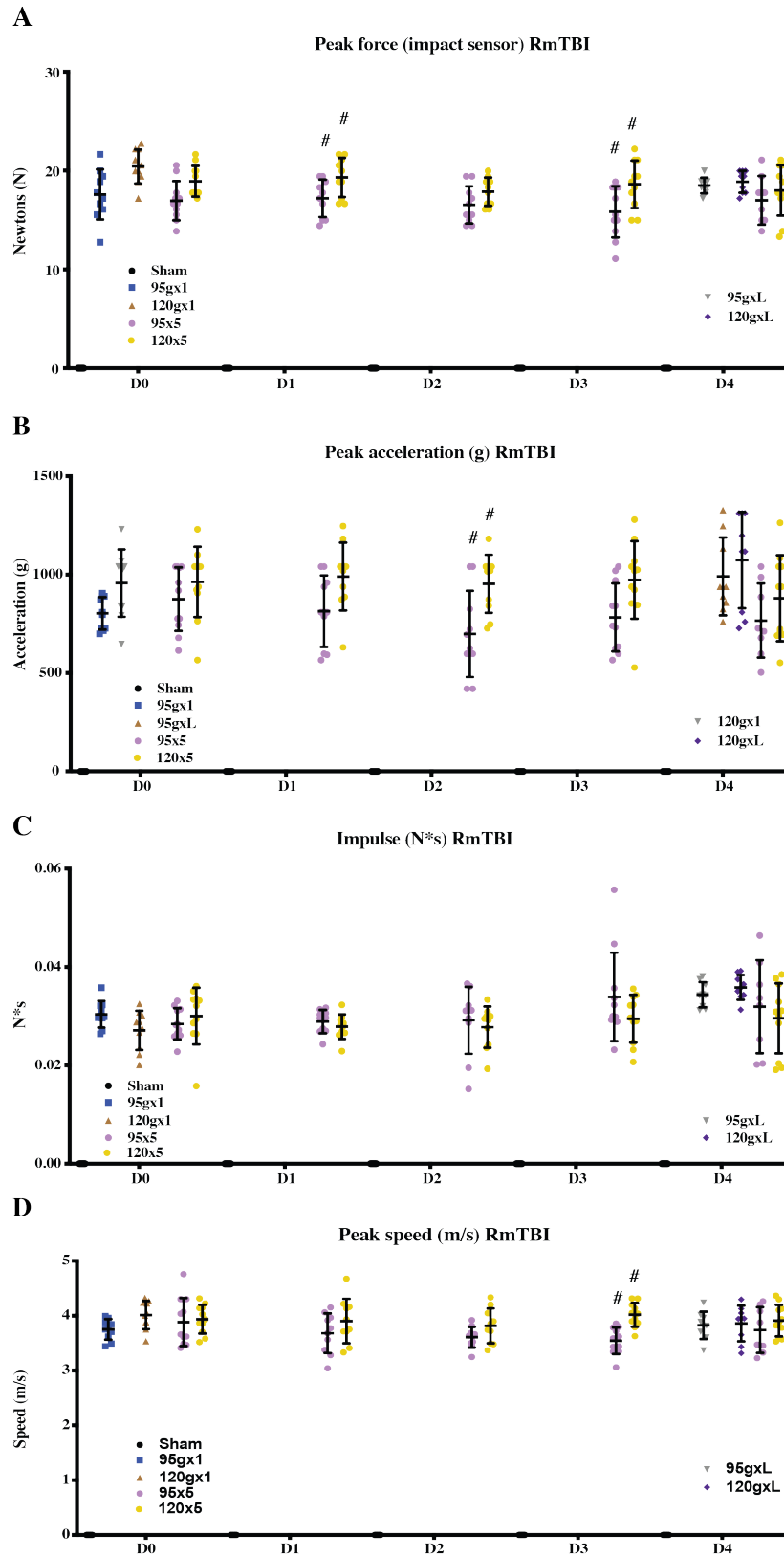
## **RESULTS OF REPETITIVE MILD TBI**

### **Peak force and acceleration are affected by object-weight at 1.0 m**

The new model of weight-drop TBI showed similar peak forces between the sTBI groups and their RmTBI counterparts on days D0 and D4 of injuries. On days D1 and D3, RmTBI group 120 g x 5 injuries group with a higher peak force than the 95 g x 5 injuries group (Figure 3.15, A). The same was seen in peak acceleration on D2, where the heads of the animals of the 120 g x 5 injuries group exhibited higher accelerations after impact than the 95 g x 5 injuries group (Figure 3.15, B). The impulse (N·s) was not different between any of the groups. The speed of head after impact followed a similar trend as the peak force on D3, being significantly higher in the 120 g x 5 injuries group when compared to 95 g x 5 injuries group (Figure 3.15, C). Additionally, there were no differences in the velocity of

the falling objects and, as expected, the KE was different between the 95 g and 120 g objects in all timepoints.

Figure 3.15. Biomechanics of repetitive mild TBI



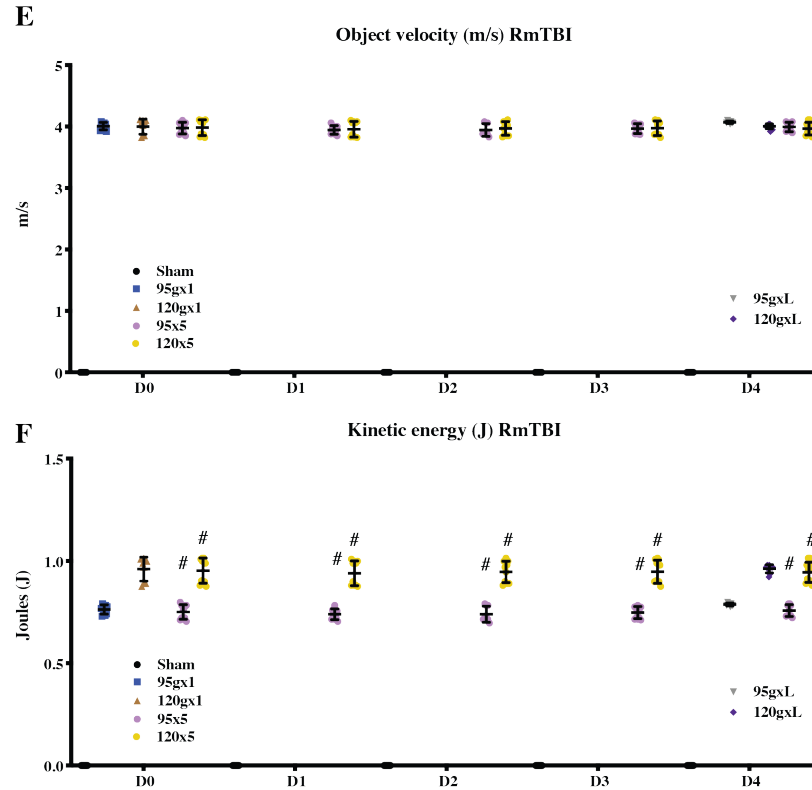


**Figure 3.15. Injury biomechanics of RmTBI.** A) Peak force in Newtons (N) was higher in 120 g x 5 group than the 95 g x 5 group on days D1 and D3. B) Peak acceleration in g (acceleration due to gravity) of the head of the animal was higher in the 120 g x 5 injuries group on D2. C) There were no differences in impulse in Newtons seconds (N·s) between any of the groups. D) Peak speed of the head was higher in the 120 g x 5 injuries group on D3. E) The velocity of the falling object showed no differences among groups. F) Calculated kinetic energy was higher in the 120 g x 5 group than 95 g x 5 group at all timepoints. (sham, 95 g x 1.0 m and 120 g x 1.0 m, n=10; rmTBI 95 g and 120 g x 5 injuries, n=11; and 95 g x L and 120 g x L n=9). Data shown as mean  $\pm$  SD. D0 and D4 were analyzed by one-way ANOVA, specific comparisons, Bonferroni's post hoc test. D1-D3 were analyzed by mixed-model ANOVA repeated measures, Tukey's post hoc test. # $p$ <0.05.

### **Repetitive mild TBI increases RR and neurological deficits**

RR was longer in the RmTBI groups when compared to sham after every injury, and no differences were found between the RmTBI groups and their respective sTBI controls (Table 3.3) (Figure 3.16, A). Neurological deficits increased with the number of injuries in the RmTBI groups. The 95 g x 5 injuries group showed earlier deficits than 120 g x 5 injuries group. Beginning on D1, neurological deficits were found in the 95 g x 5 injuries group when compared to sham and the 120 g x 5 injuries group (Figure 3.16, B). This difference persisted on D3, with 95 g x 5 injuries group vs. sham and 95 g x 1.0 m. However, on D3 and D5 both RmTBI groups show higher neurological deficits than sham and their sTBI counterparts (95 g x 5 vs. 95 g x L and 120 g x 5 vs. 120 g x L).

Figure 3.16. Neurological deficits increase with the number of injuries

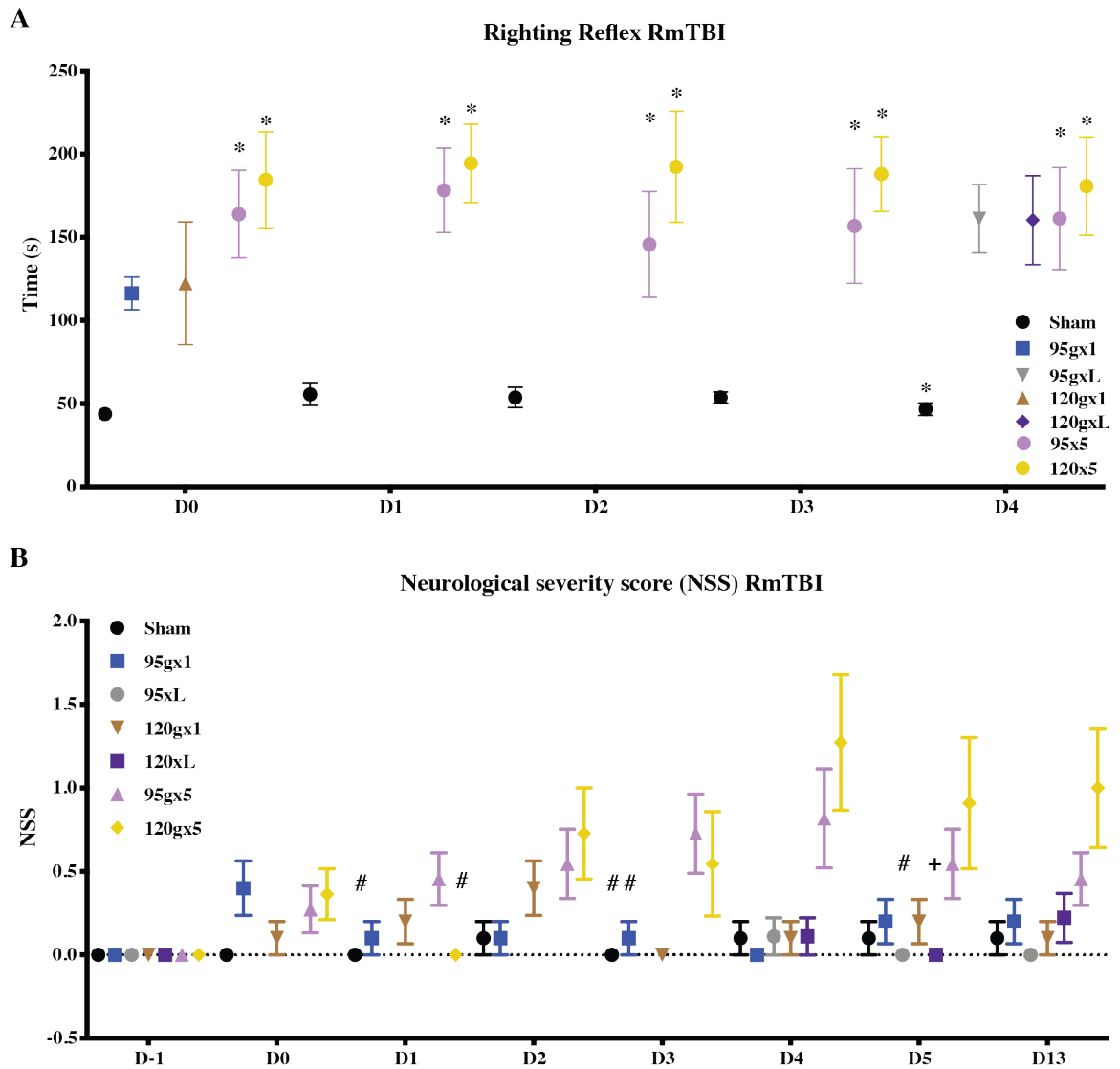


**Figure 3.16. Neurological deficits increase with the number of injuries.** A) Righting reflex was longer in the RmTBI groups when compared to sham at all timepoints. B) Neurological deficits increased with the number of injuries in the RmTBI groups. (sham, n=10; 95 g x 1.0 m and 120 g x 1.0 m, n=10; rmTBI 95 g and 120 g x 5 injuries, n=11; and 95 g x L and 120 g x L n=9). Data shown as mean  $\pm$  SEM. RR on D0 and D4 were analyzed by one-way ANOVA, specific comparisons (Table 3.3 for comparisons), Bonferroni's post hoc test, and D1-D3 were analyzed by two-way ANOVA repeated measures. NSS was analyzed D-1 and D4 to D13 with two-way ANOVA repeated measures, and D0-D3 with

two-way ANOVA repeated measures. Multiple comparison analysis using Tukey's post hoc test unless otherwise stated.  $p < 0.05$ . \* compared to sham, # compared to 95 g x 5 injuries, and + compared to 120 g x 5 injuries.

### **Repetitive mild TBI affects fine motor function but not locomotion**

GS was used to assess fine motor function. The RmTBI groups presented decreased GS when compared to sham, and the animals in 95 g x 5 injuries group also had weaker GS than their single injury counterpart (95 g x 1.0 m) on D5 (Figure 3.17, A). To assess locomotor coordination after RmTBI, mice were subjected to the rotarod test. On D6, sTBI group 120 g x L showed increased latency to fall when compared with its RmTBI counterpart 120 g x 5 injuries, this can be explained by potential hyperlocomotion activity after TBI. However, no differences were found when compared to sham (Figure 3.17, B).

Spontaneous locomotor behavior was analyzed with the PAS on days D-1, D8 and D13 and OF tests on days D6 and D7 after RmTBI. Repetitive injuries did not induce changes in gross locomotion, as assessed by vertical or horizontal exploration (rearing and distance traveled) measured by PAS, on days D-1, D8 and D15, and distance traveled in the OF test, on days D9 and D10 (Figure 3.17, C, D, and E).

Figure 3.17. RmTBI affects fine but not gross locomotion

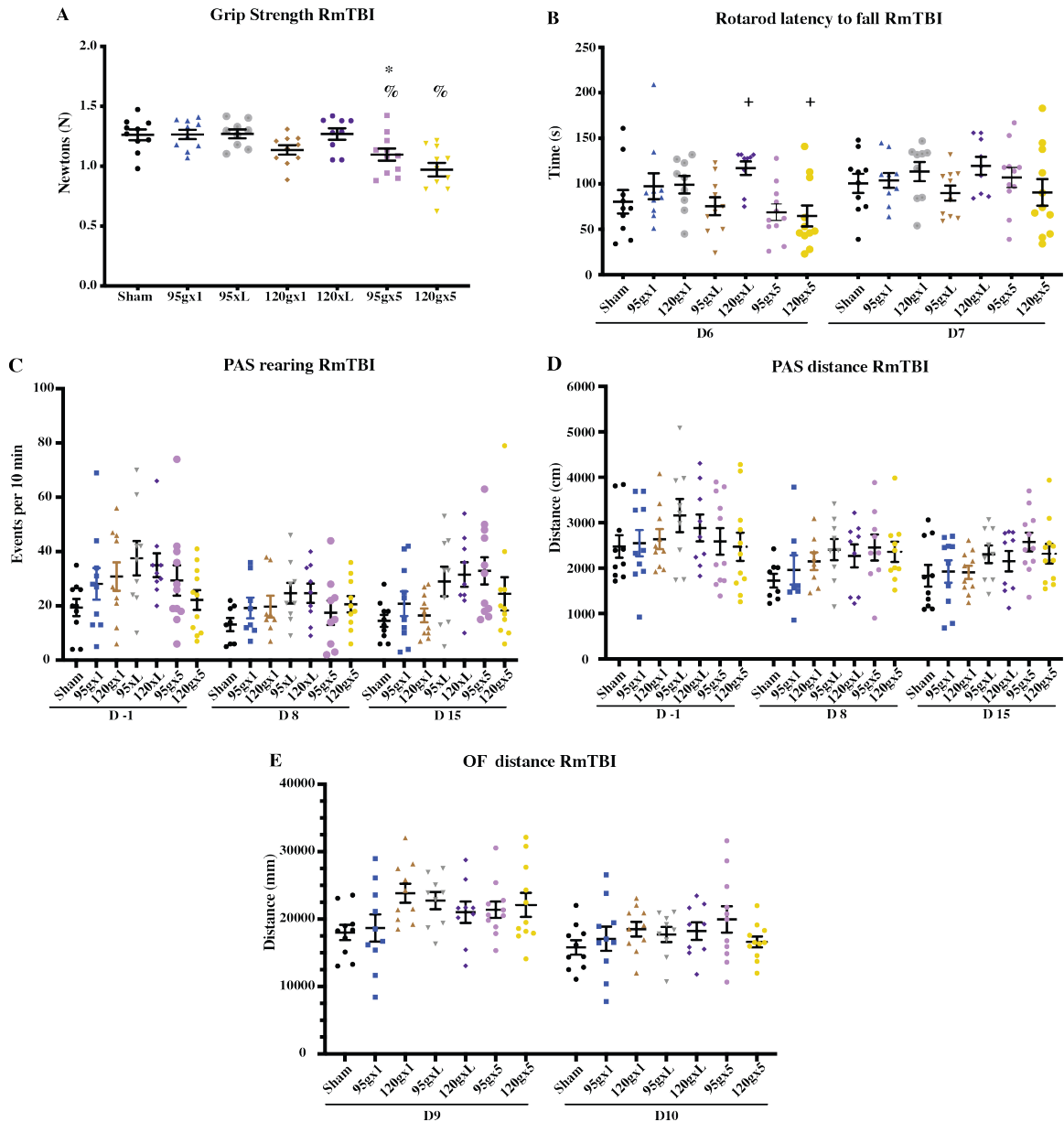


**Figure 3.17. RmTBI affects fine but not gross locomotion.** A) RmTBI reduced grip strength in the 95 g x 5 and 120 g x 5 groups when compared with control. B) sTBI 120 g x L had higher latency to fall than the 120 g x 5 injuries. C) Rearing events were not affected by TBI. D-E) No differences between groups were observed in the distance traveled in the PAS or OF. (sham, 95 g x 1.0 m and 120 g x 1.0 m, n=10; rmTBI 95 g and 120 g x 5 injuries, n=11; and 95 g x L and 120 g x L n=9). Data is shown as mean ± SEM.

GS was analyzed by one-way ANOVA and specific comparisons with Bonferroni's post hoc test. Rotarod and OF were analyzed with two-way ANOVA repeated measures. PAS was analyzed with a repeated measures mixed model. Multiple comparisons were assessed by Tukey's post hoc test unless otherwise stated.  $p < 0.05$  % compared to sham, \* compared to 95 g x 1.0 m.

### **Contextual memory is affected after RmTBI**

Contextual memory was enhanced in the animals injured with 95 g object x 1.0 m when compared to the sham group (as shown in the sTBI analysis). In contrast, RmTBI 95 g x 5 injuries group showed deficits in contextual memory when compared to the sham group and both of its sTBI controls (95 g x 1.0 m and 95 g x L) measured by the percentage of time showing freezing behavior in the aversive context. Also, the RmTBI 120 g x 5 injuries groups showed decreased freezing behavior when compared to its sTBI control 120 g x L (Figure 3.18, A). Cued memory was preserved in all groups (Figure 3.18, B). Time of exploration of the novel object was not significantly higher than the familiar object in the sTBI control groups 95 g and 120 g x L in NOR (Figure 3.18, C). Conversely, discrimination and investigation indexes showed that all groups recognized the novel object above chance (Figure 3.18, D). In NLR test, only the sTBI control group 120 g x L showed a predilection beyond chance towards the object in the novel location.

Figure 3.18. Contextual memory is affected after RmTBI

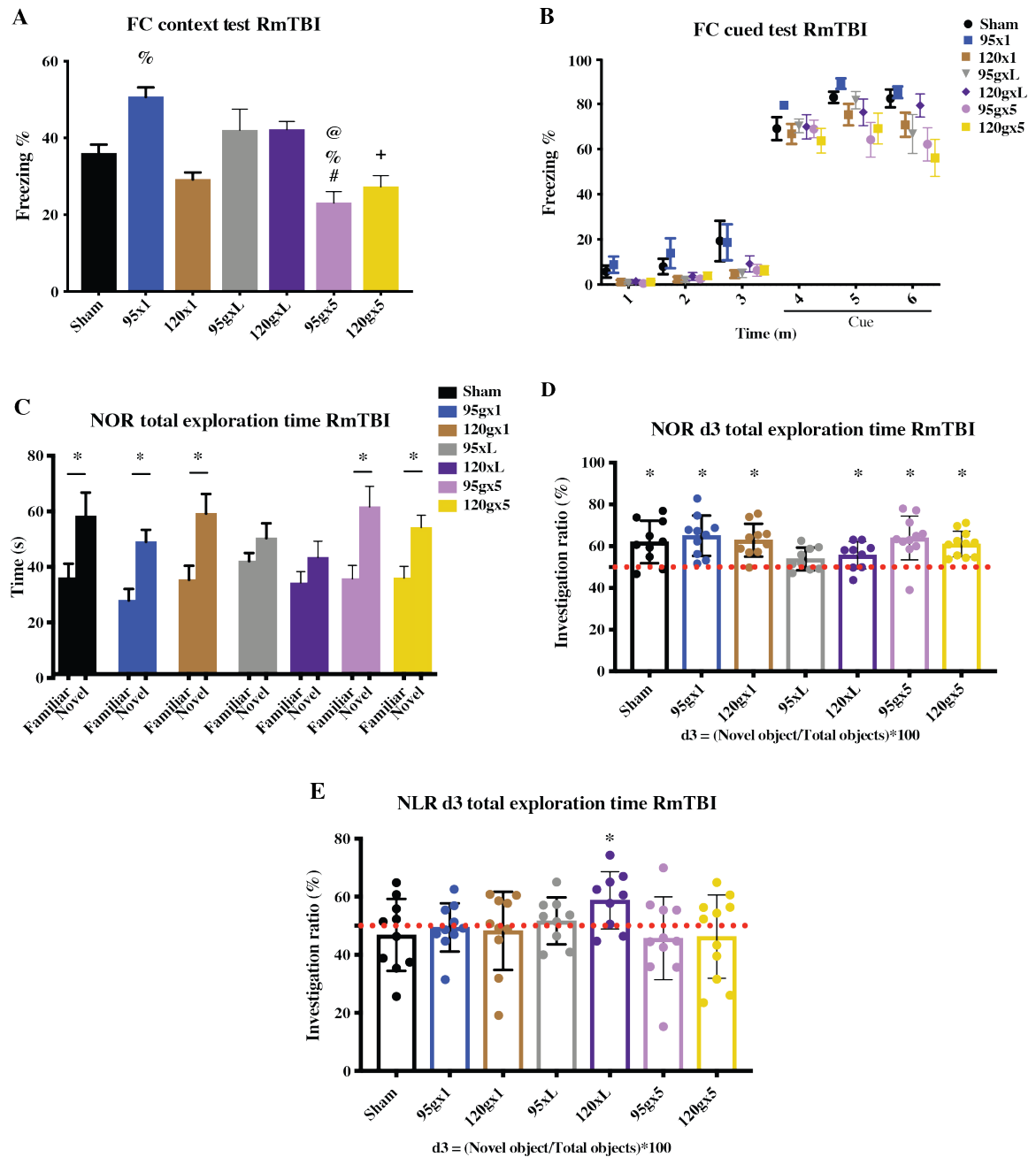


**Figure 3.18. Contextual memory is affected after RmTBI.** A) RmTBI showed decreased freezing behavior in the 95 g x 5 group when compared to sham and both sTBI controls. 120 g x 5 group froze less than 120 g x L. B) Cued memory is preserved after sTBI and RmTBI. C) sTBI groups 95 g and 120 g x L did not show preference for the novel object. D) The investigation ratio d3 (calculated to account for animal exploration differences),

showed that all groups recognized the novel object beyond chance. E) The sTBI group 120 g x L showed higher exploration of the novel location. (sham, 95 g x 1.0 m and 120 g x 1.0 m, n=10; rmTBI 95 g and 120 g x 5 injuries, n=11; and 95 g x L and 120 g x L n=9). Data shown as mean  $\pm$  SEM. FC context was analyzed by two-way ANOVA and Tukey's post hoc test. Total exploration time was analyzed with two-way ANOVA with Bonferroni's multiple comparisons post hoc test. d3 of NOR and NLR were calculated with one sample T and Wilcoxon test against a 50% theoretical mean. \*  $p < 0.05$ . % compared to sham, # compared to 95 g x 1.0 m, @ compared to 95 g x L, and + compared to 120 g x L. \* different from 50% theoretical mean.

### **RmTBI reduces acrophobia but not agoraphobia**

Multiple situations can generate anxiety-like behavior, we tested if RmTBI increased acrophobia-related anxiety with the EPM test on D5, or agoraphobia-related anxiety with thigmotaxis in the PAS, on days D-1, D8 and D15, and the OF test, on days D9 and D10. RmTBI decrease acrophobia when injured with a 95 g x 5 injuries group in comparison to sham. Entries into, time spent exploring, and distance traveled on the open arms are metrics used to assess anxiety-like behavior (Figure 3.19, A, B, and C, respectively). The measurement of thigmotaxis yielded differences in the baseline (D -1) measurement between sham and the 120 g x L (sTBI control for RmTBI, Figure 3.19, D). These sets of controls (95 g and 120 g x L) were all in the last experimental cohort, variations in the environment could have increased their willingness to explore the center of the box in the PAS at baseline, no further differences were detected afterward. Interestingly, differences in thigmotaxis between the 120 g x 5 injuries group and its sTBI (120 g x 1.0 m) control were recorded in the OF on D9, with longer exploration time of the center of the open field by the sTBI group. No differences were found when compared to sham (Figure 3.19, E).

No differences were seen in depressive-like behavior assessed by tail suspension test (data not shown).

Figure 3.19. RmTBI reduces acrophobia but not agoraphobia

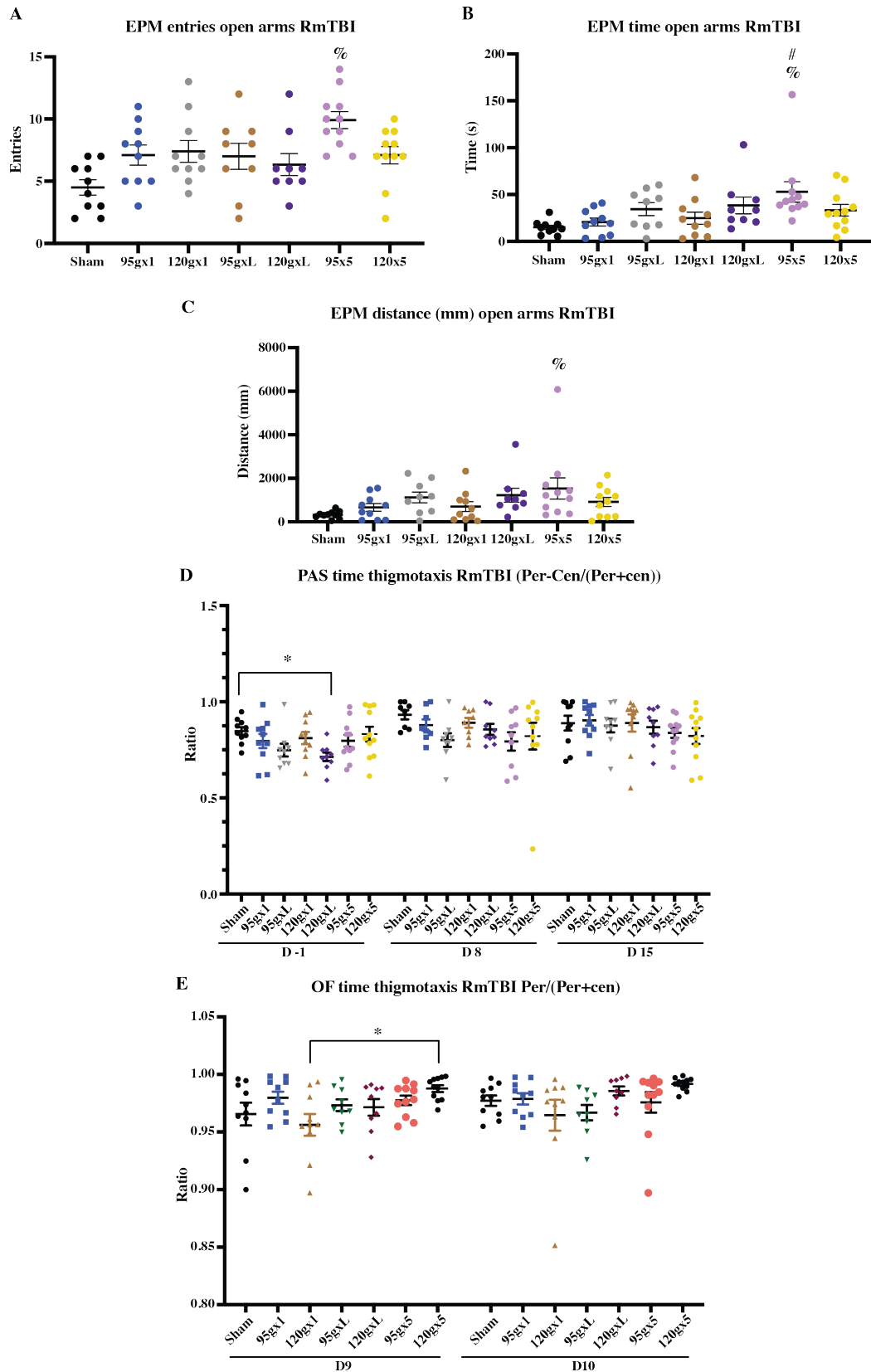


**Figure 3.19. RmTBI reduces acrophobia but not agoraphobia.** RmTBI reduced acrophobia only in the 95 g x 5 group, A) assessed by increased number of entries, B) increased time of exploration and C) distance traveled on the open arms of the EPM on D5. D) Differences in thigmotaxis were found, 120 g x L group showed increased exploration of the center. No further differences were found. F) OF exploration showed an increase in exploration of the center by the sTBI group 120 g x 1.0 m when compared to 120 g x 5 group. Per = Periphery and Cen = Center. (sham, 95 g x 1.0 m and 120 g x 1.0 m, n=10; rmTBI 95 g and 120 g x 5 injuries, n=11; and 95 g x L and 120 g x L n=9). Data shown as mean  $\pm$  SEM. EPM was analyzed with one-way ANOVA, selected comparisons and Bonferroni's post hoc test. OF was analyzed with two-way ANOVA repeated measures, and PAS was analyzed by a repeated measures mixed model analysis, Tukey's post hoc test was used for multiple comparisons. \*  $p < 0.05$ . % different from sham, # different from 95 g x 1.0 m.

### **Marble burying and nestlet shredding test show no differences after RmTBI**

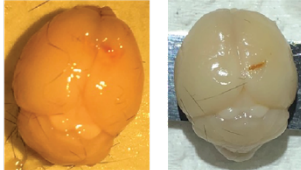
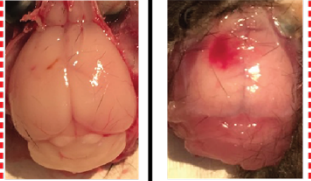
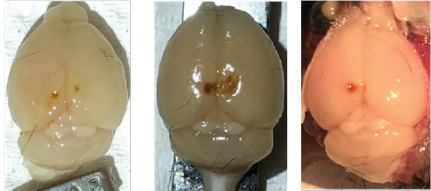
MBT and NST were used as behavioral correlates of hippocampal damage. No differences in performance were found between groups after RmTBI in these tests. (data not showed).

### **Gross morphology**

The primary injuries that this new model generates are concussion, contusion, and hematomas (Figure 3.20). The extension of the primary injury increased in an object weight-dependent manner. RmTBI showed the highest proportion of contusions and the

only hematoma which appeared to be extracranial (Figure 3.20, red box). Brain tissue was collected on day D 18.

Figure 3.20. sTBI and RmTBI can produce concussion, contusion and hematomas

	Concussion	Contusion	Hematoma
95g x 1.5m			
120g x 1.5m			
150g x 1.5m			
95g x 1m x 5 TBI			
120g x 1m x 5 TBI			

**Figure 3.20. sTBI and RmTBI can produce concussion, contusion, and hematomas.**

Columns divide concussions, contusions, and hematomas and rows separate the different injury groups. All gross morphological injuries of each group are shown in this table. Each photograph corresponds to an individual animal, except for the images in the dashed line red square, that shows an extracranial hematoma (right image in red square). After opening

the skull, no intracranial hematoma was visible, and a small contusive injury was discovered (left image in red square).

## **DISCUSSION AND CONCLUSIONS**

The last decade has seen an increased interest in the study of mild TBI (mTBI) and RmTBI. This increase is mainly due to the prevalence of mTBI in the military, named the signature injury of the US war in Iraq and Afghanistan (Elder and Cristian 2009), and the realization of neurodegenerative consequences of concussions in athletes (Omalu et al. 2005, Omalu et al. 2006, Omalu et al. 2010). This interest sparked the production of a new generation of animal models taking on the challenge to reproduce the sometimes subtle sequelae of mTBI and the more robust seen in RmTBI (Mannix et al. 2014, Mannix et al. 2013, Meehan et al. 2012, Kobeissy et al. 2016, Dapul et al. 2013, Khuman et al. 2011, Yates et al. 2017, Kane et al. 2012, Mychasiuk et al. 2014, Bodnar et al. 2019, Dewitt et al. 2013, Namjoshi et al. 2014, Sauerbeck et al. 2018, Ren et al. 2013).

Many of the recent models designed for repetitive injuries have originated from modifications of the Marmarou weight-drop impact-acceleration model. These new models reduced mortality, skull fractures and double impacts with the addition of a support system that allows animals to fall through it (made of aluminum foil or Kimwipes) (Kane et al. 2012, Mychasiuk et al. 2014, Khuman et al. 2011, Meehan et al. 2012). This design is clinically significant due to their impact-acceleration mechanics, commonly seen in humans. However, the variability concern remains.

Our newly generated closed-skull weight-drop animal model of TBI was based on a model that was designed for repetitive mild injuries. However, our newly designed apparatus and optimizations enable us to carry out a spectrum of sTBI with graded

severities, while still allowing the induction of repetitive mild TBIs. The overall purpose of this study was to extensively characterize the biomechanics of injury and behavioral outcomes in a spectrum of sTBI severities and RmTBI generated by this novel system. This model shares important characteristics with its predecessors and contemporaneous models. This model, like the other new impact-acceleration models, does not require surgery and can be performed under short exposures of inhalational anesthetics (isoflurane 2.5%), which permits to assess neurobehavioral outcomes shortly after injury (Kane et al. 2012, Mychasiuk et al. 2014, Khuman et al. 2011, Meehan et al. 2012, Namjoshi et al. 2014, Ren et al. 2013). Although this model requires some practice to get comfortable with the process of inducing the injury (due to the placement of the sensor, pulse-oximeter and arming the system to initiate recording), it quickly becomes consistent. The short time required from the start of the anesthesia induction to the end of the injury (three to four minutes) makes this model high throughput. To our knowledge, this is the first time that one of these new generation models of impact-acceleration with breakthrough supports have been biomechanically characterized.

Our results suggest that the model is biomechanically reproducible and that the responses of the head of the animal show consistency. When comparing these results with Marmarou based models (use foam as a support system for the head) in which biomechanics have been measured, consistency is similar or better in some parameters. The peak speed the head of the animals reached after impact ranged from  $3.75 \pm 0.19$  to  $4.01 \pm 0.26$  m/s (95 g and 120 g objects x 1.0 m) and  $4.83 \pm 0.27$  to  $4.94 \pm 0.18$  m/s (95 g and 150 g objects x 1.5 m, mean  $\pm$  SD), as compared to  $4.15 \pm 0.50$  m/s (450 g object x 1.0 m) and  $5.05 \pm 0.38$  m/s (450 g object x 1.5 m, Mean  $\pm$  SEM) in a weight-drop rat model (Hsieh et al. 2017). The CHIMERA model (a piston-based model) with an injury force set to 0.5 joules, show a peak speed of the animal's head of  $6.6 \pm 0.8$  m/s (Mean  $\pm$  SD), this was a faster speed and a higher variability than our model (Namjoshi et al. 2014). Peak

acceleration was higher in our model, ranging from  $804.00 \pm 82.18$  (g) to  $1110 \pm 145$  (g) ( $95$  g x  $1.0$  m and  $150$  g x  $1.5$  m respectively, mean  $\pm$  SD) when compared to the foam support weight-drop rat models,  $211.19 \pm 11.12$  (g) ( $450$  g x  $1.0$  m),  $249.24 \pm 5.83$  ( $450$  g x  $1.5$  m, mean  $\pm$  SEM),  $666 \pm 165$  (g) ( $450$  g x  $1.25$  m) and,  $907 \pm 501$  (g) ( $450$  g at  $2.25$  m, mean  $\pm$  SD), and the variability of our model was lower when compared to the latter model (Hsieh et al. 2017, Li et al. 2011). Our model provides almost double the linear acceleration with slightly higher variability than the CHIMERA model in the mild injuries ( $95$  g x  $1.0$  m, see above),  $385.3 \pm 52$  (g) (mean  $\pm$  SD) (Namjoshi et al. 2014). However, when compared with the recent modCHIIMERA, our model produces a smaller peak linear acceleration against  $1398$  (g) and  $1446$  (g) in its both configurations  $1.7$  and  $2.1$  Joules (Sauerbeck et al. 2018).

The results from the force (N) applied to the head of the animal were surprising because the objects dropped from  $1.5$  m formed a plateau, and yet the behavioral outcome followed an object-weight and drop-height dependent trend. Experiments done in Chapter 2 show that when the material being impacted resists compression, the force applied to the top of the animal's head increases in an object-weight and height-drop dependent manner. These results also show an increase in the force applied to the center and the bottom of the animal's head as object-weight and height of the drop increase. These findings suggest that a compression of the skull on the brain might be occurring after reaching a certain threshold. No deaths or skull fractures were seen in these experiments representing a lower mortality and fracture rate than those reported by Kane et al. (Kane et al. 2012). We found differences in the injuries produced by the two iterations of the model used in our laboratory. In the weight-drop model without the impactor but with a fishing line attached to the falling object, injuries had a mortality of  $16 - 20\%$ , intracranial hemorrhagic events  $27-30\%$ , severe neurological deficits  $13\%$  (that warranted euthanasia, as per our protocol) and  $1.8\%$  skull fractures ( $150$  g x  $1.5$  m). The mortality in this version of the model was

mostly due to intracranial hemorrhage. In the novel apparatus with the impactor and the sensor-based system used for this study (impactor with no fishing line), concussion was seen in 10% and 20% of the injuries induced by 95 g object x 1.5 m and 120 g x 1.5 m, respectively. Contusions were induced at a rate of 20% by both injuries with the 120 g and 150 g objects dropped from 1.5 m (Figure 3.20). RmTBI produced contusions on 27% of the animals injured with each object, one of which showed an extracranial hematoma induced by the 95 g object dropped from 1.0 m. Further, skull fractures appeared in this model when a 160 g (1 out of 4 TBIs) and 210 g (4 out of 7 TBIs) objects were dropped from 1.5 m (Data not shown, and forces were not recorded).

The behavioral characterization allowed to find sensitive tests that can identify differences in outcomes of the various severities of injuries. Neurological deficits were detected in sTBI and RmTBI by the NSS. The 120 g and 150 g x 1.5 m groups showed neurological deficits after sTBI. In the 150 g x 1.5 m, deficits were observed 2 hrs post injury and did not return to baseline by D13. These results show deficits longer than other closed skull models, the “Hit & Run” model, showed deficits in a “moderate” injury that resolved seven days after TBI (Ren et al. 2013). An open scalp weight drop model (333 g rod dropped 3 cm) with a “severe” injury produced neurological deficits that were also resolved after one week (Flierl et al. 2009). Our results were similar to those reported by Kahlin, (250 g rod dropped from 2 cm) that reached an NSS score of 6.83, 1 hr post-injury and remained elevated at seven days post-injury (Khalin et al. 2016).

On the other hand, RmTBI started without deficits and got worse as the number of injuries increased. The results of RmTBI, two injuries with the CHIMERA model showed a sustained increase in NSS score from 1 hour to 7 days post-injury (Namjoshi et al. 2014). One probability for these differences is that the individual injuries we are producing are

milder than those seen in the CHIMERA model. Thus, it requires multiple impacts before neurological deficits are severe enough to be detected.

GS results followed an object-weight and height dependent trend in the sTBI and RmTBI with decreased strength in the 120 g and 150 g x 1.5 m groups and 95 g and 120 g x 1.0 m x 5 injuries, respectively. Interestingly, the weight-drop studies that look at grip focus on the ability of the mouse to hang for more than 10 seconds (Khuman et al. 2011), and not the actual strength of the grip. Studies in humans report a reduction of GS after injury, that usually resolves within one year (Haaland et al. 1994, Hellal et al. 2003, Jin et al. 2011, Song et al. 2015). The GS is a sensitive test to assess TBI deficits and should be included as part of the evaluation of this TBI model in experiments of sTBI and RmTBI.

Anxiety-like behavior was not increased in this animal model of TBI as assessed by EPM, PAS or OF, instead TBI reduced acrophobia which can be correlated with risk-seeking behavior. TBI increased open arm exploration in sTBI (injuries from 1.5 m), and in the RmTBI (95 g x 5 injuries group, but not the 120 g x 5 injuries group). There was also an increase in center exploration (95 g and 120 g x 1.5 m) and decreased closed arm exploration (all 1.5 m groups). Multiple studies have reported an increase in anxiety-like behavior after TBI assessed by both the EPM and the OF (Popovitz, Mysore, and Adwanikar 2019, Broussard et al. 2018, Malkesman et al. 2013). While other groups have suggested that TBI increases risk-seeking behavior and this can be seen in higher exploration of the open arms of the EPM (Malkesman et al. 2013, Cheng et al. 2019, Gold et al. 2018, Petraglia, Dashnaw, et al. 2014, Petraglia, Plog, et al. 2014), as well as in impulsivity or gambling tasks (Vonder Haar et al. 2017, Shaver et al. 2019). The discrepancies among all these studies (including ours) may be explained by the previous finding of a “U” shape response in which mild or severe injuries show anxiety phenotypes while the middle shows the increase in risk-seeking behavior (Budde et al. 2013). This

could also serve as a potential explanation for the reduced open arm exploration in the 120 g RmTBI group.

The results obtained from NOR and NLR were unexpected since we have shown that the previous iteration of our model induces deficits in NOR (Chapter 4). All groups recognized the novel object, although all groups spent longer time exploring the novel object, this difference was not significant in some groups (95 g and 120 g x 1.5 m and the control groups for the last day of injuries of the RmTBI 95 g and 120 g x L). This similarity disappeared when discrimination or investigation ratio was calculated. This measure accounts for the differences in total time of exploration of each animal. The opposite was true in the NLR, where there was no distinction of the novel location by almost every group. Potential problems in this test are the use of new objects, although similar to the ones used in Chapter 4, the filling was different and the objects appeared brighter. These differences could have led to object preference making animal be more interested in the 150 ml Nalgene filter, than the T75 flask, and continued through the location. For these reasons, both of these tests are recommended to be used with this model regardless of the results presented here. However, the order of testing is recommended to be inversed (NLR followed by NOR) to avoid an object preference in both tests and obtain results unbiased due to the object at least in the spatial recognition task.

FC was used to assess memory learning, the results indicate a reduction in contextual memory, yet cued memory remained unaffected. This combination of results has been correlated with a hippocampal deficits since the cued memory is hippocampus-independent (Hernandez et al. 2010) and contextual has both hippocampal and amygdala (lateral nucleus) components (Goosens and Maren 2001). Although not significantly different, post-cue freezing showed trends to decrease in some groups when compared to the enhanced 95 g x 1.0 m group. In RmTBI this difference was significant between the 95

g x 1.0 m and the 95 g x 5 injuries group (Data not shown). This decrease in amygdala activation after TBI has been previously reported (Palmer et al. 2016). We additionally report an enhancement of FC contextual memory when comparing 95 g x 1.0 m group with sham. This enhancement of fear conditioning after mild TBI has been reported elsewhere (Reger et al. 2012), and was discussed as potential signs of post-traumatic stress disorder. This theory requires further studies. The findings in contextual memory deficits provide further motives to retest NOR and NLR in the assessment of injury outcomes in this model.

This study had several limitations, one technical limitation was the lack of a three-axis accelerometer that could allow us to analyze angular as well linear acceleration. In order to perform the broad ranges of injuries, the study was most likely underpowered for the multiple comparisons and the number of groups. This was in part planned, it would allow us to detect the most sensitive tests to assess outcome differences even with a low n. Another limitation was the type of statistical analysis used. This analysis was chosen as the basic tests for the different analyses shown in this study, but they are by no means the optimal. More complex analyses would be ideal to obtain a clearer picture of the differences between the groups. The analyses used, added to the complexity due to the number of comparisons made and the adjustment of the p-values, may lead to type II errors. Further plans before the publication of this work are to modify the statistical analysis shown here, to a multivariate linear regression model for the spectrum of injuries. For the repetitive injury analysis, a full repeated measures analysis that may include a spline to level off the behavior, accounting for the baseline. A final option, albeit more complex, would be to perform principal component analysis, this may be better once the results from the immunohistological data and the immediate physiological response to the injury are added to the study. Such analyses will allow us to correlate the results for all tests to the individual biomechanical measurements, which might allow us to have a better

understanding of injury predictors in this animal model. However, this will require a trained statistician to guide the complex analysis.

Immediate actions for this project are the analysis of the already acquired immunohistochemical images, including microglial activation (Iba-1), Phosphorylated c-Jun and fibrinogen. It is also pending to receive the images and analysis for Phosphorylated Tau being carried out by our collaborators. Future directions for biomechanical studies with this model are to test the outcomes after lateral impact in the head (Mychasiuk et al. 2016) and incorporate the angular acceleration measurement. Additionally, potential changes to the shape of the impactor may improve the contact with the head of the mouse, and changes in the tip of the impactor may allow for higher weighted objects and heights to be used while reducing skull fractures (seen with the 160 g and 210 g x 1.5 m). Higher levels of severity of injury should also be explored.

We have shown a model that produces robust behavioral changes, both in single and repetitive injuries. This model has proven to be a useful tool for high throughput studies that can be used to assess therapeutic efficacy in a spectrum of sTBI with different severities as well as in RmTBI.

## **Chapter 4 Repurposing of an FDA-approved Poly (ADP-ribose) polymerase 1 (PARP1) inhibitor (olaparib) to treat neurotrauma**

### **INTRODUCTION**

Poly(ADP-ribose) polymerase 1 (PARP1, EC 2.4.2.30) is the major isoform of a family of enzymes, present in the nucleus and mitochondria. It is responsible for a posttranslational modification called poly(ADP-ribosylation) (PARylation), which is achieved by the transfer of ADP-ribose units from NAD<sup>+</sup> (Du et al. 2003, Jagtap and Szabo 2005, Long, Klimova, and Kristian 2017). PARP1 has been implicated in DNA repair, transcriptional and cell cycle regulation, activation transcription factors for pro-inflammatory signaling, mitochondria metabolic regulation, and several forms of cell death such as necrosis, apoptosis and parthanatos (Berger et al. 2018, Thomas and Tulin 2013, Charriaut-Marlangue et al. 2018, Brunyanszki et al. 2016, Fujikawa 2015, Narne et al. 2017). The overactivation of PARP1 increases the production of PARylated proteins (PARs) consuming the NAD<sup>+</sup> in the cells, which leads to the consumption of ATP and depletion of ATP stores, generating a metabolic crisis that ultimately ends in necrotic cell death. Alternatively, mitochondrial PARP1 activation can induce mitochondrial dysfunction and induce parthanatos or apoptosis (Abramov and Duchon 2008, Alano et al. 2010, LaPlaca et al. 2001, Hortobagyi et al. 2003, Duan, Gross, and Sheu 2007, Du et al. 2003, Lai et al. 2008).

We and others have reported PARP1 activation in human TBI (Berger et al. 2018, Sarnaik et al. 2010, Fink et al. 2008). Single nucleotide polymorphisms in the PARP1 gene were correlated with favorable outcomes after TBI (Sarnaik et al. 2010). PARP activation was found in the neurons of the pericontusional tissue of patients that suffered severe TBI (Berger et al. 2018), and PARylated proteins in the cerebrospinal fluid of children that

suffered a TBI (Fink et al. 2008). Furthermore, PARP1 deficient mice have shown remarkable resilience against TBI (Zaremba et al. 2010). Pharmacological inhibition of PARP1 has shown to be neuroprotective in *in vitro* models of neuronal excitotoxicity, and oxygen-glucose deprivation. Additionally, the neuroprotective effects have also been described in *in vivo* murine models of stroke and TBI (Whalen et al. 1999, Rom et al. 2015, LaPlaca et al. 2001, Besson et al. 2005, Clark et al. 2007, Stoica et al. 2014, Besson et al. 2003, Satchell et al. 2003, Lacza et al. 2003).

In late 2014, the first PARP1 inhibitor was approved by the FDA for its use in ovarian cancer (Drew 2015, Deeks 2015), since then more have been approved. Olaparib (Lynparza™) was the first ultrapotent PARP inhibitor approved and is also the only clinically used PARP inhibitor with efficacy data outside of oncological indications. It has shown cytoprotective and neuroprotective characteristics in oxygen-glucose deprivation and NMDA receptor activation models of neuronal death (Xu et al. 2016). Additionally, only partial PARP inhibition is necessary to confer neuroprotection, which translates into a much lower dose (1-5mg/kg/day) (Berger et al. 2018) than its oncological indication (50-200 mg/kg/day) (To et al. 2014, Henneman et al. 2015). This dose has a lower probability of presenting side effects while maintaining cytoprotective efficacy.

The lack of effective treatments for TBI and the neuroprotective effects of olaparib, along with the pathophysiological characteristics of TBI, make olaparib an attractive candidate to test for potential repurposing for use in neurotrauma. The objective of this study is to provide evidence that olaparib protects against neurological and cognitive deficits in TBI.

## **MATERIALS AND METHODS**

### **Cell culture and injuries**

#### ***OXIDATIVE STRESS INJURY AND KINETIC LACTATE DEHYDROGENASE (LDH) ASSAY***

Rat B35 neuroblastoma cells, obtained from the American Type Culture Collection (ATCC, Manassas, VA), were cultured in collagen-treated plates according to previous description (Lopez-Garcia et al. 2018). Cells differentiation was induced with the addition of all-trans retinoic acid (ATRA) (10  $\mu$ M) and incubated at 37°C in 5% CO<sub>2</sub>. Fresh medium was supplemented with 600  $\mu$ M H<sub>2</sub>O<sub>2</sub> to induce oxidative stress, and one subset was treated with PARP inhibitors: olaparib (1  $\mu$ M) or PJ34 (10  $\mu$ M, as a positive control) for 24 hours. LDH activity after oxidative stress injury was performed as per our previously described methods (Gero et al. 2007, Lopez-Garcia et al. 2018) with minor modifications. Cell culture supernatant collected 24 hours after injury was mixed with 100 $\mu$ l of an LDH assay reagent, freshly prepared. The LDH assay reagent was composed of lactic acid (110 mM), NAD<sup>+</sup> (1350 mM), N-methylphenazonium methyl sulfate (290 mM), 2-(4-iodophenyl)-3-(4-nitrophenyl)-5-phenyl-2H-tetrazolium chloride (685 mM), and Tris at pH8.2 (200 mM). The absorbance changes over 15 minutes were measured kinetically at 492 nm (kinetic LDH assay). Results are shown as maximal velocity of LDH activity (mOD/min).

#### ***PROLIFERATION AND DIFFERENTIATION OF hNSCs***

Human neural stem cells (hNSCs) from the K048 line, derived from an 8-week human fetal forebrain, were kindly provided by C.N. Svendsen (Wu et al. 2002, Svendsen et al. 1998). Cells were cultured in a T75 culture flask, as previously described (Wu et al. 2002), with slightly modified methods. Briefly, K048 cells (0.5x10<sup>6</sup>/mL) were maintained in basic medium (composed of Dulbecco's Modified Eagle Medium [DMEM; 11965-092,

Gibco, Waltham, MA] and F12 [11765-054, Gibco, Waltham, MA] with a 3:1 ratio, in addition to 4-(2-hydroxyethyl)-1-piperazineethanesulfonic acid [HEPES] 15mM, 1.5% glucose, L-glutamine 2mM and 1x penicillin/streptomycin). The medium was supplemented with TPPS (transferrin 100µg/mL putrescine 100µM, progesterone 20 nM, insulin 25µg/mL and 30nM sodium selenite), epidermal growth factor (EGF) 20ng/mL (236-EG-200, R&D Systems, Minneapolis, MN), bFGF 20ng/mL (233-FB-025, R&D Systems, Minneapolis, MN), LIF 10ng/mL (7734-LF-025, R&D Systems, Minneapolis, MN) and heparin 5µg/mL (H3149-100KU, Sigma, St. Louis, MO). Two-thirds of the proliferation medium was replaced every 3-4 days and cells were incubated at 37°C with 8.5% CO<sub>2</sub>. Neurospheres were dissociated every 8 to 10 days with 0.25% trypsin and mechanical trituration into single cells.

For differentiation of hNSCs to a co-culture of neurons and astrocytes, 3-day neurospheres were transferred and seeded (at a density of  $0.5 \times 10^6/\text{cm}^2$ ) onto Bioflex® plate collagen type I, 6-well culture plates with a silicone membrane bottom (BF-3001A, Flexcell International Co., Burlington, NC), pre-coated with poly-D-Lysine 0.01% and mouse laminin 1 µg/cm<sup>2</sup> (23017-015, Invitrogen, Carlsbad, CA). Cells were primed for 4 days with ELL medium (composed of basic medium and supplemented with TPPS, L-glutamine 2mM, Insulin 25µg/mL, EGF 20ng/mL, LIF 10ng/mL and Laminin 1µg/mL); and then differentiated in B27 medium [composed of basic medium with the addition of B27® Supplement (50x)(17504-044, Gibco, Waltham, MA) at the concentration of 1µl/ml] for 10 days with half of the differentiation medium replaced every 3-4 days. Cells were incubated at 37°C with 5% CO<sub>2</sub>.

### ***RAPID STRETCH INJURY AND TREATMENT***

The injury was performed using a stretch injury model, with small modifications to our and other's published methods (Wang et al. 2012, Ellis et al. 1995). Briefly, Bioflex® plate collagen type I, containing hNSCs-derived neurons and astrocytes, was placed on a culture tray holder. Each well was hermetically sealed with the pressure transducer of the **Cell Injury Controller II** (Biomedical Engineering Facility, Medical College of Virginia, Richmond, VA). A controlled pulse of nitrogen gas set at 65 psi was exerted over the silicone membrane to produce stretch deformation. Thirty minutes after injury, two-thirds of the medium was replaced with fresh B27 medium with olaparib (3, 10 or 30  $\mu$ M) dissolved in 10% dimethyl sulfoxide (DMSO) or vehicle and incubated at 37°C with 8.5% CO<sub>2</sub> for two and a half hours, 24 hours or 4 days.

### ***MOLECULAR ANALYSIS***

#### ***NECROSIS AND APOPTOSIS ASSAY***

Cell death was assessed to investigate the effect of olaparib on neuronal and astrocyte survival after stretch injury using the Apoptotic Necrotic and Healthy Cells Detection Kit (A028, GeneCopoeia™, Rockville, MD). This kit labels annexin V for apoptotic cells, propidium iodine for necrotic cells and Hoechst 33342 as a nuclear counterstain. Briefly, hNSC were differentiated into a co-culture of neurons and astrocytes and underwent rapid stretch injury. Half an hour post-injury cells were treated with 10  $\mu$ M olaparib in 10% DMSO or vehicle. Twenty-four hours post-injury each silicone membrane with the cells attached was cut into four pieces and placed in a 12-well plate with B27 differentiation media. For the staining and detection of apoptotic necrotic and healthy cells, the manufacturer's protocol was followed. Images were acquired with a Nikon TE2000-E microscope with a C1si confocal system (Nikon Instruments Inc., Lewisville, Tx.).

### ***NAD, NADH, AND NAD/NADH MEASUREMENTS***

NAD and NADH were used to assess if olaparib improved metabolic state after stretch injury. Total NAD and NADH (ab186032, Abcam, Cambridge, MA) and NAD/NADH assay kits (ab65348, Abcam, Cambridge, MA) were used to quantify total NAD+NADH levels, and total NAD and total NADH levels respectively. Briefly, hNSCs derived neurons and astrocytes underwent rapid stretch injury and were treated with 10  $\mu$ M olaparib in 10% DMSO or vehicle 30-min after injury. Cells were collected 3 hours post-injury, and NAD+NADH or NAD and NADH were quantified as per the manufacturer's protocol. Absorbance was detected and quantified with a plate reader GM3500 and the GloMax® Explorer System software (Promega, Madison, WI).

### ***IMMUNOFLUORESCENCE (IMMUNOCYTOCHEMISTRY)***

Immunostaining procedures were previously described in detail (Gao et al. 2006). Briefly, cells in plates were fixed four days after injury with ice-cold 4% paraformaldehyde for 20 minutes, then blocked with 5% normal serum plus 0.3% bovine serum albumin (BSA, Sigma, St. Louis, MO) and permeabilized with 0.25% Triton X-100 in TBS. Incubation with Primary antibodies took place at 4°C overnight. Mouse anti-Tubulin  $\beta$  3 antibody (TuJ1 1:1000, MMS-435P, Covance, Princeton, NJ) stained neurons, anti-rabbit Glial fibrillary acidic protein (GFAP) (1:2000, 103M4756, Sigma-Aldrich, St. Louis, MO) for astrocytes, and 4', 6-diamidino-2-phenylindole (DAPI) as a nuclear counterstain (1:1000, D1306, Molecular Probes, Life sciences, Eugene, OR). Signals were visualized by incubation of species-specific secondary antibodies conjugated with Alexa Fluor 488 or 568 (1:500, A-11008 and A-11004, Invitrogen, Carlsbad, CA) at room temperature for two hours in the dark. Imaging was done using epifluorescent microscope Nikon Eclipse 80i with Nikon elements software (Nikon Instruments Inc., Lewisville, TX).

Figure 4.1. In vitro experimental design

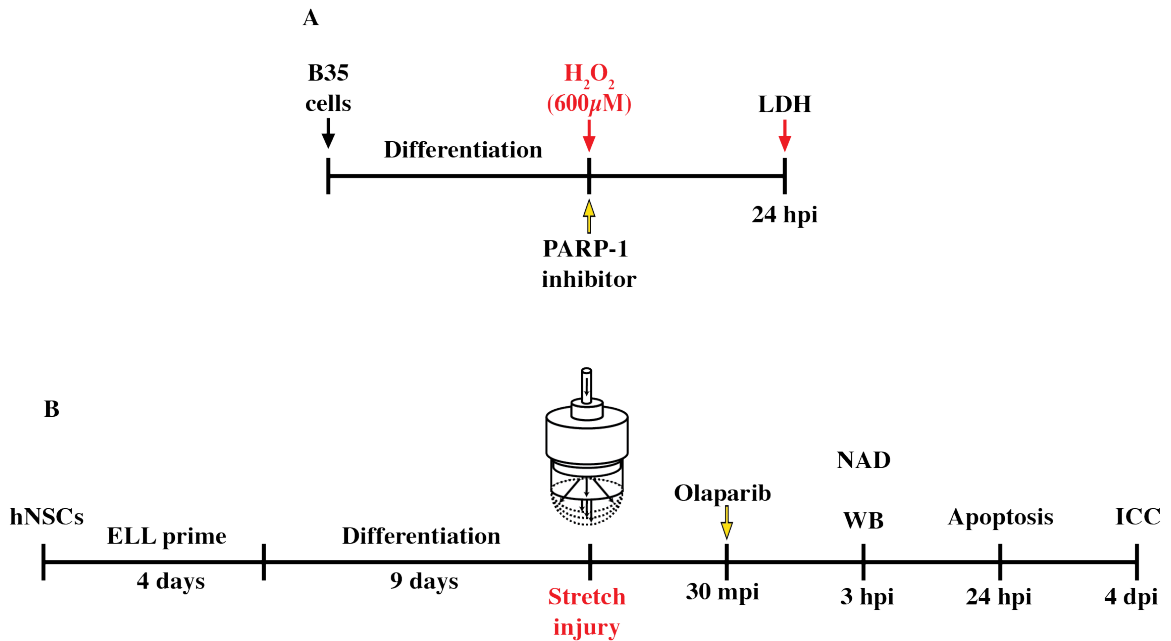


**Figure 4.1. In vitro experimental design.** Experimental design for all cell types and outcomes. A) Experimental design to measure the effect of poly(ADP-ribose) polymerase (PARP) inhibition against oxidant-induced cell death, B35 rat neuroblastoma cells were differentiated and treated with H<sub>2</sub>O<sub>2</sub> (600 μM) ± PARP inhibitors olaparib (1 μM) or PJ34 (10 μM; positive control) and kinetic LDH assay was measured after 24 hours of incubation. B) Human neural stem cells (hNSCs) were primed and differentiated (13 days) into a co-culture of neurons and astrocytes. The differentiated cells were subjected to a stretch injury and treated with olaparib 30 min post injury (mpi). Samples were collected 3 hours post injury (hpi) for WB analysis of expression of PARP1 and poly (ADP-ribose) proteins (PAR), as well as NAD and NADH analysis; 24 hours post injury to measure apoptotic and necrotic cell death and 4 days post injury (dpi) to assess neuronal survival via immunocytochemistry.

## **Animals and groups**

All procedures involving animals in this study were reviewed and approved by the Institutional Animal Care and Use Committee (IACUC) of the University of Texas Medical Branch. Thirty-eight male C57BL/6j mice, 8 to 10-week-old (000664, Jackson Lab, Sacramento, CA), were randomly assigned into four groups: sham + vehicle (n=9), sham + treatment (n=9), TBI + vehicle (n=12) and TBI + treatment (n=12). Animals that presented brain hemorrhage due to the injury, TBI + vehicle (n=2), TBI + treatment (n=4), were removed from further analysis.

## **Apparatus**

A closed-skull non-fixed head weight-drop injury system based on the model developed by Kane et al., in 2012 (Mychasiuk et al. 2014, Kane et al. 2012) was built in our laboratory with modifications. The model consists of a cylindrical brass object (19 mm in diameter, 150 g) with a brass disc (10 mm in diameter x 2 mm height) on its lower end to focus the impact on the mouse head between the ears. A fishing line (Super Strong Trilene® Big Game™ 20 LB, BGQS20C-81, Berkley®) suspends the brass object to restrain the travel distance (measured to the top of the aluminum foil) of the falling object and avoid double impacts on the animals. The object is then placed inside a polycarbonate guide tube (20 mm in internal diameter x 1.7 m length) to ensure it remains perpendicular to the ground. The guiding tube ends above an open acrylic chamber (38 cm length x 28 cm width x 22 cm depth) containing a foam cushion (10 cm height). The top of the chamber is covered by an aluminum foil that is slit along the midline. Three additional modifications were implemented to ensure higher reproducibility. First, a sensor to measure the velocity of the falling object (composed of two photodiodes and two phototransistors) placed in the last 10 cm of the guiding tube to accurately monitor the velocity and calculate the kinetic

energy of the falling object. Second, a pulley system, to avoid drag generated by the fishing line scraping the tube of the PC guiding tube. Third, a head guide device, built with a triangular clamp with padding materials, allowed to accurately position the mouse head underneath the guiding tube.

### **Closed-skull weight drop injury**

Closed-skull TBI was induced as reported by Kane et al. (Kane et al. 2012) with minor modifications. Briefly, mice were placed in an anesthesia chamber (9.6 L volume) with isoflurane 2.5% until unconsciousness was reached. Mice were then removed from the chamber and placed on a nose cone (2.5% isoflurane and 3 L flow) until they lost paw withdrawal reflex to pinch. Immediately after, mice were placed in the prone position, with its head placed within the triangular clamp, nose touching the vertex and head located directly underneath the aperture of the polycarbonate (PC) tube (3.5 cm above the aluminum foil). Mice lay on top of a previously slit sheet of aluminum foil, secured on the uppermost part of the box. The object of 150 g (secured to travel no farther than 1 cm after impact) was dropped from a height of 1.5 m (marked and secured with a bolt that crosses the width of the PC tube). Upon impact, the mice broke the aluminum foil and underwent acceleration while falling on the foam cushion 10 cm below. Animals were placed on a warm pad until they recovered consciousness. After regaining consciousness, they were placed in a warmed recovery chamber until fully awake and then transferred to their home cage.

## **Dose and route of administration**

Mice received an intraperitoneal (IP) injection of olaparib (3 mg/kg) or Vehicle (10% DMSO) 2 hours after injury followed by a subsequent dose every 12 hours until six doses were reached.

## **Neurological and behavioral assessment**

### ***RIGHTING REFLEX (RR)***

Used as a correlate of consciousness, the RR is a cerebellar reflex that drives the animal to be in a prone position whenever they are conscious. When the animal was exposed to anesthesia, the paw or tail pinch reflexes were assessed (to determine the depth of anesthesia). Once these reflexes were lost (analgesia was achieved) a chronometer was started, the anesthesia was shut down, and the animal received the injury. Immediately after injury, the mice were placed in the supine position over a warm area with a heating pad (set to Lo), where the righting reflex was continued to be assessed. The chronometer was stopped once the animal acquired the prone position, indicating that it had regained consciousness.

### ***LOCOMOTION ACTIVITY***

Locomotion was assessed in two different apparatuses, open field (One- and two-days post-injury as part of the novel object recognition paradigm, see below) and photobeam activity system (PAS) (at baseline, one, and three days post-injury). Spontaneous locomotion (distance traveled and speed), exploration (distance traveled, rearing, time in the center and the periphery of the box) as well as thigmotaxis ( $\frac{\text{Periphery}}{\text{Center+Periphery}}$ ) were measured based on time and distance explored. Briefly, animals

were placed in a 40x40x40 cm open field box and their behavior was recorded for 10 minutes by digital video capture and analyzed by the TopScan software (Ver 3.0, CleverSys Inc., Reston, VA) or through photo-cell beam breaks in the photobeam activity system (San Diego Instruments, San Diego, CA). The frames with the photobeams were positioned at 2.5cm from the ground for horizontal exploration and 4.5cm from the ground for rearing events. Equipment was thoroughly cleaned with 50% ethanol and allowed to air dry in between each animal.

### ***NOVEL OBJECT RECOGNITION (NOR)***

Spontaneous memory was assessed using the protocol described elsewhere (Ennaceur and Delacour 1988) with minor modifications. Briefly, animals underwent a three-day paradigm. On days one and two post-injury (habituation stage) mice were exposed to a white Plexiglas™ open field box (38x38x38cm) for 10 minutes in order to habituate to the new environment and reduce neophobia. During this period, we measured the same parameters mentioned in the PAS. On day three after injury mice underwent the familiarization stage for 10 minutes. During this stage two equal objects (two T75 culture flasks with non-vented caps [156472, Thermo Scientific, Waltham, MA] filled with sand for added weight and sealed with parafilm to avoid the release of smell from the sand) were placed in the corners, 10cm apart from either wall, of the open field box. A mouse was introduced on each open field box and allowed to explore the objects. Object exploration and all open field measurements were performed. On day four post-injury, after a 24-hour inter-trial period, mice were reintroduced in the open field box for the test stage. During this stage, one of the objects was replaced with a novel object (a 150 ml analytical filter, [130-4045, Nalgene, Waltham, MA] filled with sand for added weight, every opening filled with cold silicon and covered by parafilm, and profusely cleaned with 50% ethanol and allowed to dry to avoid odors). Mice were allowed to explore freely for ten minutes, object

exploration and open field measurements were recorded and analyzed. The open field box and objects were thoroughly cleaned with a 50% ethanol in water solution before and after every animal and allow to air dry to eliminate any odor cues.

### ***ELEVATED PLUS MAZE (EPM)***

Anxiety-like behavior was assessed using the single exposure paradigm of the elevated plus maze (Walf and Frye 2007). Locomotion and anxiety-like behaviors (entries, time, distance and percentage of time in the center, open and closed arms) were measured. Briefly, on day four post injury each mouse was placed in the center of the maze, facing the open arm and allowed free exploration for 5 minutes. Recording began immediately after placing the mouse on the center of the maze. Recording and analysis were performed by the TopScan software (Ver 3.0, CleverSys Inc., Reston, VA). Equipment was thoroughly cleaned with 50% ethanol and allowed to air dry in between each animal.

Figure 4.2. In vivo experimental design for assessment of olaparib treated TBI

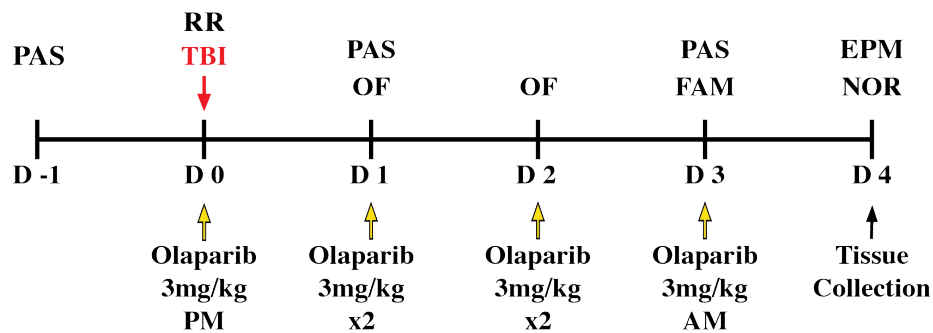


**Figure 4.2. *In vivo* experimental design for assessment of olaparib treated TBI.** Mice were subjected to impact-acceleration closed-skull weight drop traumatic brain injury. TBI was induced with a 150 g object dropped from 1.5 meters, where time to righting reflex (RR) was recorded. Two hours after injury mice received the first dose of olaparib (3 mg/kg, i.p.) in the afternoon, followed by five more doses, one every 12 hours. Animal

locomotion activity was assessed by photobeam activity system (PAS) and open field (OF). Cognitive assessment was conducted by novel object recognition (NOR), and anxiety-like behavior evaluated by elevated plus maze (EPM). Brain tissue was collected 4 days post injury.

### **Tissue processing**

Tissue collection was performed as per our previous protocol (Gao et al. 2006), with modifications. Briefly, animals were euthanized four days post-injury by ketamine/xylazine (90 mg/kg and 10 mg/kg) injection (i.p.). After mice lost pain reflex, the thoracic cavity was opened, and 0.3-0.5 ml of blood was collected from the heart into an EDTA microtainer collection tube (365974, BD, Franklin Lakes, NJ). For immunohistochemistry, 4-6 animals per group were perfused as following: a 5 mL intracardiac perfusion with ice-cold 0.1 M phosphate-buffered saline (PBS) was administered, followed by 30 mL of ice-cold 4% paraformaldehyde in PB, pH 7.4. Brains were collected and post-fixed overnight and immersed in sucrose 30% until tissue became isotonic (2 or 3 days). After cryoprotection, tissue was embedded in OCT (Fisher Scientific, Hampton, NH) and flash-frozen by immersing in 2-methyl butane in a cold bath of dry-ice with isopropyl alcohol and stored at -80°C until used. Serial coronal sections of 30  $\mu$ m were cut (Leica CM1900, Meyer Instruments Inc., Houston, TX) and mounted onto Superfrost™ Plus microscope slides (FisherBrand, Hampton, NH). Four sections were mounted per slide, separated 300  $\mu$ m apart. Tissue sections were stored at -20°C until used.

For protein and cytokine analysis, mice were perfused with 5 mL of PBS, followed by 10 mL of PBS with 1 mM phenylmethylsulfonyl fluoride (PMSF, Enzo Life Sciences Inc./Alexis Biochemicals), 1X protease inhibitor cocktail (P8340-5ml, Sigma, St. Louis, MO), 30 mM sodium fluoride (201154-100G, Sigma, St. Louis, MO) and 1 mM sodium

vanadate (56508-50G, Sigma, St. Louis, MO). Following perfusion, mice were decapitated, and brains were dissected into five brain regions: cerebellum, brainstem, hippocampus, midbrain and cortex. Samples were collected in cryogenic vials (430659, Corning, Corning, NY), fast frozen in liquid nitrogen and stored at -80°C until used.

## **Immunohistochemistry**

Immunohistochemistry was performed as previously described (Gao et al. 2006) with modifications. Briefly, brain tissue sections were blocked for one hour to reduce non-specific binding and cell membranes were permeabilized using a solution with 5% normal goat serum, 10% bovine serum albumin (0.3% final working concentration) and 85% of 0.25% Triton X-100 in Tris-buffered saline (TBS).

All antibodies were tested for optimal concentrations and centrifuged at 13,500 x g for 2 minutes at 4°C to avoid unspecific staining due to degraded antibodies. Tissue was then incubated overnight with primary antibodies at 4°C. Primary antibodies included: rabbit polyclonal anti-gial fibrillary acidic protein (GFAP, 1:2000, G9269, Sigma-Aldrich), rabbit polyclonal anti Iba-1 (1:250, 019-19741, Wako, Japan), rabbit polyclonal phosphorylated c-Jun, Serine 73 (Pc-Jun, 1:100, ab30620, Abcam, Cambridge, MA), rabbit polyclonal activated caspase 3 (aCas3, 1:1000, ab49822, Abcam, Cambridge, MA), and mouse monoclonal anti NeuN (1:1000, MAB377, Millipore, Burlington, MA).

Following incubation, tissue sections underwent three 10-min rinses in TBS and was later incubated for 3 hours at room temperature in species-specific Alexa Fluor 488 or 568 secondary antibody (1:500, A-11008 and A-11011, Invitrogen, Carlsbad, CA). Following incubation tissue was rinsed with TBS three times for 10-min each, and nuclei was counterstained with DAPI (1 µg/mL D9542, Sigma, St. Louis, MO) in TBS for 5-min

at room temperature. Coverslips were mounted onto the tissue sections with Fluoromount G (0100-01, SouthernBiotech, Birmingham, AL). Tissue sections were scanned and imaged with a Nikon TE2000-E microscope with a C1si confocal system (Nikon Instruments Inc., Lewisville, TX), and Fibrinogen/lectin imaging was obtained with All-in-one fluorescence microscope BZ-X710 (KEYENCE, Austin, TX).

## **Molecular analysis**

### ***MALONDIALDEHYDE (MDA) ABUNDANCE***

MDA is the most abundant reactive aldehyde secondary to decomposition of fatty acids due to lipid peroxidation, and thus it is used as a marker for lipid peroxidation and oxidative stress. MDA was quantified in tissue from different brain regions of these animals following the manufacturer's instructions for the ALdetect (MDA-Specific) Lipid Peroxidation Assay Kit (BML-AK171, Enzo Life Sciences, Farmingdale, NY). This kit measures free MDA through a reaction between N-methyl-2-phenylindole with MDA (2:1) at 45°C producing a stable carbocyanine dye that can be measured at 586 nm.

### ***MYELOPEROXIDASE (MPO) ACTIVITY***

MPO is a protein present in monocytes and primarily polymorphonuclear leukocytes (PMN). It produces substrate radicals by oxidizing aromatic compounds with the use of hydrogen peroxide produced by the neutrophils. When produced in excess, these radicals can generate oxidative stress and ultimately oxidative tissue damage. MPO can be used as a measure of MPO activity in neutrophils and macrophages, PMN infiltration and oxidative tissue damage. MPO activity was measured in tissue samples from different brain regions with the Myeloperoxidase fluorometric detection kit (ADI-907-029, Enzo Life Sciences, Farmingdale, NY). In the presence of MPO, a non-fluorescent reagent gets

oxidized into its fluorescent analog. The fluorescence can be measured with an excitation wavelength of 530-571 nm and an emission of 590-600nm.

### ***QUANTIFICATION OF CYTOKINE LEVELS IN PLASMA AND TISSUE***

Cytokine levels in plasma and tissue were used to assess the inflammatory environment and changes induced by injury and treatment. Quantitation was performed following the company's protocol and as previously described (Ahmad et al. 2016) with modifications. Animal blood collected in EDTA tubes was centrifuged at 1000 x g for 10 minutes, plasma was collected and stored at -80°C until use.

Simultaneous cytokine and chemokine quantitation in plasma and brain tissue (cortex and hippocampus) was done with EMD Millipore's MILLIPLEX™ MAP Mouse Cytokine/Chemokine Magnetic Bead Panel kit (MCYTOMAG-70K-PX32, EMD Millipore, Burlington, MA). The following cytokines and chemokines were analyzed: granulocyte-colony stimulating factor (G-CSF), granulocyte-macrophage-colony stimulating factor (GM-CSF), interferon (INF)  $\gamma$ , interleukin (IL)-1 $\alpha$ , IL-1 $\beta$ , IL-2, IL-4, IL-5, IL-6, IL-7, IL-9, IL-10, IL-12 (p40), IL-12 (p70), IL-13, IL-15, IL-17, INF  $\gamma$ -induced protein 10 (IP-10), keratinocyte chemoattractant (KC), monocyte chemoattractant protein 1 (MCP-1), macrophage inflammatory protein 1 $\alpha$  (MIP-1 $\alpha$ ), MIP-1 $\beta$ , MIP-2, RANTES (regulated upon activation normal T cell expressed and secreted), and tumor necrosis factor (TNF)  $\alpha$ . Data acquisition and analysis were done with the LuminexMAP fluorescent detection method via the LuminexPONENT™ acquisition software (Thermo Fisher Scientific, Waltham, MA).

## Statistical analysis

Statistical analysis for the photobeam activity system test was performed as follows. Each outcome was modeled by mixed analysis of variance with relation to group and day, including the interaction between them, blocking on the animal to control for repeated measures. Hommel-adjusted contrasts were used to assess differences among groups by day. Rear events, beam breaks, distance, zone entries and times (A-H) were log-transformed to a better approximation of normality before analysis. For log-transformed variables, the y-axis is on the (natural) log scale. For one of the thigmotaxis measurements, (Zone PctTime\*Distance) the percentage of time spent in each concentric zone was calculated and multiplied by the distance from the wall of each zone. Thus, a higher value represents a higher willingness of the mouse to move closer to the center. For NOR, to assess object preference above chance a Welch's 2-way 2-sample t-test with a reference of 50% was done. To compare differences in exploration between the novel and familiar object, and EPM analysis was modeled by a mixed analysis of variance concerning group differences, multiple comparisons were assessed by Tukey-adjusted contrasts.

Cytokine, MPO and MDA analysis was modeled by mixed analysis of variance with regard to group and differences among groups were assessed by Tukey-adjusted contrasts. For a better approximation of normality, data was Log base 2 transformed before the analysis. Figures for behavior, cytokines, MPO and MDA data, show Catseye plots, illustrating the normal distribution of the model-adjusted means by day, with shaded +/- standard error and overlaid on scatterplots of the raw data.

A mixed-effects model RM was used to assess change in animal weight over time with Tukey's multiple comparisons post hoc test. RR, image analysis, and WB were analyzed by one-way ANOVA with Tukey's multiple comparisons post hoc test.

## RESULTS

### Olaparib protects neurons from oxidant-induced cell death

To test the effect of olaparib on oxidant-induced neuronal cell death, we used a well-established model of oxidative damage. In this model B35 rat neuroblastoma cells were differentiated into neurons with ATRA. ATRA-differentiated B35 cells were exposed to hydrogen peroxide ( $\text{H}_2\text{O}_2$ ) ( $600 \mu\text{M}$ ) with or without a PARP-1 inhibitor (olaparib  $1 \mu\text{M}$  or PJ34  $10 \mu\text{M}$  as a positive control). After 24 hours of exposure to  $\text{H}_2\text{O}_2$ , LDH release was measured to assess necrotic cell death. Twenty-four hours post-injury the neurons exposed to  $\text{H}_2\text{O}_2$  showed an increase in LDH release when compared to non-exposed controls. On the other hand, both groups of cells exposed to  $\text{H}_2\text{O}_2$  and treated with a PARP-1 inhibitor prevented the increase in LDH release (Figure 4.3).

Figure 4.3. Olaparib protects neurons from oxidant-induced cell death

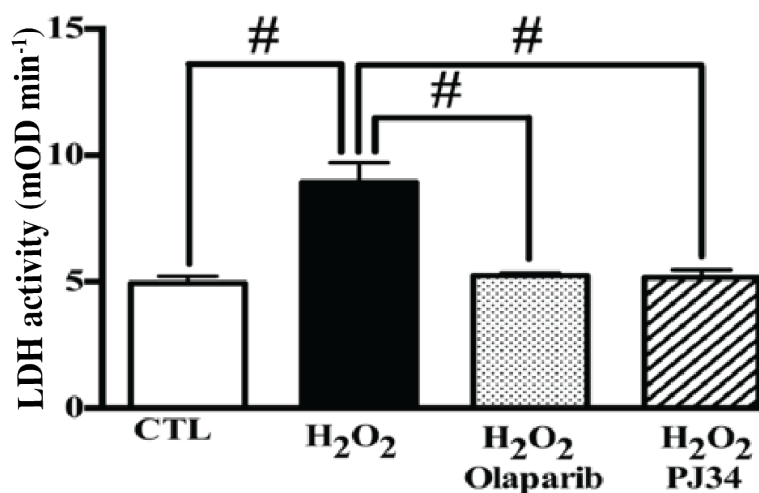


**Figure 4.3. Olaparib protects neurons from oxidant-induced cell death.** PARP inhibition reduces oxidant-induced cell death in differentiated rat neuroblastoma cells (B35) challenged with  $600 \mu\text{M}$  of  $\text{H}_2\text{O}_2$  and with or without treatment with PARP inhibitors olaparib ( $1 \mu\text{M}$ ) or PJ34 ( $10 \mu\text{M}$ ; positive control). Kinetic LDH assay was measured 24 hours post-injury. Both PARP inhibitors prevented the oxidative stress-

induced LDH release in the cell culture supernatant, LDH activity is shown in mOD/min. Data is shown as mean  $\pm$  SEM, n=4/group. <sup>#</sup>  $p < 0.05$ , analyzed by one-way ANOVA with Tukey's post hoc test

### **Olaparib reduces the formation of PARs and increases PARP1 expression**

PARP1 is responsible for PARylation, which is a NAD-dependent posttranslational modification where PAR units are added to proteins. PARs are essential in many aspects of cell signaling and produce both beneficial and detrimental events such as DNA repair, NAD depletion or cell death (Andrabi et al. 2006, Andrabi et al. 2014, Berger et al. 2018, Kim, Zhang, and Kraus 2005). As competitive inhibitor of PARP1, olaparib it binds to the catalytic site of the enzyme and prevents NAD binding, thus it is expected to prevent these processes. To determine the effect of olaparib on human neurons and astrocytes under stretch injury, we used western blotting to assess the expression of PARP1 and PAR. Cells were treated with olaparib or vehicle 30 min post-injury, and proteins were collected 3 hr post-injury. Olaparib increased PARP1 expression, while significantly reduced PAR accumulation. The increase in PARP1 expression suggests a compensatory mechanism (Figure 4.4, A, B, and D). Interestingly, the stretch injury did not increase the production of PAR in human neuro stem cell derived neurons and astrocytes. Olaparib also reduced the amount of cleaved PARP1 (cPARP1), indicating a reduction in apoptosis through caspase 3. PAR and cPARP1 are both suggested to contribute to cell death yet stretch injury did not increase either one of them. Thus, it remains to be determined whether an additional insult, such as H<sub>2</sub>O<sub>2</sub> is required to induce this response.

Figure 4.4. Olaparib reduces expression of PAR and cleaved PARP after stretch injury

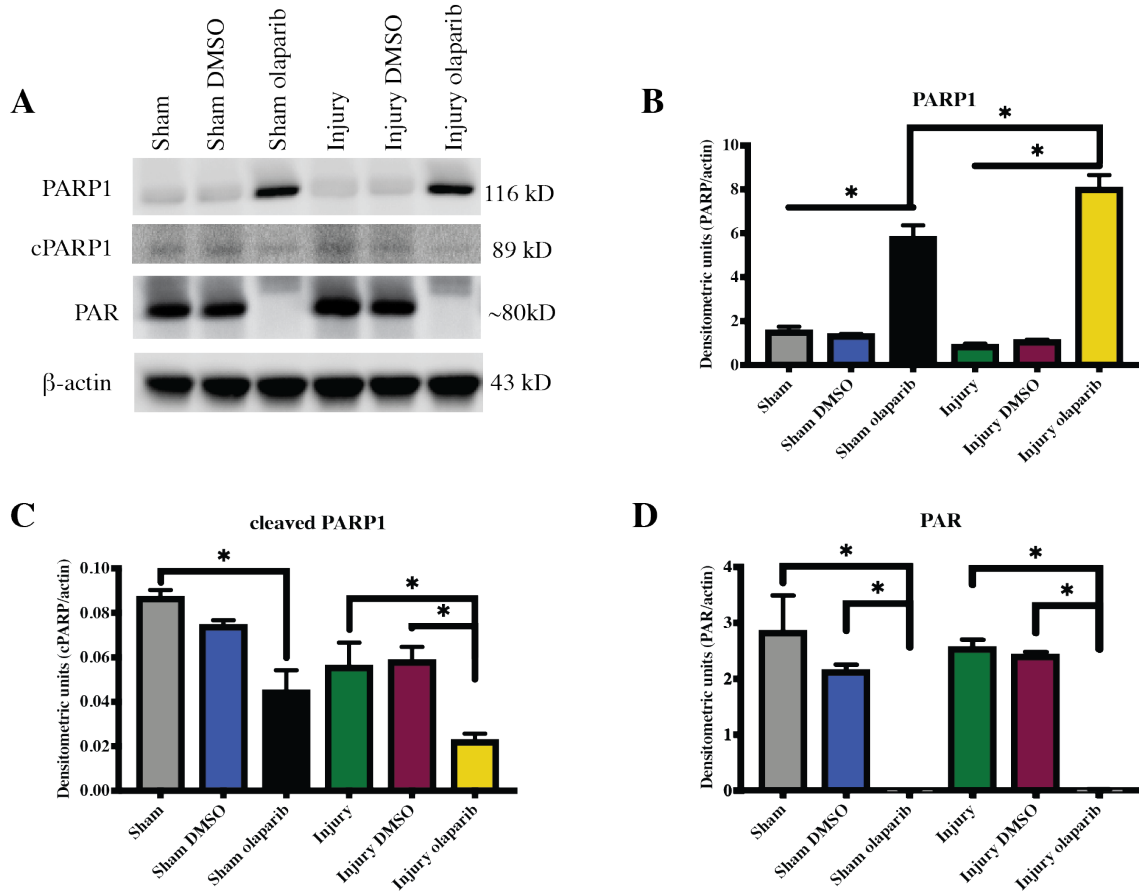


**Figure 4.4. Olaparib reduces expression of PAR and cleaved PARP after stretch injury.** A) Representative images of western blots. (B-D) Quantitative analyses of signals normalized over  $\beta$ -actin, 10  $\mu$ M olaparib 30 minutes after stretch injury increases the expression of PARP1 while reducing the amount of cleaved PARP1 and PAR polymers in hNSCs derived astrocytes and neurons collected 3 hours post-injury. Values are Mean  $\pm$  SEM, n=3, \*  $p$ <0.05, one-way ANOVA with Tukey's post hoc test.

### Olaparib reduces cell death and is neuroprotective after stretch injury

TBI is a condition known to induce PARP1 activation in humans and rodents (Ang et al. 2003, Fink et al. 2008, Sarnaik et al. 2010, LaPlaca et al. 1999). Furthermore, PARP1 and the production of PARs have been shown to induce cell death by multiple pathways

including apoptosis, necrosis, and parthanatos (Berger et al. 2018). A human brain neural stem cell (hNSCs)-derived co-culture of neurons and astrocytes was subjected to a well-established stretch injury model, to test the effect of olaparib on neuronal survival and stretch injury-induced cell death. Neuron and astrocyte co-cultures on 6-well plates with silicon bottom were subjected to stretch injury by applying a nitrogen pulse (65 psi) for 99 ms. Thirty minutes after injury cells were treated with olaparib (10  $\mu$ M) or vehicle (10% DMSO) and assessed for necrotic and apoptotic cell death 24 hours post-injury. As expected, olaparib reduced apoptotic cell death measured by annexin V (Figure 4.5, A and B); as well as “necrotic” cell death, assessed by propidium iodide, when compared to untreated injured cells (Figure 4.5, A and C). Neuronal survival was quantified to assess if this reduction in cell death was neuroprotective. A hNSCs-derived co-culture of neurons and astrocytes, treated with vehicle (10% DMSO) or olaparib (1  $\mu$ M, 10  $\mu$ M, and 30  $\mu$ M) 30 minutes after injury, was fixed four days post-injury and stained for neuronal and astrocytic markers. Neurons were quantified as a percentage of the total number of cells. Treatment with olaparib 10  $\mu$ M significantly increased neuronal cell survival following stretch injury. This beneficial effect disappears at 30  $\mu$ M. (Figure 4.5, D and E).

Figure 4.5. Olaparib reduces cell death and is neuroprotective after stretch injury

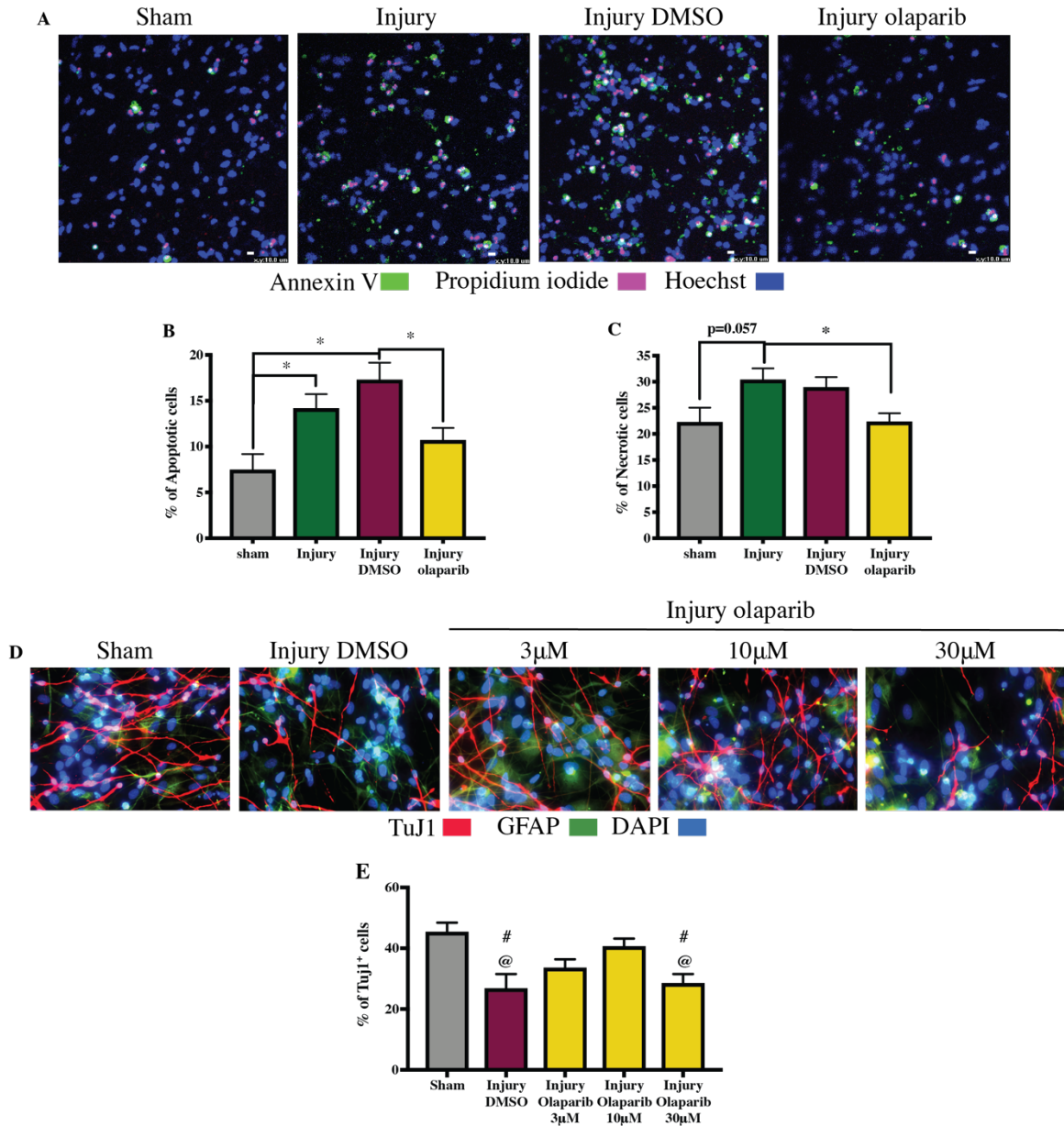


**Figure 4.5. Olaparib reduces apoptotic cell death and increases neuronal survival following stretch-injury.** A human neural stem cell-derived co-culture of neurons and astrocytes was subjected to stretch injury and treated with olaparib. A) Representative images of cell death, where green cells are undergoing apoptosis (annexin V), red are cells with compromised membrane integrity, undergoing “necrosis” (propidium iodide), and blue is a nuclear counterstain (Hoechst). B) Quantitative analysis of cells undergoing

apoptosis. Olaparib treatment (10  $\mu$ M) reduces apoptotic cell death after stretch injury. C) Quantitative analysis of necrotic cell death. Olaparib reduced “necrosis” after stretch-induced injury. D) Representative images of neuronal survival after stretch injury.  $\beta$ -tubulin III (Tuj1) was used as a neuronal marker (red), glial fibrillary acidic protein (GFAP) to stain astrocytes (green), and 4', 6-diamidino-2-phenylindole (DAPI) as a nuclear counterstain (blue). E) Quantification of Tuj1 positive cells. Olaparib shows an inverted “U” shape dose-response and increased neuronal survival at 10  $\mu$ M. Data showing mean  $\pm$  SEM, n=3 for each experiment. \*  $p < 0.05$ . one-way ANOVA with Tukey’s post hoc test. @ compared to sham, # compared to Injury olaparib 10  $\mu$ M

### **NAD levels are not restored with olaparib after stretch injury**

Activation of PARP for DNA repair catalyzes the cleavage of NAD<sup>+</sup> into nicotinamide and ADP-ribose. Injury through Ca<sup>2+</sup> influx and formation of ROS causes over-activation of PARP1 and may consequently deplete NAD<sup>+</sup>, initiating a metabolic crisis that will induce necrotic cell death (Abramov and Duchen 2008, Alano et al. 2010, LaPlaca et al. 2001, Hortobagyi et al. 2003, Duan, Gross, and Sheu 2007, Du et al. 2003, Lai et al. 2008). NAD<sup>+</sup> and NADH levels were measured to determine if the neuroprotective effects of olaparib are mediated by preservation of the NAD<sup>+</sup> stores. We collected samples at 3 hr after injury, 2 hr after olaparib treatment to assess NAD and NADH. Stretch injury reduces NAD<sup>+</sup> and NAD/NADH ratio, olaparib treatment did not alter NADH. This data indicates that olaparib inhibition in our system may not be sufficient to prevent NAD depletion.

Figure 4.6. NAD levels are not restored with olaparib after stretch injury in human neurons and astrocytes

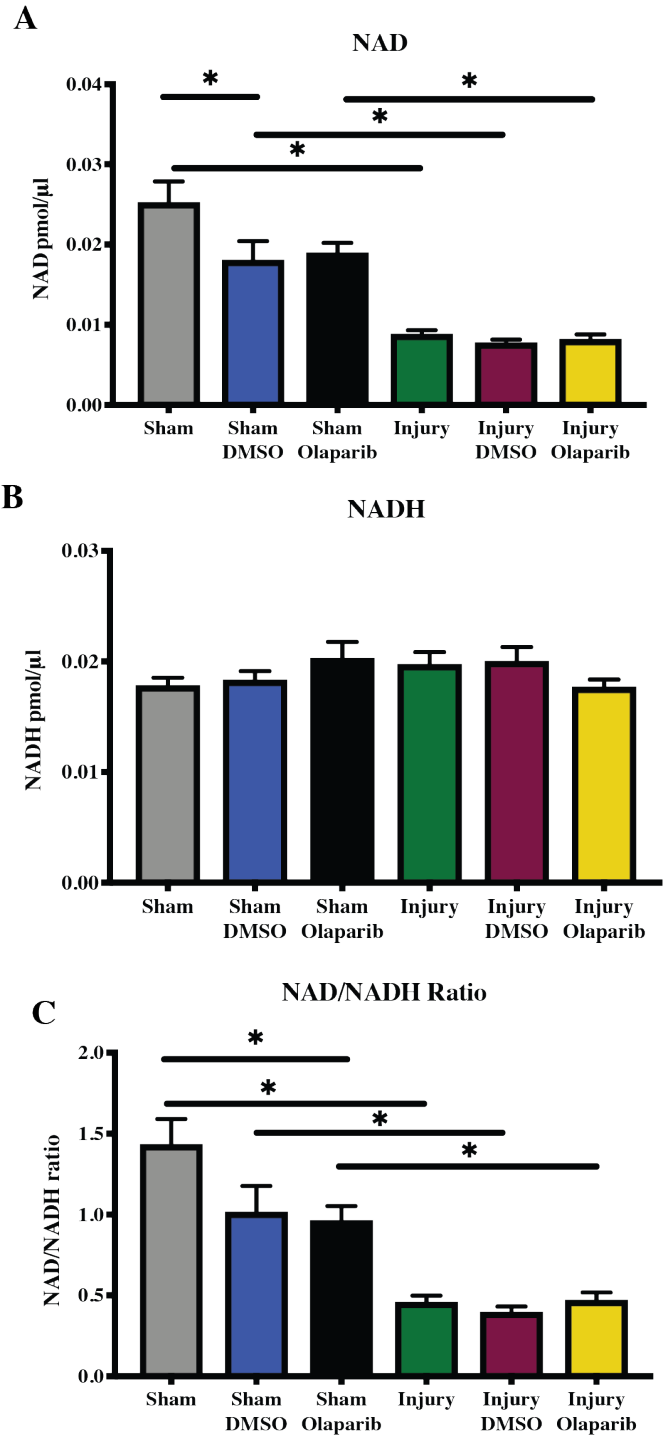


**Figure 4.6. NAD levels are not restored with olaparib after stretch injury in human neurons and astrocytes.** A) Stretch injury reduces the concentration of NAD in the cells

and olaparib does not prevent this decrease. B) No differences were found in NADH. C) NAD/NADH ratio as expected shows a similar trend as NAD. Values are mean  $\pm$  SEM, n=6, one-way ANOVA with Tukey's post hoc test for multiple comparisons.

The results showing the neuroprotective effects of olaparib in TBI models *in vitro* warranted the exploration of its effects *in vivo*.

### **Biomechanics of injury and RR**

Velocity of the falling object was measured, and kinetic energy was calculated. No differences in velocity of impact or kinetic energy was found between the groups (Figure 4.7, A-B). Also, no differences in anesthesia exposure or RR after injury were recorded (Figure 4.7, C-D), confirming that the level of loss of consciousness between the groups was comparable. Interestingly, the group that received TBI and 10% DMSO vehicle treatment lost weight after TBI and was unable to recover. In contrast, the group treated with olaparib lost weight after injury but was insignificantly different from the baseline 48 hrs. after injury onward.

Figure 4.7. Injury parameters and physiological outcomes

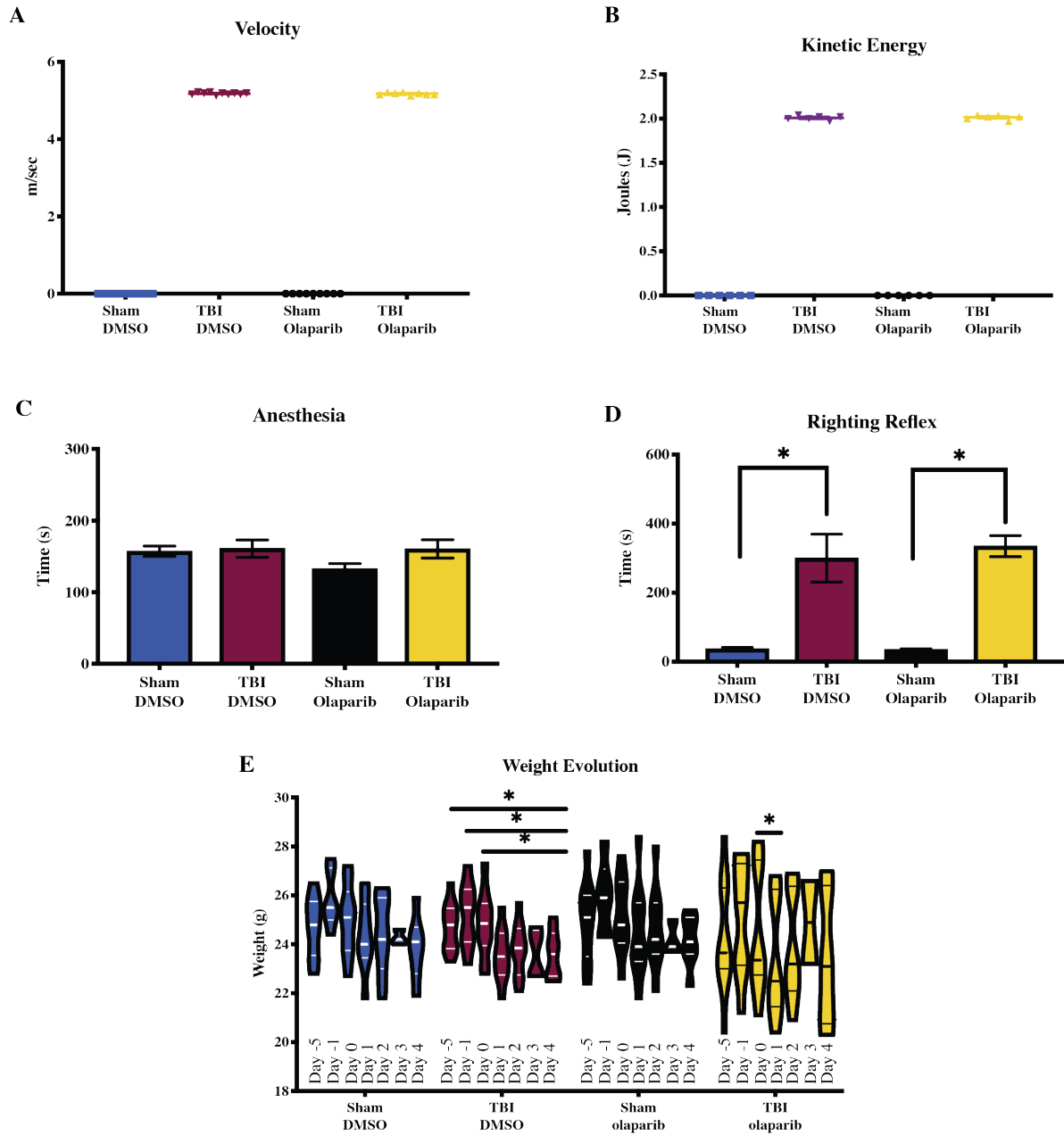


**Figure 4.7. Injury parameters and physiological outcomes.** A) Comparable velocity between the falling objects. B) Calculated Kinetic energy shows no difference among the injured groups. C) All groups had comparable exposure to 2.5% isoflurane prior to injury. D) No differences in righting reflex (RR) were recorded between the two injured groups prior to treatment administration. E) Mice undergoing TBI lost weight at 24 hours

following injury, however TBI group treated with vehicle maintained statistically significant lower weight when compared to baseline. Data in A) and B) reported as mean  $\pm$  SD, analyzed with Student's T test between the injured groups. C, D, and E) Data is shown as mean  $\pm$  SEM, anesthesia and RR were analyzed by one-way ANOVA with Tukey's post hoc test for multiple comparisons. Change in body weight was analyzed with a mixed-effects model RM with comparisons over time, with Tukey's multiple comparisons post hoc test.

### **Both olaparib and TBI independently increase locomotor activity without a synergistic effect**

Changes in locomotor activity have been reported after TBI (Tucker, Fu, and McCabe 2016, Yen et al. 2018). PAS and OF were used to assess the effects of olaparib on the normalization of the increase in locomotor activity seen after TBI. While no changes were seen in the OF, mice that suffered a TBI and were treated with vehicle showed an increase in locomotor activity as measured by the total number of beam breaks (includes horizontal and vertical exploration) and distance covered (horizontal exploration) (Figure 4.8, A and B). This increase in exploration is in part mediated by an increase in the speed of the mice in the TBI treated with DMSO 10% (Figure 4.8, C). Surprisingly, the sham group treated with olaparib also increased in locomotor activity assessed by beam breaks (Figure 4.8, A). The TBI group treated with olaparib did not show a further increase in locomotor activity compared with the olaparib sham group.

Figure 4.8. Olaparib and TBI increase locomotor activity without synergistic effect

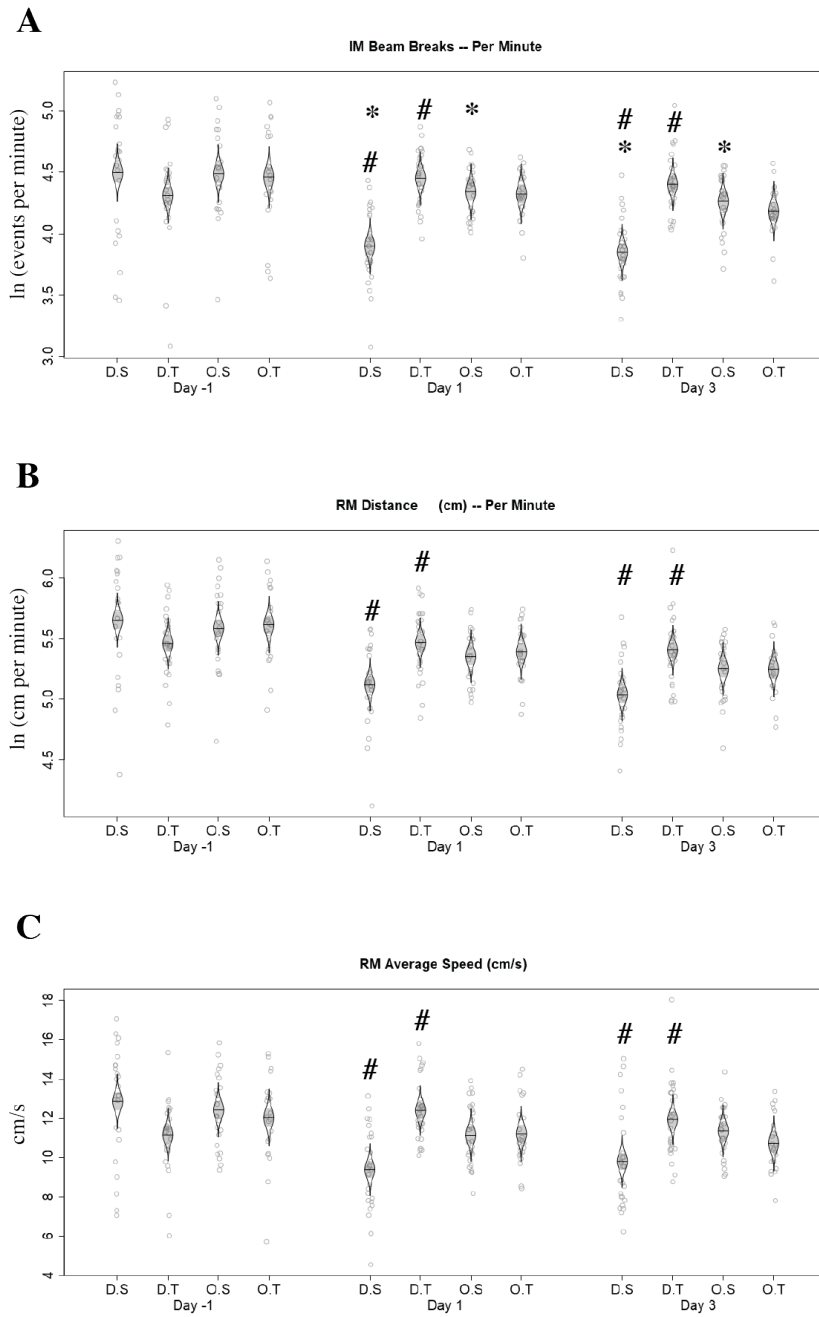


**Figure 4.8. Olaparib and TBI increase locomotor activity without synergistic effect.**

Groups are labeled on the X axis as D.S. (DMSO sham), D.T. (DMSO TBI), O.S. (olaparib TBI) and O.T. (olaparib TBI). On the Y axis, ln (natural logarithm) A) TBI and olaparib independently increased locomotor activity. No differences in exploration in were found

between olaparib sham and olaparib TBI. B) DMSO TBI mice traveled a longer distance (horizontal exploration) than DMSO sham mice. C) Average speed showed the same differences as distance. Data is shown as a normal distribution of the model-adjusted means  $\pm$  SEM. \*  $p < 0.05$  between sham + DMSO and sham + olaparib groups, #  $p < 0.05$  between DMSO sham and DMSO TBI. Each outcome was modeled by mixed analysis of variance with relation to group and day, including an interaction between them, blocking on the animal to control for repeated measures. Differences among groups by day were assessed by Hommel-adjusted contrasts.

### **Olaparib protects mice from TBI-induced cognitive deficits**

Cognitive improvement after treatment with PARP1 inhibitors has been reported in TBI injured animals (Clark et al. 2007). NOR was used to determine the effects of TBI and olaparib treatment on cognitive function. The injured mice treated with 10% DMSO did not show increased exploration time of the novel object (Figure 4.9, A) even when accounted for individual exploration times (Discrimination index) (Figure 4.9, B). These results were confirmed by the failure of the TBI group treated with 10% DMSO to recognize the novel object beyond the probability of picking one object at random (50% theoretical mean). The injury-induced deficit was rescued in the TBI group treated with olaparib. This group showed higher exploration in time and discrimination index of the novel object when compared to the familiar and did so above the 50% chance of picking one object randomly (Figure 4.9, C).

Figure 4.9. Olaparib protects mice from TBI-induced cognitive deficits

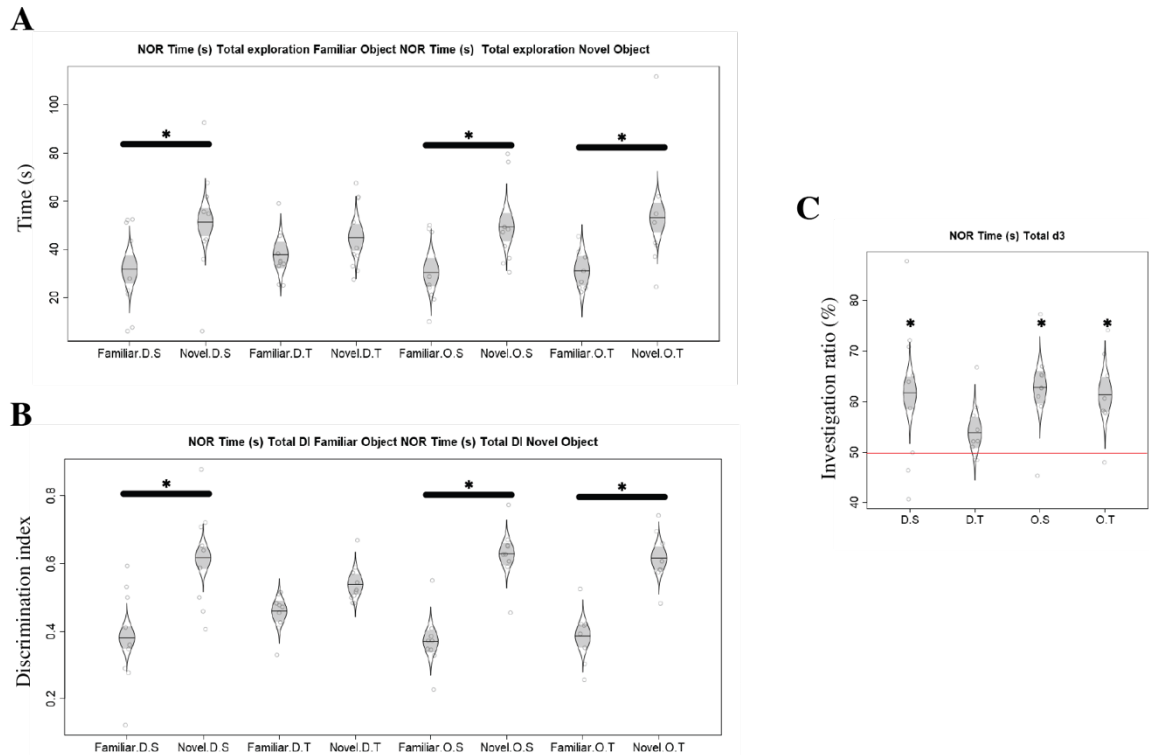


**Figure 4.9. Olaparib protects mice from TBI-induced cognitive deficits.** Groups are labeled on the X axis as D.S. (DMSO sham), D.T. (DMSO TBI), O.S. (olaparib TBI) and O.T. (olaparib TBI). A) Time spent exploring the novel object was significantly higher than the time exploring the familiar object in all groups except DMSO TBI. B) To account for potential individual differences in time of exploration, a discrimination index (DI) was calculated for each object (time exploring novel or familiar object/total exploration time). All groups except DMSO TBI showed significantly higher exploration of the novel object over the familiar. C) Novel object exploration compared to a theoretical mean of 50 to elucidate if the animals preferentially explored the novel object beyond chance. TBI+DMSO group failed to explore the novel object beyond 50-50 chance. (DMSO sham and olaparib sham, n=9; olaparib TBI, n=8; and DMSO TBI, n=10). Data is shown as a normal distribution of the model-adjusted means  $\pm$  SE. \*  $p < 0.05$ . For differences between the objects per group one-way ANOVA with Tukey's post hoc test were done. Each group

was compared against a reference of 50% to test whether the data for each group differed from the chance of picking one object at random, Welch's 2-way 2-sample t-tests were used.

### **TBI and olaparib individually decrease agoraphobia-related anxiety**

Next, we tested if olaparib had an effect on anxiety-related behavior after TBI. TBI is known to have a paradoxical effect on the anxiety-related behavior, while TBI increases anxiety (Popovitz, Mysore, and Adwanikar 2019, Broussard et al. 2018, Malkesman et al. 2013), there are reports of increases in risk-seeking behavior (Malkesman et al. 2013, Cheng et al. 2019, Gold et al. 2018, Petraglia, Dashnaw, et al. 2014, Petraglia, Plog, et al. 2014). While we saw no differences in acrophobia-related anxiety (EPM, Figure 4.10), both TBI and olaparib, individually decreased agoraphobia-related anxiety (thigmotaxis in open field, Figure 4.11, A-D). Interestingly, the results shown with impactor in Chapter 3 are different from these results, which may suggest differential areas of the brain being injured in the two iterations of the model.

TBI injured mice treated with DMSO increase the exploration of the center of the arena as assessed by the number of entries (Figure 4.11, A). However, the measurement done by concentric squares improved the resolution of that exploration. On Day 1 post-injury only the DMSO TBI showed a willingness to explore the center for a longer period of time. On day three post-injury the olaparib sham group also showed an increased willingness to explore closer to the center. The olaparib TBI group showed no difference in exploration when compared to the olaparib sham group (Figure 4.11, B). Finally, when measuring the individual areas explored, it is noticeable that all groups increased their exploration of every square in comparison to DMSO sham, except on day three where the group olaparib TBI entered the central square significantly less than the DMSO TBI group

(Figure 4.11 C). The time spent exploring each square showed fewer differences, with a significant increase in exploration of the center square by DMSO TBI and olaparib sham groups when compared to the DMSO TBI group on both days Figure 4.11, D).

Figure 4.10. No differences are found in acrophobia-related anxiety

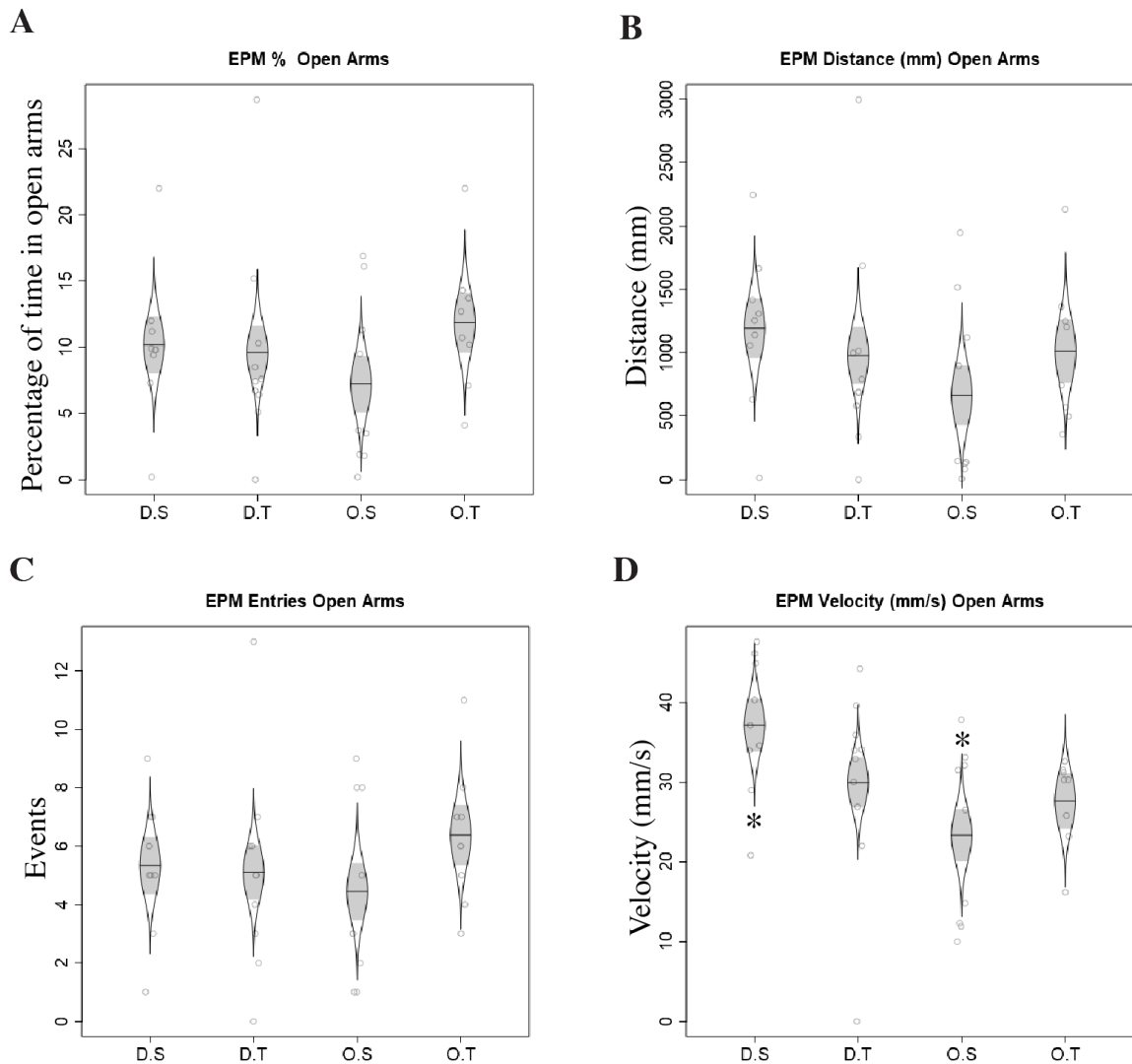


**Figure 4.10. No differences are found in acrophobia related anxiety.** Groups are labeled on the X axis as D.S. (DMSO sham), D.T. (DMSO TBI), O.S. (olaparib TBI) and O.T. (olaparib TBI). There were no differences in acrophobia-related anxiety induced by TBI or

olaparib in the exploration of the elevated plus maze. A) There were no significant differences in the percentage of time spent, B) distance covered, or C) entries into the open arms between the different groups. D) Interestingly, olaparib sham mice were slower when exploring the open arms when compared to DMSO sham. Data is shown as a normal distribution of the model-adjusted means  $\pm$  SEM. \*  $p < 0.05$ . For differences between groups one-way ANOVA with Tukey's post hoc test was done.

Figure 4.11. TBI and olaparib individually decrease agoraphobia-related anxiety

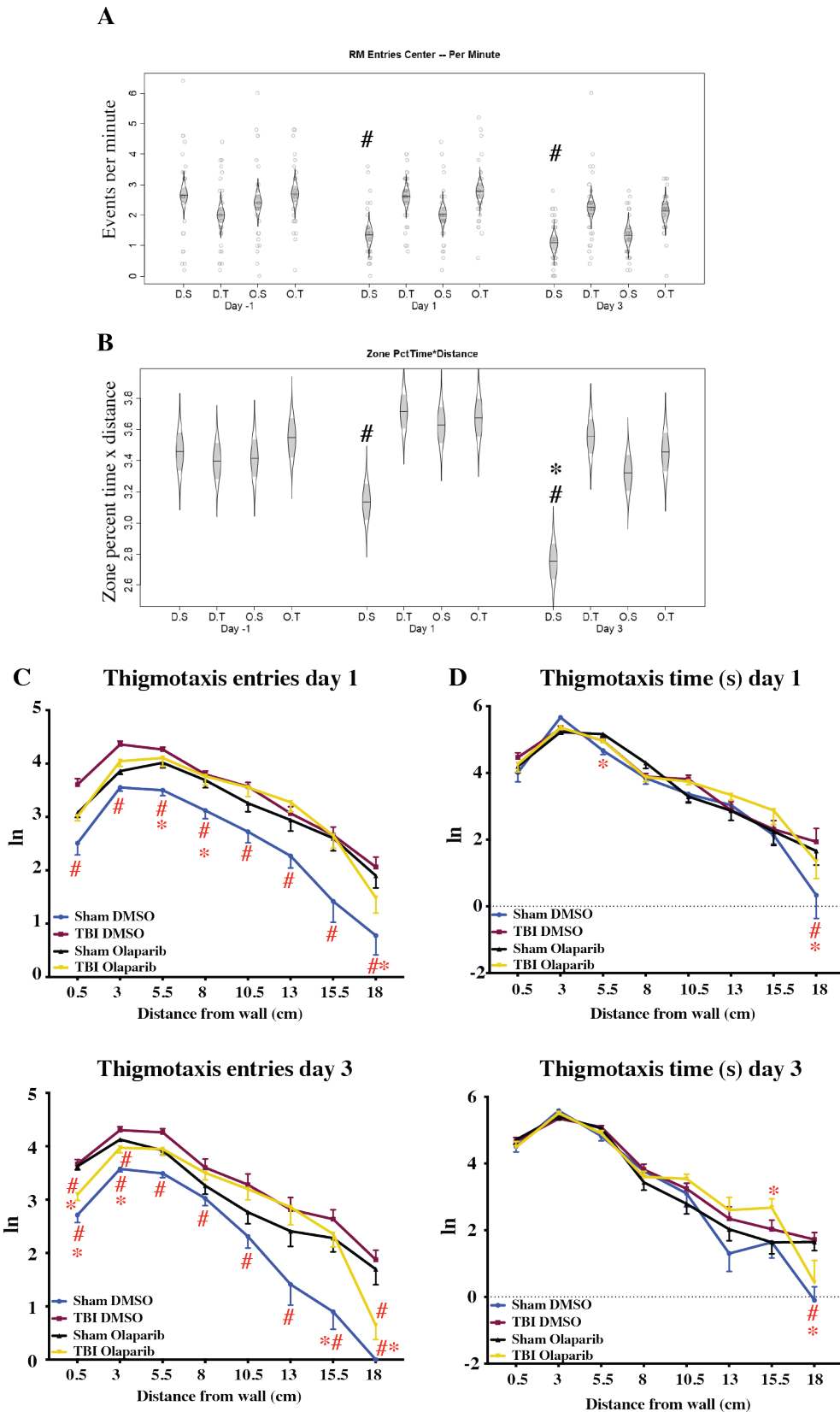


**Figure 4.11. TBI and olaparib individually decrease agoraphobia-related anxiety.** A)

The DMSO TBI group showed increase entries into the center of the arena when compared to the sham DMOS group. B) This increased exploration of the center was also seen when measuring the willingness of the mice to explore longer times closer to the center. On day three the olaparib sham group also showed a significant increase when compared to DMSO sham. C) Increased number of entries to every concentric square in the PAS by DMSO TBI on days 1 and 3 when compared to DMSO sham and on the central square on day 3 when compared with olaparib TBI. This increase was also seen in the olaparib sham group with differences in most of the squares when compared to sham. D) DMSO TBI group showed a significant increase in time spent in the central square when compared to DMSO sham. This difference was also seen between olaparib sham and DMSO sham. Data was log transformed to approach normality before the analysis and is shown as a normal distribution of the model-adjusted means  $\pm$  SEM.  $p < 0.05$ , where # compared to DMSO TBI; \* compared to olaparib sham. Each outcome was modeled by mixed analysis of variance with relation to group and day, including an interaction between them, blocking on the animal to control for repeated measures. Differences among groups by day were assessed by Hommel-adjusted contrasts.

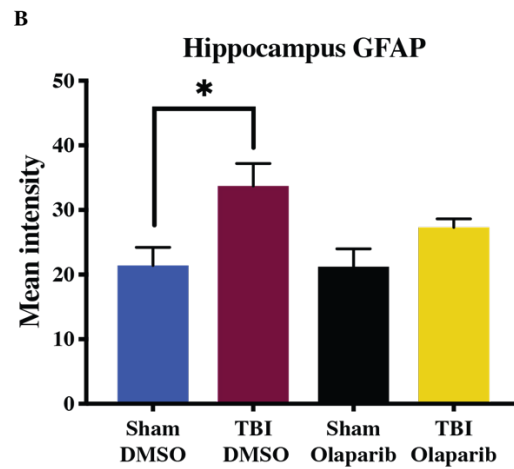
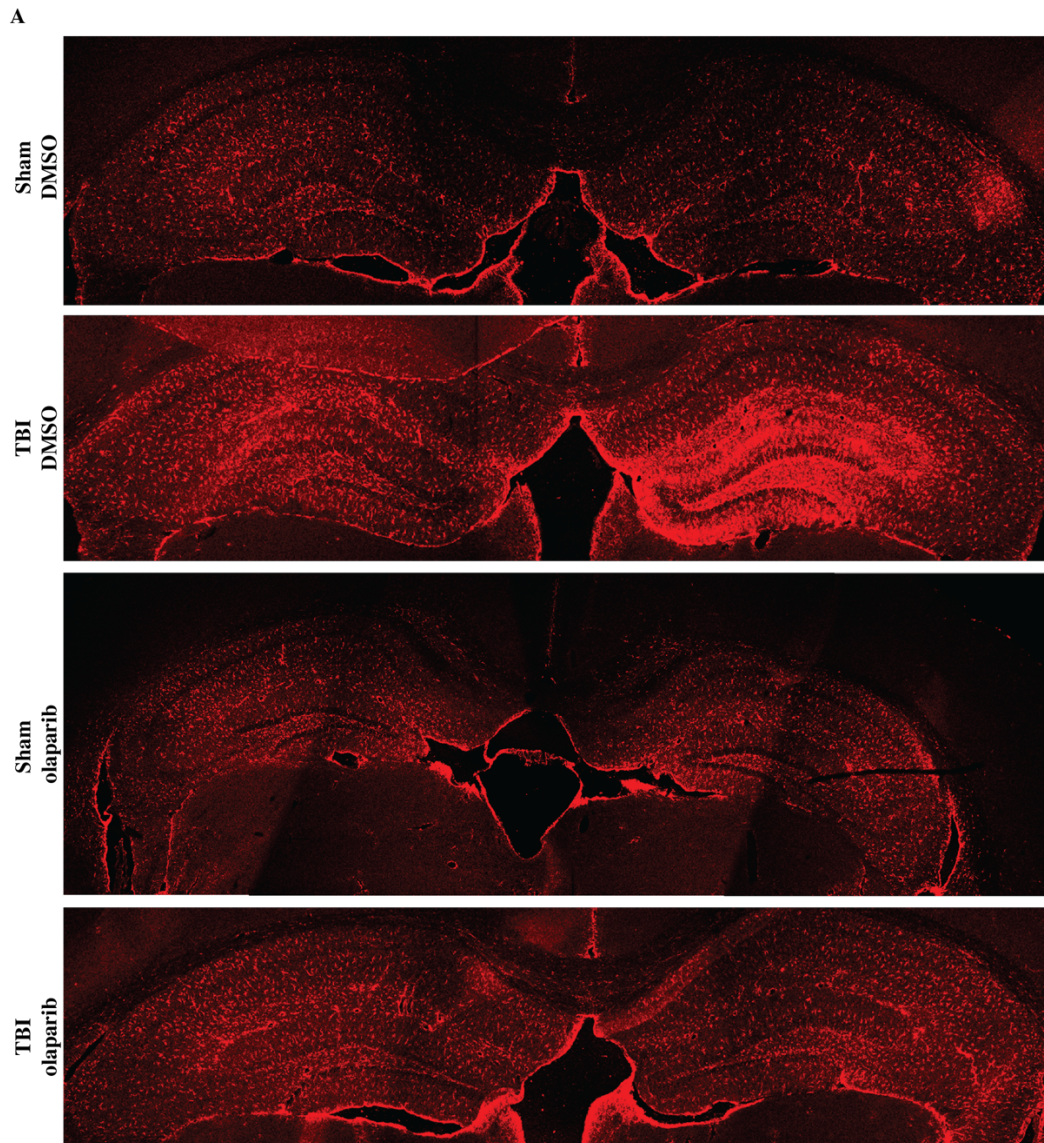
**Olaparib reduces astrogliosis and increases microglial activation after TBI**

PARP1 inhibition is known to reduce neuroinflammation (Stoica et al. 2014, d'Avila et al. 2012, Kauppinen et al. 2009). To understand the neuroprotective mechanism of olaparib the tissue was examined for neuroinflammation using immunohistochemical analysis. For this motive, astrogliosis and microgliosis were examined with GFAP and Iba-1 respectively. The DMSO TBI group showed an increase in astrogliosis in the hippocampus. As expected, this astrocytic reaction was reduced by olaparib showing no

difference in GFAP immunoreactivity when compared with the olaparib sham group (Figure 4.12).

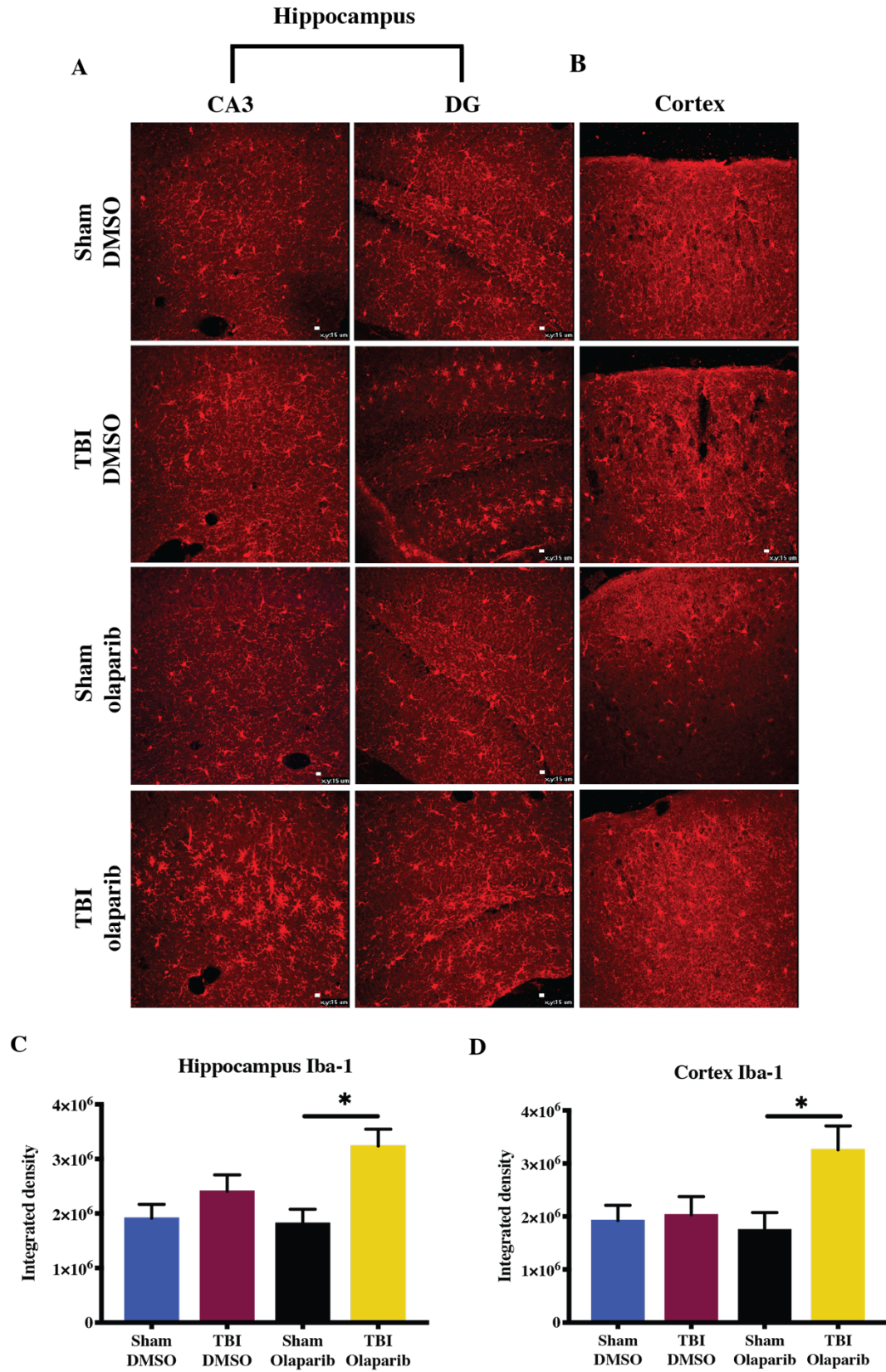
Microglial changes after TBI and olaparib treatment were examined next. Surprisingly, animals that received an injury and were treated with olaparib showed higher integrated density measurements for Iba-1 in the hippocampus and cortex, which correlates with microgliosis. Additionally, morphological changes were evident in the microglia of this group, showing enlarged cell bodies and thick ramifications at this subacute stage of injury (Figure 4.13, A).

Figure 4.12. Olaparib reduces astrogliosis in the hippocampus after TBI



**Figure 4.12. Olaparib reduces astrogliosis in the hippocampus after TBI.** A) Olaparib promotes a reduction of TBI-induced reactive astrogliosis in the hippocampus, as seen in the representative images. B) Quantification of fluorescence intensity shows a significant increase in astrogliosis in the hippocampus of the DMSO TBI group, but not seen in the olaparib TBI group. Data is shown as mean  $\pm$  SEM. n=3 per group. Analyzed by one-way ANOVA with Tukey's post hoc test. \* $p$ <0.05.

Figure 4.13. Olaparib increases TBI-induced microgliosis



**Figure 4.13. Olaparib increases TBI-induced microgliosis.** A) Representative images of Iba-1 staining in the hippocampus, note morphology of the microglia in the olaparib TBI group. B) representative images of the cortex. C and D) Integrated density analysis of IBA-1 staining in the hippocampus and cortex above a preset threshold set per region, with a significant increase in the olaparib TBI group when compared to olaparib sham. Data is shown as mean  $\pm$  SEM. n=3 per group and about 18 sections per animal. Analyzed by one-way ANOVA with Tukey's post hoc test. \* $p$ <0.05.

### **Olaparib shows neuroprotection after TBI in vivo**

After observing the unexpected increase in microglial activation with olaparib treatment after TBI, we proceeded to examine the tissue for axonal injury, assessed by phosphorylated c-Jun immunoreactivity, which is a sensitive marker for axonal damage (Greer, McGinn, and Povlishock 2011). The higher concentration of positive staining for phosphorylated c-Jun, in this iteration of our animal model, was in the hypothalamus, surrounding the 3rd ventricle. The number of phosphorylated c-Jun positive cells drastically increased after TBI, whereas animals injured and treated with olaparib showed protection against axonal injury. These results are significant since the hypothalamic area is involved in metabolic regulations, hormonal and circadian signaling, memory, and the regulation of the pituitary gland, among a multitude of additional functions (Delgado, Cerda-Reverter, and Soengas 2017, Coll and Yeo 2013, Coppari 2012, van Wimersma Greidanus, Jolles, and De Wied 1985).

Figure 4.14. Olaparib protects neurons from injury assessed by phosphorylated c-Jun

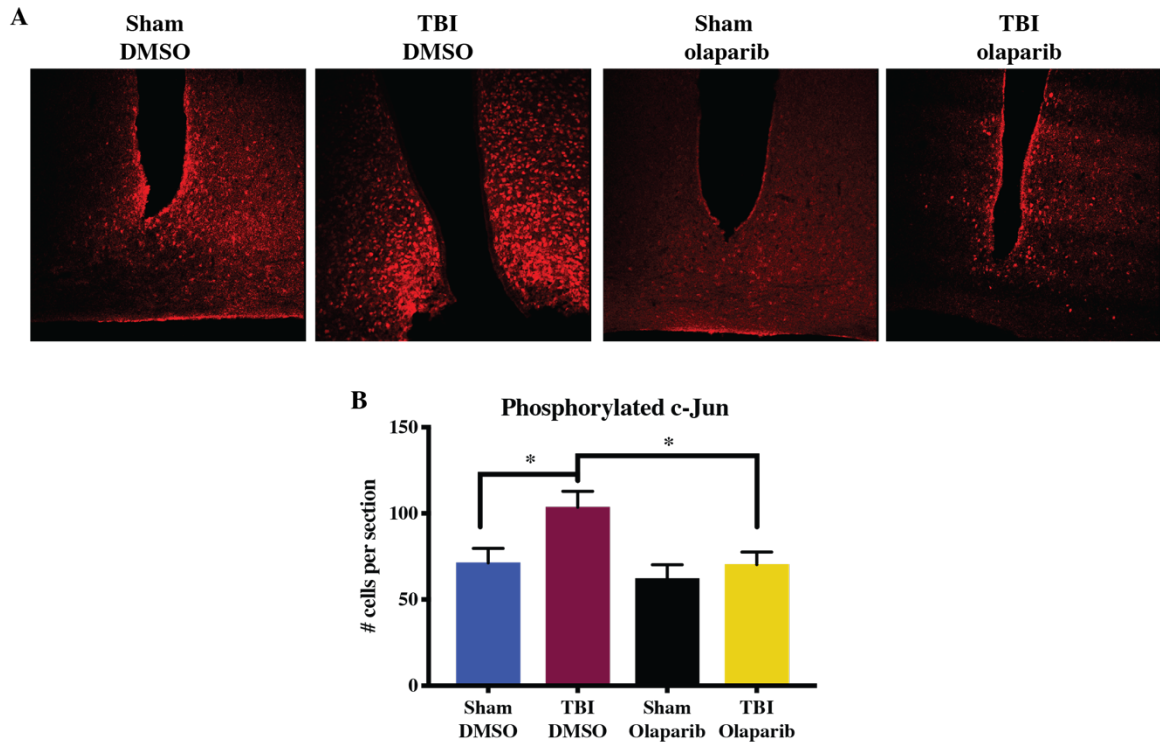


**Figure 4.14. Olaparib protects neurons from injury assessed by phosphorylated c-Jun.** A) Olaparib protects from axonal injury assessed by the TBI-induced expression of phosphorylated c-Jun in the hypothalamus, seen in the representative images. B) Quantitation of phosphorylated c-Jun positive cells per section shows a significant increase in Phosphorylated c-Jun immunoreactivity in the hypothalamus of the DMSO TBI group when compared to DMSO sham and olaparib TBI. Data is shown in Mean  $\pm$  SEM.  $n=3/\text{group}$  and  $\sim 12$  sections per animal. One-way ANOVA with Tukey's post hoc test.  $*p<0.05$ .

### Olaparib increases activated caspase 3 positive cells in uninjured controls

A complicated interplay between apoptotic effectors and PARP1 has been the focus of multiple studies. Interestingly, most of these studies have shown that an increase in PARP1 leads to an increase in activation of Caspase 3, and that cleaved PARP reduces the

activation of Caspase 3 (Hong, Dawson, and Dawson 2004, Zhang, Lau, and Monks 2012, Boulares et al. 1999). However, we found that olaparib increases the number of activated Caspase 3 positive cells in the hypothalamic area of the uninjured control group when compared to the DMSO sham group. Albeit present in the olaparib TBI group, the increase in activated caspase 3 positive cell is smaller than in the olaparib sham group (Figure 4.15).

Figure 4.15. Olaparib increases the number of activated caspase 3 positive cells

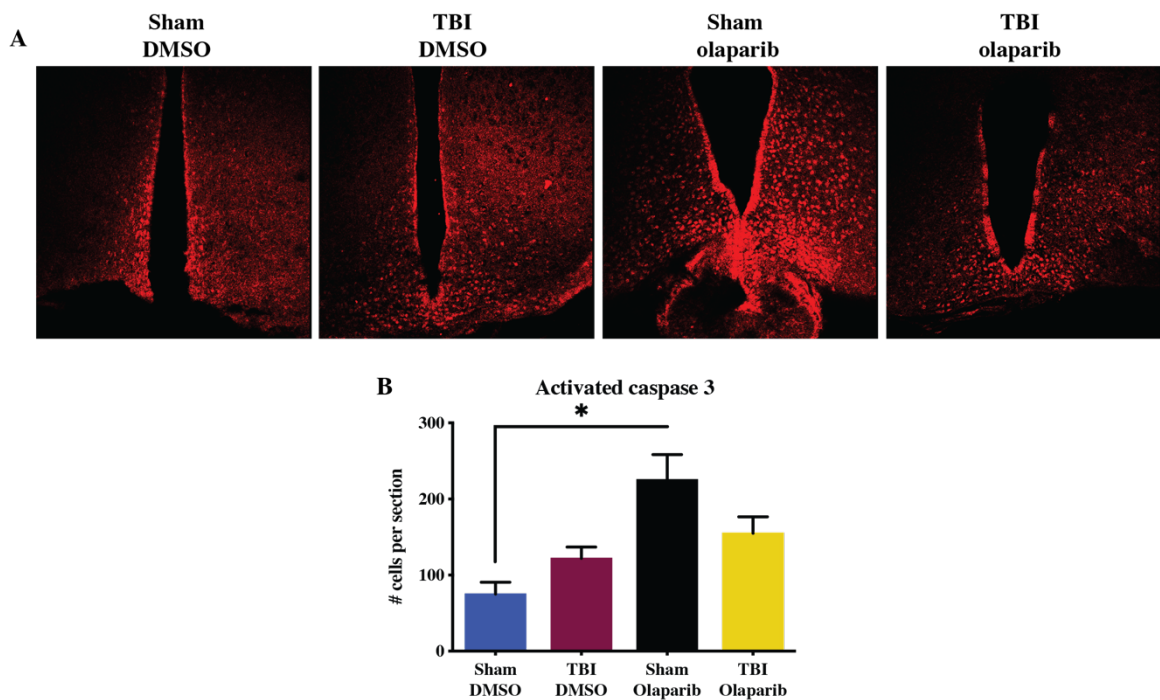


**Figure 4.15. Olaparib increases the number of activated caspase 3 positive cells.** A) Olaparib increases the number of activated caspase 3 positive cells in uninjured control animals as seen in the representative images. B) Quantification of the cells shows a significant increase in the number of activated caspase 3 positive cells per section in the olaparib sham group when compared to the DMSO sham group. Data is shown in Mean ± SEM. n=3/group with approximately 12 sections per animal. One-way ANOVA with Tukey's post hoc test. \* $p < 0.05$ .

## TBI shows no changes in lipid peroxidation and hydrogen peroxide levels 4 days post injury

TBI increases the formation of ROS through several pathways including excitotoxicity through calcium homeostasis and acidosis of the extracellular space (Shohami et al. 1997). Additionally, PARP1 inhibition has proven to reduce the formation of ROS (Ahmad et al. 2018). We found no differences in the levels of lipid peroxidation and hydrogen peroxide between the groups. Although, not surprising since this increase has an early onset and decreases shortly after injury (Cristofori et al. 2001, Scholpp et al. 2004).

Figure 4.16. No differences in lipid peroxidation and hydrogen peroxide levels assessed by MPO and MDA

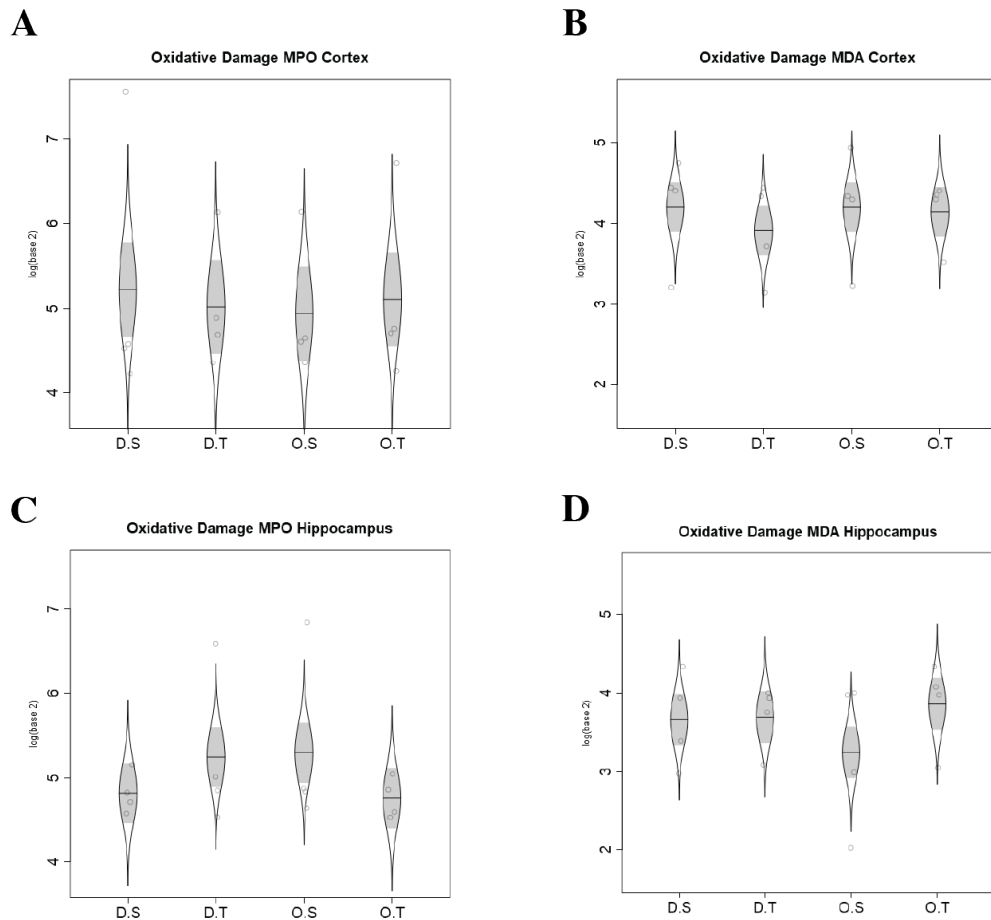


**Figure 4.16. No differences in lipid peroxidation and hydrogen peroxide levels assessed by MPO and MDA.** A-D) Two of the five brain regions analyzed for lipid peroxidation damage (A and C) and hydrogen peroxide levels (B and D) after TBI are shown. Data was log transformed to approach normality before the analysis. Analysis was modeled by mixed analysis of variance with regard to group, and differences among groups were assessed by Tukey-adjusted contrasts. For a better approximation of normality, data was Log base 2 transformed before the analysis. Data shows the normal distribution of the model-adjusted means  $\pm$  SEM.  $p < 0.05$

#### **Differences in cytokine and chemokine profiles after TBI and olaparib treatment.**

Since PARP1 was suggested to regulate inflammatory signaling in stroke and heart diseases and its inhibition has been associated with anti-inflammatory signaling (Berger, et al., 2017 British J Pharmacol), we evaluated the changes in the cytokine and chemokine profiles on brain samples collected 4 days post-injury. Some of the changes in the hippocampal expression of cytokines and chemokines were: A reduction in TNF- $\alpha$  in the hippocampus of olaparib TBI when compared to the olaparib sham group (Figure 4.17, A). Also, olaparib sham had significantly more IL- $\beta$  than the DMSO sham or olaparib TBI groups (Figure 4.17, B). IL-6 was decreased in the DMSO TBI sham in respect to DMSO sham (Figure 4.17, C). Increase in MCP-1 in olaparib TBI when compared to DMSO TBI (Figure 4.18, E), and DMSO TBI has a reduction in the MIP-2 when compared to DMSO sham (Figure 4.18, F).

Two chemokines were differentially expressed in the cortex, KC, which had higher expression in the olaparib sham group vs. DMSO sham and olaparib TBI, and RANTES, with lower expression in olaparib TBI against olaparib sham. Finally, LIF, was increased in the plasma of the olaparib TBI group when compared with DMSO TBI.

Figure 4.17. Differences in cytokine and chemokine profiles after TBI

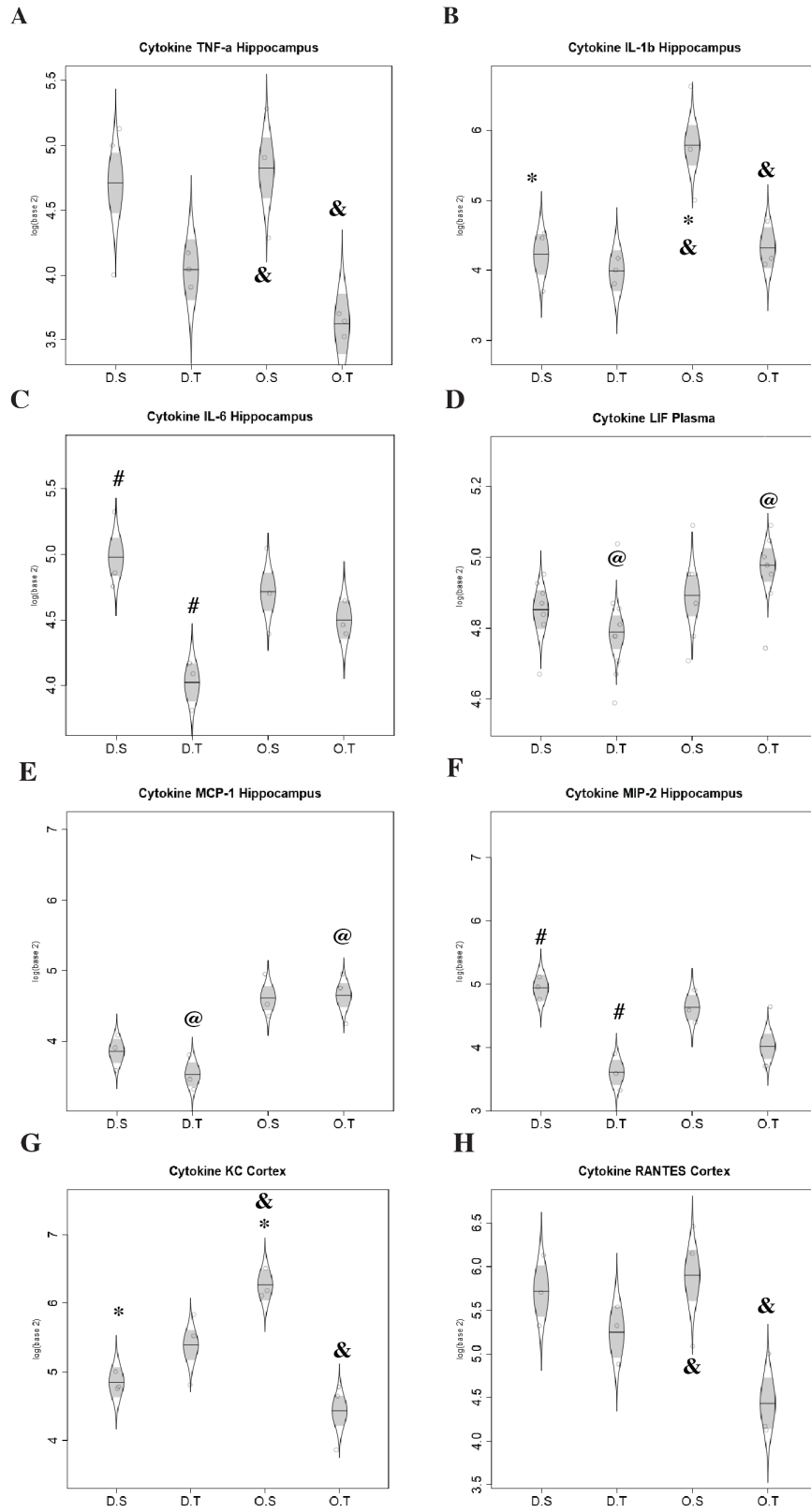


**Figure 4.17. Differences in cytokine and chemokine profiles after TBI.** A) TNF- $\alpha$  is decreased in TBI vs. olaparib sham. B) IL- $\beta$  is increased in olaparib sham vs. olaparib TBI and DMSO sham. C) IL-6 decreases in DMSO TBI vs. DMSO sham. D) LIF increases in plasma of the olaparib TBI group when compared to DMSO TBI. E) MCP-1 increases in olaparib TBI vs. DMSO TBI. F) MIP-2 decreases in DMSO TBI vs. DMSO sham, G) KC increases in olaparib sham vs. olaparib TBI and DMSO sham. H) Rantes decreases in olaparib TBI vs. olaparib sham. Analysis was modeled by mixed analysis of variance with regard to group, and differences among groups were assessed by Tukey-adjusted contrasts. For a better approximation of normality, data was Log base 2 transformed before the analysis. Data shows the normal distribution of the model-adjusted means +/- standard error.  $p < 0.05$ . & difference between olaparib sham and olaparib TBI, \* difference between DMSO sham and olaparib sham, # difference between DMSO TBI and DMSO sham and @ difference between olaparib TBI and DMSO TBI.

## DISCUSSION AND CONCLUSIONS

The generation of a viable treatment option for TBI remains elusive. The recent availability of PARP inhibitors fit for treating certain cancers in humans increases the potential for repurposing these compounds to non-oncological diseases (Berger et al. 2018). There is plenty of preclinical data demonstrating the efficacy of various PARP inhibitors in models of TBI showing morphological and behavioral improvements (Whalen et al. 1999, Rom et al. 2015, LaPlaca et al. 2001, Besson et al. 2005, Clark et al. 2007, Stoica et al. 2014, Besson et al. 2003, Satchell et al. 2003, Lacza et al. 2003, Zaremba et al. 2010). However, other studies showed detrimental effects of PARP inhibition when treating sublethal stroke (Nagayama et al. 2000), or affecting cognitive testing (Satchell et al. 2003). It was later discovered the PARP1 activation is required for long-term memory formation (Cohen-Armon et al. 2004).

Olaparib (Lynparza™) was the first FDA approved PARP inhibitor for the treatment of ovarian and breast cancer (Deeks 2015). However, outside of cancer, olaparib has shown neuroprotection in oxygen-glucose deprivation and excitotoxicity models of neuronal death (Xu et al. 2016). TBI treatment only requires partial PARP inhibition to obtain its neuroprotective effects. Thus, we hypothesized that a much lower dose is required (1-5mg/kg/day) (Berger et al. 2018), at which the occurrence of side-effects is less likely. This work is the first in a series of studies to show the efficacy of olaparib in the treatment of TBI.

There are a plethora of mechanisms through which PARP1 activation can affect outcomes post-TBI. Of these, the most prevalent is the metabolic disruption and cell death. This mechanism follows the depletion of NAD<sup>+</sup>, due to activation of PARP1 stimulated by ROS and excitotoxicity induced DNA damage (Virag, Salzman, and Szabo 1998, Ha and Snyder 1999, Andrabi et al. 2006, Fatokun, Dawson, and Dawson 2014). In order to assess if olaparib might be a suitable therapeutic to repurpose for TBI, we investigate its effect in neuroprotection in two in vitro models and on the posttraumatic neurological outcome on a murine closed-skull weight drop injury model, in vivo.

Our results show that olaparib confers neuroprotection to differentiated B35 cells from oxidant-induced cell death, at a comparable level with PJ34 yet at one-tenth of the dose. Olaparib also showed protection against necrosis and apoptosis in a stretch injury model of neurons and astrocytes derived from human neural stem cells, as assessed by annexin V and propidium iodide. It is important to point out that parthanatos is known to also exhibit annexin V and propidium iodide positive staining (Wang, Dawson, and Dawson 2009). Thus, the decrease in cell death may likely include necrosis, apoptosis, and parthanatos. Further experiments are needed to establish which type of cell death is being

prevented by olaparib. PARP1 has been implicated in all of these types of cell death (Ethier et al. 2012, Wang, Kim, et al. 2011, Aredia and Scovassi 2014, Zhang, Lau, and Monks 2012). Further, we showed that this decrease in cell death was partly mediated by neuronal survival with a “U” shape dose response, where 10  $\mu$ M conferred the most protection. This type of response has been reported in the past with other PARP1 inhibitors (Calabrese 2008).

To observe the efficacy of olaparib on an *in vitro* stretch injury model, the expression of PARP1 and its byproducts were quantified by western blotting. Surprisingly, stretch injury did not increase PARP1, its cleavage or the production of PAR polymers. However, olaparib increased the expression of PARP1 and reduced cPARP1 while decreasing the production of PAR polymers in cells with or without stretch injury. These results suggest a compensatory mechanism at 3hr post injury, 2.5hr post treatment in human neural stem cell derived neurons and astrocytes. Also, a decrease in cleaved PARP1 (89 kD fragment) was found in olaparib treated cells with or without stretch injury. These results suggest a high efficacy of PARP1 in these cells; even a compensatory PARP1 increase, does not result in an increased production of PAR polymers. Additionally, the decrease in cleaved PARP1 suggests a decrease in caspase-3 mediated apoptosis (Zhang, Lau, and Monks 2012, Virag et al. 2013). A potential explanation for the lack of PAR production and the increase in PARP1 expression in this *in vitro* injury model is that the time point at which the cells were collected is too short. Other models of chemical injuries with increases in PAR expression have measured 24 hr after initiation of exposure (Brochier et al. 2015).

Once the cytoprotective and neuroprotective effects of olaparib were established, NAD<sup>+</sup> levels after stretch injury were measured to explore if improvement in metabolic status of the cell after injury was responsible for this beneficial effects. As expected we

found a decrease in NAD<sup>+</sup> levels after injury (Lai et al. 2008, Clark et al. 2007, Satchell et al. 2003), however, olaparib did not prevent the NAD<sup>+</sup> depletion after stretch injury, which is contrary to previous findings. Although it is important to point out that these studies were done in animals and PARP inhibitors were administered immediately after injury (Clark et al. 2007, Satchell et al. 2003) this is also the case in studies with cells, where they administered the PARP1 inhibitor pre-injury (Krainz et al. 2018). For NAD<sup>+</sup> to be used as an indicator, a shorter time of administration after injury may prove beneficial due to its rapid depletion (Bai and Canto 2012). Furthermore, the detection accomplished by this method measures the whole cell NAD<sup>+</sup> levels. Recent studies have suggested that the preservation of mitochondrial NAD<sup>+</sup> pools and not the total NAD<sup>+</sup> levels may be responsible for cell survival (Yang et al. 2007, Long, Klimova, and Kristian 2017). This hypothesis is also supported by the recent finding of the existence of mitochondrial PARP1 and the PARylation of proteins in the complexes of the respiratory chain (Brunyanszki et al. 2016), as well as the reports suggesting that PAR can induce cell death even in the absence of cytosolic NAD<sup>+</sup> depletion (Andrabi et al. 2006).

Our findings *in vivo* with olaparib on protection from TBI-induced cognitive impairments are in accordance with others using different PARP inhibitors (Whalen et al. 1999, Clark et al. 2007, Satchell et al. 2003). As expected, mice displayed an increase in locomotor activity following TBI (Tucker, Fu, and McCabe 2016, Yen et al. 2018), However, it was unexpected that the sham grouped treated with olaparib showed a similar response. Also, the TBI animals treated with olaparib showed no further increase (than the one seen in the olaparib sham) in locomotor activity. These results suggest that there is not an additive or synergistic effect between TBI and olaparib in the increment of locomotion. Interestingly, a study on aging using PARP<sup>-/-</sup> mice found a similar increase in locomotion, assessed as squares crossed in the OF and rearing time, this was suspected of being associated with a faster metabolism in this strain of mice (Piskunova et al. 2008). The way

this study quantified the horizontal locomotion, could have missed the increase in central exploration that the sham group treated with olaparib showed in this study as reduced agoraphobia. Others have looked at the effects of PARP1 inhibition in mood disorders and found decreases in depressive-like behavior at a dose of 40 mg/kg of 3-aminobenzamide (3-AB) a prototypical PARP inhibitor (Ordway et al. 2017). Regrettably, no other tests of mood disorder behavior were conducted.

Likewise, TBI showed a robust reduction in this anxiety-like behavior both in the number of entries and the time spent in the squares closer to the center of the open field. These results concur with others which have seen increases in risk-seeking behavior after TBI (Malkesman et al. 2013, Cheng et al. 2019, Gold et al. 2018, Petraglia, Dashnaw, et al. 2014, Petraglia, Plog, et al. 2014). This impulsivity and risk-seeking behavior is also seen in humans and is one of the reasons why TBI is one of the main risk factors for subsequent TBIs (Kocka and Gagnon 2014, Antonius et al. 2014, James, Strom, and Leskela 2014). It was surprising that no changes in acrophobia were seen in the TBI group since this behavior was seen in the later iteration of this model (Chapter 3).

The beneficial effect of olaparib was also observed in the reduction of astrogliosis (Irvine et al. 2017). The reduction in astrogliosis is significant since PARP1 activation in astrocytes has been correlated with impaired glutamate uptake. This process can extend the excitotoxic environment and lead to further damage (Tang et al. 2010). There were additional neuroprotective effects by preventing axonal damage. This effect is a similar finding as several reports that associate PARP1 inhibition with a decreased neuronal loss (Stoica et al. 2014, Satchell et al. 2003). This effect was not seen in a study in pigs using veliparib (another PARP1 inhibitor) assessed by amyloid precursor protein (APP) staining (Irvine et al. 2017).

Two unexpected results were the increase in microglial activation measured as Iba-1 integrated density in the TBI group treated with olaparib and the increase in the number of activated caspase 3 positive cells in the sham group treated with olaparib.

The activation of microglia in the TBI group treated with olaparib was surprising because other studies reported that PARP-1 inhibition decreases microglial activation (Kauppinen et al. 2011, Kauppinen et al. 2009, d'Avila et al. 2012, Stoica et al. 2014, Irvine et al. 2017). However, a significant result was the increase in the MCP-1 chemokine in the olaparib TBI group when compared to DMSO TBI. This chemokine is involved in the proliferation and migration of microglia, yet, some reports mention that this particular chemokine is not directly involved with the activation of an inflammatory response (Hinojosa et al. 2011). Furthermore, the MCP-1 increase was accompanied by decreases in pro-inflammatory chemokines released by microglia TNF- $\alpha$  and IL-1 $\beta$  (Kumar and Loane 2012) when compared to the olaparib sham group. These results suggest that while an activation and migration of microglia is occurring in the olaparib TBI group it may not be as part of a pro-inflammatory response at this timepoint.

Additionally, the olaparib TBI group showed non-significant trends to decrease IL-5, MIP-1a, and MIP-2 vs. the olaparib sham group (data not shown). This cytokine and two chemokines are pro-inflammatory. IL-5 has shown a diffuse expression in blast injury and is co-expressed with MCP-1 (Siva Sai Sujith Sajja et al. 2014). IL-5 induces proliferation and promotes activation of microglia, leading to a pro-inflammatory pathway (Liva and de Vellis 2001). MIP-1a and MIP-2 are chemoattractant and chemotactic agents. Expression of MIP-1a and MIP-2 has been correlated with recruitment and neutrophil infiltration into the brain (Johnson et al. 2011, Diab et al. 1999). The olaparib TBI group also showed decreases in RANTES, that promotes homing and migration of T cells, and KC which is another neutrophil chemoattractant. Lastly, there are reports that link the elevation of MIP-

1a, MIP-2, RANTES and KC with BBB disruption (Shigemoto-Mogami, Hoshikawa, and Sato 2018). These results taken together led us to hypothesize that the morphological changes in the microglia of the olaparib TBI group may follow a non-inflammatory activation which showed beneficial effects, as assessed behaviorally.

As mentioned above, we found an increase in activated caspase 3 cells in the hypothalamus of animals in the olaparib sham group. This was surprising, since most reports that discuss the association between PARP1 and caspase 3 show a mutual regulation where caspase 3 cleaves PARP1, to avoid energy stores depletion, in the process of apoptosis and PARP1 inhibition can reduce activation of caspase 3 (Levrant et al. 2006, Los et al. 2002, Zhang, Lau, and Monks 2012). Although no clear correlation was found in the literature between PARP1 inhibition and an increase in caspase 3 activation, (normally as PARP1 increases so does activated caspase 3 and viceversa), both PARP1 inhibition and caspase 3 activation are involved in neural stem cell differentiation. Moreover, when this caspase 3 activation occurs, no PARP1 cleavage takes place. When the increase of caspase 3 activation or inhibition of PARP1 induce differentiation, it follows mainly an astrocytic lineage (Plane, Grossenbacher, and Deng 2012). Further studies are required to understand further understand these results and dilucidated the effect of low dose PARP1 inhibitor in hypothalamic caspase 3 activation.

We also reported an increase in IL-1 $\beta$  in the hippocampus of the sham group treated with olaparib when compared with DMSO sham and olaparib TBI groups. PARP1 inhibition has been shown to inhibit IL-1 $\beta$  inflammatory response by reducing the expression of IL-1R (receptor) (Sun et al. 2008), this may be a compensatory mechanism due to this reduction in the receptor. The DMSO TBI group showed decreased IL-6 cytokine in the hippocampus. IL-6 is a cytokine that has been extensively studied in the healthy and diseased brain with multiple functions. In an early stage of injury, IL-6 has

shown neuroprotective effects by reducing the firing of neurons and inhibiting the release of glutamate, thus reducing excitotoxicity. Additionally, IL-6 is involved in the inhibition of TNF- $\alpha$  and the reduction of diapedesis by neutrophils and inducing their apoptosis (Erta, Quintana, and Hidalgo 2012) It is understandably that a reduction in IL-6 at early timepoints after injury is correlated with decreased neuronal survival and slower recovery after TBI (Jassam et al. 2017). The loss of this protective mechanisms by a reduction in IL-6 could have influenced the outcome in the DMSO TBI group and contributed to the astrogliosis and neuronal compromise.

In conclusion, the present study shows that olaparib is neuroprotective and prevents cognitive deficits after TBI. We have shown a reduction in astrogliosis and pro-inflammatory markers at this early timepoint (4dpi), such as TNF- $\alpha$  and IL-1 $\beta$ , MIP-1a, MIP-2, KC and RANTES. These results suggest that additional mechanisms may be at play in the cell survival, some of these may include the decrease in PAR signaling, the maintenance in mitochondrial integrity by the preservation of mitochondrial NAD<sup>+</sup> stores as well as maintenance of the glycolytic pathway. Further studies are necessary to determine the optimal dose and time points of administration, the sex differences in the effect of olaparib, and a better understanding of the changes we observed in this study. Among these changes it is important to determine the phenotype of the microglia in the olaparib TBI group, and to further explore the consequences of the activation of caspase 3 in the hypothalamic area in olaparib sham group. The present work shows that the use of olaparib in the treatment of TBI is beneficial and may be a suitable candidate for repurposing to treat neurotrauma. This could be considered once its efficacy has been proven in this and other preclinical models of TBI.

## **Chapter 5 Discussion and future directions**

### **CONCLUSIONS**

#### **Overall impression of findings**

The physicians and researchers that aim to cure TBI face a great challenge. The complexity of the response the brain towards an injury, in addition to the incredible heterogeneity of this pathology, makes this one of the most complex questions in medicine. In order to study TBI, certain characteristics and outcomes of this disease need to be modeled. Up to this day, no single model has been able to replicate the entirety of this disease. Additionally, the vast array of models and their variations have made it difficult to compare outcomes among laboratories. This lack of comparability complicates the generation of meta-analysis to select the best therapeutic candidates for translation into clinical trials.

The present dissertation is a complex project that includes the complete process in research, from model development, optimization and characterization to therapeutic evaluation of a disease with the use of a model. The first chapter of this work includes the development of a murine closed-skull weight drop TBI model that incorporates a system to measure the biomechanical characteristics of the injury. Further, it shows the development of the Professional mouse, a second system that allows for the detection of variability between impacts and could facilitate comparison among devices. With these two systems, a full mechanical characterization of the new apparatus was done. Followed by a comparison of the mechanical properties of similar models commonly used in the field, these results are compiled in chapter 2. In chapter 3, a full characterization of the injury and behavioral outcomes was done with the new model and its integrated sensor system. This characterization includes a range of different sTBI and RmTBI severities.

Finally, in Chapter 4, the therapeutic evaluation of the efficacy of a recent FDA approved drug was carried out to assess the potential for repurposing from cancer to neurotrauma.

The newly generated apparatus and system were comprised of a guiding tube for a falling object that ends on an impactor on top of a support for the mouse. This support is based on a sheet of aluminum foil placed on top of an open acrylic box with a foam cushion inside. Once the animal is impacted, the aluminum foil breaks, and it accelerates downward until it lands on the cushion. Other supports commonly used by models in the field are trap doors suspended by magnets and Kimwipes. The system embedded in the model is formed by a velocity sensor placed at the end of the tube and a force sensor placed inside the impactor (impact sensor). The Professional mouse is a cast model with the shape and approximate weight of a young adult mouse with three sensors inside the silicone head. The first sensor and second sensor are force sensors and were placed in the center and on the bottom of the head, respectively. The third sensor, an accelerometer, was placed inside the bottom of the head.

The new model proved to have a high mechanical reproducibility, beginning with the velocity of the falling objects. These measurements detected that friction inside the tube plays a role in the speed at impact reached by the falling object. Further, with the 150 g object, these sensors showed that albeit small, there were drop related differences based on the release of the object. The model proved reproducible in the similar forces generated at impact in the top, middle and bottom of the head of the Professional mouse. This reproducibility was also found in the speed and acceleration of the head of the Professional mouse after injury.

The impact sensor was critical in the discovery of double impacts in the model that uses trap doors as support. Also, it helped demonstrate that an increase in resistance by the

support increases the force applied on the of the mouse. The Professional mouse and the impact sensor demonstrated an object-weight and drop-height dependent increase in the force applied on the head. These results proved useful to understand and explain the results seen in the characterization of the model in chapter 3. Finally, a combination of the impact sensor and the accelerometer facilitated the generation of a tolerance curve, where differences in the impacts received by the Professional mouse on each of the supports was distinguishable. These differences support the empirical observation that animals injured in the Kimwipe model suffered more severe injuries than in the aluminum foil.

In the third chapter, the biomechanical characterization of the model showed that the impact force reached a plateau in the objects dropped from 1.5 m. Even with the same forces, animals showed increasing neurobehavioral deficits that were object-weight dependent. These results were explained by the experiments in chapter 2 in which the stepwise increase was observed in all three areas of the head of the Professional mouse. The results are highly suggestive of a threshold in the integrity of the skull after which compression occurs. As expected, it was shown that the model generated a spectrum of injuries, graded based on the object-weight and drop-height. These translated into behavioral deficits, the more sensitive tests found for this model were: the neurological severity score (NSS), the grip strength, the elevated plus maze, and fear conditioning, for both single and repetitive injuries. Recommendations were also made about the other memory tasks.

In the fourth chapter, the therapeutic evaluation of olaparib, a PARP1 inhibitor, yielded exciting results. First, as other PARP1 inhibitors, it showed neuroprotection *in vivo* and *in vitro* in response to different type of insults and prevented neurocognitive deficits in our animal model of TBI. As expected, it showed a decrease in neuro-inflammation assessed with astrogliosis and cytokine concentrations. Second, three unexpected yet

interesting findings occurred. One, there was no improvement in NAD<sup>+</sup> levels after stretch injury in olaparib treated cells while there is a decrease in neuronal and astrocytic cell death. This suggests that other mechanisms may be responsible for this outcome, such as preservation of mitochondrial pools of NAD<sup>+</sup>, a decrease in the formation of PAR (“the signal of death”), maintenance of the mitochondrial membrane integrity, among others. Two, the TBI group treated with olaparib showed increase Iba-1 immunoreactivity and morphology change that suggests activation. This finding counters every other publication found while conducting this study and writing this dissertation. The interesting part is that this “activation” happened in an environment where the concentration of pro-inflammatory cytokines and chemokines are either decreased or with a tendency to decrease when compared to the uninjured control. Which could indicate that the microglial activation is protective; in either case, this is the first time this phenomenon is reported in animals treated with PARP1 inhibitors. Three, the activation of caspase 3 in the hypothalamic area of the sham animals treated with olaparib proved surprising. Animals that were treated with a compound that is tightly intertwined with caspases and both serve as regulators of each other. In which the increase of PARP1 leads to an increase of activated caspase 3. The one correlation that was found in the elaboration of this dissertation was that the inhibition of PARP1 and the activation of caspase 3 (in a non-apoptotic manner) play a significant role in the differentiation of neural stem cells and their commitment toward an astrocytic differentiation. These outcomes and its mechanism should be further studied and dilucidated, as well as its implications for the brain microenvironment.

In conclusion, olaparib prevented from TBI-induced cognitive deficits showed neuroprotective and anti-neuroinflammatory properties. It also showed decreases in agoraphobia, primarily in the sham group, which could suggest anti-anxiolytic properties. This compound should continue the efficacy evaluation to determine if it’s repurposing to TBI is feasible and will improve the lives of those suffering from this devastating disease.

## **Overview of impact, significance and innovation**

This project generated an optimized, low cost, murine model of closed-skull weight-drop traumatic brain injury. The model is part of a system that has the capability to measure, in real time, the forces being applied on the head of the animal to generate the TBI. The sensors embedded in the apparatus can provide the much-needed standardization to the weight-drop models, and can be used on every animal and every experiment. We propose to add these parameters (force of impact, impulse, acceleration of the head, speed of the head) to the common data elements database. Reporting the forces applied in the TBI has the potential of making data and outcomes more comparable, potentially leading to stronger evidence when deciding the promise of individual therapeutics for advancing to clinical testing.

This study also yielded a system to understand the forces and their effects on the head of an animal. With the artificial mouse we created, different variations of closed skull models could be compared to understand differences in the outcomes, as we showed here. This “mouse” could be used to calibrate devices in different laboratories working in multicenter studies such as the Operation Brain Trauma Therapy, if more than one laboratory is using the same or similar model. It could aid in our understanding of the variability among operators or devices, and help standardize practices within researchers or laboratories. While the size of the model that we generated is that of a mouse, scaling this system should pose no problems, if the weight and size of a rat is required for the calibration.

With the generation of a novel model of TBI we also did extensive behavioral characterization of the model. This was done with the intent of highlighting behavior tests that yield robust changes that can show differences even with a low number of animals. At

the same time, we were able to eliminate some of the tests that did not show any trends in this particular model. We hope that those who choose to use this model will have the required information to plan an effective experimental design, and that this design is aimed at answering their question with the least number of animals and most robust behavioral effects.

Finally, this project was, to our knowledge, the first to assess the use of the FDA-approved compound olaparib as a potential therapeutic for TBI. This project has generated data that suggests that olaparib protects from neurological damage and cognitive deficits after TBI. Also, the results collected can be the first step in determining the appropriate dose range to test in a larger pharmacokinetic and pharmacodynamic project, to optimize the beneficial effects of this potential treatment. These next preclinical studies could open the door for the repurposing of the clinically available medications as an experimental therapeutic for TBI.

#### **CAVEATS AND ALTERNATIVE EXPLANATIONS**

There were two main caveats in the development of this project. The statistical analysis of the characterization of the model is not optimal. There is a high number of comparisons conducted for each test which could lead to a type II error. This shows the robustness of the injury induced-effects and the sensitivity of the tests that detect those deficits. One limitation was the lack of correlations with morphological data. The image analysis is pending. This result will allow generating associations between the behavioral findings and sites of anatomical damage. The statistical analysis suited for this data is a multivariate linear regression model for the spectrum of injuries and a repeated measures model including a spline to level off the behavior for the repetitive injury analysis. An exciting possibility is the use of principal component analysis to observe correlations

between all the different variables studied, that could allow the clustering of data and the analysis of the modifying variables in the outcomes.

A second caveat was the lack of biodisponibility data of olaparib and the use of DMSO as a solvent. The latter is essential. There is a report that DMSO at a concentration of 5 to 30% can react with PARP1 as a competitive inhibitor. This could have masked the results and decrease the difference in effect due to treatment in TBI. Improvements may have been more robust than reported here.

## **FUTURE DIRECTIONS**

The development of this model and the study of biomechanics for this dissertation has opened a multitude of possibilities and interesting questions with the use of this model.

Recently, an animal model of TBI named "Hit & Run" was developed. This model has the peculiarity that it induces lateral impacts (Ren et al. 2013). An interest notion of this position for an impact is the induction of rotational acceleration in the mouse. In humans, rotational accelerations are correlated with higher severity and in particular diffuse axonal injury. Is the weight-drop TBI model capable of producing rotational acceleration in the brain of a mouse? if so, do these types of impact generate higher severity of the injury and worse outcomes?

One exciting characteristic of this animal model is the time required to induce and TBI, which makes it a semi-high throughput method for drug screening. This property allows the model to be used to make quick go/no go decisions by morphological outcomes after injury, before a full pharmacological analysis of the drug is with a full therapeutic assessment of behavioral outcomes. The characterization of behavioral deficits done in this

work can aid in determining power analysis and choosing specific behavioral tests that can offer tailored results based on the effects of the injury or treatment. Additionally, based on our results in the characterization of the model, two of the questions that remain are if the behavior detected by the EPM corresponds with locomotor impulsivity or risk-seeking behavior. An attractive approach to this question could be to conduct the go/no go test for locomotor impulsivity or the gambling test for risk-seeking behavior. Additionally, the understanding of the anatomical correlates and the areas and connections affected could prove exciting in the understanding of a systems biology approach to the correlations between behaviors and morphological alterations.

In my view, an important future direction of this development is the promotion of the use of the sensor systems incorporated into the model or the Professional mouse. The objective of this is to promote a low-cost, easy to implement system to measure biomechanical characteristics of TBI. This will be a first step in generating comparable data that can standardize the way we report the injury. Also, by introducing this kind of measurements, it will change the way we understand the trauma and maybe even the stratification of its severity. An additional step to this is to make the schematic of the apparatus and sensors available and open source, so other laboratories can build the sensor systems or the TBI apparatus as a low-cost secondary injury model that will allow the test of therapeutics in more than one injury type. The cost of building the apparatus is around \$2,000 with the optical grade materials and all the sensors. This can be much cheaper if conventional materials are used and should have no effect on the mechanics of the model. Even with the \$2,000 cost of construction, it is low-cost when compared to commercially available weight-drop setups that span from \$1,290 for an acrylic box a tube and a stand (\$1,490 if it's for rats) to \$10,000 for a Kimwipe model. If more complex systems are taken into account, then the price difference will be even more significant for the CHIMERA or CCI models.

Multiple questions remained unanswered in the olaparib project:

- Positive caspase 3 cells in the hypothalamus:
  - What is the effect of olaparib on neural stem cells?
  - Does olaparib promote activation of caspase 3?
  - Does this activation lead to caspase 3-dependent differentiation or apoptosis?
- Microglial activation:
  - What type of microglial activation was seen in the olaparib TBI group?
  - What is the phenotype of these cells and what effect are they having on other populations of cells in the area?
- Neuroprotective mechanism:
  - Does olaparib improve NAD<sup>+</sup> levels after closed-skull weight-drop TBI?
  - What is the effect of olaparib on glycolysis?

A particular line of inquiry I am excited about is the effect of olaparib on glutamate uptake and GABA regulation. This can have monumental effects on the regulation of differentiation of the stem cells in the dentate gyrus, subventricular and subgranular zone and could have lasting effects on regeneration after injury.

Also, there are reports of PARP-1 inhibition on enzymes that affect cytoskeletal proteins in neurons associated with neurite outgrowth through the RhoA pathway. This can be an exciting line of inquiry since our laboratory found the increased expression of alpha-smooth muscle actin after TBI and its inhibition shows protection from axonal shortening after stretch injury. Could this be another mechanism through which it conferred neuroprotection in this experiment?

Further studies are needed to continue the process towards the repurposing of this medication. For this, it is necessary to establish the full olaparib pharmacodynamic and pharmacokinetic profile as well as bioavailability analysis of the drug. Additionally, it is paramount to determine the optimal dose for the inhibition of PARP1 in the central nervous system and the therapeutic window after TBI to assess clinical feasibility. Following these studies, further safety profiles need to be conducted at the doses tested, and the analysis of the effects seen in this work and their meaning.

## Appendix A Biomechanical comparison of the models

All sensors	Object (g)	Height (m)	Impactor	Support		Object velocity (m/s)	Kinetic Energy Object (J)	Max Force (N)	Max Impulse (N*s)	Time (ms)	Max Acceleration (g)	Max Speed (m/s)	Max Force middle (N)	Max impulse middle (N*s)	Time (ms)	Max Force bottom (N)	Max impulse bottom (N*s)	Time (ms)
1	95	1	Yes	Aluminum	Average	4.22900	0.84953	39.47233	0.04505	1.14064	1339.81905	6.16052	51.01663	0.03206	0.62080	91.30507	0.08776	0.96249
					SD	0.01861	0.00748	1.57667	0.00634	0.15221	49.57710	0.20767	1.55253	0.00106	0.01384	5.05665	0.02726	0.29912
					N	20	20	21	21	21	21	21	21	21	21	21	21	21
1	95	1	Yes	Kimwipe	Average	4.23350	0.85133	41.48300	0.06254	1.51020	1389.38182	6.64964	48.99202	0.03131	0.63927	95.10327	0.05501	0.57673
					SD	0.01461	0.00587	1.75470	0.00765	0.19914	53.10336	0.23122	2.05314	0.00124	0.01433	4.07850	0.01151	0.10744
					N	20	20	22	22	22	22	22	22	22	22	22	22	22
1	95	1	No	Aluminum	Average	4.12364	0.80772	-	-	-	1337.10000	6.89536	45.81846	0.02586	0.56903	95.55120	0.04815	0.50495
					SD	0.01690	0.00662	-	-	-	113.53074	0.40663	4.11184	0.00199	0.02722	6.79032	0.01035	0.10497
					N	11	11	0	0	14	14	14	14	14	14	14	14	
1	95	1	Yes	Doors	Average	4.22850	0.84933	64.86133	0.18088	2.79650	1397.29048	5.00181	58.68006	0.06490	1.10788	146.11307	0.42143	2.89864
					SD	0.02207	0.00885	3.66832	0.00797	0.19201	334.89481	1.07872	4.93510	0.00474	0.03844	10.70870	0.03391	0.29990
					N	20.00000	20.00000	21.00000	21.00000	21.00000	21.00000	21.00000	21.00000	21.00000	21.00000	21.00000	21.00000	21.00000
2	120	1	Yes	Aluminum	Average	4.24000	1.07668	42.17633	0.04342	1.02941	1404.94762	6.49300	54.06387	0.03449	0.63006	94.42987	0.05804	0.61550
					SD	0.01892	0.00959	1.27090	0.00170	0.02192	55.53215	0.13239	1.04580	0.00054	0.01058	4.77767	0.00864	0.09355
					N	20	20	21	21	21	21	21	21	21	21	21	21	
2	120	1	Yes	Kimwipe	Average	4.24550	1.08147	43.04820	0.06364	1.47809	1451.83500	6.85575	52.21238	0.03312	0.63450	101.59856	0.07564	0.74628
					SD	0.01395	0.00710	1.49895	0.00742	0.16629	61.68763	0.30573	2.20508	0.00133	0.01510	2.80944	0.01254	0.13448
					N	20	20	20	20	20	20	20	20	20	20	20	20	
2	120	1	No	Aluminum	Average	4.15727	1.03698	-	-	-	1390.96667	6.90358	46.53543	0.02764	0.59414	93.83080	0.08987	0.75005
					SD	0.01348	0.00672	-	-	-	83.88411	0.17622	1.69609	0.00132	0.02508	15.14890	0.01587	0.15624
					N	11	11	0	0	12	12	12	12	12	12	12	12	
2	120	1	Yes	Doors	Average	4.24950	1.08352	70.84285	0.20608	2.93044	1319.86000	5.25990	67.61340	0.07393	1.09403	153.42432	0.47410	3.11093
					SD	0.01877	0.00956	5.33409	0.00666	0.31760	318.95217	2.84498	7.13607	0.00750	0.02402	13.72292	0.02571	0.29692
					N	20	20	20	20	20	20	20	20	20	20	20	20	
3	150	1	Yes	Aluminum	Average	4.23550	1.35824	43.73980	0.04585	1.04846	1486.90000	6.71595	56.71348	0.03567	0.62913	99.24096	0.05346	0.53869
					SD	0.02438	0.01546	1.31295	0.00141	0.02145	60.01379	0.27522	2.28303	0.00135	0.01164	5.04844	0.00648	0.06032
					N	20	20	20	20	20	20	20	20	20	20	20	20	
3	150	1	Yes	Doors	Average	4.23900	1.34772	74.23509	0.22706	3.07574	1416.43478	5.64909	72.18546	0.07782	1.07787	167.34456	0.50876	3.06083
					SD	0.02269	0.01437	4.72487	0.00526	0.28602	318.90905	3.25493	5.94772	0.00658	0.01651	15.43829	0.02903	0.28106
					N	20	20	23	23	23	23	23	23	23	23	23	23	
4	95	1.5	Yes	Aluminum	Average	5.27400	1.32151	48.43540	0.05133	1.05899	1617.65000	7.39280	62.67834	0.03911	0.62404	109.50576	0.08638	0.60702
					SD	0.04593	0.02292	1.32511	0.00181	0.02901	53.65254	0.29920	2.42718	0.00169	0.01261	5.65500	0.00703	0.06464
					N	20	20	20	20	20	20	20	20	20	20	20	20	
4	95	1.5	Yes	Kimwipe	Average	5.31450	1.34166	51.08468	0.06928	1.35882	1678.35909	8.10959	62.74733	0.03901	0.62191	118.89309	0.08054	0.68014
					SD	0.03940	0.01981	2.09684	0.00710	0.13060	79.18420	0.35134	2.20191	0.00130	0.01358	4.82074	0.01347	0.12805
					N	20	20	22	22	22	22	22	22	22	22	22	22	
4	95	1.5	Yes	Doors	Average	5.29750	1.33312	81.44438	0.23540	2.89929	1468.55238	6.20438	81.12710	0.08495	1.04780	185.69867	0.53641	2.89329
					SD	0.04700	0.02356	4.24826	0.00814	0.20635	351.27355	2.72642	7.05067	0.00895	0.01932	17.76925	0.02718	0.14997
					N	20	20	21	21	21	21	21	21	21	21	21	21	
5	120	1.5	Yes	Aluminum	Average	5.32300	1.70022	50.91710	0.05524	1.08507	1716.81500	7.76560	66.89114	0.04131	0.61994	117.24720	0.08993	0.59667
					SD	0.05362	0.03434	1.97391	0.00265	0.03735	91.81554	0.34223	2.99703	0.00141	0.01588	4.18962	0.00848	0.07205
					N	20	20	20	20	20	20	20	20	20	20	20	20	
5	120	1.5	Yes	Doors	Average	5.33800	1.70844	84.86205	0.26437	3.14232	1698.89500	8.82715	83.50234	0.08710	1.04572	195.82920	0.60456	3.09712
					SD	0.03331	0.02127	6.90101	0.01125	0.37038	343.60301	4.91764	10.31942	0.00949	0.03517	14.46015	0.03688	0.21217
					N	20	20	20	20	20	20	20	20	20	20	20	20	
6	150	1.5	Yes	Aluminum	Average	5.30200	2.10851	52.93352	0.05731	1.08278	1747.54286	8.14233	69.66124	0.04334	0.62243	120.79283	0.07289	0.60393
					SD	0.04927	0.03916	1.74348	0.00256	0.03542	89.10496	0.22163	2.90781	0.00169	0.01560	7.73437	0.00899	0.06603
					N	20	20	21	21	21	21	21	21	21	21	21	21	
6	150	1.5	No	Aluminum	Average	5.16667	2.00211	-	-	-	1741.55000	8.43180	56.28028	0.03155	0.56045	115.31184	0.06954	0.60645
					SD	0.02000	0.01549	-	-	-	86.75830	0.38078	4.44221	0.00279	0.02016	14.82339	0.01598	0.13155
					N	9	9	0	0	10	10	10	10	10	10	10	10	
6	150	1.5	Yes	Doors	Average	5.35050	2.14714	91.02229	0.27263	3.00165	1508.40952	7.22143	92.59225	0.08022	1.06369	203.72693	0.61929	3.04957
					SD	0.02762	0.02214	4.14887	0.01101	0.19219	317.90078	4.03385	10.50724	0.00913	0.03079	15.82496	0.04874	0.24351
					N	20	20	21	21	21	21	21	21	21	21	21	21	

## Appendix B Code

Three codes were written for the measurement of the falling weight. The first was used for the first trial experiments of the model (Chapter 2, evolution of the model) and the biological characterization of the injury (Chapter 3), we realized that the code indicated that velocity was measured when the signal reappeared. The presence of the impactor reduced the velocity, albeit this was consistent among all groups. However, for the biomechanical characterization of the model and comparison with other models, including without impactor, this posed a problem for comparison. The code was corrected for this effect changing from a while statement to an If statement. This change resulted in the measure of velocity when the signal was interrupted, eliminating the effect induced by the presence of the impactor (Chapter 2, working model).

The third code was written when testing the first impact sensor, the force sensitive resistor (FSR), during the first trial experiments (Chapter 2, evolution of the model).

### Appendix B1 Calibrator code

```
int firstsens = 4;
int secondsens = 5;

int val;
int val2;

void setup()
{Serial.begin(9600);
pinMode(firstsens, INPUT);
pinMode(secondsens, INPUT);
}

void loop()
{
val=analogRead(firstsens);
val2=analogRead(secondsens);
Serial.println("First Sensor");
Serial.println(val);
Serial.println("Second Sensor");
Serial.println(val2);
delay (1000);
}
```

### Appendix B2 Velocity sensor code for initial trials and biological characterization

```
int firstsens = 4;
int secondsens = 5;
unsigned long time1, time2;
```

```

float mps, elap;
int val;
int val2;

void setup()
{Serial.begin(9600);
pinMode(firstsens, INPUT);
pinMode(secondsens, INPUT);
}

void loop()
{Serial.println("Velocity, meters per second");
val=analogRead(firstsens);
val2=analogRead(secondsens);
while(val>40)
//change values for val and val2 depending on calibrator
{
val=analogRead(firstsens);
}
while (val <=40)
{
time1=micros();
val=analogRead(firstsens);
}
while(val2>40)
{
val2=analogRead(secondsens);
}
while (val2<=40)
{
time2=micros();
val2=analogRead(secondsens);
}
elap=(time2-time1);
mps=0.10*1000000/elap;
Serial.println(mps);
//mps=0.1*1000000/elap for 10 cm.
{

```

## Appendix B3 Velocity sensor code for biomechanical characterization

```

int firstsens = 4;
int secondsens = 5;
unsigned long time1, time2;
float mps, elap;
int val;
int val2;

void setup()
{Serial.begin(9600);
pinMode(firstsens, INPUT);
pinMode(secondsens, INPUT);
}

```

```

void loop()
{Serial.println("Velocity, meters per second");
val=analogRead(firstsens);
val2=analogRead(secondsens);
while(val>40)
//change values for val and val2 depending on calibrator
{
  val=analogRead(firstsens);
}
If
(val<=40)
{
  time1=micros();
  val=analogRead(firstsens);
}
while(val2>40)
{
  val2=analogRead(secondsens);
}
If
(val2<=40)
{
  time2=micros();
  val2=analogRead(secondsens);
}
elap=(time2-time1);
mps=0.10*1000000/elap;
Serial.println(mps);
//mps=0.1*1000000/elap for 10 cm.
{

```

## Appendix B4 Velocity sensor and force sensitive resistor (FSR) code

```

int forcesensor = 1;
int firstled = 4;
int secondled = 5;
unsigned long time1, time2, time3, time4;
float mps, elap;
int val;
int val2;
int val3;

void setup()
{
  Serial.begin(9600);
  pinMode(forcesensor, INPUT);
  pinMode(firstled, INPUT);
  pinMode(secondled, INPUT);
}
void loop()
{
  Serial.println("Projectile speed, meters per second");
  val=analogRead(firstled);

```

```

val2=analogRead(secondled);
while(val>40)
//In this while loop, the value is set for the threshold signal from the first led, which will depend on the
calibrator value
{
  val=analogRead(firstled);
  val3=analogRead(forcesensor);
}
while(val<=40)
{
  time1=micros();
  val=analogRead(firstled);
  val3=analogRead(forcesensor);
}
while(val2>40)
//Same as previous while loop, except for the other led
{
  val2=analogRead(secondled);
  val3=analogRead(forcesensor);
}
while(val2<=40)
{
  time2=micros();
  val2=analogRead(secondled);
  val3=analogRead(forcesensor);
}
elap=(time2-time1);
time4=(time2+1000000);
mps=0.1*1000000/elap;
Serial.println(mps);
while(val>40)
{
  time3=micros();
while(time4>time3)
{
  val3=analogRead(forcesensor);
  Serial.println(val3);
  time3=micros();
}
while(time3>time4)
{
  val=0;
}
}
Serial.println(elap);
}

```

## Bibliography/References

- Abdul-Muneer, P. M., N. Chandra, and J. Haorah. 2015. "Interactions of oxidative stress and neurovascular inflammation in the pathogenesis of traumatic brain injury." *Mol Neurobiol* 51 (3):966-79. doi: 10.1007/s12035-014-8752-3.
- Abramov, A. Y., and M. R. Duchen. 2008. "Mechanisms underlying the loss of mitochondrial membrane potential in glutamate excitotoxicity." *Biochim Biophys Acta* 1777 (7-8):953-64. doi: 10.1016/j.bbabi.2008.04.017.
- Adams, J. H., D. Doyle, D. I. Graham, A. E. Lawrence, and D. R. McLellan. 1984. "Diffuse axonal injury in head injuries caused by a fall." *Lancet* 2 (8417-8418):1420-2.
- Adams, J. H., D. I. Graham, L. S. Murray, and G. Scott. 1982. "Diffuse axonal injury due to nonmissile head injury in humans: an analysis of 45 cases." *Ann Neurol* 12 (6):557-63. doi: 10.1002/ana.410120610.
- Ahmad, A., D. Gero, G. Olah, and C. Szabo. 2016. "Effect of endotoxemia in mice genetically deficient in cystathionine-gamma-lyase, cystathionine-beta-synthase or 3-mercaptopyruvate sulfurtransferase." *Int J Mol Med* 38 (6):1683-1692. doi: 10.3892/ijmm.2016.2771.
- Ahmad, A., G. Olah, D. N. Herndon, and C. Szabo. 2018. "The clinically used PARP inhibitor olaparib improves organ function, suppresses inflammatory responses and accelerates wound healing in a murine model of third-degree burn injury." *Br J Pharmacol* 175 (2):232-245. doi: 10.1111/bph.13735.
- Alano, C. C., P. Garnier, W. Ying, Y. Higashi, T. M. Kauppinen, and R. A. Swanson. 2010. "NAD<sup>+</sup> depletion is necessary and sufficient for poly(ADP-ribose) polymerase-1-mediated neuronal death." *J Neurosci* 30 (8):2967-78. doi: 10.1523/JNEUROSCI.5552-09.2010.
- Albrecht, Jennifer S., Jon Mark Hirshon, Maureen McCunn, Kathleen T. Bechtold, Vani Rao, Linda Simoni-Wastila, and Gordon S. Smith. 2016. "Increased Rates of Mild Traumatic Brain Injury Among Older Adults in US Emergency Departments, 2009-2010." *The Journal of head trauma rehabilitation* 31 (5):E1-E7. doi: 10.1097/HTR.0000000000000190.
- Amat, J. A., H. Ishiguro, K. Nakamura, and W. T. Norton. 1996. "Phenotypic diversity and kinetics of proliferating microglia and astrocytes following cortical stab wounds." *Glia* 16 (4):368-82. doi: 10.1002/(SICI)1098-1136(199604)16:4<368::AID-GLIA9>3.0.CO;2-W.
- Andelic, N. 2013. "The epidemiology of traumatic brain injury." *Lancet Neurol* 12 (1):28-9. doi: 10.1016/S1474-4422(12)70294-6.

- Andrabi, S. A., N. S. Kim, S. W. Yu, H. Wang, D. W. Koh, M. Sasaki, J. A. Klaus, T. Otsuka, Z. Zhang, R. C. Koehler, P. D. Hurn, G. G. Poirier, V. L. Dawson, and T. M. Dawson. 2006. "Poly(ADP-ribose) (PAR) polymer is a death signal." *Proc Natl Acad Sci U S A* 103 (48):18308-13. doi: 10.1073/pnas.0606526103.
- Andrabi, S. A., G. K. Umanah, C. Chang, D. A. Stevens, S. S. Karuppagounder, J. P. Gagne, G. G. Poirier, V. L. Dawson, and T. M. Dawson. 2014. "Poly(ADP-ribose) polymerase-dependent energy depletion occurs through inhibition of glycolysis." *Proc Natl Acad Sci U S A* 111 (28):10209-14. doi: 10.1073/pnas.1405158111.
- Andriessen, T. M., B. Jacobs, and P. E. Vos. 2010. "Clinical characteristics and pathophysiological mechanisms of focal and diffuse traumatic brain injury." *J Cell Mol Med* 14 (10):2381-92. doi: 10.1111/j.1582-4934.2010.01164.x.
- Ang, B. T., E. Yap, J. Lim, W. L. Tan, P. Y. Ng, I. Ng, and T. T. Yeo. 2003. "Poly(adenosine diphosphate-ribose) polymerase expression in human traumatic brain injury." *J Neurosurg* 99 (1):125-30. doi: 10.3171/jns.2003.99.1.0125.
- Angoa-Perez, M., M. J. Kane, D. I. Briggs, D. M. Francescutti, and D. M. Kuhn. 2013. "Marble burying and nestlet shredding as tests of repetitive, compulsive-like behaviors in mice." *J Vis Exp* (82):50978. doi: 10.3791/50978.
- Angoa-Perez, M., M. J. Kane, D. I. Briggs, N. Herrera-Mundo, D. C. Viano, and D. M. Kuhn. 2014. "Animal models of sports-related head injury: bridging the gap between pre-clinical research and clinical reality." *J Neurochem* 129 (6):916-31. doi: 10.1111/jnc.12690.
- Antonius, D., N. Mathew, J. Picano, A. Hinds, A. Cogswell, J. Olympia, T. Brooks, M. DiGiacomo, J. Baker, B. Willer, and J. Leddy. 2014. "Behavioral health symptoms associated with chronic traumatic encephalopathy: a critical review of the literature and recommendations for treatment and research." *J Neuropsychiatry Clin Neurosci* 26 (4):313-22. doi: 10.1176/appi.neuropsych.13090201.
- Aredia, F., and A. I. Scovassi. 2014. "Involvement of PARPs in cell death." *Front Biosci (Elite Ed)* 6:308-17.
- Ari, C., D. P. D'Agostino, D. M. Diamond, M. Kindy, C. Park, and Z. Kovacs. 2019. "Elevated Plus Maze Test Combined with Video Tracking Software to Investigate the Anxiolytic Effect of Exogenous Ketogenic Supplements." *J Vis Exp* (143). doi: 10.3791/58396.
- Bai, P., and C. Canto. 2012. "The role of PARP-1 and PARP-2 enzymes in metabolic regulation and disease." *Cell Metab* 16 (3):290-5. doi: 10.1016/j.cmet.2012.06.016.

- Bailey, Z. S., W. B. Hubbard, and P. J. VandeVord. 2016. "Cellular Mechanisms and Behavioral Outcomes in Blast-Induced Neurotrauma: Comparing Experimental Setups." *Methods Mol Biol* 1462:119-38. doi: 10.1007/978-1-4939-3816-2\_8.
- Bandak, F. A., G. Ling, A. Bandak, and N. C. De Lanerolle. 2015. "Injury biomechanics, neuropathology, and simplified physics of explosive blast and impact mild traumatic brain injury." *Handb Clin Neurol* 127:89-104. doi: 10.1016/B978-0-444-52892-6.00006-4.
- Barkhoudarian, G., D. A. Hovda, and C. C. Giza. 2011. "The molecular pathophysiology of concussive brain injury." *Clin Sports Med* 30 (1):33-48, vii-iii. doi: 10.1016/j.csm.2010.09.001.
- Barkhoudarian, G., D. A. Hovda, and C. C. Giza. 2016. "The Molecular Pathophysiology of Concussive Brain Injury - an Update." *Phys Med Rehabil Clin N Am* 27 (2):373-93. doi: 10.1016/j.pmr.2016.01.003.
- Barlow, K. M., S. Crawford, A. Stevenson, S. S. Sandhu, F. Belanger, and D. Dewey. 2010. "Epidemiology of postconcussion syndrome in pediatric mild traumatic brain injury." *Pediatrics* 126 (2):e374-81. doi: 10.1542/peds.2009-0925.
- Barlow, P. 2012. "A practical review of the Glasgow Coma Scale and Score." *Surgeon* 10 (2):114-9. doi: 10.1016/j.surge.2011.12.003.
- Barnett, S. A. 1976. *The rat : a study in behaviour*: Canberra, ACT : Australian National University Press.
- Begonia, M. T., R. Prabhu, J. Liao, W. R. Whittington, A. Claude, B. Willeford, J. Wardlaw, R. Wu, S. Zhang, and L. N. Williams. 2014. "Quantitative analysis of brain microstructure following mild blunt and blast trauma." *J Biomech* 47 (15):3704-11. doi: 10.1016/j.jbiomech.2014.09.026.
- Bennett, R. E., and D. L. Brody. 2014. "Acute reduction of microglia does not alter axonal injury in a mouse model of repetitive concussive traumatic brain injury." *J Neurotrauma* 31 (19):1647-63. doi: 10.1089/neu.2013.3320.
- Berger, N. A., V. C. Besson, A. H. Boulares, A. Burkle, A. Chiarugi, R. S. Clark, N. J. Curtin, S. Cuzzocrea, T. M. Dawson, V. L. Dawson, G. Hasko, L. Liaudet, F. Moroni, P. Pacher, P. Radermacher, A. L. Salzman, S. H. Snyder, F. G. Soriano, R. P. Strosznajder, B. Sumegi, R. A. Swanson, and C. Szabo. 2018. "Opportunities for the repurposing of PARP inhibitors for the therapy of non-oncological diseases." *Br J Pharmacol* 175 (2):192-222. doi: 10.1111/bph.13748.
- Bergsneider, M., D. A. Hovda, E. Shalmon, D. F. Kelly, P. M. Vespa, N. A. Martin, M. E. Phelps, D. L. McArthur, M. J. Caron, J. F. Kraus, and D. P. Becker. 1997. "Cerebral hyperglycolysis following severe traumatic brain injury in humans: A positron emission tomography study." *Journal of Neurosurgery* 86 (2):241-251. doi: Doi 10.3171/Jns.1997.86.2.0241.

- Besson, V. C., N. Croci, R. G. Boulu, M. Plotkine, and C. Marchand-Verrecchia. 2003. "Deleterious poly(ADP-ribose)polymerase-1 pathway activation in traumatic brain injury in rat." *Brain Res* 989 (1):58-66.
- Besson, V. C., Z. Zsengeller, M. Plotkine, C. Szabo, and C. Marchand-Verrecchia. 2005. "Beneficial effects of PJ34 and INO-1001, two novel water-soluble poly(ADP-ribose) polymerase inhibitors, on the consequences of traumatic brain injury in rat." *Brain Res* 1041 (2):149-56. doi: 10.1016/j.brainres.2005.01.096.
- Bianchi, M. E. 2007. "DAMPs, PAMPs and alarmins: all we need to know about danger." *J Leukoc Biol* 81 (1):1-5. doi: 10.1189/jlb.0306164.
- Biedermann, S. V., D. G. Biedermann, F. Wenzlaff, T. Kurjak, S. Nouri, M. K. Auer, K. Wiedemann, P. Briken, J. Haaker, T. B. Lonsdorf, and J. Fuss. 2017. "An elevated plus-maze in mixed reality for studying human anxiety-related behavior." *BMC Biol* 15 (1):125. doi: 10.1186/s12915-017-0463-6.
- Blennow, K., J. Hardy, and H. Zetterberg. 2012. "The Neuropathology and Neurobiology of Traumatic Brain Injury." *Neuron* 76 (5):886-899. doi: Doi 10.1016/J.Neuron.2012.11.021.
- Blumbergs, Peter C. 2005. "Pathology." In *Head Injury 2Ed: Pathophysiology & Management*, edited by P Reilly and R Bullock. London: CRC Press.
- Bodnar, C. N., K. N. Roberts, E. K. Higgins, and A. D. Bachstetter. 2019. "A Systematic Review of Closed Head Injury Models of Mild Traumatic Brain Injury in Mice and Rats." *J Neurotrauma*. doi: 10.1089/neu.2018.6127.
- Boulares, A. H., A. G. Yakovlev, V. Ivanova, B. A. Stoica, G. Wang, S. Iyer, and M. Smulson. 1999. "Role of poly(ADP-ribose) polymerase (PARP) cleavage in apoptosis. Caspase 3-resistant PARP mutant increases rates of apoptosis in transfected cells." *J Biol Chem* 274 (33):22932-40.
- Breasted, J. H. 1930. *The Edwin Smith surgical papyrus: published in, facsimile hieroglyphic transliteration with, translation commentary in two volumes,:* Chicago, Ill. : The University of Chicago Press, 1930.
- Briggs, D. I., M. Angoa-Perez, and D. M. Kuhn. 2016. "Prolonged Repetitive Head Trauma Induces a Singular Chronic Traumatic Encephalopathy-Like Pathology in White Matter Despite Transient Behavioral Abnormalities." *Am J Pathol* 186 (11):2869-2886. doi: 10.1016/j.ajpath.2016.07.013.
- Brochier, C., J. I. Jones, D. E. Willis, and B. Langley. 2015. "Poly(ADP-ribose) polymerase 1 is a novel target to promote axonal regeneration." *Proc Natl Acad Sci U S A* 112 (49):15220-5. doi: 10.1073/pnas.1509754112.
- Broekkamp, C. L., H. W. Rijk, D. Joly-Gelouin, and K. L. Lloyd. 1986. "Major tranquilizers can be distinguished from minor tranquilizers on the basis of

effects on marble burying and swim-induced grooming in mice." *Eur J Pharmacol* 126 (3):223-9.

- Broussard, J. I., L. Acion, H. De Jesus-Cortes, T. Yin, J. K. Britt, R. Salas, M. Costa-Mattioli, C. Robertson, A. A. Pieper, D. B. Arciniegas, and R. Jorge. 2018. "Repeated mild traumatic brain injury produces neuroinflammation, anxiety-like behaviour and impaired spatial memory in mice." *Brain Inj* 32 (1):113-122. doi: 10.1080/02699052.2017.1380228.
- Brown, M. R., P. G. Sullivan, and J. W. Geddes. 2006. "Synaptic mitochondria are more susceptible to Ca<sup>2+</sup> overload than nonsynaptic mitochondria." *J Biol Chem* 281 (17):11658-68. doi: 10.1074/jbc.M510303200.
- Bruns, J., Jr., and W. A. Hauser. 2003. "The epidemiology of traumatic brain injury: a review." *Epilepsia* 44 (s10):2-10.
- Brunyanszki, A., B. Szczesny, L. Virag, and C. Szabo. 2016. "Mitochondrial poly(ADP-ribose) polymerase: The Wizard of Oz at work." *Free Radic Biol Med* 100:257-270. doi: 10.1016/j.freeradbiomed.2016.02.024.
- Budde, M. D., A. Shah, M. McCrea, W. E. Cullinan, F. A. Pintar, and B. D. Stemper. 2013. "Primary blast traumatic brain injury in the rat: relating diffusion tensor imaging and behavior." *Front Neurol* 4:154. doi: 10.3389/fneur.2013.00154.
- Buki, A., and J. T. Povlishock. 2006. "All roads lead to disconnection?--Traumatic axonal injury revisited." *Acta Neurochir (Wien)* 148 (2):181-93; discussion 193-4. doi: 10.1007/s00701-005-0674-4.
- Calabrese, E. J. 2008. "Drug therapies for stroke and traumatic brain injury often display U-shaped dose responses: occurrence, mechanisms, and clinical implications." *Crit Rev Toxicol* 38 (6):557-77. doi: 10.1080/10408440802014287.
- Carre, E., E. Cantais, O. Darbin, J. P. Terrier, M. Lonjon, B. Palmier, and J. J. Risso. 2004. "Technical aspects of an impact acceleration traumatic brain injury rat model with potential suitability for both microdialysis and PtiO<sub>2</sub> monitoring." *J Neurosci Methods* 140 (1-2):23-8. doi: 10.1016/j.jneumeth.2004.04.037.
- Carroll, L. J., J. D. Cassidy, L. Holm, J. Kraus, and V. G. Coronado. 2004. "Methodological issues and research recommendations for mild traumatic brain injury: The WHO Collaborating Centre Task Force on Mild Traumatic Brain Injury." *Journal of Rehabilitation Medicine* 36:113-125. doi: 10.1080/16501960410023877.
- Castagne, V., P. Moser, S. Roux, and R. D. Porsolt. 2010. "Rodent models of depression: forced swim and tail suspension behavioral despair tests in rats and mice." *Curr Protoc Pharmacol* Chapter 5:Unit 5 8. doi: 10.1002/0471141755.ph0508s49.

- Centers for Disease Control and Prevention. 2010. "Injury and Prevention Control: Traumatic Brain Injury." accessed Sept 20 2014. [http://www.cdc.gov/traumaticbraininjury/get\\_the\\_facts.html](http://www.cdc.gov/traumaticbraininjury/get_the_facts.html).
- Centers for Disease Control and Prevention. 2015. Report to Congress on Traumatic Brain Injury in the United States: Epidemiology and Rehabilitation. Atlanta, GA: National Center for Injury Prevention and Control.
- Cernak, I. 2005. "Animal models of head trauma." *NeuroRx* 2 (3):410-22. doi: 10.1602/neurorx.2.3.410.
- Chandra, N., A. Sundaramurthy, and R. K. Gupta. 2017. "Validation of Laboratory Animal and Surrogate Human Models in Primary Blast Injury Studies." *Mil Med* 182 (S1):105-113. doi: 10.7205/MILMED-D-16-00144.
- Charriaut-Marlangue, C., C. Leconte, Z. Csaba, L. Chafa, J. Pansiot, M. Talatizi, K. Simon, R. Moretti, C. Marchand-Leroux, O. Baud, and V. C. Besson. 2018. "Sex differences in the effects of PARP inhibition on microglial phenotypes following neonatal stroke." *Brain Behav Immun* 73:375-389. doi: 10.1016/j.bbi.2018.05.022.
- Chen, A. Y., and A. Colantonio. 2011. "Defining neurotrauma in administrative data using the International Classification of Diseases Tenth Revision." *Emerg Themes Epidemiol* 8 (1):4. doi: 10.1186/1742-7622-8-4.
- Chen, Y., S. Constantini, V. Trembovler, M. Weinstock, and E. Shohami. 1996. "An experimental model of closed head injury in mice: pathophysiology, histopathology, and cognitive deficits." *J Neurotrauma* 13 (10):557-68. doi: 10.1089/neu.1996.13.557.
- Cheng, J., J. Gu, Y. Ma, T. Yang, Y. Kuang, B. Li, and J. Kang. 2010. "Development of a rat model for studying blast-induced traumatic brain injury." *J Neurol Sci* 294 (1-2):23-8. doi: 10.1016/j.jns.2010.04.010.
- Cheng, W. H., K. M. Martens, A. Bashir, H. Cheung, S. Stukas, E. Gibbs, D. R. Namjoshi, E. B. Button, A. Wilkinson, C. J. Barron, N. R. Cashman, P. A. Cripton, and C. L. Wellington. 2019. "CHIMERA repetitive mild traumatic brain injury induces chronic behavioural and neuropathological phenotypes in wild-type and APP/PS1 mice." *Alzheimers Res Ther* 11 (1):6. doi: 10.1186/s13195-018-0461-0.
- Chiu, C. C., Y. E. Liao, L. Y. Yang, J. Y. Wang, D. Tweedie, H. K. Karnati, N. H. Greig, and J. Y. Wang. 2016. "Neuroinflammation in animal models of traumatic brain injury." *J Neurosci Methods* 272:38-49. doi: 10.1016/j.jneumeth.2016.06.018.
- Christman, C. W., M. S. Grady, S. A. Walker, K. L. Holloway, and J. T. Povlishock. 1994. "Ultrastructural studies of diffuse axonal injury in humans." *J Neurotrauma* 11 (2):173-86. doi: 10.1089/neu.1994.11.173.

- Cipriani, G., E. Rapizzi, A. Vannacci, R. Rizzuto, F. Moroni, and A. Chiarugi. 2005. "Nuclear poly(ADP-ribose) polymerase-1 rapidly triggers mitochondrial dysfunction." *J Biol Chem* 280 (17):17227-34. doi: 10.1074/jbc.M414526200.
- Clark, D. P. Q., V. M. Perreau, S. R. Shultz, R. D. Brady, E. Lei, S. Dixit, J. M. Taylor, P. M. Beart, and W. C. Boon. 2019. "Inflammation in Traumatic Brain Injury: Roles for Toxic A1 Astrocytes and Microglial-Astrocytic Crosstalk." *Neurochem Res*. doi: 10.1007/s11064-019-02721-8.
- Clark, R. S., V. A. Vagni, P. D. Nathaniel, L. W. Jenkins, C. E. Dixon, and C. Szabo. 2007. "Local administration of the poly(ADP-ribose) polymerase inhibitor INO-1001 prevents NAD<sup>+</sup> depletion and improves water maze performance after traumatic brain injury in mice." *J Neurotrauma* 24 (8):1399-405. doi: 10.1089/neu.2007.0305.
- Cohen-Armon, M., L. Visochek, A. Katzoff, D. Levitan, A. J. Susswein, R. Klein, M. Valbrun, and J. H. Schwartz. 2004. "Long-term memory requires polyADP-ribosylation." *Science* 304 (5678):1820-2. doi: 10.1126/science.1096775.
- Coll, A. P., and G. S. Yeo. 2013. "The hypothalamus and metabolism: integrating signals to control energy and glucose homeostasis." *Curr Opin Pharmacol* 13 (6):970-6. doi: 10.1016/j.coph.2013.09.010.
- Coppari, R. 2012. "Metabolic actions of hypothalamic SIRT1." *Trends Endocrinol Metab* 23 (4):179-85. doi: 10.1016/j.tem.2012.01.002.
- Coqueugniot, H., O. Dutour, B. Arensburg, H. Duday, B. Vandermeersch, and A. M. Tillier. 2014. "Earliest cranio-encephalic trauma from the Levantine Middle Palaeolithic: 3D reappraisal of the Qafzeh 11 skull, consequences of pediatric brain damage on individual life condition and social care." *PLoS One* 9 (7):e102822. doi: 10.1371/journal.pone.0102822.
- Coronado, V. G., L. C. McGuire, K. Sarmiento, J. Bell, M. R. Lionbarger, C. D. Jones, A. I. Geller, N. Khoury, and L. Xu. 2012. "Trends in Traumatic Brain Injury in the U.S. and the public health response: 1995-2009." *J Safety Res* 43 (4):299-307. doi: 10.1016/j.jsr.2012.08.011.
- Corrigan, J. D., and F. M. Hammond. 2013. "Traumatic brain injury as a chronic health condition." *Arch Phys Med Rehabil* 94 (6):1199-201. doi: 10.1016/j.apmr.2013.01.023.
- Corrigan, J. D., A. W. Selassie, and J. A. Orman. 2010. "The epidemiology of traumatic brain injury." *J Head Trauma Rehabil* 25 (2):72-80. doi: 10.1097/HTR.0b013e3181ccc8b4.
- Cortez, I., D. V. Bulavin, P. Wu, E. L. McGrath, K. A. Cunningham, M. Wakamiya, J. Papaconstantinou, and K. T. Dineley. 2017. "Aged dominant negative p38alpha MAPK mice are resistant to age-dependent decline in adult-neurogenesis and

context discrimination fear conditioning." *Behav Brain Res* 322 (Pt B):212-222. doi: 10.1016/j.bbr.2016.10.023.

Courville, Cyril Brian. 1953. *Commotio cerebri*. Los Angeles: San Lucas Press.

Cristofori, L., B. Tavazzi, R. Gambin, R. Vagnozzi, C. Vivenza, A. M. Amorini, D. Di Pierro, G. Fazzina, and G. Lazzarino. 2001. "Early onset of lipid peroxidation after human traumatic brain injury: a fatal limitation for the free radical scavenger pharmacological therapy?" *J Investig Med* 49 (5):450-8. doi: 10.2310/6650.2001.33790.

Cryan, J. F., C. Mombereau, and A. Vassout. 2005. "The tail suspension test as a model for assessing antidepressant activity: review of pharmacological and genetic studies in mice." *Neurosci Biobehav Rev* 29 (4-5):571-625. doi: 10.1016/j.neubiorev.2005.03.009.

d'Avila, J. C., T. I. Lam, D. Bingham, J. Shi, S. J. Won, T. M. Kauppinen, S. Massa, J. Liu, and R. A. Swanson. 2012. "Microglial activation induced by brain trauma is suppressed by post-injury treatment with a PARP inhibitor." *J Neuroinflammation* 9:31. doi: 10.1186/1742-2094-9-31.

Dapul, H. R., J. Park, J. Zhang, C. Lee, A. DanEshmand, J. Lok, C. Ayata, T. Gray, A. Scalzo, J. Qiu, E. H. Lo, and M. J. Whalen. 2013. "Concussive injury before or after controlled cortical impact exacerbates histopathology and functional outcome in a mixed traumatic brain injury model in mice." *J Neurotrauma* 30 (5):382-91. doi: 10.1089/neu.2012.2536.

Dawson, V. L., and T. M. Dawson. 2004. "Deadly conversations: nuclear-mitochondrial cross-talk." *J Bioenerg Biomembr* 36 (4):287-94. doi: 10.1023/B:JOB.0000041755.22613.8d.

Deacon, R. 2012. "Assessing burrowing, nest construction, and hoarding in mice." *J Vis Exp* (59):e2607. doi: 10.3791/2607.

Deacon, R. M. 2006. "Digging and marble burying in mice: simple methods for in vivo identification of biological impacts." *Nat Protoc* 1 (1):122-4. doi: 10.1038/nprot.2006.20.

Deacon, R. M., A. Croucher, and J. N. Rawlins. 2002. "Hippocampal cytotoxic lesion effects on species-typical behaviours in mice." *Behav Brain Res* 132 (2):203-13.

Deacon, R. M., and J. N. Rawlins. 2005. "Hippocampal lesions, species-typical behaviours and anxiety in mice." *Behav Brain Res* 156 (2):241-9. doi: 10.1016/j.bbr.2004.05.027.

Deck, C., and Daniel Baumgartner. 2007. "Influence of rotational acceleration on intracranial mechanical parameters under accidental circumstances." *Proceedings*

of the International Research Council on the Biomechanics of Injury conference 35:185.

- Deeks, E. D. 2015. "Olaparib: first global approval." *Drugs* 75 (2):231-40. doi: 10.1007/s40265-015-0345-6.
- DeKosky, S. T., P. M. Kochanek, R. S. Clark, J. R. Ciallella, and C. E. Dixon. 1998. "Secondary Injury After Head Trauma: Subacute and Long-term Mechanisms." *Semin Clin Neuropsychiatry* 3 (3):176-185.
- Delgado, M. J., J. M. Cerda-Reverter, and J. L. Soengas. 2017. "Hypothalamic Integration of Metabolic, Endocrine, and Circadian Signals in Fish: Involvement in the Control of Food Intake." *Front Neurosci* 11:354. doi: 10.3389/fnins.2017.00354.
- Denny-Brown, D., and W. R. Russell. 1940. "Experimental cerebral concussion." *J Physiol* 99 (1):153.
- Department of Defense. 2010. *Mild Traumatic Brain Injury Pocket Guide (CONUS)*. Washington, D.C.: The Defense Centers of Excellence for Psychological Health and Traumatic Brain Injury (DCoE) and the Defense and Veterans Brain Injury Center (DVBIC).
- Dere, E., J. P. Huston, and M. A. De Souza Silva. 2007. "The pharmacology, neuroanatomy and neurogenetics of one-trial object recognition in rodents." *Neurosci Biobehav Rev* 31 (5):673-704. doi: 10.1016/j.neubiorev.2007.01.005.
- Dewan, M. C., A. Rattani, S. Gupta, R. E. Baticulon, Y. C. Hung, M. Punchak, A. Agrawal, A. O. Adeleye, M. G. Shrima, A. M. Rubiano, J. V. Rosenfeld, and K. B. Park. 2018. "Estimating the global incidence of traumatic brain injury." *J Neurosurg*:1-18. doi: 10.3171/2017.10.JNS17352.
- Dewitt, D. S., R. Perez-Polo, C. E. Hulsebosch, P. K. Dash, and C. S. Robertson. 2013. "Challenges in the development of rodent models of mild traumatic brain injury." *J Neurotrauma* 30 (9):688-701. doi: 10.1089/neu.2012.2349.
- Diab, A., H. Abdalla, H. L. Li, F. D. Shi, J. Zhu, B. Hojberg, L. Lindquist, B. Wretling, M. Bakhiet, and H. Link. 1999. "Neutralization of macrophage inflammatory protein 2 (MIP-2) and MIP-1alpha attenuates neutrophil recruitment in the central nervous system during experimental bacterial meningitis." *Infect Immun* 67 (5):2590-601.
- Dineley, K. T., X. Xia, D. Bui, J. D. Sweatt, and H. Zheng. 2002. "Accelerated plaque accumulation, associative learning deficits, and up-regulation of alpha 7 nicotinic receptor protein in transgenic mice co-expressing mutant human presenilin 1 and amyloid precursor proteins." *J Biol Chem* 277 (25):22768-80. doi: 10.1074/jbc.M200164200.

- Ditty, B. J., N. B. Omar, P. M. Foreman, D. M. Patel, P. R. Pritchard, and M. O. Okor. 2015. "The nonsurgical nature of patients with subarachnoid or intraparenchymal hemorrhage associated with mild traumatic brain injury." *J Neurosurg* 123 (3):649-53. doi: 10.3171/2014.10.JNS132713.
- Drew, Y. 2015. "The development of PARP inhibitors in ovarian cancer: from bench to bedside." *Br J Cancer* 113 Suppl 1:S3-9. doi: 10.1038/bjc.2015.394.
- Du, L., X. Zhang, Y. Y. Han, N. A. Burke, P. M. Kochanek, S. C. Watkins, S. H. Graham, J. A. Carcillo, C. Szabo, and R. S. Clark. 2003. "Intra-mitochondrial poly(ADP-ribosylation) contributes to NAD<sup>+</sup> depletion and cell death induced by oxidative stress." *J Biol Chem* 278 (20):18426-33. doi: 10.1074/jbc.M301295200.
- Duan, Y., R. A. Gross, and S. S. Sheu. 2007. "Ca<sup>2+</sup>-dependent generation of mitochondrial reactive oxygen species serves as a signal for poly(ADP-ribose) polymerase-1 activation during glutamate excitotoxicity." *J Physiol* 585 (Pt 3):741-58. doi: 10.1113/jphysiol.2007.145409.
- Eisenberg, H. M., H. E. Gary, Jr., E. F. Aldrich, C. Saydjari, B. Turner, M. A. Foulkes, J. A. Jane, A. Marmarou, L. F. Marshall, and H. F. Young. 1990. "Initial CT findings in 753 patients with severe head injury. A report from the NIH Traumatic Coma Data Bank." *J Neurosurg* 73 (5):688-98. doi: 10.3171/jns.1990.73.5.0688.
- Elder, G. A., and A. Cristian. 2009. "Blast-related mild traumatic brain injury: mechanisms of injury and impact on clinical care." *Mt Sinai J Med* 76 (2):111-8. doi: 10.1002/msj.20098.
- Ellis, E. F., J. S. McKinney, K. A. Willoughby, S. Liang, and J. T. Povlishock. 1995. "A new model for rapid stretch-induced injury of cells in culture: characterization of the model using astrocytes." *J Neurotrauma* 12 (3):325-39.
- Engelborghs, K., J. Verlooy, J. Van Reempts, B. Van Deuren, M. Van de Ven, and M. Borgers. 1998. "Temporal changes in intracranial pressure in a modified experimental model of closed head injury." *J Neurosurg* 89 (5):796-806. doi: 10.3171/jns.1998.89.5.0796.
- Ennaceur, A., and J. Delacour. 1988. "A new one-trial test for neurobiological studies of memory in rats. 1: Behavioral data." *Behav Brain Res* 31 (1):47-59.
- Erta, M., A. Quintana, and J. Hidalgo. 2012. "Interleukin-6, a major cytokine in the central nervous system." *Int J Biol Sci* 8 (9):1254-66. doi: 10.7150/ijbs.4679.
- Ethier, C., M. Tardif, L. Arul, and G. G. Poirier. 2012. "PARP-1 modulation of mTOR signaling in response to a DNA alkylating agent." *PLoS One* 7 (10):e47978. doi: 10.1371/journal.pone.0047978.

- Eugenin, E. A., D. Eckardt, M. Theis, K. Willecke, M. V. Bennett, and J. C. Saez. 2001. "Microglia at brain stab wounds express connexin 43 and in vitro form functional gap junctions after treatment with interferon-gamma and tumor necrosis factor-alpha." *Proc Natl Acad Sci U S A* 98 (7):4190-5. doi: 10.1073/pnas.051634298.
- Faden, A. I. 1993. "Experimental neurobiology of central nervous system trauma." *Crit Rev Neurobiol* 7 (3-4):175-86.
- Faden, A. I., P. Demediuk, S. S. Panter, and R. Vink. 1989. "The role of excitatory amino acids and NMDA receptors in traumatic brain injury." *Science* 244 (4906):798-800.
- Fang, B., M. Liang, G. Yang, Y. Ye, H. Xu, X. He, and J. H. Huang. 2014. "Expression of S100A6 in rat hippocampus after traumatic brain injury due to lateral head acceleration." *Int J Mol Sci* 15 (4):6378-90. doi: 10.3390/ijms15046378.
- Faria, M. A. 2015. "Neolithic trepanation decoded- A unifying hypothesis: Has the mystery as to why primitive surgeons performed cranial surgery been solved?" *Surg Neurol Int* 6:72. doi: 10.4103/2152-7806.156634.
- Farkas, O., J. Lifshitz, and J. T. Povlishock. 2006. "Mechanoporation induced by diffuse traumatic brain injury: An irreversible or reversible response to injury?" *Journal of Neuroscience* 26 (12):3130-3140. doi: Doi 10.1523/Jneurosci.5119-05.2006.
- Fatokun, A. A., V. L. Dawson, and T. M. Dawson. 2014. "Parthanatos: mitochondrial-linked mechanisms and therapeutic opportunities." *Br J Pharmacol* 171 (8):2000-16. doi: 10.1111/bph.12416.
- Faul, Mark, Likang Xu, Marlana Wald, and Victor Coronado. 2010. *Traumatic Brain Injury in the United States: Emergency Department Visits, Hospitalizations and Deaths*.
- Feeney, D. M., M. G. Boyeson, R. T. Linn, H. M. Murray, and W. G. Dail. 1981. "Responses to cortical injury: I. Methodology and local effects of contusions in the rat." *Brain Res* 211 (1):67-77.
- Filali, M., R. Lalonde, and S. Rivest. 2009. "Cognitive and non-cognitive behaviors in an APP<sup>swe</sup>/PS1 bigenic model of Alzheimer's disease." *Genes Brain Behav* 8 (2):143-8. doi: 10.1111/j.1601-183X.2008.00453.x.
- Fink, E. L., Y. Lai, X. Zhang, K. Janesko-Feldman, P. D. Adelson, C. Szabo, R. P. Berger, A. A. Sarnaik, P. M. Kochanek, and R. S. Clark. 2008. "Quantification of poly(ADP-ribose)-modified proteins in cerebrospinal fluid from infants and children after traumatic brain injury." *J Cereb Blood Flow Metab* 28 (9):1523-9. doi: 10.1038/jcbfm.2008.52.
- Finnie, J. 2001. "Animal models of traumatic brain injury: a review." *Aust Vet J* 79 (9):628-33.

- Finnie, J. W. 2016. "Forensic Pathology of Traumatic Brain Injury." *Vet Pathol* 53 (5):962-78. doi: 10.1177/0300985815612155.
- Finnie, J. W., and P. C. Blumbergs. 2002. "Traumatic brain injury." *Vet Pathol* 39 (6):679-89. doi: 10.1354/vp.39-6-679.
- Flierl, M. A., P. F. Stahel, K. M. Beauchamp, S. J. Morgan, W. R. Smith, and E. Shohami. 2009. "Mouse closed head injury model induced by a weight-drop device." *Nat Protoc* 4 (9):1328-37. doi: 10.1038/nprot.2009.148.
- Foda, M. A., and A. Marmarou. 1994. "A new model of diffuse brain injury in rats. Part II: Morphological characterization." *J Neurosurg* 80 (2):301-13. doi: 10.3171/jns.1994.80.2.0301.
- Fujikawa, D. G. 2015. "The role of excitotoxic programmed necrosis in acute brain injury." *Comput Struct Biotechnol J* 13:212-21. doi: 10.1016/j.csbj.2015.03.004.
- Fujimoto, S. T., L. Longhi, K. E. Saatman, V. Conte, N. Stocchetti, and T. K. McIntosh. 2004. "Motor and cognitive function evaluation following experimental traumatic brain injury." *Neurosci Biobehav Rev* 28 (4):365-78. doi: 10.1016/j.neubiorev.2004.06.002.
- Furukawa, Y., M. Okada, N. Akaike, T. Hayashi, and J. Nabekura. 2000. "Reduction of voltage-dependent magnesium block of N-methyl-D-aspartate receptor-mediated current by in vivo axonal injury." *Neuroscience* 96 (2):385-92.
- Gao, J., R. J. Grill, T. J. Dunn, S. Bedi, J. Allende Labastida, R. A. Hetz, H. Xue, J. R. Thonhoff, D. S. DeWitt, D. S. Prough, C. S. Cox, Jr., and P. Wu. 2016. "Human Neural Stem Cell Transplantation-Mediated Alteration of Microglial/Macrophage Phenotypes after Traumatic Brain Injury." *Cell Transplant* 25 (10):1863-1877. doi: 10.3727/096368916X691150.
- Gao, Junling, Donald S. Prough, David J. McAdoo, James J. Grady, Margaret O. Parsley, Long Ma, Yevgeniya I. Tarensenko, and Ping Wu. 2006. "Transplantation of primed human fetal neural stem cells improves cognitive function in rats after traumatic brain injury." *Experimental Neurology* 201 (2):281-292. doi: <http://dx.doi.org/10.1016/j.expneurol.2006.04.039>.
- Gardner, R. C., and K. Yaffe. 2015. "Epidemiology of mild traumatic brain injury and neurodegenerative disease." *Mol Cell Neurosci*. doi: 10.1016/j.mcn.2015.03.001.
- Gennarelli, T. A. 1994. "Animate models of human head injury." *J Neurotrauma* 11 (4):357-68. doi: 10.1089/neu.1994.11.357.
- Gennarelli, T. A., L. E. Thibault, J. H. Adams, D. I. Graham, C. J. Thompson, and R. P. Marcincin. 1982. "Diffuse axonal injury and traumatic coma in the primate." *Ann Neurol* 12 (6):564-74. doi: 10.1002/ana.410120611.

- Gero, D., K. Modis, N. Nagy, P. Szoleczky, Z. D. Toth, G. Dorman, and C. Szabo. 2007. "Oxidant-induced cardiomyocyte injury: identification of the cytoprotective effect of a dopamine 1 receptor agonist using a cell-based high-throughput assay." *Int J Mol Med* 20 (5):749-61.
- Giustini, A., C. Pistarini, and C. Pisoni. 2013. Traumatic and nontraumatic brain injury. In *Neurological Rehabilitation*: Elsevier.
- Giza, C. C., and D. A. Hovda. 2001. "The Neurometabolic Cascade of Concussion." *J Athl Train* 36 (3):228-235.
- Giza, C. C., and D. A. Hovda. 2014. "The new neurometabolic cascade of concussion." *Neurosurgery* 75 Suppl 4:S24-33. doi: 10.1227/NEU.0000000000000505.
- Giza, Christopher C., Jeffrey S. Kutcher, Stephen Ashwal, Jeffrey Barth, Thomas S. D. Getchius, Gerard A. Gioia, Gary S. Gronseth, Kevin Guskiewicz, Steven Mandel, Geoffrey Manley, Douglas B. McKeag, David J. Thurman, and Ross Zafonte. 2013. "Summary of evidence-based guideline update: Evaluation and management of concussion in sports." *Neurology* 80 (24):2250. doi: 10.1212/WNL.0b013e31828d57dd.
- Gold, E. M., V. Vasilevko, J. Hasselmann, C. Tiefenthaler, D. Hoa, K. Ranawaka, D. H. Cribbs, and B. J. Cummings. 2018. "Repeated Mild Closed Head Injuries Induce Long-Term White Matter Pathology and Neuronal Loss That Are Correlated With Behavioral Deficits." *ASN Neuro* 10:1759091418781921. doi: 10.1177/1759091418781921.
- Goldstein, L. E., A. M. Fisher, C. A. Tagge, X. L. Zhang, L. Velisek, J. A. Sullivan, C. Upreti, J. M. Kracht, M. Ericsson, M. W. Wojnarowicz, C. J. Goletiani, G. M. Maglakelidze, N. Casey, J. A. Moncaster, O. Minaeva, R. D. Moir, C. J. Nowinski, R. A. Stern, R. C. Cantu, J. Geiling, J. K. Blusztajn, B. L. Wolozin, T. Ikezu, T. D. Stein, A. E. Budson, N. W. Kowall, D. Chargin, A. Sharon, S. Saman, G. F. Hall, W. C. Moss, R. O. Cleveland, R. E. Tanzi, P. K. Stanton, and A. C. McKee. 2012. "Chronic traumatic encephalopathy in blast-exposed military veterans and a blast neurotrauma mouse model." *Sci Transl Med* 4 (134):134ra60. doi: 10.1126/scitranslmed.3003716.
- Goosens, K. A., and S. Maren. 2001. "Contextual and auditory fear conditioning are mediated by the lateral, basal, and central amygdaloid nuclei in rats." *Learn Mem* 8 (3):148-55. doi: 10.1101/lm.37601.
- Greer, J. E., M. J. McGinn, and J. T. Povlishock. 2011. "Diffuse traumatic axonal injury in the mouse induces atrophy, c-Jun activation, and axonal outgrowth in the axotomized neuronal population." *J Neurosci* 31 (13):5089-105. doi: 10.1523/JNEUROSCI.5103-10.2011.
- Gross, C. G. 2012. *A Hole in the Head: More Tales in the History of Neuroscience*, The MIT Press: MIT Press.

- Gubata, M. E., E. R. Packnett, C. D. Blandford, A. L. Piccirillo, D. W. Niebuhr, and D. N. Cowan. 2014. "Trends in the epidemiology of disability related to traumatic brain injury in the US Army and Marine Corps: 2005 to 2010." *J Head Trauma Rehabil* 29 (1):65-75. doi: 10.1097/HTR.0b013e318295f590.
- Gurdjian, E. S., H. R. Lissner, F. G. Evans, L. M. Patrick, and W. G. Hardy. 1961. "Intracranial pressure and acceleration accompanying head impacts in human cadavers." *Surg Gynecol Obstet* 113:185-90.
- Ha, H. C., and S. H. Snyder. 1999. "Poly(ADP-ribose) polymerase is a mediator of necrotic cell death by ATP depletion." *Proc Natl Acad Sci U S A* 96 (24):13978-82.
- Haaland, K. Y., N. Temkin, G. Randahl, and S. Dikmen. 1994. "Recovery of simple motor skills after head injury." *J Clin Exp Neuropsychol* 16 (3):448-56. doi: 10.1080/01688639408402655.
- Hagos, F. T., S. M. Adams, S. M. Poloyac, P. M. Kochanek, C. M. Horvat, R. S. B. Clark, and P. E. Empey. 2019. "Membrane transporters in traumatic brain injury: Pathological, pharmacotherapeutic, and developmental implications." *Exp Neurol* 317:10-21. doi: 10.1016/j.expneurol.2019.02.011.
- Hale, A. C., K. M. Bohnert, R. Grekin, and R. K. Sripada. 2019. "Traumatic Brain Injury in the General Population: Incidence, Mental Health Comorbidity, and Functional Impact." *J Nerv Ment Dis* 207 (1):38-42. doi: 10.1097/NMD.0000000000000915.
- Hardman, J. M., and A. Manoukian. 2002. "Pathology of head trauma." *Neuroimaging Clin N Am* 12 (2):175-87, vii.
- Hayes, R. L., D. Stalhammar, J. T. Povlishock, A. M. Allen, B. J. Galinat, D. P. Becker, and H. H. Stonnington. 1987. "A new model of concussive brain injury in the cat produced by extradural fluid volume loading: II. Physiological and neuropathological observations." *Brain Inj* 1 (1):93-112.
- Hellal, F., D. Pruneau, B. Palmier, P. Faye, N. Croci, M. Plotkine, and C. Marchand-Verrecchia. 2003. "Detrimental role of bradykinin B2 receptor in a murine model of diffuse brain injury." *J Neurotrauma* 20 (9):841-51. doi: 10.1089/089771503322385773.
- Henneman, L., M. H. van Miltenburg, E. M. Michalak, T. M. Braumuller, J. E. Jaspers, A. P. Drenth, R. de Korte-Grimmerink, E. Gogola, K. Szuhai, A. Schlicker, R. Bin Ali, C. Pritchard, I. J. Huijbers, A. Berns, S. Rottenberg, and J. Jonkers. 2015. "Selective resistance to the PARP inhibitor olaparib in a mouse model for BRCA1-deficient metaplastic breast cancer." *Proc Natl Acad Sci U S A* 112 (27):8409-14. doi: 10.1073/pnas.1500223112.
- Hernandez, C. M., I. Cortez, Z. Gu, J. O. Colon-Saez, P. W. Lamb, M. Wakamiya, J. L. Yakel, and K. T. Dineley. 2014. "Research tool: Validation of floxed alpha7

- nicotinic acetylcholine receptor conditional knockout mice using in vitro and in vivo approaches." *J Physiol* 592 (15):3201-14. doi: 10.1113/jphysiol.2014.272054.
- Hernandez, C. M., R. Kaye, H. Zheng, J. D. Sweatt, and K. T. Dineley. 2010. "Loss of alpha7 nicotinic receptors enhances beta-amyloid oligomer accumulation, exacerbating early-stage cognitive decline and septohippocampal pathology in a mouse model of Alzheimer's disease." *J Neurosci* 30 (7):2442-53. doi: 10.1523/JNEUROSCI.5038-09.2010.
- Hinojosa, A. E., B. Garcia-Bueno, J. C. Leza, and J. L. Madrigal. 2011. "CCL2/MCP-1 modulation of microglial activation and proliferation." *J Neuroinflammation* 8:77. doi: 10.1186/1742-2094-8-77.
- Holbourn, A. H. S. 1943. "MECHANICS OF HEAD INJURIES." *The Lancet* 242 (6267):438-441. doi: [https://doi.org/10.1016/S0140-6736\(00\)87453-X](https://doi.org/10.1016/S0140-6736(00)87453-X).
- Homer, and W. H. D. Rouse. 1995. *The Iliad: The Story of Achillês*. Translated by W. H. D. Rouse, *Mentor*. New York, NY: Penguin Publishing Group.
- Hong, S. J., T. M. Dawson, and V. L. Dawson. 2004. "Nuclear and mitochondrial conversations in cell death: PARP-1 and AIF signaling." *Trends Pharmacol Sci* 25 (5):259-64. doi: 10.1016/j.tips.2004.03.005.
- Hortobagyi, T., C. Gorlach, Z. Benyo, Z. Lacza, S. Hortobagyi, M. Wahl, and T. Harkany. 2003. "Inhibition of neuronal nitric oxide synthase-mediated activation of poly(ADP-ribose) polymerase in traumatic brain injury: neuroprotection by 3-aminobenzamide." *Neuroscience* 121 (4):983-90.
- Hsieh, T. H., J. W. Kang, J. H. Lai, Y. Z. Huang, A. Rotenberg, K. Y. Chen, J. Y. Wang, S. Y. Chan, S. C. Chen, Y. H. Chiang, and C. W. Peng. 2017. "Relationship of mechanical impact magnitude to neurologic dysfunction severity in a rat traumatic brain injury model." *PLoS One* 12 (5):e0178186. doi: 10.1371/journal.pone.0178186.
- Institute of Medicine National Research Council. 2014. *Sports-Related Concussions in Youth: Improving the Science, Changing the Culture*. Edited by Graham Robert, P. Rivara Frederick, A. Ford Morgan and Spicer Carol Mason. Washington, DC: The National Academies Press.
- Irvine, K., R. Bishop, S. J. Won, J. Xu, K. Hamel, V. Coppes, P. Singh, A. Sondag, E. Rome, J. Basu, G. Santos, S. S. Panter, and R. Swanson. 2017. "Effects of veliparib on microglial activation and functional outcomes following traumatic brain injury in the rat and pig." *J Neurotrauma*. doi: 10.1089/neu.2017.5044.
- Ivancevic, V. G. 2009. "New mechanics of traumatic brain injury." *Cogn Neurodyn* 3 (3):281-93. doi: 10.1007/s11571-008-9070-0.

- Iwakuma, T., and C. V. Brunngraber. 1973. "Chronic extradural hematomas. A study of 21 cases." *J Neurosurg* 38 (4):488-93. doi: 10.3171/jns.1973.38.4.0488.
- Jagtap, P., and C. Szabo. 2005. "Poly(ADP-ribose) polymerase and the therapeutic effects of its inhibitors." *Nat Rev Drug Discov* 4 (5):421-40. doi: 10.1038/nrd1718.
- James, L. M., T. Q. Strom, and J. Leskela. 2014. "Risk-taking behaviors and impulsivity among veterans with and without PTSD and mild TBI." *Mil Med* 179 (4):357-63. doi: 10.7205/MILMED-D-13-00241.
- Jamnia, N., J. H. Urban, G. E. Stutzmann, S. G. Chiren, E. Reisenbigler, R. Marr, D. A. Peterson, and D. A. Kozlowski. 2017. "A Clinically Relevant Closed-Head Model of Single and Repeat Concussive Injury in the Adult Rat Using a Controlled Cortical Impact Device." *J Neurotrauma* 34 (7):1351-1363. doi: 10.1089/neu.2016.4517.
- Jassam, Y. N., S. Izzy, M. Whalen, D. B. McGavern, and J. El Khoury. 2017. "Neuroimmunology of Traumatic Brain Injury: Time for a Paradigm Shift." *Neuron* 95 (6):1246-1265. doi: 10.1016/j.neuron.2017.07.010.
- Jedynak, P., P. Jaholkowski, G. Wozniak, C. Sandi, L. Kaczmarek, and R. K. Filipkowski. 2012. "Lack of cyclin D2 impairing adult brain neurogenesis alters hippocampal-dependent behavioral tasks without reducing learning ability." *Behav Brain Res* 227 (1):159-66. doi: 10.1016/j.bbr.2011.11.007.
- Jin, W., J. Kong, T. Lu, H. Wang, H. Ni, J. Wu, Y. Dai, J. Jiang, and W. Liang. 2011. "Erythropoietin prevents secondary brain injury induced by cortical lesion in mice: possible involvement of Nrf2 signaling pathway." *Ann Clin Lab Sci* 41 (1):25-32.
- Jirkof, P. 2014. "Burrowing and nest building behavior as indicators of well-being in mice." *J Neurosci Methods* 234:139-46. doi: 10.1016/j.jneumeth.2014.02.001.
- Johnson, E. A., T. L. Dao, M. A. Guignet, C. E. Geddes, A. I. Koemeter-Cox, and R. K. Kan. 2011. "Increased expression of the chemokines CXCL1 and MIP-1alpha by resident brain cells precedes neutrophil infiltration in the brain following prolonged soman-induced status epilepticus in rats." *J Neuroinflammation* 8:41. doi: 10.1186/1742-2094-8-41.
- Johnson, V. E., W. Stewart, and D. H. Smith. 2013. "Axonal pathology in traumatic brain injury." *Experimental Neurology* 246:35-43. doi: 10.1016/J.Expneurol.2012.01.013.
- Kanayama, G., M. Takeda, H. Niigawa, Y. Ikura, H. Tamii, N. Taniguchi, T. Kudo, Y. Miyamae, T. Morihara, and T. Nishimura. 1996. "The effects of repetitive mild brain injury on cytoskeletal protein and behavior." *Methods Find Exp Clin Pharmacol* 18 (2):105-15.

- Kane, M. J., M. Angoa-Perez, D. I. Briggs, D. C. Viano, C. W. Kreipke, and D. M. Kuhn. 2012. "A mouse model of human repetitive mild traumatic brain injury." *J Neurosci Methods* 203 (1):41-9. doi: 10.1016/j.jneumeth.2011.09.003.
- Kane, M. J., H. Hatic, V. Delic, J. S. Dennis, C. L. Butler, J. N. Saykally, and B. A. Citron. 2011. "Modeling the pathobiology of repetitive traumatic brain injury in immortalized neuronal cell lines." *Brain Res* 1425:123-31. doi: 10.1016/j.brainres.2011.09.047.
- Katayama, Y., D. P. Becker, T. Tamura, and D. A. Hovda. 1990. "Massive increases in extracellular potassium and the indiscriminate release of glutamate following concussive brain injury." *J Neurosurg* 73 (6):889-900. doi: 10.3171/jns.1990.73.6.0889.
- Kauppinen, T. M., S. W. Suh, A. E. Berman, A. M. Hamby, and R. A. Swanson. 2009. "Inhibition of poly(ADP-ribose) polymerase suppresses inflammation and promotes recovery after ischemic injury." *J Cereb Blood Flow Metab* 29 (4):820-9. doi: 10.1038/jcbfm.2009.9.
- Kauppinen, T. M., S. W. Suh, Y. Higashi, A. E. Berman, C. Escartin, S. J. Won, C. Wang, S. H. Cho, L. Gan, and R. A. Swanson. 2011. "Poly(ADP-ribose)polymerase-1 modulates microglial responses to amyloid beta." *J Neuroinflammation* 8:152. doi: 10.1186/1742-2094-8-152.
- Kawamata, T., Y. Katayama, D. A. Hovda, A. Yoshino, and D. P. Becker. 1995. "Lactate Accumulation Following Concussive Brain Injury - the Role of Ionic Fluxes Induced by Excitatory Amino-Acids." *Brain Research* 674 (2):196-204. doi: Doi 10.1016/0006-8993(94)01444-M.
- Khalin, I., N. L. Jamari, N. B. Razak, Z. B. Hasain, M. A. Nor, M. H. Zainudin, A. B. Omar, and R. Alyautdin. 2016. "A mouse model of weight-drop closed head injury: emphasis on cognitive and neurological deficiency." *Neural Regen Res* 11 (4):630-5. doi: 10.4103/1673-5374.180749.
- Khuman, J., W. P. Meehan, 3rd, X. Zhu, J. Qiu, U. Hoffmann, J. Zhang, E. Giovannone, E. H. Lo, and M. J. Whalen. 2011. "Tumor necrosis factor alpha and Fas receptor contribute to cognitive deficits independent of cell death after concussive traumatic brain injury in mice." *J Cereb Blood Flow Metab* 31 (2):778-89. doi: 10.1038/jcbfm.2010.172.
- Kim, M. Y., T. Zhang, and W. L. Kraus. 2005. "Poly(ADP-ribosyl)ation by PARP-1: 'PAR-laying' NAD<sup>+</sup> into a nuclear signal." *Genes Dev* 19 (17):1951-67. doi: 10.1101/gad.1331805.
- King, A I, K H Yang, L Zhang, W Hardy, and D C Viano. 2003. "Is Head Injury caused by Linear or Angular Acceleration?" IRCOBI Conference, Lisbon, Portugal.

- King, A. I. 2017. "Basics of the Biomechanics of Brain Injury." In *The Biomechanics of Impact Injury: Biomechanical Response, Mechanisms of Injury, Human Tolerance and Simulation*. Springer International Publishing.
- King, J. T., Jr., P. M. Carlier, and D. W. Marion. 2005. "Early Glasgow Outcome Scale scores predict long-term functional outcome in patients with severe traumatic brain injury." *J Neurotrauma* 22 (9):947-54. doi: 10.1089/neu.2005.22.947.
- Kobeissy, Firas H., C. Edward Dixon, Ronald L. Hayes, Stefania Mondello, and Ralph G. DePalma. 2016. *Injury models of the central nervous system : methods and protocols, Methods in molecular biology*,. New York: Humana Press.
- Kocka, A., and J. Gagnon. 2014. "Definition of Impulsivity and Related Terms Following Traumatic Brain Injury: A Review of the Different Concepts and Measures Used to Assess Impulsivity, Disinhibition and other Related Concepts." *Behav Sci (Basel)* 4 (4):352-70. doi: 10.3390/bs4040352.
- Kondratiuk, I., H. Devijver, B. Lechat, F. Van Leuven, L. Kaczmarek, and R. K. Filipkowski. 2013. "Glycogen synthase kinase-3beta affects size of dentate gyrus and species-typical behavioral tasks in transgenic and knockout mice." *Behav Brain Res* 248:46-50. doi: 10.1016/j.bbr.2013.03.045.
- Korley, F. K., G. D. Kelen, C. M. Jones, and R. Diaz-Arrastia. 2016. "Emergency Department Evaluation of Traumatic Brain Injury in the United States, 2009-2010." *J Head Trauma Rehabil* 31 (6):379-387. doi: 10.1097/HTR.0000000000000187.
- Krainz, T., A. M. Lamade, L. Du, T. S. Maskrey, M. J. Calderon, S. C. Watkins, M. W. Epperly, J. S. Greenberger, H. Bayir, P. Wipf, and R. S. B. Clark. 2018. "Synthesis and Evaluation of a Mitochondria-Targeting Poly(ADP-ribose) Polymerase-1 Inhibitor." *ACS Chem Biol* 13 (10):2868-2879. doi: 10.1021/acscchembio.8b00423.
- Kumar, A., and D. J. Loane. 2012. "Neuroinflammation after traumatic brain injury: opportunities for therapeutic intervention." *Brain Behav Immun* 26 (8):1191-201. doi: 10.1016/j.bbi.2012.06.008.
- Kurhe, Y. V., M. Radhakrishnan, D. Thangaraj, and D. Gupta. 2014. "Anti-anxiety effect of a novel 5-HT(3) receptor antagonist N-(benzo[d]thiazol-2-yl)-3-ethoxyquinoxalin-2-carboxamide (6k) using battery tests for anxiety in mice." *Indian J Pharmacol* 46 (1):100-4. doi: 10.4103/0253-7613.125186.
- Kuriakose, M., M. Skotak, A. Misistia, S. Kahali, A. Sundaramurthy, and N. Chandra. 2016. "Tailoring the Blast Exposure Conditions in the Shock Tube for Generating Pure, Primary Shock Waves: The End Plate Facilitates Elimination of Secondary Loading of the Specimen." *PLoS One* 11 (9):e0161597. doi: 10.1371/journal.pone.0161597.

- Lacza, Z., E. M. Horvath, K. Komjati, T. Hortobagyi, C. Szabo, and D. W. Busija. 2003. "PARP inhibition improves the effectiveness of neural stem cell transplantation in experimental brain trauma." *Int J Mol Med* 12 (2):153-9.
- Lai, Y., Y. Chen, S. C. Watkins, P. D. Nathaniel, F. Guo, P. M. Kochanek, L. W. Jenkins, C. Szabo, and R. S. Clark. 2008. "Identification of poly-ADP-ribosylated mitochondrial proteins after traumatic brain injury." *J Neurochem* 104 (6):1700-11. doi: 10.1111/j.1471-4159.2007.05114.x.
- Lajtha, Abel, and Naren L. Banik. 2007. *Handbook of neurochemistry and molecular neurobiology. Neural protein metabolism and function*. 3rd ed, Springer reference. New York: Springer.
- Laker, S. R. 2011. "Epidemiology of concussion and mild traumatic brain injury." *PM R* 3 (10 Suppl 2):S354-8. doi: 10.1016/j.pmrj.2011.07.017.
- Lange, R. T., G. L. Iverson, and M. D. Franzen. 2009. "Neuropsychological functioning following complicated vs. uncomplicated mild traumatic brain injury." *Brain Inj* 23 (2):83-91. doi: 10.1080/02699050802635281.
- Langlois, J. A., W. Rutland-Brown, and M. M. Wald. 2006. "The epidemiology and impact of traumatic brain injury: a brief overview." *J Head Trauma Rehabil* 21 (5):375-8.
- LaPlaca, M. C., R. Raghupathi, A. Verma, A. A. Pieper, K. E. Saatman, S. H. Snyder, and T. K. McIntosh. 1999. "Temporal patterns of poly(ADP-ribose) polymerase activation in the cortex following experimental brain injury in the rat." *J Neurochem* 73 (1):205-13.
- LaPlaca, M. C., C. M. Simon, G. R. Prado, and D. K. Cullen. 2007. "CNS injury biomechanics and experimental models." *Prog Brain Res* 161:13-26. doi: 10.1016/S0079-6123(06)61002-9.
- LaPlaca, M. C., J. Zhang, R. Raghupathi, J. H. Li, F. Smith, F. M. Bareyre, S. H. Snyder, D. I. Graham, and T. K. McIntosh. 2001. "Pharmacologic inhibition of poly(ADP-ribose) polymerase is neuroprotective following traumatic brain injury in rats." *J Neurotrauma* 18 (4):369-76. doi: 10.1089/089771501750170912.
- Leger, M., A. Quiedeville, V. Bouet, B. Haelewyn, M. Boulouard, P. Schumann-Bard, and T. Freret. 2013. "Object recognition test in mice." *Nat Protoc* 8 (12):2531-7. doi: 10.1038/nprot.2013.155.
- Levin, H. S., A. L. Benton, and R. G. Grossman. 1982. *Neurobehavioral Consequences of Closed Head Injury*: Oxford University Press.
- Levrاند, S., C. Vannay-Bouchiche, B. Pesse, P. Pacher, F. Feihl, B. Waeber, and L. Liaudet. 2006. "Peroxyntirite is a major trigger of cardiomyocyte apoptosis in

- vitro and in vivo." *Free Radic Biol Med* 41 (6):886-95. doi: 10.1016/j.freeradbiomed.2006.04.034.
- Li, Y., L. Zhang, S. Kallakuri, R. Zhou, and J. M. Cavanaugh. 2011. "Quantitative relationship between axonal injury and mechanical response in a rodent head impact acceleration model." *J Neurotrauma* 28 (9):1767-82. doi: 10.1089/neu.2010.1687.
- Lissner, H.R. , M. Lebow, and F.G. Evans. 1960. "Experimental studies on the relation between acceleration and intracranial pressure changes in man." *Surgery, Gynecology & Obstetrics* 111:329-338.
- Liva, S. M., and J. de Vellis. 2001. "IL-5 induces proliferation and activation of microglia via an unknown receptor." *Neurochem Res* 26 (6):629-37.
- Londei, T., A. M. Valentini, and V. G. Leone. 1998. "Investigative burying by laboratory mice may involve non-functional, compulsive, behaviour." *Behav Brain Res* 94 (2):249-54.
- Long, A., N. Klimova, and T. Kristian. 2017. "Mitochondrial NUDIX hydrolases: A metabolic link between NAD catabolism, GTP and mitochondrial dynamics." *Neurochem Int* 109:193-201. doi: 10.1016/j.neuint.2017.03.009.
- Long, J. B., T. L. Bentley, K. A. Wessner, C. Cerone, S. Sweeney, and R. A. Bauman. 2009. "Blast overpressure in rats: recreating a battlefield injury in the laboratory." *J Neurotrauma* 26 (6):827-40. doi: 10.1089/neu.2008.0748.
- Lopez-Garcia, I., D. Gero, B. Szczesny, P. Szoleczky, G. Olah, K. Modis, K. Zhang, J. Gao, P. Wu, L. C. Sowers, D. DeWitt, D. S. Prough, and C. Szabo. 2018. "Development of a stretch-induced neurotrauma model for medium-throughput screening in vitro: identification of rifampicin as a neuroprotectant." *Br J Pharmacol* 175 (2):284-300. doi: 10.1111/bph.13642.
- Los, M., M. Mozoluk, D. Ferrari, A. Stepczynska, C. Stroh, A. Renz, Z. Herceg, Z. Q. Wang, and K. Schulze-Osthoff. 2002. "Activation and caspase-mediated inhibition of PARP: a molecular switch between fibroblast necrosis and apoptosis in death receptor signaling." *Mol Biol Cell* 13 (3):978-88. doi: 10.1091/mbc.01-05-0272.
- Ma, X., A. Aravind, B. J. Pfister, N. Chandra, and J. Haorah. 2019. "Animal Models of Traumatic Brain Injury and Assessment of Injury Severity." *Mol Neurobiol*. doi: 10.1007/s12035-018-1454-5.
- Maas, A. I., C. L. Harrison-Felix, D. Menon, P. D. Adelson, T. Balkin, R. Bullock, D. C. Engel, W. Gordon, J. L. Orman, H. L. Lew, C. Robertson, N. Temkin, A. Valadka, M. Verfaellie, M. Wainwright, D. W. Wright, and K. Schwab. 2010. "Common Data Elements for Traumatic Brain Injury: Recommendations From the Interagency Working Group on Demographics and Clinical Assessment."

- Maas, A. I. R., D. K. Menon, P. D. Adelson, N. Andelic, M. J. Bell, A. Belli, P. Bragge, A. Brazinova, A. Buki, R. M. Chesnut, G. Citerio, M. Coburn, D. J. Cooper, A. T. Crowder, E. Czeiter, M. Czosnyka, R. Diaz-Arrastia, J. P. Dreier, A. C. Duhaime, A. Ercole, T. A. van Essen, V. L. Feigin, G. Gao, J. Giacino, L. E. Gonzalez-Lara, R. L. Gruen, D. Gupta, J. A. Hartings, S. Hill, J. Y. Jiang, N. Ketharanathan, E. J. O. Kompanje, L. Lanyon, S. Laureys, F. Lecky, H. Levin, H. F. Lingsma, M. Maegele, M. Majdan, G. Manley, J. Marsteller, L. Mascia, C. McFadyen, S. Mondello, V. Newcombe, A. Palotie, P. M. Parizel, W. Peul, J. Piercy, S. Polinder, L. Puybasset, T. E. Rasmussen, R. Rossaint, P. Smielewski, J. Soderberg, S. J. Stanworth, M. B. Stein, N. von Steinbuchel, W. Stewart, E. W. Steyerberg, N. Stocchetti, A. Synnot, B. Te Ao, O. Tenovuo, A. Theadom, D. Tibboel, W. Videtta, K. K. W. Wang, W. H. Williams, L. Wilson, K. Yaffe, Tbir Participants In, and Investigators. 2017. "Traumatic brain injury: integrated approaches to improve prevention, clinical care, and research." *Lancet Neurol* 16 (12):987-1048. doi: 10.1016/S1474-4422(17)30371-X.
- MacFarlane, M. P., and T. C. Glenn. 2015. "Neurochemical cascade of concussion." *Brain Inj* 29 (2):139-53. doi: 10.3109/02699052.2014.965208.
- Malkesman, O., L. B. Tucker, J. Ozl, and J. T. McCabe. 2013. "Traumatic brain injury - modeling neuropsychiatric symptoms in rodents." *Front Neurol* 4:157. doi: 10.3389/fneur.2013.00157.
- Management of Concussion/mTBI Working Group. 2009. "VA/DoD Clinical Practice Guideline for Management of Concussion/Mild Traumatic Brain Injury." *J Rehabil Res Dev* 46 (6):CP1-68.
- Manley, G. T., G. Rosenthal, M. Lam, D. Morabito, D. Yan, N. Derugin, A. Bollen, M. M. Knudson, and S. S. Panter. 2006. "Controlled cortical impact in swine: pathophysiology and biomechanics." *J Neurotrauma* 23 (2):128-39. doi: 10.1089/neu.2006.23.128.
- Mannix, R., J. Berglass, J. Berkner, P. Moleus, J. Qiu, N. Andrews, G. Gunner, L. Berglass, L. L. Jantzie, S. Robinson, and W. P. Meehan, 3rd. 2014. "Chronic gliosis and behavioral deficits in mice following repetitive mild traumatic brain injury." *J Neurosurg* 121 (6):1342-50. doi: 10.3171/2014.7.JNS14272.
- Mannix, R., W. P. Meehan, J. Mandeville, P. E. Grant, T. Gray, J. Berglass, J. Zhang, J. Bryant, S. Rezaie, J. Y. Chung, N. V. Peters, C. Lee, L. W. Tien, D. L. Kaplan, M. Feany, and M. Whalen. 2013. "Clinical correlates in an experimental model of repetitive mild brain injury." *Ann Neurol* 74 (1):65-75. doi: 10.1002/ana.23858.
- Mao, H., L. Zhang, K. H. Yang, and A. I. King. 2006. "Application of a finite element model of the brain to study traumatic brain injury mechanisms in the rat." *Stapp Car Crash J* 50:583-600.

- Maragakis, N. J., M. Dykes-Hoberg, and J. D. Rothstein. 2004. "Altered expression of the glutamate transporter EAAT2b in neurological disease." *Ann Neurol* 55 (4):469-77. doi: 10.1002/ana.20003.
- Marmarou, A., M. A. Foda, W. van den Brink, J. Campbell, H. Kita, and K. Demetriadou. 1994. "A new model of diffuse brain injury in rats. Part I: Pathophysiology and biomechanics." *J Neurosurg* 80 (2):291-300. doi: 10.3171/jns.1994.80.2.0291.
- Masel, B. E., and D. S. DeWitt. 2010. "Traumatic brain injury: a disease process, not an event." *J Neurotrauma* 27 (8):1529-40. doi: 10.1089/neu.2010.1358.
- Maxwell, W. L., J. T. Povlishock, and D. L. Graham. 1997. "A mechanistic analysis of nondisruptive axonal injury: a review." *J Neurotrauma* 14 (7):419-40.
- McCrorry, P., W. Meeuwisse, J. Dvorak, M. Aubry, J. Bailes, S. Broglio, R. C. Cantu, D. Cassidy, R. J. Echemendia, R. J. Castellani, G. A. Davis, R. Ellenbogen, C. Emery, L. Engebretsen, N. Feddermann-Demont, C. C. Giza, K. M. Guskiewicz, S. Herring, G. L. Iverson, K. M. Johnston, J. Kissick, J. Kutcher, J. J. Leddy, D. Maddocks, M. Makdissi, G. T. Manley, M. McCrea, W. P. Meehan, S. Nagahiro, J. Patricios, M. Putukian, K. J. Schneider, A. Sills, C. H. Tator, M. Turner, and P. E. Vos. 2017. "Consensus statement on concussion in sport-the 5(th) international conference on concussion in sport held in Berlin, October 2016." *Br J Sports Med* 51 (11):838-847. doi: 10.1136/bjsports-2017-097699.
- McCrorry, P. R., and S. F. Berkovic. 2001. "Concussion: the history of clinical and pathophysiological concepts and misconceptions." *Neurology* 57 (12):2283-9.
- McIntosh, T. K., L. Noble, B. Andrews, and A. I. Faden. 1987. "Traumatic brain injury in the rat: characterization of a midline fluid-percussion model." *Cent Nerv Syst Trauma* 4 (2):119-34.
- McKee, A. C., and M. E. Robinson. 2014. "Military-related traumatic brain injury and neurodegeneration." *Alzheimers Dement* 10 (3 Suppl):S242-53. doi: 10.1016/j.jalz.2014.04.003.
- Meaney, D. F., and D. K. Cullen. 2017. "Biomechanical Basis of Traumatic Brain Injury." In *Youmans & Winn neurological surgery*, edited by H. R. Winn and J. R. Youmans, 2755-2764. Philadelphia, PA: Elsevier.
- Meaney, D. F., and D. H. Smith. 2011. "Biomechanics of concussion." *Clin Sports Med* 30 (1):19-31, vii. doi: 10.1016/j.csm.2010.08.009.
- Meehan, W. P., 3rd, J. Zhang, R. Mannix, and M. J. Whalen. 2012. "Increasing recovery time between injuries improves cognitive outcome after repetitive mild concussive brain injuries in mice." *Neurosurgery* 71 (4):885-91. doi: 10.1227/NEU.0b013e318265a439.

- Menon, D. K., K. Schwab, D. W. Wright, A. I. Maas, Demographics, International Clinical Assessment Working Group of the, Injury Interagency Initiative toward Common Data Elements for Research on Traumatic Brain, and Health Psychological. 2010. "Position statement: definition of traumatic brain injury." *Arch Phys Med Rehabil* 91 (11):1637-40. doi: 10.1016/j.apmr.2010.05.017.
- Meythaler, J. M., J. D. Peduzzi, E. Eleftheriou, and T. A. Novack. 2001. "Current concepts: diffuse axonal injury-associated traumatic brain injury." *Arch Phys Med Rehabil* 82 (10):1461-71.
- Mishra, V., M. Skotak, H. Schuetz, A. Heller, J. Haorah, and N. Chandra. 2016. "Primary blast causes mild, moderate, severe and lethal TBI with increasing blast overpressures: Experimental rat injury model." *Sci Rep* 6:26992. doi: 10.1038/srep26992.
- Morales, D. M., N. Marklund, D. Lebold, H. J. Thompson, A. Pitkanen, W. L. Maxwell, L. Longhi, H. Laurer, M. Maegele, E. Neugebauer, D. I. Graham, N. Stocchetti, and T. K. McIntosh. 2005. "Experimental models of traumatic brain injury: do we really need to build a better mousetrap?" *Neuroscience* 136 (4):971-89. doi: 10.1016/j.neuroscience.2005.08.030.
- Mychasiuk, R., A. Farran, M. Angoa-Perez, D. Briggs, D. Kuhn, and M. J. Esser. 2014. "A novel model of mild traumatic brain injury for juvenile rats." *J Vis Exp* (94). doi: 10.3791/51820.
- Nagayama, T., R. P. Simon, D. Chen, D. C. Henshall, W. Pei, R. A. Stetler, and J. Chen. 2000. "Activation of poly(ADP-ribose) polymerase in the rat hippocampus may contribute to cellular recovery following sublethal transient global ischemia." *J Neurochem* 74 (4):1636-45.
- Namjoshi, D. R., W. H. Cheng, K. A. McInnes, K. M. Martens, M. Carr, A. Wilkinson, J. Fan, J. Robert, A. Hayat, P. A. Crompton, and C. L. Wellington. 2014. "Merging pathology with biomechanics using CHIMERA (Closed-Head Impact Model of Engineered Rotational Acceleration): a novel, surgery-free model of traumatic brain injury." *Mol Neurodegener* 9:55. doi: 10.1186/1750-1326-9-55.
- Namjoshi, D. R., C. Good, W. H. Cheng, W. Panenka, D. Richards, P. A. Crompton, and C. L. Wellington. 2013. "Towards clinical management of traumatic brain injury: a review of models and mechanisms from a biomechanical perspective." *Dis Model Mech* 6 (6):1325-38. doi: 10.1242/dmm.011320.
- Narne, P., V. Pandey, P. K. Simhadri, and P. B. Phanithi. 2017. "Poly(ADP-ribose)polymerase-1 hyperactivation in neurodegenerative diseases: The death knell tolls for neurons." *Semin Cell Dev Biol* 63:154-166. doi: 10.1016/j.semcdb.2016.11.007.
- Nichols, J. N., A. S. Deshane, T. L. Niedzielko, C. D. Smith, and C. L. Floyd. 2016. "Greater neurobehavioral deficits occur in adult mice after repeated, as compared

- to single, mild traumatic brain injury (mTBI)." *Behav Brain Res* 298 (Pt B):111-24. doi: 10.1016/j.bbr.2015.10.052.
- Nicolas, L. B., Y. Kolb, and E. P. Prinssen. 2006. "A combined marble burying-locomotor activity test in mice: a practical screening test with sensitivity to different classes of anxiolytics and antidepressants." *Eur J Pharmacol* 547 (1-3):106-15. doi: 10.1016/j.ejphar.2006.07.015.
- Nilsson, P., L. Hillered, Y. Olsson, M. J. Sheardown, and A. J. Hansen. 1993. "Regional Changes in Interstitial K<sup>+</sup> and Ca<sup>2+</sup> Levels Following Cortical Compression Contusion Trauma in Rats." *Journal of Cerebral Blood Flow and Metabolism* 13 (2):183-192.
- Ninchoji, T., K. Uemura, I. Shimoyama, K. Hinokuma, T. Bun, and S. Nakajima. 1984. "Traumatic intracerebral haematomas of delayed onset." *Acta Neurochir (Wien)* 71 (1-2):69-90.
- Nyanzu, M., F. Siaw-Debrah, H. Ni, Z. Xu, H. Wang, X. Lin, Q. Zhuge, and L. Huang. 2017. "Improving on Laboratory Traumatic Brain Injury Models to Achieve Better Results." *Int J Med Sci* 14 (5):494-505. doi: 10.7150/ijms.18075.
- O'Connor, W. T., A. Smyth, and M. D. Gilchrist. 2011. "Animal models of traumatic brain injury: a critical evaluation." *Pharmacol Ther* 130 (2):106-13. doi: 10.1016/j.pharmthera.2011.01.001.
- Omalu, B. I., S. T. DeKosky, R. L. Hamilton, R. L. Minster, M. I. Kamboh, A. M. Shakir, and C. H. Wecht. 2006. "Chronic traumatic encephalopathy in a national football league player: part II." *Neurosurgery* 59 (5):1086-92; discussion 1092-3. doi: 10.1227/01.NEU.0000245601.69451.27.
- Omalu, B. I., S. T. DeKosky, R. L. Minster, M. I. Kamboh, R. L. Hamilton, and C. H. Wecht. 2005. "Chronic traumatic encephalopathy in a National Football League player." *Neurosurgery* 57 (1):128-34; discussion 128-34.
- Omalu, B. I., R. L. Hamilton, M. I. Kamboh, S. T. DeKosky, and J. Bailes. 2010. "Chronic traumatic encephalopathy (CTE) in a National Football League Player: Case report and emerging medicolegal practice questions." *J Forensic Nurs* 6 (1):40-6. doi: 10.1111/j.1939-3938.2009.01064.x.
- Ommaya, A. K., and T. A. Gennarelli. 1974. "Cerebral concussion and traumatic unconsciousness. Correlation of experimental and clinical observations of blunt head injuries." *Brain* 97 (4):633-54.
- Ommaya, A. K., and A. E. Hirsch. 1971. "Tolerances for cerebral concussion from head impact and whiplash in primates." *J Biomech* 4 (1):13-21.

- Ommaya, A. K., P. Yarnell, A. E. Hirsch, and E. H. Harris. 1967. "Scaling of Experimental Data on Cerebral Concussion in Sub-Human Primates to Concussion Threshold for Man."
- Onaya, M. 2002. "Neuropathological investigation of cerebral white matter lesions caused by closed head injury." *Neuropathology* 22 (4):243-51.
- Ordway, G. A., A. Szebeni, L. J. Hernandez, J. D. Crawford, K. Szebeni, M. J. Chandley, K. C. Burgess, C. Miller, E. Bakkalbasi, and R. W. Brown. 2017. "Antidepressant-Like Actions of Inhibitors of Poly(ADP-Ribose) Polymerase in Rodent Models." *Int J Neuropsychopharmacol* 20 (12):994-1004. doi: 10.1093/ijnp/pyx068.
- Orliaguet, G. A., P. G. Meyer, and T. Bagnon. 2008. "Management of critically ill children with traumatic brain injury." *Paediatr Anaesth* 18 (6):455-61. doi: 10.1111/j.1460-9592.2008.02507.x.
- Owens, K., J. H. Park, R. Schuh, and T. Kristian. 2013. "Mitochondrial dysfunction and NAD(+) metabolism alterations in the pathophysiology of acute brain injury." *Transl Stroke Res* 4 (6):618-34. doi: 10.1007/s12975-013-0278-x.
- Ozdogan, Selcuk, Firat Zeynep, and Atalay Basar. 2013. "Mild Traumatic Brain Injury." *J Neurol Neurophysiol* 4:172. doi: 10.4172/2155-9562.1000172.
- Palmer, C. P., H. E. Metheny, J. A. Elkind, and A. S. Cohen. 2016. "Diminished amygdala activation and behavioral threat response following traumatic brain injury." *Exp Neurol* 277:215-226. doi: 10.1016/j.expneurol.2016.01.004.
- Pearson, William S., David E. Sugerman, Lisa C. McGuire, and Victor G. Coronado. 2012. "Emergency department visits for traumatic brain injury in older adults in the United States: 2006-08." *The western journal of emergency medicine* 13 (3):289-293. doi: 10.5811/westjem.2012.3.11559.
- Perel, P., I. Roberts, O. Bouamra, M. Woodford, J. Mooney, and F. Lecky. 2009. "Intracranial bleeding in patients with traumatic brain injury: a prognostic study." *BMC Emerg Med* 9:15. doi: 10.1186/1471-227X-9-15.
- Pervez, M., R. S. Kitagawa, and T. R. Chang. 2018. "Definition of Traumatic Brain Injury, Neurosurgery, Trauma Orthopedics, Neuroimaging, Psychology, and Psychiatry in Mild Traumatic Brain Injury." *Neuroimaging Clin N Am* 28 (1):1-13. doi: 10.1016/j.nic.2017.09.010.
- Petraglia, A. L., M. L. Dashnaw, R. C. Turner, and J. E. Bailes. 2014. "Models of mild traumatic brain injury: translation of physiological and anatomic injury." *Neurosurgery* 75 Suppl 4:S34-49. doi: 10.1227/NEU.0000000000000472.
- Petraglia, A. L., B. A. Plog, S. Dayawansa, M. Chen, M. L. Dashnaw, K. Czerniecka, C. T. Walker, T. Viterise, O. Hyrien, J. J. Iliff, R. Deane, M. Nedergaard, and J. H.

- Huang. 2014. "The spectrum of neurobehavioral sequelae after repetitive mild traumatic brain injury: a novel mouse model of chronic traumatic encephalopathy." *J Neurotrauma* 31 (13):1211-24. doi: 10.1089/neu.2013.3255.
- Piper, I. R., D. Thomson, and J. D. Miller. 1996. "Monitoring weight drop velocity and foam stiffness as an aid to quality control of a rodent model of impact acceleration neurotrauma." *J Neurosci Methods* 69 (2):171-4. doi: 10.1016/S0165-0270(96)00046-5.
- Piskunova, T. S., M. N. Yurova, A. I. Ovsyannikov, A. V. Semenchenko, M. A. Zabezhinski, I. G. Popovich, Z. Q. Wang, and V. N. Anisimov. 2008. "Deficiency in Poly(ADP-ribose) Polymerase-1 (PARP-1) Accelerates Aging and Spontaneous Carcinogenesis in Mice." *Curr Gerontol Geriatr Res*:754190. doi: 10.1155/2008/754190.
- Plane, J. M., S. K. Grossenbacher, and W. Deng. 2012. "PARP-1 deletion promotes subventricular zone neural stem cells toward a glial fate." *J Neurosci Res* 90 (8):1489-506. doi: 10.1002/jnr.23040.
- Pop, V., and J. Badaut. 2011. "A neurovascular perspective for long-term changes after brain trauma." *Transl Stroke Res* 2 (4):533-45. doi: 10.1007/s12975-011-0126-9.
- Popovitz, J., S. P. Mysore, and H. Adwanikar. 2019. "Long-Term Effects of Traumatic Brain Injury on Anxiety-Like Behaviors in Mice: Behavioral and Neural Correlates." *Front Behav Neurosci* 13:6. doi: 10.3389/fnbeh.2019.00006.
- Post, A., T. B. Hoshizaki, C. Karton, J. M. Clark, L. Dawson, J. Cournoyer, K. Taylor, R. A. Oeur, M. D. Gilchrist, and M. D. Cusimano. 2019. "The biomechanics of concussion for ice hockey head impact events." *Comput Methods Biomech Biomed Engin*:1-13. doi: 10.1080/10255842.2019.1577827.
- Povlishock, J. T. 1993. "Pathobiology of traumatically induced axonal injury in animals and man." *Ann Emerg Med* 22 (6):980-6.
- Povlishock, J. T., and D. I. Katz. 2005. "Update of neuropathology and neurological recovery after traumatic brain injury." *J Head Trauma Rehabil* 20 (1):76-94.
- Povlishock, J. T., A. Marmarou, T. McIntosh, J. Q. Trojanowski, and J. Moroi. 1997. "Impact acceleration injury in the rat: Evidence for focal axolemmal change and related neurofilament sidearm alteration." *Journal of Neuropathology and Experimental Neurology* 56 (4):347-359. doi: Doi 10.1097/00005072-199704000-00003.
- Reger, M. L., A. M. Poulos, F. Buen, C. C. Giza, D. A. Hovda, and M. S. Fanselow. 2012. "Concussive brain injury enhances fear learning and excitatory processes in the amygdala." *Biol Psychiatry* 71 (4):335-43. doi: 10.1016/j.biopsych.2011.11.007.

- Ren, Z., J. J. Iliff, L. Yang, J. Yang, X. Chen, M. J. Chen, R. N. Giese, B. Wang, X. Shi, and M. Nedergaard. 2013. "'Hit & Run' model of closed-skull traumatic brain injury (TBI) reveals complex patterns of post-traumatic AQP4 dysregulation." *J Cereb Blood Flow Metab* 33 (6):834-45. doi: 10.1038/jcbfm.2013.30.
- Risling, M., and J. Davidsson. 2012. "Experimental animal models for studies on the mechanisms of blast-induced neurotrauma." *Front Neurol* 3:30. doi: 10.3389/fneur.2012.00030.
- Rodriguez-Grande, B., A. Ichkova, S. Lemarchant, and J. Badaut. 2017. "Early to Long-Term Alterations of CNS Barriers After Traumatic Brain Injury: Considerations for Drug Development." *AAPS J* 19 (6):1615-1625. doi: 10.1208/s12248-017-0123-3.
- Rodriguez-Rivera, J., L. Denner, and K. T. Dineley. 2011. "Rosiglitazone reversal of Tg2576 cognitive deficits is independent of peripheral gluco-regulatory status." *Behav Brain Res* 216 (1):255-61. doi: 10.1016/j.bbr.2010.08.002.
- Rom, S., H. Dykstra, V. Zuluaga-Ramirez, N. L. Reichenbach, and Y. Persidsky. 2015. "miR-98 and let-7g\* protect the blood-brain barrier under neuroinflammatory conditions." *J Cereb Blood Flow Metab* 35 (12):1957-65. doi: 10.1038/jcbfm.2015.154.
- Romeu-Mejia, R., C. C. Giza, and J. T. Goldman. 2019. "Concussion Pathophysiology and Injury Biomechanics." *Curr Rev Musculoskelet Med*. doi: 10.1007/s12178-019-09536-8.
- Rose, F. C. 1997. "The history of head injuries: an overview." *J Hist Neurosci* 6 (2):154-180. doi: 10.1080/09647049709525700.
- Rotatori, Anthony F., and Sandra Burkhardt. 2011. "Chapter 13 History of Traumatic Brain Injury." In *History of Special Education*, 315-342. Emerald Group Publishing Limited.
- Saatman, K. E., K. J. Feeko, R. L. Pape, and R. Raghupathi. 2006. "Differential behavioral and histopathological responses to graded cortical impact injury in mice." *J Neurotrauma* 23 (8):1241-53. doi: 10.1089/neu.2006.23.1241.
- Sanchez, G. M., and A. L. BurrIDGE. 2007. "Decision making in head injury management in the Edwin Smith Papyrus." *Neurosurg Focus* 23 (1):E5. doi: 10.3171/foc.2007.23.1.5.
- Sarnaik, A. A., Y. P. Conley, D. O. Okonkwo, T. L. Barr, E. L. Fink, C. Szabo, P. M. Kochanek, and R. S. Clark. 2010. "Influence of PARP-1 polymorphisms in patients after traumatic brain injury." *J Neurotrauma* 27 (3):465-71. doi: 10.1089/neu.2009.1171.

- Satchell, M. A., X. Zhang, P. M. Kochanek, C. E. Dixon, L. W. Jenkins, J. Melick, C. Szabo, and R. S. Clark. 2003. "A dual role for poly-ADP-ribosylation in spatial memory acquisition after traumatic brain injury in mice involving NAD<sup>+</sup> depletion and ribosylation of 14-3-3gamma." *J Neurochem* 85 (3):697-708.
- Sauerbeck, A. D., C. Fanizzi, J. H. Kim, M. Gangolli, P. V. Bayly, C. L. Wellington, D. L. Brody, and T. T. Kummer. 2018. "modCHIMERA: a novel murine closed-head model of moderate traumatic brain injury." *Sci Rep* 8 (1):7677. doi: 10.1038/s41598-018-25737-6.
- Scholpp, J., J. K. Schubert, W. Miekisch, and G. F. Noeldge-Schomburg. 2004. "Lipid peroxidation early after brain injury." *J Neurotrauma* 21 (6):667-77. doi: 10.1089/0897715041269632.
- Shaver, T. K., J. E. Ozga, B. Zhu, K. G. Anderson, K. M. Martens, and C. Vonder Haar. 2019. "Long-term deficits in risky decision-making after traumatic brain injury on a rat analog of the Iowa gambling task." *Brain Res* 1704:103-113. doi: 10.1016/j.brainres.2018.10.004.
- Shaw, N. A. 1985. "A simple device for experimentally concussing the rat." *Physiol Behav* 35 (4):637-9.
- Shaw, N. A. 1986. "Somatosensory evoked potentials after experimental head injury in the awake rat." *J Neurol Sci* 74 (2-3):257-70.
- Shigemoto-Mogami, Y., K. Hoshikawa, and K. Sato. 2018. "Activated Microglia Disrupt the Blood-Brain Barrier and Induce Chemokines and Cytokines in a Rat in vitro Model." *Front Cell Neurosci* 12:494. doi: 10.3389/fncel.2018.00494.
- Shohami, E., E. Beit-Yannai, M. Horowitz, and R. Kohen. 1997. "Oxidative stress in closed-head injury: brain antioxidant capacity as an indicator of functional outcome." *J Cereb Blood Flow Metab* 17 (10):1007-19. doi: 10.1097/00004647-199710000-00002.
- Siedler, D. G., M. I. Chuah, M. T. Kirkcaldie, J. C. Vickers, and A. E. King. 2014. "Diffuse axonal injury in brain trauma: insights from alterations in neurofilaments." *Front Cell Neurosci* 8:429. doi: 10.3389/fncel.2014.00429.
- Simon, D. W., M. J. McGeachy, H. Bayir, R. S. B. Clark, D. J. Loane, and P. M. Kochanek. 2017. "The far-reaching scope of neuroinflammation after traumatic brain injury." *Nat Rev Neurol* 13 (9):572. doi: 10.1038/nrneurol.2017.116.
- Siva Sai Sujith Sajja, B., C. Tenn, L. J. McLaws, and P. VandeVord. 2014. "IL-5; a diffuse biomarker associated with brain inflammation after blast exposure." *Biomed Sci Instrum* 50:375-82.

- Skaper, S. D., L. Facci, M. Zusso, and P. Giusti. 2018. "An Inflammation-Centric View of Neurological Disease: Beyond the Neuron." *Front Cell Neurosci* 12:72. doi: 10.3389/fncel.2018.00072.
- Skotak, M., E. Alay, and N. Chandra. 2018. "On the Accurate Determination of Shock Wave Time-Pressure Profile in the Experimental Models of Blast-Induced Neurotrauma." *Front Neurol* 9:52. doi: 10.3389/fneur.2018.00052.
- Smith, D. H., R. R. Hicks, V. E. Johnson, D. A. Bergstrom, D. M. Cummings, L. J. Noble, D. Hovda, M. Whalen, S. T. Ahlers, M. LaPlaca, F. C. Tortella, A. C. Duhaime, and C. E. Dixon. 2015. "Pre-Clinical Traumatic Brain Injury Common Data Elements: Toward a Common Language Across Laboratories." *J Neurotrauma* 32 (22):1725-35. doi: 10.1089/neu.2014.3861.
- Smith, D. H., D. F. Meaney, and W. H. Shull. 2003. "Diffuse axonal injury in head trauma." *J Head Trauma Rehabil* 18 (4):307-16.
- Smith, D. H., M. Nonaka, R. Miller, M. Leoni, X. H. Chen, D. Alsop, and D. F. Meaney. 2000. "Immediate coma following inertial brain injury dependent on axonal damage in the brainstem." *J Neurosurg* 93 (2):315-22. doi: 10.3171/jns.2000.93.2.0315.
- Song, Q., D. Xie, S. Pan, and W. Xu. 2015. "Rapamycin protects neurons from brain contusion-induced inflammatory reaction via modulation of microglial activation." *Mol Med Rep* 12 (5):7203-10. doi: 10.3892/mmr.2015.4407.
- Staal, J. A., T. C. Dickson, R. Gasperini, Y. Liu, L. Foa, and J. C. Vickers. 2010. "Initial calcium release from intracellular stores followed by calcium dysregulation is linked to secondary axotomy following transient axonal stretch injury." *J Neurochem* 112 (5):1147-55. doi: 10.1111/j.1471-4159.2009.06531.x.
- Stalhammar, D., B. J. Galinat, A. M. Allen, D. P. Becker, H. H. Stonnington, and R. L. Hayes. 1987. "A new model of concussive brain injury in the cat produced by extradural fluid volume loading: I. Biomechanical properties." *Brain Inj* 1 (1):73-91.
- Stemper, B. D., A. S. Shah, M. D. Budde, C. M. Olsen, A. Glavaski-Joksimovic, S. N. Kurpad, M. McCrea, and F. A. Pintar. 2016. "Behavioral Outcomes Differ between Rotational Acceleration and Blast Mechanisms of Mild Traumatic Brain Injury." *Front Neurol* 7:31. doi: 10.3389/fneur.2016.00031.
- Steru, L., R. Chermat, B. Thierry, and P. Simon. 1985. "The tail suspension test: a new method for screening antidepressants in mice." *Psychopharmacology (Berl)* 85 (3):367-70.
- Stiefel, M., A. Shaner, and S. D. Schaefer. 2006. "The Edwin Smith Papyrus: the birth of analytical thinking in medicine and otolaryngology." *Laryngoscope* 116 (2):182-8. doi: 10.1097/01.mlg.0000191461.08542.a3.

- Stoica, B. A., D. J. Loane, Z. Zhao, S. V. Kabadi, M. Hanscom, K. R. Byrnes, and A. I. Faden. 2014. "PARP-1 inhibition attenuates neuronal loss, microglia activation and neurological deficits after traumatic brain injury." *J Neurotrauma* 31 (8):758-72. doi: 10.1089/neu.2013.3194.
- Strauss, Israel, and Nathan Savitsky. 1934. "HEAD INJURY: NEUROLOGIC AND PSYCHIATRIC ASPECTS." *Archives of Neurology & Psychiatry* 31 (5):893-955. doi: 10.1001/archneurpsyc.1934.02250050011001.
- Strich, S. J. 1956. "Diffuse degeneration of the cerebral white matter in severe dementia following head injury." *J Neurol Neurosurg Psychiatry* 19 (3):163-85.
- Sullivan, H. G., J. Martinez, D. P. Becker, J. D. Miller, R. Griffith, and A. O. Wist. 1976. "Fluid-percussion model of mechanical brain injury in the cat." *J Neurosurg* 45 (5):521-34.
- Sun, D. A., L. S. Deshpande, S. Sombati, A. Baranova, M. S. Wilson, R. J. Hamm, and R. J. DeLorenzo. 2008. "Traumatic brain injury causes a long-lasting calcium (Ca<sup>2+</sup>)-plateau of elevated intracellular Ca levels and altered Ca<sup>2+</sup> homeostatic mechanisms in hippocampal neurons surviving brain injury." *Eur J Neurosci* 27 (7):1659-72. doi: 10.1111/j.1460-9568.2008.06156.x.
- Svendsen, C. N., M. G. ter Borg, R. J. Armstrong, A. E. Rosser, S. Chandran, T. Ostenfeld, and M. A. Caldwell. 1998. "A new method for the rapid and long term growth of human neural precursor cells." *J Neurosci Methods* 85 (2):141-52.
- Tang, K. S., S. W. Suh, C. C. Alano, Z. Shao, W. T. Hunt, R. A. Swanson, and C. M. Anderson. 2010. "Astrocytic poly(ADP-ribose) polymerase-1 activation leads to bioenergetic depletion and inhibition of glutamate uptake capacity." *Glia* 58 (4):446-57. doi: 10.1002/glia.20936.
- Taylor, C. A., J. M. Bell, M. J. Breiding, and L. Xu. 2017. "Traumatic Brain Injury-Related Emergency Department Visits, Hospitalizations, and Deaths - United States, 2007 and 2013." *MMWR Surveill Summ* 66 (9):1-16. doi: 10.15585/mmwr.ss6609a1.
- Taylor, G. T., S. Lerch, and S. Chourbaji. 2017. "Marble burying as compulsive behaviors in male and female mice." *Acta Neurobiol Exp (Wars)* 77 (3):254-260.
- Teasdale, G., and B. Jennett. 1974. "Assessment of coma and impaired consciousness. A practical scale." *Lancet* 2 (7872):81-4.
- Teasdale, G., A. Maas, F. Lecky, G. Manley, N. Stocchetti, and G. Murray. 2014. "The Glasgow Coma Scale at 40 years: standing the test of time." *The Lancet Neurology* 13 (8):844-854. doi: [https://doi.org/10.1016/S1474-4422\(14\)70120-6](https://doi.org/10.1016/S1474-4422(14)70120-6).
- Thomas, A., A. Burant, N. Bui, D. Graham, L. A. Yuva-Paylor, and R. Paylor. 2009. "Marble burying reflects a repetitive and perseverative behavior more than

- novelty-induced anxiety." *Psychopharmacology (Berl)* 204 (2):361-73. doi: 10.1007/s00213-009-1466-y.
- Thomas, C., and A. V. Tulin. 2013. "Poly-ADP-ribose polymerase: machinery for nuclear processes." *Mol Aspects Med* 34 (6):1124-37. doi: 10.1016/j.mam.2013.04.001.
- Thornhill, S., G. M. Teasdale, G. D. Murray, J. McEwen, C. W. Roy, and K. I. Penny. 2000. "Disability in young people and adults one year after head injury: prospective cohort study." *BMJ* 320 (7250):1631-5.
- Thurman, D.J., Kraus, J.F., Romer, C.J., & World Health Organization. Division of Emergency and Humanitarian Action. 1995. Standards for surveillance of neurotrauma / editors : David J. Thurman, Jess F. Kraus and Claude J. Romer. Geneva: World Health Organization.
- To, C., E. H. Kim, D. B. Royce, C. R. Williams, R. M. Collins, R. Risingsong, M. B. Sporn, and K. T. Liby. 2014. "The PARP inhibitors, veliparib and olaparib, are effective chemopreventive agents for delaying mammary tumor development in BRCA1-deficient mice." *Cancer Prev Res (Phila)* 7 (7):698-707. doi: 10.1158/1940-6207.CAPR-14-0047.
- Tomlinson, B. E. 1970. "Brain-stem lesions after head injury." *J Clin Pathol Suppl (R Coll Pathol)* 4:154-65.
- Tsenter, J., L. Beni-Adani, Y. Assaf, A. G. Alexandrovich, V. Trembovler, and E. Shohami. 2008. "Dynamic changes in the recovery after traumatic brain injury in mice: effect of injury severity on T2-weighted MRI abnormalities, and motor and cognitive functions." *J Neurotrauma* 25 (4):324-33. doi: 10.1089/neu.2007.0452.
- Tucker, L. B., A. H. Fu, and J. T. McCabe. 2016. "Performance of Male and Female C57BL/6J Mice on Motor and Cognitive Tasks Commonly Used in Pre-Clinical Traumatic Brain Injury Research." *J Neurotrauma* 33 (9):880-94. doi: 10.1089/neu.2015.3977.
- Vagnozzi, R., B. Tavazzi, S. Signoretti, A. M. Amorini, A. Belli, M. Cimatti, R. Delfini, V. Di Pietro, A. Finocchiaro, and G. Lazzarino. 2007. "Temporal window of metabolic brain vulnerability to concussions: mitochondrial-related impairment--part I." *Neurosurgery* 61 (2):379-88; discussion 388-9. doi: 10.1227/01.NEU.0000280002.41696.D8.
- Vaishnavi, S., V. Rao, and J. R. Fann. 2009. "Neuropsychiatric problems after traumatic brain injury: unraveling the silent epidemic." *Psychosomatics* 50 (3):198-205. doi: 10.1176/appi.psy.50.3.198.
- van Wimersma Greidanus, T. B., J. Jolles, and D. De Wied. 1985. "Hypothalamic neuropeptides and memory." *Acta Neurochir (Wien)* 75 (1-4):99-105.

- Virag, L., A. Robaszkiewicz, J. M. Rodriguez-Vargas, and F. J. Oliver. 2013. "Poly(ADP-ribose) signaling in cell death." *Mol Aspects Med* 34 (6):1153-67. doi: 10.1016/j.mam.2013.01.007.
- Virag, L., A. L. Salzman, and C. Szabo. 1998. "Poly(ADP-ribose) synthetase activation mediates mitochondrial injury during oxidant-induced cell death." *J Immunol* 161 (7):3753-9.
- Vonder Haar, C., K. M. Martens, L. K. Riparip, S. Rosi, C. L. Wellington, and C. A. Winstanley. 2017. "Frontal Traumatic Brain Injury Increases Impulsive Decision Making in Rats: A Potential Role for the Inflammatory Cytokine Interleukin-12." *J Neurotrauma* 34 (19):2790-2800. doi: 10.1089/neu.2016.4813.
- Vosler, P. S., D. Sun, S. Wang, Y. Gao, D. B. Kintner, A. P. Signore, G. Cao, and J. Chen. 2009. "Calcium dysregulation induces apoptosis-inducing factor release: cross-talk between PARP-1- and calpain-signaling pathways." *Exp Neurol* 218 (2):213-20. doi: 10.1016/j.expneurol.2009.04.032.
- Wahab, R. A., E. J. Neuberger, B. G. Lyeth, V. Santhakumar, and B. J. Pfister. 2015. "Fluid percussion injury device for the precise control of injury parameters." *J Neurosci Methods* 248:16-26. doi: 10.1016/j.jneumeth.2015.03.010.
- Walf, A. A., and C. A. Frye. 2007. "The use of the elevated plus maze as an assay of anxiety-related behavior in rodents." *Nature Protocols* 2 (2):322-328. doi: 10.1038/nprot.2007.44.
- Walz, N., A. Muhlberger, and P. Pauli. 2016. "A Human Open Field Test Reveals Thigmotaxis Related to Agoraphobic Fear." *Biol Psychiatry* 80 (5):390-7. doi: 10.1016/j.biopsych.2015.12.016.
- Wang, E., J. Gao, Q. Yang, M. O. Parsley, T. J. Dunn, L. Zhang, D. S. DeWitt, L. Denner, D. S. Prough, and P. Wu. 2012. "Molecular mechanisms underlying effects of neural stem cells against traumatic axonal injury." *J Neurotrauma* 29 (2):295-312. doi: 10.1089/neu.2011.2043.
- Wang, G., Y. P. Zhang, Z. Gao, L. B. E. Shields, F. Li, T. Chu, H. Lv, T. Moriarty, X. M. Xu, X. Yang, C. B. Shields, and J. Cai. 2018. "Pathophysiological and behavioral deficits in developing mice following rotational acceleration-deceleration traumatic brain injury." *Dis Model Mech* 11 (1). doi: 10.1242/dmm.030387.
- Wang, H. C., C. F. Sun, H. Chen, M. S. Chen, G. Shen, Y. B. Ma, and B. D. Wang. 2014. "Where are we in the modelling of traumatic brain injury? Models complicated by secondary brain insults." *Brain Inj* 28 (12):1491-503. doi: 10.3109/02699052.2014.943288.
- Wang, H., S. W. Yu, D. W. Koh, J. Lew, C. Coombs, W. Bowers, H. J. Federoff, G. G. Poirier, T. M. Dawson, and V. L. Dawson. 2004. "Apoptosis-inducing factor

- substitutes for caspase executioners in NMDA-triggered excitotoxic neuronal death." *J Neurosci* 24 (48):10963-73. doi: 10.1523/JNEUROSCI.3461-04.2004.
- Wang, Y., V. L. Dawson, and T. M. Dawson. 2009. "Poly(ADP-ribose) signals to mitochondrial AIF: a key event in parthanatos." *Exp Neurol* 218 (2):193-202. doi: 10.1016/j.expneurol.2009.03.020.
- Wang, Y., N. S. Kim, J. F. Haince, H. C. Kang, K. K. David, S. A. Andrabi, G. G. Poirier, V. L. Dawson, and T. M. Dawson. 2011. "Poly(ADP-ribose) (PAR) binding to apoptosis-inducing factor is critical for PAR polymerase-1-dependent cell death (parthanatos)." *Sci Signal* 4 (167):ra20. doi: 10.1126/scisignal.2000902.
- Wang, Y., Y. Wei, S. Oguntayo, W. Wilkins, P. Arun, M. Valiyaveetil, J. Song, J. B. Long, and M. P. Nambiar. 2011. "Tightly coupled repetitive blast-induced traumatic brain injury: development and characterization in mice." *J Neurotrauma* 28 (10):2171-83. doi: 10.1089/neu.2011.1990.
- Weber, J. T. 2012. "Altered calcium signaling following traumatic brain injury." *Front Pharmacol* 3:60. doi: 10.3389/fphar.2012.00060.
- Weber, J. T., B. A. Rzigalinski, and E. F. Ellis. 2001. "Traumatic injury of cortical neurons causes changes in intracellular calcium stores and capacitative calcium influx." *J Biol Chem* 276 (3):1800-7. doi: 10.1074/jbc.M009209200.
- Weber, John T. 2007. "Experimental models of repetitive brain injuries." In *Progress in Brain Research*, edited by T. Weber John and I. R. Maas Andrew, 253-261. Elsevier.
- Werner, C., and K. Engelhard. 2007. "Pathophysiology of traumatic brain injury." *Br J Anaesth* 99 (1):4-9. doi: 10.1093/bja/aem131.
- Whalen, M. J., R. S. Clark, C. E. Dixon, P. Robichaud, D. W. Marion, V. Vagni, S. H. Graham, L. Virag, G. Hasko, R. Stachlewitz, C. Szabo, and P. M. Kochanek. 1999. "Reduction of cognitive and motor deficits after traumatic brain injury in mice deficient in poly(ADP-ribose) polymerase." *J Cereb Blood Flow Metab* 19 (8):835-42. doi: 10.1097/00004647-199908000-00002.
- Wheble, J. L., and D. K. Menon. 2016. "TBI-the most complex disease in the most complex organ: the CENTER-TBI trial-a commentary." *J R Army Med Corps* 162 (2):87-9. doi: 10.1136/jramc-2015-000472.
- Whyte, J., J. Vasterling, and G. T. Manley. 2010. "Common data elements for research on traumatic brain injury and psychological health: current status and future development." *Arch Phys Med Rehabil* 91 (11):1692-6. doi: 10.1016/j.apmr.2010.06.031.

- Williams, A. J., J. A. Hartings, X. C. Lu, M. L. Rolli, J. R. Dave, and F. C. Tortella. 2005. "Characterization of a new rat model of penetrating ballistic brain injury." *J Neurotrauma* 22 (2):313-31. doi: 10.1089/neu.2005.22.313.
- Williams, D. H., H. S. Levin, and H. M. Eisenberg. 1990. "Mild head injury classification." *Neurosurgery* 27 (3):422-8.
- Wirth, P., W. Yu, A. L. Kimball, J. Liao, P. Berkner, and M. J. Glenn. 2017. "New method to induce mild traumatic brain injury in rodents produces differential outcomes in female and male Sprague Dawley rats." *J Neurosci Methods* 290:133-144. doi: 10.1016/j.jneumeth.2017.07.030.
- Witcher, K. G., D. S. Eiferman, and J. P. Godbout. 2015. "Priming the inflammatory pump of the CNS after traumatic brain injury." *Trends Neurosci* 38 (10):609-620. doi: 10.1016/j.tins.2015.08.002.
- Wolf, J. A., P. K. Stys, T. Lusardi, D. Meaney, and D. H. Smith. 2001. "Traumatic axonal injury induces calcium influx modulated by tetrodotoxin-sensitive sodium channels." *J Neurosci* 21 (6):1923-30.
- Wolmarans, D. W., D. J. Stein, and B. H. Harvey. 2016. "Of mice and marbles: Novel perspectives on burying behavior as a screening test for psychiatric illness." *Cogn Affect Behav Neurosci* 16 (3):551-60. doi: 10.3758/s13415-016-0413-8.
- World Health Organization. 2006. "Neurological disorders: public health challenges." World Health Organization, accessed Sept 22 2014. [http://www.who.int/mental\\_health/neurology/neurological\\_disorders\\_report\\_web.pdf?ua=1](http://www.who.int/mental_health/neurology/neurological_disorders_report_web.pdf?ua=1).
- Wu, P., Y. I. Tarasenko, Y. Gu, L. Y. Huang, R. E. Coggeshall, and Y. Yu. 2002. "Region-specific generation of cholinergic neurons from fetal human neural stem cells grafted in adult rat." *Nat Neurosci* 5 (12):1271-8. doi: 10.1038/nn974.
- Xiong, Y., A. Mahmood, and M. Chopp. 2013. "Animal models of traumatic brain injury." *Nat Rev Neurosci* 14 (2):128-42. doi: 10.1038/nrn3407.
- Xiong, Y., A. Mahmood, and M. Chopp. 2018. "Current understanding of neuroinflammation after traumatic brain injury and cell-based therapeutic opportunities." *Chin J Traumatol* 21 (3):137-151. doi: 10.1016/j.cjtee.2018.02.003.
- Xu, J. C., J. Fan, X. Wang, S. M. Eacker, T. I. Kam, L. Chen, X. Yin, J. Zhu, Z. Chi, H. Jiang, R. Chen, T. M. Dawson, and V. L. Dawson. 2016. "Cultured networks of excitatory projection neurons and inhibitory interneurons for studying human cortical neurotoxicity." *Sci Transl Med* 8 (333):333ra48. doi: 10.1126/scitranslmed.aad0623.

- Yang, H., T. Yang, J. A. Baur, E. Perez, T. Matsui, J. J. Carmona, D. W. Lamming, N. C. Souza-Pinto, V. A. Bohr, A. Rosenzweig, R. de Cabo, A. A. Sauve, and D. A. Sinclair. 2007. "Nutrient-sensitive mitochondrial NAD<sup>+</sup> levels dictate cell survival." *Cell* 130 (6):1095-107. doi: 10.1016/j.cell.2007.07.035.
- Yates, N. J., S. Lydiard, B. Fehily, G. Weir, A. Chin, C. A. Bartlett, J. Alderson, and M. Fitzgerald. 2017. "Repeated mild traumatic brain injury in female rats increases lipid peroxidation in neurons." *Exp Brain Res* 235 (7):2133-2149. doi: 10.1007/s00221-017-4958-8.
- Yen, T. L., C. C. Chang, C. L. Chung, W. C. Ko, C. H. Yang, and C. Y. Hsieh. 2018. "Neuroprotective Effects of Platonin, a Therapeutic Immunomodulating Medicine, on Traumatic Brain Injury in Mice after Controlled Cortical Impact." *Int J Mol Sci* 19 (4). doi: 10.3390/ijms19041100.
- Ying, W. 2006. "NAD<sup>+</sup> and NADH in cellular functions and cell death." *Front Biosci* 11:3129-48.
- Yokobori, S., A. T. Mazzeo, S. Gajavelli, and M. R. Bullock. 2014. "Mitochondrial Neuroprotection in Traumatic Brain Injury: Rationale and Therapeutic Strategies." *Cns & Neurological Disorders-Drug Targets* 13 (4):606-619.
- Yokobori, S., R. Nakae, H. Yokota, M. S. Spurlock, S. Mondello, S. Gajavelli, and R. M. Bullock. 2018. "Subdural hematoma decompression model: A model of traumatic brain injury with ischemic-reperfusional pathophysiology: A review of the literature." *Behav Brain Res* 340:23-28. doi: 10.1016/j.bbr.2016.05.055.
- Yoshino, A., D. A. Hovda, T. Kawamata, Y. Katayama, and D. P. Becker. 1991. "Dynamic Changes in Local Cerebral Glucose-Utilization Following Cerebral Concussion in Rats - Evidence of a Hypermetabolic and Subsequent Hypometabolic State." *Brain Research* 561 (1):106-119. doi: Doi 10.1016/0006-8993(91)90755-K.
- Yue, John K., Caitlin K. Robinson, Ethan A. Winkler, Pavan S. Upadhyayula, John F. Burke, Romain Pirracchio, Catherine G. Suen, Hansen Deng, Laura B. Ngwenya, Sanjay S. Dhall, Geoffrey T. Manley, and Phiroz E. Tarapore. 2017. "Circadian variability of the initial Glasgow Coma Scale score in traumatic brain injury patients." *Neurobiology of Sleep and Circadian Rhythms* 2:85-93. doi: <https://doi.org/10.1016/j.nbscr.2016.09.002>.
- Zaremba, T., H. Thomas, M. Cole, E. R. Plummer, and N. J. Curtin. 2010. "Doxorubicin-induced suppression of poly(ADP-ribose) polymerase-1 (PARP-1) activity and expression and its implication for PARP inhibitors in clinical trials." *Cancer Chemother Pharmacol* 66 (4):807-12. doi: 10.1007/s00280-010-1359-0.
- Zhang, F., S. S. Lau, and T. J. Monks. 2012. "A dual role for poly(ADP-ribose) polymerase-1 during caspase-dependent apoptosis." *Toxicol Sci* 128 (1):103-14. doi: 10.1093/toxsci/kfs142.

- Zhang, Y. P., J. Cai, L. B. Shields, N. Liu, X. M. Xu, and C. B. Shields. 2014. "Traumatic brain injury using mouse models." *Transl Stroke Res* 5 (4):454-71. doi: 10.1007/s12975-014-0327-0.
- Ziebell, Jenna M., Frances Corrigan, and Robert Vink. 2012. "Animal models of mild and severe TBI: what have we learned in the past 30 years?" In *Traumatic Brain and Spinal Cord Injury: Challenges and Developments*, edited by Andrew Maas, Cristina Morganti-Kossmann and Ramesh Raghupathi, 114-125. Cambridge: Cambridge University Press.
- Zou, J., Y. X. Wang, F. F. Dou, H. Z. Lu, Z. W. Ma, P. H. Lu, and X. M. Xu. 2010. "Glutamine synthetase down-regulation reduces astrocyte protection against glutamate excitotoxicity to neurons." *Neurochem Int* 56 (4):577-84. doi: 10.1016/j.neuint.2009.12.021.
- Zuercher, Mathias, Wolfgang Ummenhofer, Anja Baltussen, and Bernhard Walder. 2009. "The use of Glasgow Coma Scale in injury assessment: A critical review." *Brain Injury* 23 (5):371-384. doi: 10.1080/02699050902926267.

## **Vita**

Javier Allende Labastida was born in San Luis Potosí, México on August 28<sup>a</sup>, 1982. He was born to Mr. Javier Jose Allende Perogordo and Mrs. Maria del Pilar Labastida Aguirre. Javier attended Bachillerato Anahuac Highschool in San Luis Potosi. He earned an M.D. degree from Universidad de Monterrey at San Pedro Garza García, N.L., México. Javier has co-authored three peer-reviewed original research articles.

Permanent address: Cañada de Gómez 160, Lomas 4a secc. San Luis Potosí, San Luis Potosí, México, 78216

This dissertation was typed by Javier Allende Labastida.

## Summary of Dissertation

Traumatic brain injury (TBI) is a major public health problem. It represents the leading cause of morbidity and mortality in children and young adults, resulting in long-term sequelae for a considerable number of survivors. Development of effective therapeutics for patients with TBI is an unmet need. A critical step to address this need is to establish reproducible and comparable animal models that will allow preclinical meta-analyses, and has led to an increasing interest in generating common data elements in TBI research.

This project addresses TBI and research-related issues in three ways. First, an existing closed-skull weight drop TBI model was optimized by the incorporation of three novel sensors, which allowed the detection of important factors that could induce variability. This finding led to the redesign of the model and the addition of an impactor. Additionally, the sensors allowed measurement and comparison of forces applied on the head of the animal to monitor mechanical reproducibility. The outcomes of these injuries were further evaluated with a comprehensive battery of behavioral and pathological analyses. Second, an artificial model of a mouse, “the professional mouse” was developed to aid the precise measurement for reproducibility of closed-head injury models or compare between models. Finally, this newly optimized TBI model was used to initiate the assessment of a potentially therapeutic drug to treat neurotrauma. Olaparib (Lynparza®) is a Poly(ADP-polymerase) 1 (PARP1) inhibitor approved by the FDA for the treatment of breast and ovarian cancer. Several studies reported the activation of PARP1 after injury in the central nervous system. This activation has been correlated with increased inflammation, mitochondrial dysfunction and necrosis. Furthermore, the inhibition of PARP1 is neuroprotective in different models of brain injury. This study shows that olaparib administered after TBI reduces astrogliosis and cognitive deficits. Although

further studies are needed, we are enthusiastic that PARP inhibition may prove efficacious in the acute phase, as well as prevent the later-stage neurological deterioration secondary to single or repetitive TBI.